THE PHOTOPHYSICAL PROPERTIES OF RUTHENIUM(II) POLYPYRIDYL COMPLEXES IMMOBILISED IN SOL-GEL MATRICES.

BY

KAREN MONGEY, B. Sc.

A THESIS PRESENTED TO DUBLIN CITY UNIVERSITY FOR THE DEGREE OF DOCTOR OF PHILOSOPHY.

SUPERVISOR PROF. JOHANNES G. VOS.
SCHOOL OF CHEMICAL SCIENCES
DUBLIN CITY UNIVERSITY.

JANUARY 1996.

This thesis is dedicated to my parents.

This thesis has not previously been submitted as an exercise for a degree at this or at any other university. Except as otherwise indicated, this work has been carried out by the author alone.

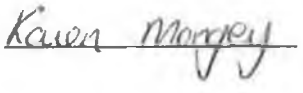

Karen Mongey

Acknowledgements.

First and foremost I would like to thank my supervisor Prof. Hans Vos for his support, advice and encouragement throughout my postgraduate years. His assistance in the preparation of this manuscript is greatly appreciated. I would also like to thank him for the use of his office (which I have become quite fond of) and I grudgingly return the key.

I also extend my gratitude to all the academic and technical staff of the Chemistry department, both past and present. In particular I would like to thank Dr. Conor Long (and the members of his research group), Dr. Dermot Diamond and Suzanne Walsh for their assistance in the dreadful "double exponential" era and to Vinnie for supplying my Smartie addiction during this time.

I would also like to thank Dr. John McGarvey of the Chemistry Department at Queens University for the resonance Raman measurements.

Many thanks to all my fellow research group both past and present; Helen, Rachel, Dave, Margaret, Noel, Christine, Luke and Una. Thanks to Tia for her expert advice and training in the low temperature work without which I would undoubtedly have lost a finger or two and Frances for her help and remarkable listening skills over the last three years without whom I would definitely have lost my mind. Special thanks to (my other half) Miriam for her friendship in good and bad times over the past few years (Up Kilkenny !), for putting up with me over the last six months while concocting this thesis and for resisting the temptation to belt me every time I said "I think I have it sorted now".

Thanks also to Dr. Brian MacCraith, Dr. Colette McDonagh and Aisling McEvoy of the physics department, firstly, for their insight on a vast number of sol-gel issues over the past three years and secondly, for their company on the Portuguese expedition.

I would like to thank all of the postgrads in the chemistry department: Ciara, Mary, Fiona, Orla, Siobhan, Rod, Colette, James, Farmer, Paul (thanks for the driving lesson), Ciaran, Pat (for the dream interpretations), Joe, Tom, Mick (× 4) all the class of '92 and many more. To "the lads", Cormac, Shane,

James and Ollie, I extend my gratitude for the amusement at coffee times and I eagerly await dinner invitations.

Outside of DCU, I wish to thank all of the gang, in particular Grainne (for replacement of lost marbles!), Terri, Catherine, Miriam and Una for their support over the past few months and their willingness to celebrate prematurely. I would also like to thank the girls in the house and wish them every success in the future.

Finally I would like to thank my siblings (too numerous to name), and my parents, Dolores and Jimmy. This thesis is dedicated to them and I thank them for everything.

Abstract.

This thesis involves the synthesis and characterisation of sol-gel monoliths doped with Ru(II) polypyridyl complexes. In Chapter 1 an overview of the chemistry of the sol-gel process is given along with an introduction to the photophysical properties of Ru(II) complexes in solution.

In the first section of this thesis, the Ru(II) dopants are employed as spectroscopic probes of the sol-gel process, following the reactions as they proceed from the initial sol to the final xerogel. Variations in the photophysical properties of these immobilised complexes were found to accompany changes in the sol-gel microenvironment. As such, these Ru(II) dopants can be employed to yield information on the evolution of the sol-gel reactions. On the one hand, the blue shift in the emission energy of $[Ru(bpy)_3]^{2+}$ and $[Ru(phen)_3]^{2+}$ associated with the restrictive nature of the sol-gel matrix as compared to solution, was used to probe the early stages of the sol-gel process. Investigations into a number of parameters (*i.e.* pH, temperature and water/silane ratio) which effect these reactions were carried out. On the other hand, the photophysical behaviour of the immobilised $[Ru(dpp)_3]^{2+}$ was found to probe the final stages (the drying reactions) of the sol-gel process. This section also investigates the potential application of the acid/base chemistry of a pyridyltriazole complex as a probe of changes in acidity which may occur during the sol-gel process.

The final section of this thesis involves using the known information of the sol-gel system to examine the excited state processes of Ru(II) polypyridyl complexes under a novel environment. Chapters 5 and 6 investigate the temperature dependence of the excited-state decay of a range of complexes in solution and in the sol-gel matrix. Significant differences were found depending on the individual complex and also on the nature of the host matrix. These studies suggest that the population of the ^3MC state which is responsible for the photodecomposition of these complexes in solution may be inhibited in the sol-gel matrix and that as such, the photolability of a number of these complexes decreases upon immobilisation.

Table of Contents.

Chapter 1.

Introduction.

1.1 General introduction.

The sol-gel process is a method by which inorganic glasses, such as silicates or aluminosilicates, can be prepared from solution by hydrolysis and polycondensation of alkoxide precursors [1-2]. This method has received considerable attention in recent years, because it possesses a number of desirable characteristics [3-6]. Firstly, it enables one to prepare glasses at temperatures far lower than those employed in conventional melting techniques. In addition, the sol-gel process is a high-purity process which leads to excellent homogeneity. Finally, the sol-gel approach is adaptable to producing bulk monoliths as well as films and fibres.

One of the major applications in this area is the ability to dope inorganic glasses with photoactive molecules. Organic and biological molecules with poor thermal stability can be encapsulated intact in the inorganic glass while retaining their optical properties. The flexible solution chemistry and the ability to prepare an essentially inorganic matrix with little or no heating means that the sol-gel process is compatible with a wide variety of dopant molecules, leading to a constantly increasing list of doped sol-gels of diverse applications. Room temperature polymerisation of metal alkoxides has led to the preparation of materials of optical interest, such as solid laser dye blocks and films [7], hole-burning materials [8], photochromic glasses [9,10] and non-linear optical materials [11].

The prospects for using encapsulants for a new generation of highly specific optical sensors are very promising [12-14]. The dopant cannot be easily leached out from the solid, but a significant fraction is exposed to the intrapore region of the matrix where it can participate in a diverse variety of chemical reactions. The high transparency of the sol-gel matrix allows this reactivity to be quantified spectroscopically. These beneficial features together with the chemical inertness of the matrix have led to the application of sol-gels in chemical sensor technology.

Another very active area in sol-gel technology, is the use of photoprobes to gain a more comprehensive understanding of the sol-gel process [15]. By this approach, a low concentration of a probe molecule with the desired photophysical or

photochemical properties is added to the system under investigation. Changes in the properties exerted by changes in the environment are then monitored. The ability to observe the sol-gel-xerogel transitions by this method has produced and continues to produce much needed information.

1.2 The sol-gel process.

The current status of sol-gel preparation [1,16], can be traced back to the work of Dislich [17] in 1971 on the low temperature preparation of a borosilicate glass by heating metal alkoxide-derived gel powder and that of Mazdiyashni and co-workers [18] in 1969 on the low temperature preparation of ferroelectric ceramics by sintering metal alkoxide-derived gel powder. Primarily, much attention was given to the low temperature nature of the sol-gel process. However, sol-gel researchers soon became aware of the of the potential of the sol-gel method to provide new advanced functional materials. The prospects of this novel glass forming technique to produce new or improved glasses, glass-ceramics with superior and unique properties, environmental insensitivity and reproducibility were realised [5].

For millennia, ceramics have been prepared with essentially the same technology. Powders have been shaped into objects and subsequently densified at extremely high temperatures. The technology of making glass has also remained fundamentally the same since prehistory. Particles are melted, homogenised, and shaped into objects from the liquid. The motivation for sol-gel processing is primarily the potentially higher purity and homogeneity of the resulting glass and the fore mentioned lower processing temperatures associated with sol-gels compared with traditional glass melting or ceramic powder methods [19]. Major advances in the production of ceramics and glasses using the sol-gel method depends on an approach which emphasises control of formation through chemistry [20]. This approach has been named "ultrastructure processing" and has been the subject of several recent symposia [21-22]. The goal of sol-gel processing in general is to control the surfaces and interfaces of materials during the earliest stages of production. Long term reliability of a material is usually limited by localised variations in the physical chemistry of the surface and interfaces within the material. The emphasis on ultrastructure processing is on limiting and controlling physical chemical variability by the production of uniquely homogeneous structures and achieving unique physical properties by combining inorganic and organic materials.

1.2.1 An overview of the sol-gel process.

Alkoxysilanes play an important role in the development of silicon-containing materials. Perhaps the most investigated sol-gel method is that which employs tetraalkoxysilanes for the preparation of silica glasses. The principal synthetic route used by researchers to form sol-gels is through the hydrolysis and condensation polymerisation of tetraalkoxysilanes [23], as shown in the following reactions:

$$\equiv Si - OR + H_2O \rightleftharpoons \equiv Si\text{-}OH + ROH \qquad (1.1)$$

$$\equiv Si - OR + HO - Si \equiv \rightleftharpoons \equiv Si - O - Si \equiv + ROH \qquad (1.2)$$

$$\equiv Si - OH + HO - Si \equiv \rightleftharpoons \equiv Si - O - Si \equiv + H_2O \qquad (1.3)$$

It is evident from these equations that the structure of the sol-gel glass evolves sequentially as the product of successive hydrolysis and condensation reactions (and the reverse reactions, esterification and alcoholic or hydrolytic depolymerisation). The major variables in this reaction sequence include the type of alkoxysilane and its functionality, the catalyst (OH^- or H^+) and its concentration (*i.e.* pH), the reaction temperature and finally, whether the system is open or closed to the atmosphere. These variables control the polymerisation growth and aggregation of the silica species throughout the transition from the sol to the gel state.

It is important to remember that the hydrolysis and condensation reactions occur at different rates but concurrently and so once hydrolysis has begun it is unlikely that the two reactions can be separated. However, in the following sections these two reactions are reviewed separately to allow for a more clear explanation.

1.2.2 Hydrolysis.

Hydrolysis occurs by the nucleophilic attack of the oxygen contained in water on the silicon atom [24]. Hydrolysis is most rapid and complete when catalysts are employed [25].

1.2.2.1 Mechanisms involved in hydrolysis.

Solution pH affects the sol-gel process by modifying the relative rates of the hydrolysis and condensation reactions. In effect, it controls the reaction mechanisms involved. Under acidic conditions, the reaction sequence for hydrolysis is as follows: the alkoxide is protonated by the acid, thus increasing the acidity of the group and allowing the central silicon atom to be attacked from the rear by a water molecule [24-26].

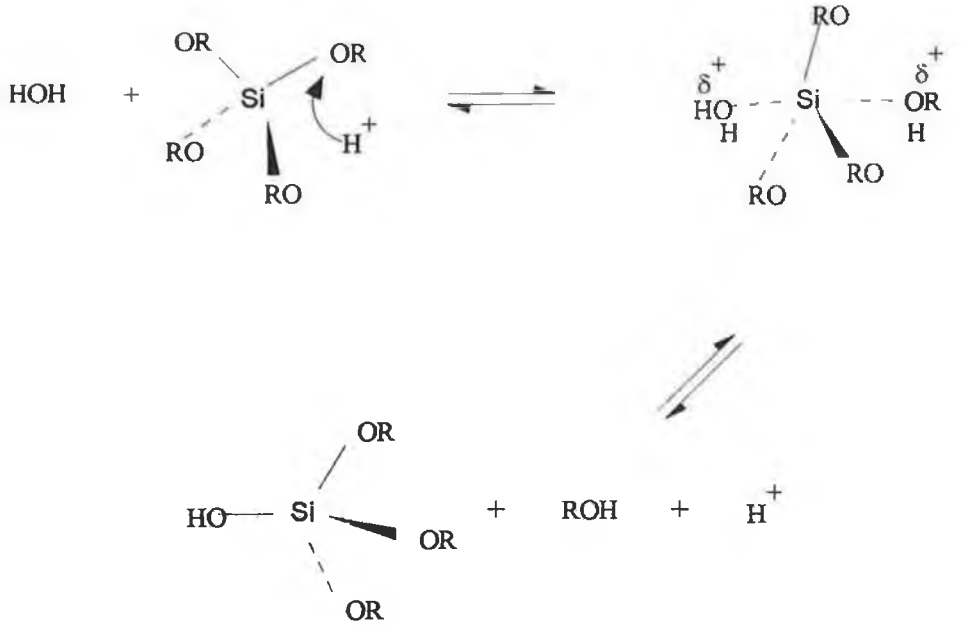

Figure 1.1 Reaction mechanism involved in the acid catalysed hydrolysis reaction of tetraalkoxysilanes.

The water acquires a partial positive charge and consequently partially reduces the charge on the alkoxide thus making it a better leaving group. Under acidic conditions, hydrolysis is rapid, producing a rapid increase of Si-OH containing monomers. These monomers are then slowly polymerised by a cluster-cluster growth mechanism into lightly branched polymers which entangle to form a cross-linked gel. This type of gel is usually referred to as a 'polymeric' gel [27].

The base catalysed reaction proceeds with a hydroxyl anion directly attacking the electropositive silicon, resulting in a partial negative charge developing on the silicon atom. Redistribution of charge occurs with the partial negative charge becoming accommodated by an alkoxy group. The alkoxy group is then able to leave the reactive intermediate, a proton being extracted from a readily available water molecule, with additional ions being generated in the process [28].

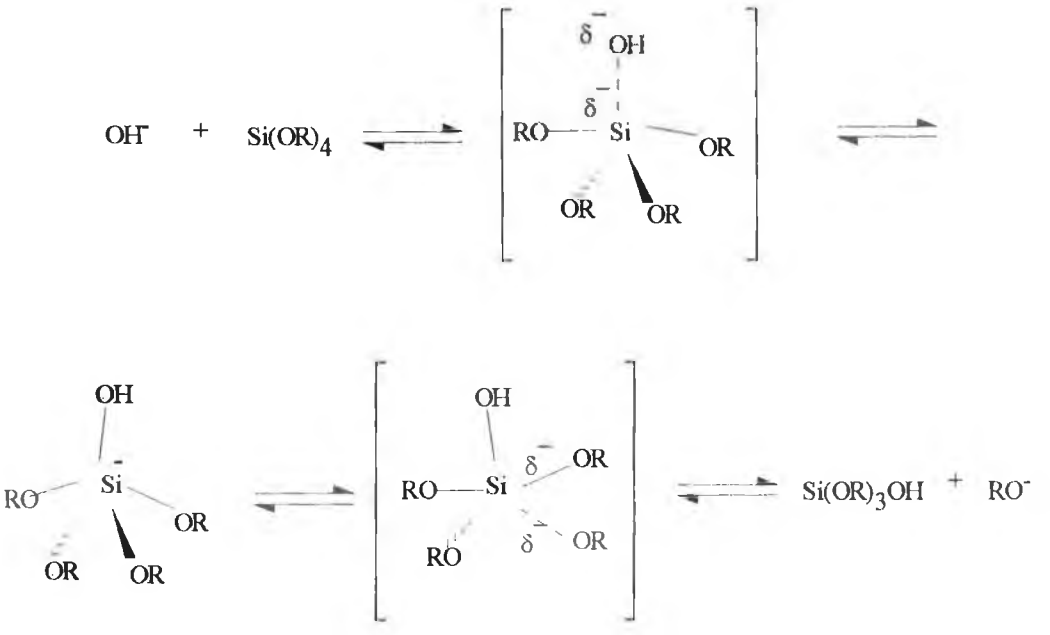

Figure 1.2 Reaction mechanism involved in the base catalysed hydrolysis reaction of tetraalkoxysilanes.

Under basic conditions, the condensation reaction is much faster than the hydrolysis reaction. The reactions proceed by quickly polymerising the newly generated

monomers by a monomer-cluster growth mechanism. Under such conditions, a highly branched structure is produced. Eventually, the clusters aggregate to become a network. This type of gel is termed 'colloidal' [27].

1.2.2.2 Steric and inductive effects in hydrolysis reactions.

The hydrolysis reaction is sensitive to both steric and inductive effects. As the alkyl substituent of the alkoxy group gets larger, the rate of the hydrolysis decreases. This is a result of steric effects. Under acidic conditions the hydrolysis rate increases with the degree of alkyl substitution (electron providing), whereas under basic conditions the reverse trend is evident [24].

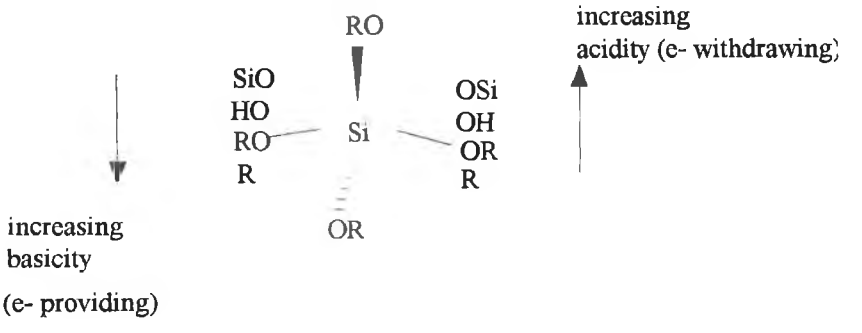

Figure 1.3 Inductive effects of substituents attached to silicon, R, OR, OH or OSi

Because increased stability of the transition state will increase the reaction rate, the inductive effects are evidence for positively and negatively charged transition states or intermediates under acidic and basic conditions, respectively. With this reasoning, under acidic conditions the hydrolysis rate decreases with each subsequent hydrolysis step, whereas under basic conditions the increased electron withdrawing capabilities of OH (and OSi) compared to OR may establish a condition in which each subsequent hydrolysis step occurs more quickly as hydrolysis and condensation proceed.

1.2.2.3 Effect of Water/Silane ratio (R) on hydrolysis.

Hydrolysis of the alkoxide precursors is achieved with R values varying from usually 1 to over 25 [27]. Figure 1.4 illustrates the effect of water concentration on the gel time [16]. The most obvious effect of increasing R, is the promotion of hydrolysis according to Equation 1.1. However, Le Chatelier's principal states that the reaction rate slows down after the water concentration exceeds the equilibrium value, since water is also the product of the condensation reaction. Thus, as the water concentration increases, the gelling time will at first decrease and then increase with a minimum at the equilibrium concentration.

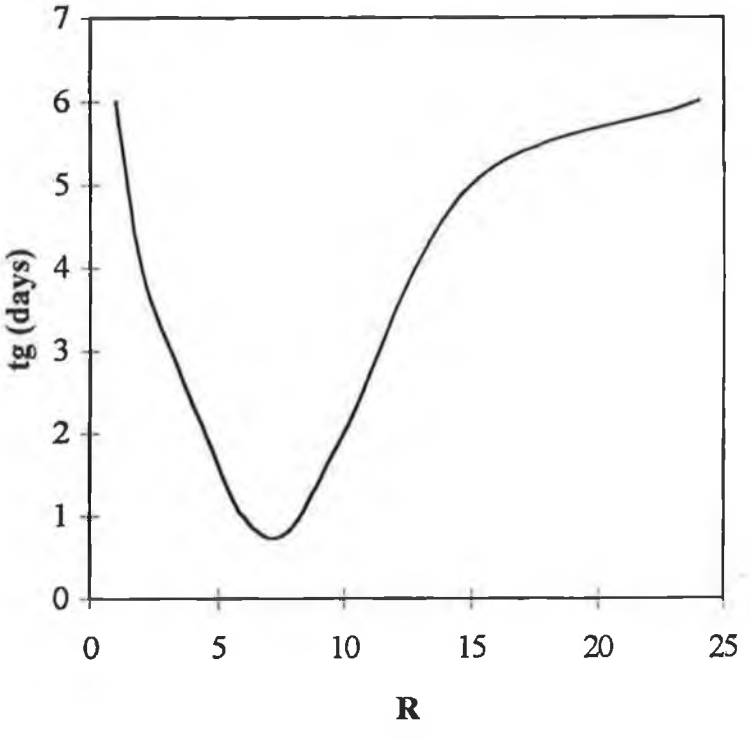

Figure 1.4 Effect of R (water/silane ratio) on the relative gel time (t_g) [16].

Equations 1.2 and 1.3 suggest two further effects of the water/silane ratio. With under-stoichiometric additions of water (R<<4), the alcohol producing condensation reaction is favoured, whereas the water producing reaction is favoured when R>>4. Excess water, however, is expected to promote depolymerisation according to the reverse of Equation 1.3, hydrolytic depolymerisation [24].

1.2.2.4 Solvent effects on hydrolysis.

The two most important characteristics of the solvent employed in the sol-gel process are firstly its polarity and secondly the availability of labile protons. The polarity of the solvent largely determines the solvating ability for the polar or nonpolar species. The second characteristic determines whether anions or cations are solvated more strongly and whether or not the solvent can participate in dissociative reactions, namely alcoholysis and hydrolytic depolymerisation *i.e.* the reverse of Equations 1.2 and 1.3 respectively. Because hydrolysis is both hydroxyl and hydronium ion catalysed, solvent molecules which hydrogen bond to hydroxyl ions or hydronium ions reduce catalytic activity under basic and acidic conditions respectively. Therefore, aprotic solvents, which do not hydrogen bond to hydroxyl ions, have the effect of making hydroxyl ions more nucleophilic, whereas protic solvents make hydronium ions more electrophilic [29].

1.2.2.5 Reverse reactions in hydrolysis.

The hydrolysis reaction may proceed in the reverse direction in which an alcohol (or protonated alcohol or alkoxide anion under acidic and basic conditions, respectively) displaces a hydroxyl group to produce a water molecule. This is known as reesterification. The extent of reesterification of polysiloxanes proceeds much further under acidic conditions than under basic conditions [24,28].

$$R'OH + Si(OR)_4 \rightleftharpoons Si(OR)_3OR' + ROH \qquad (1.4)$$

Transesterificaton occurs when an alcohol displaces an alkoxide to produce an alcohol molecule (Equation 1.4). This can be used as a method of producing various alkoxides.

1.2.3 Condensation.

Polymerisation to form siloxane bonds occurs by either an alcohol producing reaction as in Equation 1.2, or a water producing condensation reaction as in Equation 1.3.

1.2.3.1 Mechanisms involved in condensation.

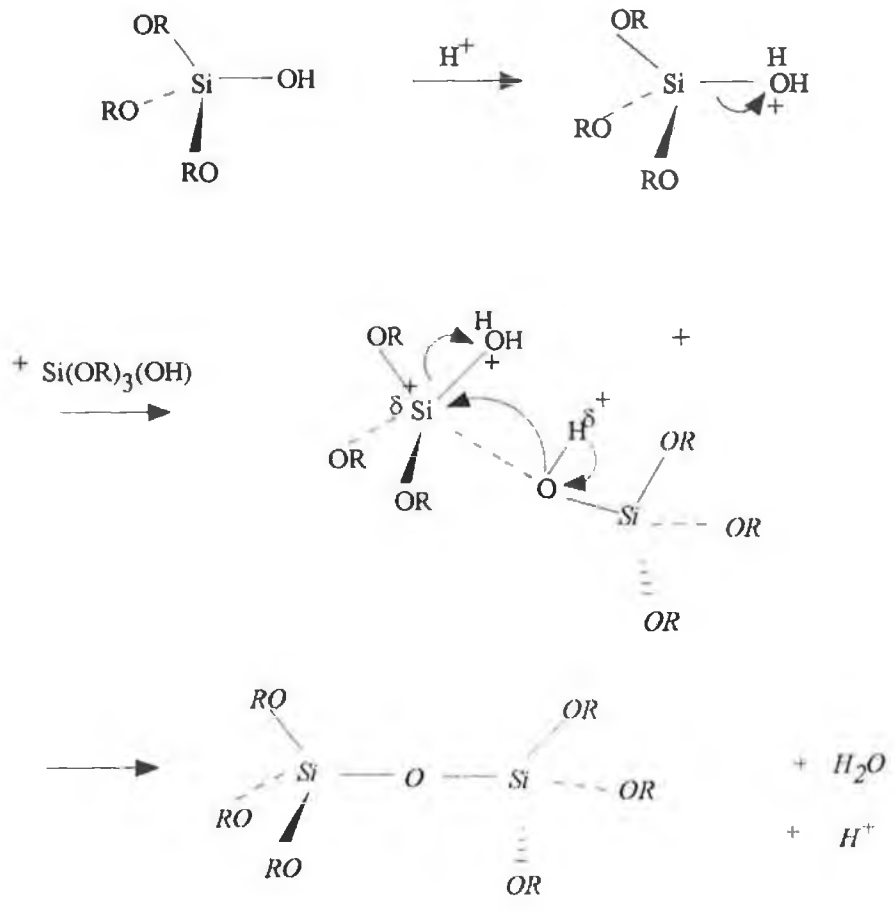

Figure 1.5 Reaction mechanism involved in acid catalysed condensation reactions.

At low pH, the most basic silanols are protonated first (monomeric singly hydrolysed species rather than oligomers). Protonation of the silanol increases the acidity of the group and renders the silicon atom more susceptible to attack by a nucleophile.

The base catalysed condensation reaction occurs via a nucleophilic reaction mechanism, and water or alcohol may be released. Water release is favoured unless water concentrations are very low ($R < 0.5$) when alcohol liberation becomes significant. The most widely accepted mechanism for the base catalysed condensation reaction involves the attack of a nucleophilic deprotonated silanol on a neutral silicate species [23-26]:

$$\equiv SiO^- + Si(OH)_4 \rightleftharpoons \equiv Si\text{-}O\text{-}Si\equiv + OH^- \qquad (1.5)$$

This reaction pertains above the isoelectric point of silica where surface silanols may be deprotonated depending on their acidity. The acidity of a silanol depends on the other substituents on the silicon atom. When basic OR and OH groups are replaced with OSi, the reduced electron density on the central silicon atom increases the acidity of the protons on the remaining silanols. This mechanism, proposed by Iler [24], favours reactions between larger, more highly branched species which contain acidic silanols, and smaller less branched species. It is generally believed that the base catalysed condensation mechanism involves penta- or hexa-coordinated silicon intermediates or transition states [24,26]. It is suggested that a silanol is deprotonated, the oxygen acquiring a formal negative charge and becoming the nucleophile for attack on another silicon centre. As the acidity of the groups attached to the silicon increases, the more stabilising effect on the expanded coordination transition states.

According to Figure 1.6 , the overall condensation rate is maximised at neutral pH and minimised at ~ pH 2.5 [24]. Under highly basic conditions, non-gelling systems are obtained. The minimum at pH 2.5 corresponds to the isoelectric point of silica. Surface silanol groups are protonated and deprotonated at lower and

higher pH, respectively. Silanols become more acidic with the extent of condensation of the siloxane network to which they are attached.

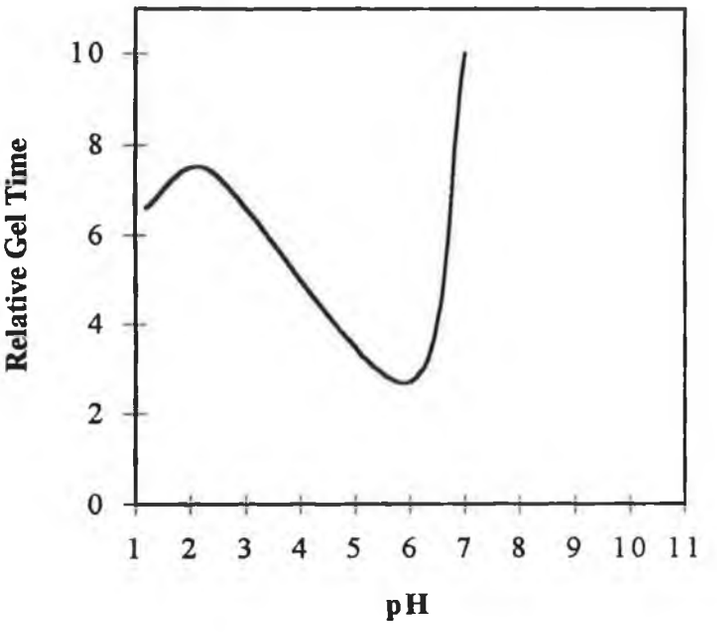

Figure 1.6 Effect of pH on the relative gel time (t_g) [16].

Regardless of the cause, the pH dependence suggests that protonated and deprotonated silanols are involved in the acid and base catalysed mechanisms. At elevated pH where the gel times are observed to increase, condensation reactions proceed but gelation does not occur. In this pH regime, particles are formed which after reaching a critical size become stable due to mutual repulsion effects [24].

1.2.3.2 Steric and inductive effects in condensation reactions.

During the sol-gel process, condensation can proceed by two different reactions which can occur between substantially different solution species (monomers, oligomers etc.) which have undergone different extents of hydrolysis, therefore steric

and inductive effects are complicated and are not well documented for tetraalkoxides. It is accepted that in tetra-functional alkoxides normally employed in sol-gel processing, substituents which increase steric crowding in the transition state will retard condensation. Voronkov and co-workers also state that the condensation rate increases with an increase in the number of silanols on the silicon atom [30].

1.2.3.3 Solvent effects on condensation.

As mentioned in section 1.2.2.4, solvents may be either protic or aprotic and may vary in their polarity. Depending on the pH, either protonated or deprotonated silanols are involved in the condensation mechanism. Because protic solvents hydrogen bond to nucleophilic deprotonated silanols and aprotic solvents hydrogen bond to electrophilic protonated silanols, protic solvents are expected to retard base-catalysed condensation and promote acid-catalysed condensation. Aprotic solvents have the reverse effect.

In addition, the mechanism of particle aggregation as well as the extent of condensation of the polymeric network have been shown to be dramatically affected by the presence of organic additives [31]. These observations can be explained in terms of hydrogen bonding and electrostatic interactions which modulate the nucleophilic substitution mechanism associated with the sol-gel condensation process.

1.2.3.4 Reverse reactions in condensation.

Alcoholysis and hydrolysis of siloxane bonds (the reverse of Equations 1.2 and 1.3, respectively) provide a method for bond breakage and reformation, allowing continual restructuring of the growing polymers. The hydrolysis reaction (dissolution of silica) exhibits a strong pH dependence [24]. It has been shown that alcoholysis occurs under basic conditions, which leads to a redistribution of siloxane bonds:

$$ROH + (RO)_3Si\text{-}O\text{-}Si(OR)_3 \rightleftharpoons Si(OR)_4 + Si(OR)_3OH \qquad (1.6)$$

It has been proposed that this reaction accounts for the common observation that under base catalysed conditions, unhydrolysed monomers persist past the gel point, even with over-stoichiometric amounts of water.

1.2.4 Gelation.

In the sol-gel process, the condensed silica species in time link together to become a three dimensional network. The physical characteristics of the gel depend greatly upon the size of the particles and the extent of crosslinking prior to gelation. Acid catalysis leads to a more polymeric form of gel with linear chains as intermediates. Base catalysis yields colloidal gels where gelation occurs by crosslinking of the colloidal particles [27]. At gelation, the viscosity increases sharply, and a solid object results, taking the shape of the mould.

The gel point of any system, including sol-gel silica, is easy to observe qualitatively and easy to define in abstract terms but extremely difficult to measure analytically. A gelling solution represents a unique state of matter because it is neither a liquid nor solid, but is in between these two states. The gelation process can be viewed as the growth process of randomly multiconnected polymer clusters starting from multifunctional monomer units, which can link together by chemical reaction. At the gel point a giant cluster appears, having a macroscopic size. The sol becomes a gel when it can support a stress elastically. It is extremely difficult to define the point at which a distinct transition from sol to gel occurs. There is not an activation energy that can be measured, nor can one precisely define the point where the sol changes from a viscous fluid to an elastic gel. The change is gradual as more and more particles become interconnected. However, the sharp increase in viscosity that accompanies gelation essentially freezes in a particular polymer structure at the gel

point. At this point gelation may be considered a rapid solidification process. This 'frozen-in' structure may change appreciably with time, depending on the temperature, solvent and pH conditions or upon the removal of solvent molecules. However, the gelation time (t_g) is also known to be influenced by the size of the container, indicating that t_g is not solely an intrinsic property of the sol.

The amount of water for hydrolysis has a dramatic influence on the gelation time. For low water content, generally an increase of the amount of hydrolysis water (*i.e.* R) decreases the gelation time, although there is a dilution effect. The location of the minimum in the curve t_g versus R, depends on the experimental conditions, such as the nature the chemicals, catalyst and temperature.

In conclusion, the extent to which the overall reactions proceed depend on the detailed conditions used. The fact that gelation has occurred does not indicate that these hydrolysis/condensation reactions have ceased [32], but merely that sufficient network has been formed to hinder motion. Under basic conditions gelation occurs rapidly but the majority of the precursors are at that point still unreacted. Under acidic conditions most of the precursors have been partially hydrolysed and have taken part in condensation, but they may still have M-OR bonds.

1.2.5 Ageing.

This process occurs when a gel is left in its mother liquid after gelation and reactions continue such that the structure and properties of the material change significantly [16]. During this time, polycondensation continues along with localised solution and reprecipitation of the gel network which increases the thickness of interparticle necks and decreases the porosity. The strength of the gel thereby increases with ageing. The reason for allowing a gel to age adequately, is to produce a gel of sufficient strength to withstand the stresses encountered during drying. Gels shrink on drying to give small pore volume and diameter. If they are wet aged they increase in coalescence and

shrink little on drying and yield materials with larger pore sizes than materials that have not been wet aged.

During ageing, three separate processes can occur, often simultaneously. These include: polycondensation, syneresis and coarsening, and are dealt with separately in the following sections.

1.2.5.1 Polycondensation.

Provided that silanol groups are close enough to react they will condense to increase the connectivity of the network. The condensation reactions continues to occur because of the large concentration of unreacted silanol groups present in a newly formed gel. This process can be accelerated by hydrothermal treatment which in effect increases the rate of the reactions [33].

1.2.5.2 Syneresis.

The shrinking of the gel and the resulting expulsion of liquid (water or alcohol) from the pores is called syneresis. Syneresis in alcoholic gel systems is generally attributed to formation of new bonds through condensation reactions, which increases the bridging bonds and causes contraction of the gel network. In aqueous gel systems, or colloidal gels, the structure is controlled by the balance between electrostatic repulsion and attractive van der Waals forces. Therefore, the extent of shrinkage is controlled by additions of electrolyte [24]. The presence of organic solvents which form hydrogen bonds with silanol groups inhibits condensation and as a result slows the rate of syneresis.

1.2.5.3 Coarsening.

This is the irreversible decrease in surface area due to dissolution and reprecipitation events. Because small particles are more soluble than larger ones, and since not all the small three-dimensional particles are the same size, the particles grow in average size and diminish in numbers as the smaller ones are deposited upon the larger ones [24]. The result of dissolution/reprecipitation is to reduce the net curvature of the solid phase: small particles disappear and small pores are filled in, so the interfacial area decreases and the average pore size increases.

In summary, there are changes in most physical properties of the gel during ageing. As well as changes to the surface area and porosity, the mechanical properties of the gel are modified. Due to the increase in bridging bonds, the stiffness of the gel network increases, as does the elastic modulus, the viscosity and the modulus of rupture [24].

1.2.6 Drying.

During drying the excess liquid is removed from the interconnected pore network. If the pores are small (< 20 nm) large capillary stresses develop during drying. These stresses cause the gels to crack catastrophically unless the drying process is controlled by decreasing the liquid surface chemistry by the addition of surfactants [34], or the elimination of very small pores by hypercritical evaporation, which avoids solid-liquid interface and hence side-steps capillary stresses. The drying process can be divided into a number of stages. During the first stage, the decrease in volume of the gel is equal to the volume of the liquid lost by evaporation and the rate of loss of solvent from the material is constant. The next stage of drying begins when the strength of the network has increased, due to the greater packing density of the solid phase, sufficient to resist further shrinkage. At this stage liquid is driven to the surface by gradients in capillary pressure, where it evaporates due to the

ambient vapour pressure being lower than inside the pores. The final stage of drying occurs when the remaining liquid evaporates within the pores and is removed by diffusion of its vapours to the surface. Cracking during the first stage of drying is rare unless the gel has not been sufficiently aged and therefore does not possess the dimensional stability to withstand the increasing compressive stress. Most failure occurs during the early part of the second stage, the point at which the gel stops shrinkage. The possibility of cracking at this stage is high due to the high stresses and low strain tolerance of the material.

1.2.7 Dehydration and Chemical Stabilisation of Gels.

For a sol-gel material to be used in ambient environment, both thermal and chemical stabilisation are often required. Chemical stabilisation involves removing the concentration of surface silanols below a critical level so that the surface does not rehydroxylate during use. Thermal stabilisation involves reducing the surface area sufficiently to enable the material to be used at a given temperature without reversible structural changes [16].

A major problem in producing silica gels suitable for optics is the removal of surface hydroxyl groups and hydrogen bonded water. These entities give rise to atomic vibrational energy absorption in almost the entire range of ultra-violet to infra-red wavelengths (160-4500 nm) and as a result decreases the optical applications of silica gel monoliths. Consequently, to accomplish the optimum optical performance of silica, complete dehydration is imperative.

To achieve dehydration it is necessary to recognise that 'water' is present in two forms. Firstly, free water within the ultraporous gel structure (*i.e.* physisorbed water) and secondly, hydroxy groups associated with the gel surface (*i.e.* chemisorbed water). The physisorbed water can be eliminated and surface silanol (Si-OH) groups condensed starting at about 170^0C. The dehydration is completely reversible, up to about 400^0C. Above 400^0C, the dehydration process is irreversible

as a result of shrinkage and sintering across the pores. Thus, the amount of existing hydroxyl groups on the gel surface is an inverse function of the temperature of densification. UV-VIS-NIR absorption data also show that the reduction of surface hydroxyl groups occurs above 400^0C. Above 800^0C only isolated silanol groups exist and these can also be removed by extended thermal treatment [16]. Heating the porous gel at high temperature causes densification to occur. The pores are eliminated and the density ultimately becomes equivalent to fused quartz or fused silica.

Dehydration can also be achieved using a variety of chlorinated compounds. Compounds such as chloroform can completely react with surface hydroxyl groups to form hydrochloric acid. This can then be desorbed from the gel at a temperature range 400-800^0C where the pores are still interconnected.

1.2.8 Densification.

Densification is the final treatment process of gels and occurs in the temperature region of 1000-1700^0C depending on the radii of the pores and their surface area [24]. Controlling the gel-glass transition is a difficult problem if one wants to retain the initial shape of the starting material. It is essential to remove volatile species from the pores prior to their closure. With successful stabilisation treatments however, it is possible to manufacture monolithic dense gel-derived glasses by using furnaces. In effect, densification is the increase in bulk density that occurs in a material as a result of the decrease in volume fraction of the pores. It is widely accepted that despite the complex manner in which the gel evolves towards a glass, once the gel has been densified and heated above the glass transition temperature, its final structure and properties become indistinguishable from those of a melt-derived glass.

1.2.9 Luminescent species in sol-gel glasses.

The sol-gel technique offers a low temperature method for synthesising amorphous materials which are either totally inorganic in nature or composed of inorganics and organics [1]. This process, as described in the previous sections, is based on the hydrolysis and condensation reactions of alkoxysilanes in alcoholic solutions. The ability to synthesise inorganic polymers using sol-gel processing with little or no heating makes it possible to dope these gels with a variety of organic, organometallic and indeed inorganic compounds, especially dyes having desired luminescent properties [6-9,15]. Prior to the employment of the sol-gel technique, the incorporation of these compounds into solids was restricted to the use of frozen solvents or organic polymer matrices. The present approach represents a totally new type of composite material because the oxide matrix not only offers a significantly more ionic environment but also it is thermally, chemically and dimensionally more stable [2]. Thus, studies of inorganic-, and indeed organic-doped sol-gels have begun to develop substantial breadth; from investigation of doped sol-gels for spectroscopic and matrix-isolation photochemistry, to the effect of solvent chemistry on luminescence properties, to the development of laser and non-linear optical materials [15].

Organometallic dyes, like transition metal complexes, can be used as photosensitisers in the photochemical conversion of solar energy, and their incorporation into solid matrices may be advantageous. In particular, the photophysical behaviour of the ruthenium tris (2,2'-bipyridyl) cation, $[Ru(bpy)_3]^{2+}$, at low temperatures in solids and in solutions at room temperature has been the subject of extensive research [35-38]. This thesis involves the photophysical behaviour of ruthenium polypyridyl complexes in sol-gel matrices. We are primarily concerned with two aspects of these doped gels. The first aspect concerns the information which the Ru(II) polypyridyl complexes relay about the sol-gel process while the second involves the effect of the rigid matrix on the photophysical properties of the immobilised complexes. Therefore it is subsequently necessary to give a review of

Ru(II) polypyridyl complexes. In the next section, detailed information concerning the properties of $[Ru(bpy)_3]^{2+}$, the archetype of such complexes, in solution, will be given.

1.3 The Photophysical properties of $[Ru(bpy)_3]^{2+}$ in solution.

The photophysical and photochemical properties of ruthenium (II) polypyridyl complexes have been studied extensively in the past fifteen years. They have attracted the attention of several research groups because of a unique combination of ground- and excited-state properties [35-37]. The prototype of these complexes is $[Ru(bpy)_3]^{2+}$ (bpy = 2,2' bipyridine) which has been used as a photoluminescent compound, an excited-state reactant in energy and electron-transfer processes, an excited-state product in chemiluminescent and electrochemiluminescent reactions, and also a mediator in the conversion of light and chemical reactions [37-38].

1.3.1. Absorption and emission properties.

Ru(II) compounds are stable low-spin d^6 species, which can be oxidised (removal of a metal-localised electron), or reduced (addition of an electron into a ligand π^* orbital) [37]. The most important photophysical properties of $[Ru(bpy)_3]^{2+}$ are depicted in Figure 1.7. The absorption spectrum of $[Ru(bpy)_3]^{2+}$ as seen in Figure 1.8, exhibits a number of distinguishing features. Transitions within the ligand π-bonding orbital to the π^*-antibonding orbital, labelled π-π^* or ligand centred transitions occur at high energies (185 and 285 nm) and have high extinction coefficients. In addition, transitions such as promotion of an electron from the metal t_{2g} orbital to an e_g orbital are possible, and give rise to weak absorption bands (322

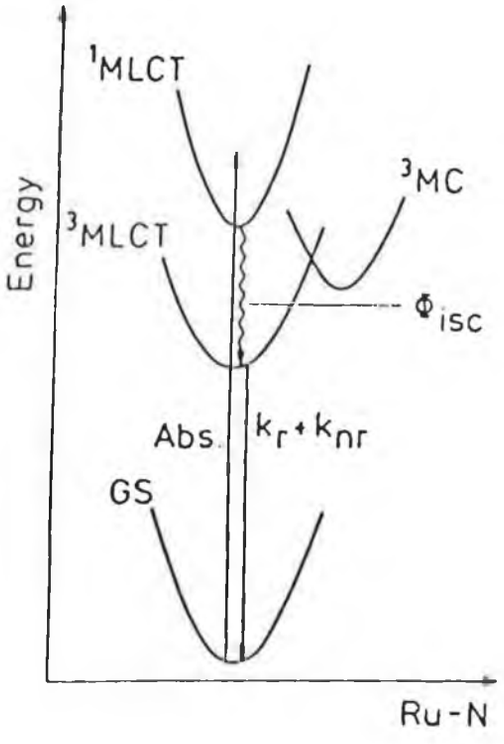

Figure 1.7 Schematic representation of the photophysical pathways of $[Ru(bpy)_3]^{2+}$.

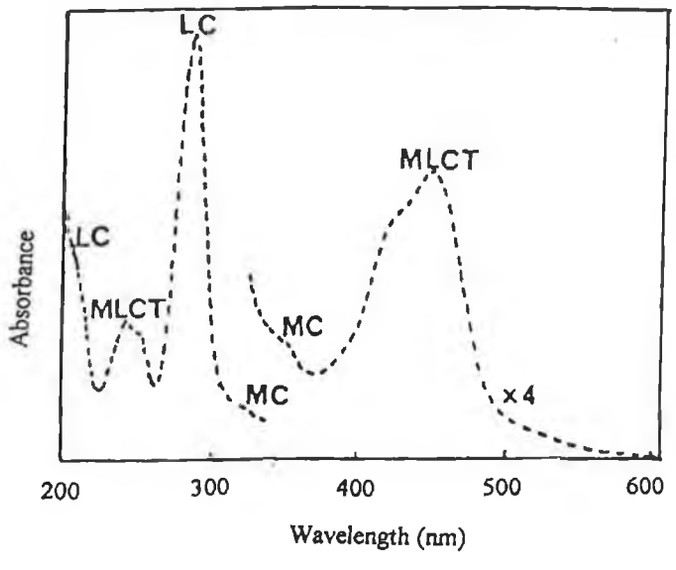

Figure 1.8 Absorption spectrum of $[Ru(bpy)_3]^{2+}$ in aqueous solution, with the assignments for the various bands.

and 344 nm) [37-38]. However, the most significant feature of this spectrum is the intense absorption band exhibited at 452 nm, which has a molar extinction coefficient (ε) of 14600 $M^{-1}cm^{-1}$. This band has been assigned to a metal-to-ligand charge-transfer transition (MLCT) [37-38]. Fast intersystem crossing (ISC), estimated to occur with a rate of 5×10^{-10} s^{-1} [40], occurs from the singlet to the triplet MLCT state with an efficiency of unity [41-42]. The large spin-orbital coupling present in this complex makes this spin-forbidden transition possible [43]. Emission from the triplet state to the ground state (k^r) or radiationless deactivation to the ground state (k^{nr}) can take place [37]. It is widely accepted that the emitting state of $[Ru(bpy)_3]^{2+}$ consists of three closely spaced ^{3}MLCT levels, each with a different triplet character and lifetime [39,44]. The fast radiationless decay of the ^{3}MLCT excited state to the ground state results in a relatively short excited-state lifetime and a small luminescence efficiency. Another deactivating pathway is the population of the metal centred (^{3}MC) excited state [45-47]. This state is strongly distorted with respect to the ground state nuclear geometry, and upon population, reduces the emission quantum yield by causing rapid radiationless decay, or more destructively, cleavage of a Ru-N bond, leading to photosubstitution [46,48-49].

1.3.2 Lifetime of the emitting state.

The large energy-gap between the lowest excited states and the ground state of $[Ru(bpy)_3]^{2+}$ allows radiative processes (emission) to compete with non-radiative ones (quenching). Consequently, luminescent decay is a competitive process whereby the quantum yield of emission is a measure of the fraction of excited states which undergo radiative decay, and may be expressed as follows:

$$\Phi_r = k^r / k^r + k^{nr} \qquad (1.7)$$

where k^r represents the radiative decay rate, k^{nr} the non-radiative decay rate of this luminescent set of states, and Φ_r the quantum yield of emission [50]. The lifetime of many polypyridyl complexes of Ru(II) in fluid solution is highly temperature dependent and the lifetime can be expressed as the sum of a temperature independent and several temperature dependent terms:

$$1/\tau = k_0 + \sum_i k_i^{nr}(T) \qquad (1.8)$$

where $k_0 = k^r + k_0^{nr}$ (the sum of the temperature independent radiative and non-radiative decays) and $\sum_i k_i^{nr}(T)$ are the temperature dependent rate constants.

The temperature-dependent terms can be associated, in a schematic way, either to:

(a) an activated surface crossing to another excited state, described by the Arrhenius equation:

$$k_i^{nr} = A_i \exp(-\Delta E_i/RT) \qquad (1.9)$$

where, A_i is the frequency factor and ΔE_i is the activation energy for surface crossing between states respectively or

(b) to the coming into play of vibrational modes that can favour the radiationless decay that are prevented at low temperature because of the frozen molecular environment. This second type of thermally activated process can be dealt with by the following equation

$$k_i^{nr} = B_i / \{1 + \exp[C_i(1/T - 1/T_{Bi})]\} \qquad (1.10)$$

which describes the stepwise behaviour centred at a certain temperature T_{Bi}. In this equation C_i is a temperature related to the smoothness of the step and B_i is the value

attained by k_i at $T >> T_{Bi}$. This equation is particularly useful for describing the behaviour of a system in the glass-fluid transition region of a solvent matrix. The $\ln(1/\tau)$ vs. $1/T$ plots can usually be fitted by using Equation 1.8, with an appropriate number of terms given by Equations 1.9 and 1.10.

The radiative rate constant can be obtained by measuring the luminescence quantum yield and lifetime at room temperature:

$$k^r = \Phi_{em} / \tau \qquad (1.11)$$

The radiative rate constant is obtained at room temperature, because it is generally accepted that k^r is temperature independent above 77 K. The temperature-independent non-radiative rate constant can be obtained from the lifetime at low temperature:

$$k_0^{nr} = 1/\tau_{77K} - k^r \qquad (1.12)$$

At 77 K, no extra deactivating processes are present (like population of the ^{3}MC state) and the value of k_0^{nr} is only governed by radiationless deactivation of the ^{3}MLCT states.

At temperatures below 77 K, the temperature dependence of excited-state lifetimes for $[Ru(bpy)_3]^{2+}$ reveals that the luminescence of this complex originates from three close lying ^{3}MLCT states whose populations are in thermal equilibrium [51-54]. A plot of $\ln(1/\tau)$ Vs $1000/T$ for $[Ru(bpy)_3]^{2+}$ shows strong temperature dependent behaviour particularly above 250 K, with luminescence lifetime decreasing with increasing temperature [45]. This has been assigned to the activated surface crossing between ^{3}MLCT and ^{3}MC states. It is generally agreed that the ligand photosubstitution reaction proceeds *via* this thermally-activated radiationless transition from this luminescent ^{3}MLCT level to a distorted ^{3}MC level, with subsequent competition between radiationless decay to the ground state and cleavage of a Ru-N bond with formation of an intermediate containing a

monodentate bipyridyl ligand [46-47]. Such an intermediate can undergo either loss of the ligand or chelate ring closure with reformation of $[Ru(bpy)_3]^{2+}$.

However, experimental evidence shows that the combination of a series of three low-lying MLCT states and a thermally activated MLCT→d-d transition is not adequate to account for the temperature dependencies of all cases. For example, more complex temperature dependent behaviour becomes evident at the glass-to-fluid transition [55]. In addition, there is direct spectroscopic and kinetic evidence for the presence of an additional MLCT state for $[Ru(bpy)_3]^{2+}$ in the solid state [44]. The presence of this fourth ^{3}MLCT state will be discussed in more detail in following chapters.

1.3.3 Chemistry and quenching reactions of the $[Ru(bpy)_3]^{2+}$ excited state.

The first step in any photochemical and photophysical process is the absorption of a photon by the molecule. The molecule is thereby promoted to an excited state. The resultant excited state molecule is a high energy unstable species which must undergo some type of deactivation process as shown in Figure 1.9.

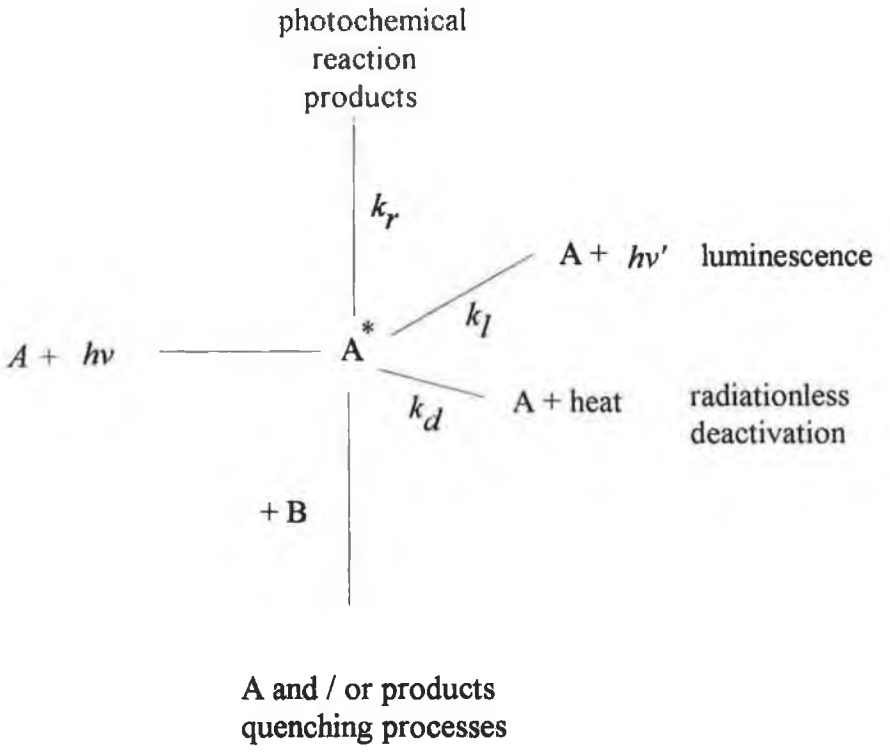

Figure 1.9 Schematic representation of excited state deactivation processes.

Deactivation may occur via:

(a) disappearance of the original molecule through photochemical reaction,
(b) emission of light (luminescence),
(c) radiationless decay (degradation of the excess energy into heat), and
(d) interaction of the excited state molecule with another species present [37].

Processes which involve radiationless deactivation, quenching or photochemical reactions are in direct competition with the luminescent decay of the excited state. In view of the relatively long-lived excited state of $^{*}[Ru(bpy)_3]^{2+}$, the complex may

partake in a range of bimolecular energy transfer processes. It is a versatile species often acting as an energy donor, electron donor or an electron acceptor.

$$^{*}[Ru(bpy)_3]^{2+} + Q \xrightarrow{k_{q(ox)}} [Ru(bpy)_3]^{3+} + Q^{-} \qquad (1.13)$$

$$^{*}[Ru(bpy)_3]^{2+} + Q \xrightarrow{k_{q(red)}} [Ru(bpy)_3]^{1+} + Q^{+} \qquad (1.14)$$

$$^{*}[Ru(bpy)_3]^{2+} + Q \xrightarrow{k_{q(E)}} [Ru(bpy)_3]^{2+} + Q^{*} \qquad (1.15)$$

where (1.13) represents oxidative quenching, (1.14) reductive quenching and (1.15) energy transfer [35,37,50]. The first two processes outlined above, involve electron transfer from/to the excited state molecule and simultaneous oxidation or reduction of another species in the proximity. The third process is a physical process where through contact, the excited state molecule transfers its energy to another molecule.

Establishment of the actual quenching mechanism is by no means trivial. The ability to undergo energy transfer is related to the zero-zero spectroscopic energy E^{0-0} of the donor-acceptor pair (spectral overlap) and that of electron transfer to their respective redox potentials. The kinetic factors are associated with the activation energy needed to reorganise the inner and outer shells before electron transfer can occur [35].

The assignment of quenching processes to 'energy transfer' requires either direct observation of the acceptor phosphorescence or at least photoreactions arising from the excitation into the acceptor-excited sites. Bimolecular quenching of the excited state of $[Ru(bpy)_3]^{2+}$ has been extensively studied employing metal ions such as Eu^{3+} and Cr^{2+} [56], amines [57], quinones [58], and particularly paraquats such as methylviologen [59].

A useful parameter in considering an excited state is its mean lifetime given by;

$$1/\tau = k_{obs} \quad (1.16)$$

where τ represents the lifetime and k_{obs} the decay rate constant. This is the average lifetime for an excited state, decaying through all possible decay mechanisms, each with its own decay constant so that;

$$1/\tau = k^r + k^{nr} + k^q[Q] \quad (1.17)$$

where k^r represents the emission rate constant, k^{nr} the internal non-radiative constant and k^q the bimolecular quenching rate constant with [Q] the concentration of quencher Q.

The Stern-Volmer equation is derived from this;

$$1/\tau = 1/\tau_0 + k^q[Q] \quad (1.18)$$

where τ and τ_0 represent the observed lifetimes in the presence and absence of the quencher respectively. This equation describes the effect of a quencher on the lifetime in solution [60]. The slope of the Stern-Volmer plot of $1/\tau$ Vs. [Q] yields the value of k^q.

Compounds which contain unpaired electrons may act as efficient quenching agents. Perhaps the most eminent of these agents is molecular oxygen which is well recognised as a paramagnetic species. It is particularly effective in removing the energy from triplet state molecules and consequently poses as an obstacle when considering phosphorescence and also relatively long-lived fluorescent species. Molecular oxygen is one of the few species which effectively quenches $^*[Ru(bpy)_3]^{2+}$ with a k^q of approximately 3.3×10^9 $M^{-1}s^{-1}$. Singlet oxygen formation by energy transfer and electron transfer mechanisms have been proposed. The lifetime of $^*[Ru(bpy)_3]^{2+}$ is reduced by about a third in aerated aqueous solutions. Bubbling with nitrogen or argon reduces oxygen quenching to less than 1% [49].

1.3.4 Fine tuning of the excited state.

Comparison with the requirements needed for photosensitisers and luminophores [61], show that the main limitation of $[Ru(bpy)_3]^{2+}$ lies in the existence of low-lying d-d states causing depletion of the relatively long-lived ^{3}MLCT states and also providing a pathway for photodecompostition. Because population of the d-d state is thermally activated, there is an appreciable increase in the deactivation rate as the temperature is raised. Thus, $[Ru(bpy)_3]^{2+}$ shows a large decrease in lifetime above room temperature, which limits its use at higher temperatures. In addition, the narrow absorption band at 452 nm limits its potential use as a catalyst for solar energy conversion, as only a small part of the solar energy spectrum can be utilised. Typically, complications arising from d-d states can be avoided by changing to analogous complexes of Os(II). Since $10Dq$ is approximately 30% greater for Os, the d-d states are no longer thermally accessible at or below room temperature. However, ruthenium(II) polypyridyl complexes are a preferred source of photosensitisers for a number of reasons. Firstly, for equivalent cases where excited-state energies are the same, Ru(II) ^{3}MLCT states are longer lived, by a factor of approximately three, when compared to their Os(II) counterparts [62]. Secondly, there exists a broad background synthetic chemistry for Ru(II), and the preparative conditions involved are less demanding [63]. Finally, the background synthetic chemistry to ligand-bridged dimers and oligomers is known, and the potential clearly exists for designing complex systems where the Ru-bpy chromophore is attached to catalytic sites [64].

Evidently, the understanding and the ability to control the factors which are involved in the determination of the relative positioning of the d-d state and the ^{3}MLCT states is extremely important. The spectroscopic properties of Ru(II) complexes are governed by the σ-donor and π-acceptor properties of the ligands which surround the ruthenium centre [65]. Therefore, by changing the ligand systems around this centre it is possible to alter the ground state and excited state properties of these metallic complexes. For a series of $[Ru^{II}(bpy)_2(L)]^{n+}$ complexes, variations in

L can significantly affect the relative position of the d-d state. Through careful selection of L, it is possible to increase the energy gap between the ^{3}MLCT and the ^{3}MC states, thereby preventing population of the deactivating state [65]. Control of the luminescence properties of complexes hinges on the control of the relative state energies and the nature of the lowest excited-state [66].

When a class *a* type ligand (where L is a weaker σ-donor but a better π-acceptor than bipyridine) is introduced, this ligand may participate directly in the excited state reactions. Such ligands alter the excited state properties by decreasing the t_{2g}-^{3}MLCT energy gap, since the π^* lowest unoccupied molecular orbital (LUMO) will reside on this ligand. The objective of using these ligands, is to isolate the ^{3}MC state from the ^{3}MLCT state. However, the weak σ-donor properties of class *a* ligands result in a reduced ligand field splitting (*i.e.* $10Dq$ will be reduced compared with $[Ru(bpy)_3]^{2+}$) and after excitation of the complex the ^{3}MC state may still be populated.

Alternatively, if a class *b* ligand is introduced, (where L is a stronger σ-donor and a weaker π-acceptor than bipyridine), then this ligand will act as a spectator ligand and will not become directly involved in the emission processes. Because of their strong σ-donating ability, this class of ligands possess π^* levels of much higher energy than bpy. As a result, in mixed chelate complexes containing both bpy and class *b* ligands, the excited state is always bpy based. This class of ligands donate much electron density into the metal d orbitals thereby increasing $10Dq$. Unfortunately, the t_{2g} level is destabilised and this may lead to a reduction in the ^{3}MC-^{3}MLCT energy gap.

The effects of the introduction of different ligand types into ruthenium polypyridyl complexes can be clearly observed in their electronic spectra. Specific examples of class *a* ligands include 2,2'-bipyrazine (bpz) [67], 2-2'-bipyrimidine (bpm) [68] and 2,2'-biquinoline (biq) [65]. The structure of these ligands, and the other ligands cited in this theses are displayed in Figure 1.10. The most attractive

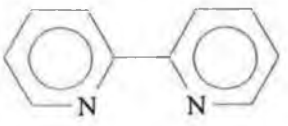

2-2'-bipyridine (bpy)

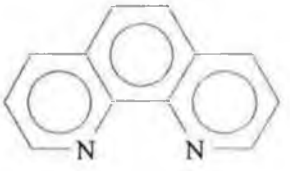

1,10'-phenanthroline (phen)

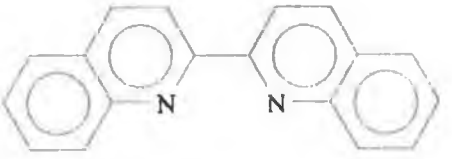

2,2'-biquinoline (biq)

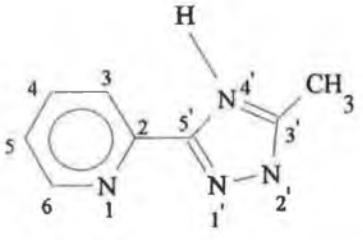

3-methyl-5-(pyridyn-2-yl)-1,2,4-triazole (H3Mptr)

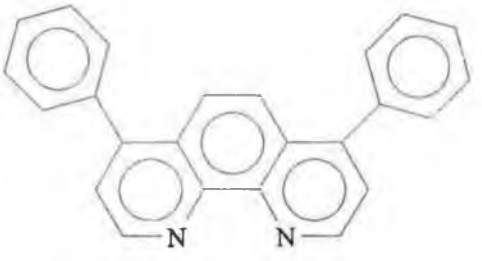

4,7-diphenyl-1,10-phenanthroline (dpp)

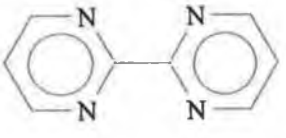

2,2'-bipyrimidine (bpm)

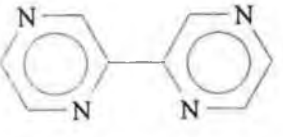

2,2'-bipyrazine (bpz)

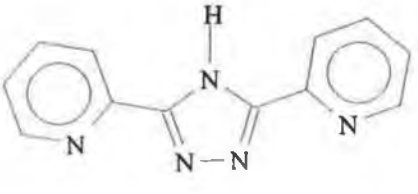

3,5-bis(pyridyn-2-yl)-1,2,4-triazole (bpt)

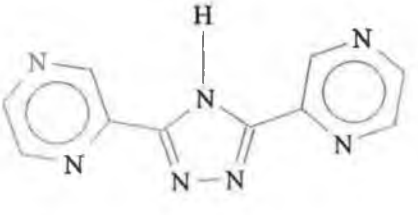

3,5-bis(pyrazin-2-yl)1,2,4-triazole (bpzt)

Figure 1.10 Ligands cited in text.

feature of complexes formed by replacing one bipyridine ligand of $[Ru(bpy)_3]^{2+}$ with a strong π-acceptor lies in the red-shifted absorption and emission energies, thus making the absorption range more accessible to the solar spectrum. However, as mentioned previously, the smaller σ-donation of these ligands, and also there propensity for accepting π-backbonding from the dπ orbitals, results in a smaller $10Dq$ thus making ^{3}MC thermally accessible at ambient temperatures and the emission yield is diminished [65]. There have, however, been some examples of stable complexes containing class *a* ligands. In some cases, a large ^{3}MC-^{3}MLCT energy gap is maintained when the effect of decreasing $10Dq$ is mitigated by the effect of very low energy ligand π^* levels [65].

Recently, there has been an increased interest in systems containing at least one class *b* ligand. Such ligands include pyrazoles [69] and also triazoles [70]. Because of their strong σ-donating ability of this class of ligand compared with bipyridine, their π^* levels are much higher in energy, and as a result, in mixed chelate complexes containing both bpy and class *b* ligands, the emission is always bpy based. The measure of σ and π donating abilities of these ligands may be modified by introduction of substituents onto the ligand [70]. In particular, the triazoles have been an important contribution to the class *b* type ligands. These complexes show interesting properties as a result of the electronic properties of the triazole ring [70]. The availability of different coordination sites on the triazole leads to variations of the magnitude of the σ-donation felt by the metal. Another important feature of the triazole ring is that it can be deprotonated, leading to an extensive ground-state and excited-state acid-base chemistry.

1.3.5 Dinuclear complexes.

Dinuclear transition metal complexes have received considerable attention in recent years [72]. Ruthenium(II) and osmium(II) dimeric complexes are of interest because,

if certain lifetime constraints are satisfied, they could in principle act as a two-electron transfer reagent when excited by two photons. A very important feature of these species, is that in a mixed-valence species containing M(II) and M(III), electron hopping from the M(II) centre to the M(III) centre can take place. Light-induced electron hopping may be detected in the near-infrared absorption spectra and is called the intervalence transition [73]. Many types of binuclear complexes with bridging ligand have been synthesised and utilised in the studies of electron-transfer processes and metal-metal interactions. The selection of bridging ligand can change the nature of metal-metal interactions. It has been suggested that preparation of luminescent bimetallic Ru(II) complexes demands a bridging ligand that correlates to 2,2'-bipyridine so that the coordination and field strength about each Ru(II) centre is in essence equivalent to that in $[Ru(bpy)_3]^{2+}$. Until quite recently, only two types of bridging ligands had been studied. Firstly, those ligands which have low-lying π^* orbitals [74]. For the most part, such bridging ligands will be directly involved in the electrochemical reduction and emission processes. Thus, this ligand acts as an electron-transfer or energy-transfer trap and may decrease the emission yield. Secondly, those bridging ligands which exhibit strong σ-donation properties, and function only as a building block for the synthesis of the dinuclear systems. The bridging ligand has much less influence on the emission properties, because the luminescence is now bpy based [75].

The 3,5-bis(pyridin-2-yl)-1,2,4-triazole (Hbpt) ligand (see Figure 1.10) allows formation of dinuclear species which retain their luminescent properties [76-77]. The Hbpt is a class *b* type ligand, and due to the stronger σ donation properties of the ligand, the ^{3}MC levels of the monomer species (*i.e.* $[Ru(bpy)_2(bpt)]^{1+}$), are expected to lie at higher energy than for $[Ru(bpy)_3]^{2+}$. Coupled with the lower energy of the ^{3}MLCT state, this infers that the ^{3}MC-^{3}MLCT energy gap for the monomer is considerably larger than for $[Ru(bpy)_3]^{2+}$. Consequently, a highly photostable monomeric species is formed. However, sharing of the negative charge of the bpt^- ligand between the two metal centres in the dimeric species results in reduced ligand field strength of the ligand and furthermore results in the formation of

a photoactive species [77]. An advantage of employing this ligand as a link between two metal centres is that it does not act as a trap for energy and electron transfer. The LUMO is in all cases, located on the bpy ligands and not on the connecting bpt^- ligand. Consequently this ligand may be an appropriate bridge for polynuclear complexes which can display photoinduced electron or energy migration properties [76]. Analogous mononuclear and dinuclear formed by replacing the ruthenium centres with osmium, results in complexes which are both photostable. The greater 10 *Dq* value for Os(II) as compared with Ru(II), results in an augmentation of the of the ^{3}MLCT-^{3}MC energy gap, causing the population of the d-d state to be impossible at ambient temperatures [75].

It is widely known that by using bipyrazine instead of bipyridine as a ligand, the LUMO of the resulting metal complex is lowered considerably. This is caused by the strong π-acceptor properties of pyrazine [37,65,78]. Replacing both pyridyl rings of Hbpt with two pyrazine substituents, results in the formation of 3,5-bis(pyrazin-2-yl)-1,2,4-triazole (Hbpzt) (see Figure 1.10). The effect of employing Hbpzt, results in complexes with quite unusual properties. The lowest absorption and emission bands displayed by the monomeric species, $[Ru(bpy)_2(bpzt)]^{1+}$, are $Ru\rightarrow\pi^*$ (bpy) transitions. Protonation of the triazole ring, or coordination of a second $Ru(bpy)_2$ moiety results in a reduction of the $\pi^*(bpzt^-)$ level so that the emission is now Hbpzt based [79]. Furthermore, the nature of the MLCT band is altered, as the $Ru\rightarrow\pi^*(bpzt)$ transition is also observed. The uncommon features observed for Hbpzt complexes are caused by a combination of the strong σ-donor properties of the triazole ring and the strong π-accepting properties of the two pyrazine rings [70].

1.4 Ruthenium(II) polypyridyl complexes in heterogeneous environments.

Ruthenium complexes display interesting photophysical and photochemical properties which make them attractive probes of their local microenvironment. In particular, the emission of such complexes can reflect the nature of their

surroundings, or provide information about other quencher molecules close to it [80]. In general, the study of transition metal complexes in solids has progressed at a much slower pace than that in fluid solution. However, because of the proliferation of practical applications upon incorporation into a membrane or solid matrix, the photophysics of such complexes in a solid environment now presents a formidable challenge to the material scientist [81]. For example, luminescence of species on or in solid supports is becoming increasingly important, particularly in the area of fibre optic sensors, which are frequently supported in polymers, in gels or on surfaces [82]. The photophysical aspects of such materials are by no means straight forward. In contrast to more conventional homogeneous luminescence materials, these supports are frequently heterogeneous on a microscopic scale, giving rise to complex and poorly characterised decay kinetics (see section 4.1). This complexity may result in obscure sensor response. In effect, heterogeneity makes the analysis of photochemical and photophysical data much more complicated than in the gas phase or even in fluid systems. However, their substantial presence in natural systems, justifies focusing attention on such systems and attempting to cope with their inherent complexity [81].

1.4.1 Photoprocesses of ruthenium(II) complexes on surfaces.

The role played by surfaces in chemical reactions is a source of intrigue for kineticists, colloid and polymer chemists, and indeed biochemists. The exterior of a material is of prime importance to industrial chemistry, as it is here that corrosion chemistry begins or a selected feature of a chemical reaction is catalysed. Photoprocesses on solid surfaces have attracted increasing attention from a practical viewpoint of uses. The crux of the matter with chemical reactions on surfaces is the enhancement of a selected chemical change or catalysis of a reaction. The mimicry of the photosynthetic process has been of major interest over the past 15 years due to its association with storage of light energy, leading the development of the field of

photochemistry in nonhomogeneous media [83]. Much of the effort in this area has focused on the use of electron-transfer reactions, as the ionic products are likely candidates for storage to convert and store solar energy. In particular, electron transfer from the excited $^{*}[Ru(bpy)_3]^{2+}$, to electron acceptors, *e.g.* methylviologen, MV^{2+}, has received detailed attention [84].

$$^{*}[Ru(bpy)_3]^{2+} + MV^{2+} \rightarrow [Ru(bpy)_3]^{3+} + MV^{+} \qquad (1.19)$$

The medium in which this process takes place is of extreme importance in establishing the yield of photoions, the more polar media promoting larger ionic yields [84]. However, the subsequent back-reaction of $[Ru(bpy)_3]^{3+}$ and MV^{+} limits the length of time during which charge separation and thus energy storage can be maintained. The suppression of this energy wasting back reaction can be achieved by a sacrificial repair agent, e.g. ethylenediaminetetraacetate, EDTA, which donates an electron to $[Ru(bpy)_3]^{3+}$ yielding $[Ru(bpy)_3]^{2+}$ and the net reaction is electron transfer from EDTA to MV^{2+}. Another possibility is to mechanically restrict the motion of these species in a rigid medium which promotes electron transfer to give $[Ru(bpy)_3]^{3+}$ and MV^{+}, but decreases the probability of the back-reaction. Cellulose provides such a medium, and it has been shown that MV^{+} is formed upon excitation of $[Ru(bpy)_3]^{2+}$ and MV^{2+} in this medium [85]. Similar photosensitised electron transfer and charge separation have also been demonstrated in redox active surfactant aggregates [86]. The layered zirconium phosphates are heterogeneous systems which could prove useful as media for solar energy conversion. Zirconium phosphates are acidic, inorganic, ion-exchange materials having a layered structure. These materials have potential applications as catalysts, ion-exchangers, solid electrolytes and hosts for various intercalants [87,88]. The microenvironment within zirconium phosphates has been shown to restrain movement of ions through the interlayer space, but diffusion leading to dynamic quenching can occur.

Hashimoto and co-workers have reported the photoinduced charge separation from photoexcited ruthenium complexes chemically and physically

adsorbed on powdered semiconductors by measuring the luminescence decays and the time-resolved spectra [89,90]. The interfacial charge-transfer process between semiconductor and adsorbed molecule is a key mechanism in fundamental aspects of powdered semiconductor photocatalysis and indeed photography. These studies contribute to the understanding of the dye sensitisation process of semiconductors because of the ability to obtain direct information for the rate of electron transfer between the excited dye and the semiconductor that are free from complications caused by various diffusion processes inevitable for experiments using solutions.

The search for efficient solar energy conversion devices continues to be an important area of research [91]. One approach is to make use of dye-sensitised, large band-gap semiconductor films to absorb solar light [92]. In such a device, a dye stuff (sensitiser) absorbs visible light and, after excitation, injects electrons into the conduction band of the semiconductor producing an electric current. The difficulties in obtaining reasonable conversion efficiencies with such systems are notorious. Apart from poor injection quantum yields, the light absorption by a monolayer of sensitiser adsorbed on a flat surface is at best a few percent. Multilayer deposition has proved to be an unsuccessful approach to solve this dilemma due to the lack of photoactivity and the filtering effect of the dye molecules which are not in direct contact with the semiconductor. As such, a major problem with the application of spectral sensitisation in photoelectrochemical devices for solar energy conversion has been low efficiency.

Recently, an order of magnitude increase in solar energy conversion efficiencies at dye sensitised photoelectrochemical cells has been realised [93-94]. This break-through was accomplished by attaching ruthenium polypyridyl complexes to high surface area titanium dioxide, TiO_2, electrodes. The general accepted model for dye sensitisation of wide gap semiconductors is illustrated in Figure 1.11 [95]. In this model, an excited dye injects an electron into the semiconductor conduction band from a normal distribution of donor levels and becomes oxidised. The electron is swept to the semiconductor bulk by the surface electric field and flows through an external cell to perform useful work.

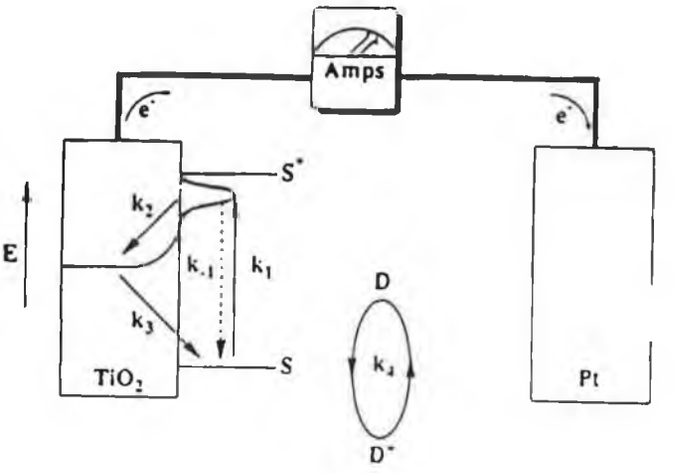

Figure 1.11 Model for dye sensitisation of wide gap semiconductors [96].

The oxidised dye is reduced by an electron donor present in the electrolyte, k_4. Reduction of the oxidised donor occurs at the counter electrode and the solar cell is therefore regenerative. Radiative and nonradiative decay of the excited state, k_{-1}, and recombination of the photoinjected electron with the oxidised dye sensitiser or the oxidised electron donor, k_3, represent loss mechanisms. These TiO_2 films have a specific fractal-type surface texture [96], and can be sensitised with strikingly high yields. When operating as anodes in a photoelectrochemical cell, these materials efficiently convert visible light to electricity [93-97]. Incident photon-to-current efficiencies exceeding 70% have been obtained. Since it is expected that most inorganic charge transfer complexes possess unique ground state properties, it is not surprising that solar energy conversion efficiencies are dependent on the nature of the molecular dye sensitiser. Another important factor is to endow the sensitiser with suitable interlocking groups which serve as electronic bridging function between its

chromophoric moiety and the conduction band of the TiO_2 [98,99]. Graetzel and co-workers have recently reported on the performance of CN-bridged trinuclear ruthenium complexes [100]. These complexes show promising features when adsorbed onto rough TiO_2 films, both with respect to efficiency of light-energy conversion as well as from their stability under long-term illumination. In effect, research on artificial photosynthetic devices based on this technology provides an opportunity to directly convert light into electricity on a molecular level.

Another prominent field in the area of immobilised luminescent ruthenium polypyridyl complexes onto surfaces which has emerged during the past 10 years, is that of modified electrodes. Much attention has been paid to polymer modified electrodes where covalent attachment of the ruthenium metal centre to pendant co-ordinating group on the polymer [101-102]. Such metallopolymeric materials offer a convenient way of creating an interface by physical adsorption onto particles in solution. The extension of homogeneous solution chemistry to polymeric materials also provides a facility for the incorporation of both catalytic and chromophoric sites, in a fixed chemical matrix. Modified electrodes differ from conventional electrodes in that a thin film of material is coated onto the electrode surface. In so doing, greater control of the electrode characteristics and surface reactivity can be achieved, thus enabling either the selective reaction of a particular analyte, or the mediation of redox reactions which are slow or not possible at a bare, unmodified electrode. The rapid charge transfer rates, the chemical and physical robustness, and the synthetic flexibility of these metallopolymers make them ideally suited for practical applications.

1.4.2 Ruthenium(II) complexes as probes of the local microenvironment.

Excited states as probe molecules comment on their environment in two basic ways leading to spectroscopic measurements commenting on:

(a) the nature of the environment of the excited state, and
(b) the relative ease of movement at the site.

Movement of other molecules (quenchers) to the excited state is also reflected in this type of kinetic measurement. Most spectroscopic studies of molecules at interfaces are obtained *via* emission spectroscopy of the excited state. This technique of fluorescence or phosphorescence probing of the system is sensitive both to probe environment and to low concentrations of the probe molecule, a necessity in order not to disturb the system under study. In recent years the emission spectroscopy of ruthenium(II) polypyridyl complexes has proven to be a sensitive and flexible tool for the investigation of a number of different environments.

Colloidal silica (SiO_2) and clays (aluminosilicates) are two class of inorganic colloids provide a particularly interesting challenge for fluorescence probing [103-105]. Solutions of colloidal silica with particles of radius in the range of 50-200 Å are commercially available today. The particles are spherical, possessing a negative surface, consisting of SiO^- groups and adsorbed OH^- ions. The counterions in most systems are Na^+, and they are readily replaced by other cations such as $[Ru(bpy)_3]^{2+}$. The silanol groups at the surface of SiO_2 particles are ionised at pH $\geq$ 5.5 and produce a diffuse double layer. The negative surface charges can aid quite significantly in the separation of photoredox products.

Wheeler and Thomas have used $[Ru(bpy)_3]^{2+}$ and 4-(1-pyrenyl)-butyltrimethylammonium bromide (PN^+), to investigate the nature of colloidal silica particles in water [103]. The fluorescence spectra of these probes show that the silica surface is very polar and similar to water. Inefficient quenching of emission of these probes by anionic quenchers (as compared to that in homogeneous solvents)

confirms the presence of negative charges. Studies with cationic quenchers show that the cations are strongly bound to the silica particles.

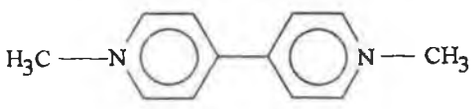

MV^{2+}

PVS

The presence of a negatively charged interface in these SiO_2^- particles should enable achievement of efficient charge separation. Calvin and co-workers have demonstrated such processes using silica-bound sensitisers and viologen salts as acceptor relays [104]. With zwitterionic viologen, propylviologen sulfonate (PVS), on electron transfer, two oppositely charged photoproducts, $[Ru(bpy)_3]^{3+}$ and PVS^-

$$^*[Ru(bpy)_3]^{2+} + PVS \underset{k_2}{\overset{k_q}{\rightleftharpoons}} [Ru(bpy)_3]^{3+} + PVS^- \qquad (1.20)$$

The former is strongly adsorbed to the silica particle, but the reduced form of the electron acceptor is repelled by the negatively charged interface, hindering the recombination process as illustrated by:

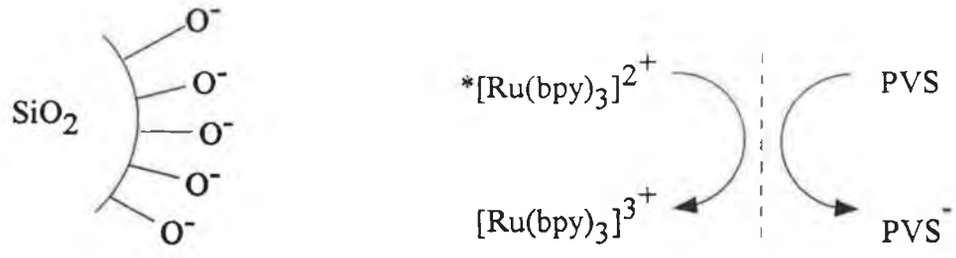

The forward quenching rate k_q is comparable in water and in SiO_2 colloids. However, the back electron transfer rate k_2 is retarded by more than 100-fold over

that observed in the homogeneous phase. In the case of dicationic methyl viologen, MV^{2+}, the quenching rate is strongly enhanced on the silica surface (100-fold). The importance of the surface potential of SiO_2 colloids in retarding the back reaction has been demonstrated by varying the ionic strength and the pH of the medium.

Ruthenium(II) probes have also been employed in the characterisation of colloidal clay systems. Clay constitutes a unique class of inorganic colloids which occur quite readily in nature with special structural features that make them versatile as catalysts and catalyst supports [105]. These aluminosilicate systems are negatively charged containing aluminium in an octahedral configuration sharing oxygen atoms with silicon, which is in tetrahedral configuration. Their ability to exchange cations has been utilised to locate cationic probes, *e.g.* $[Ru(bpy)_3]^{2+}$ on such clays as laptonite, which is a synthetic clay, and natural hectorite and montmorillonite. The absorption and luminescence of $[Ru(bpy)_3]^{2+}$ undergo significant perturbations in clays. The charge transfer absorption band shifts towards the red (maxima at 472, 462 and 465 nm in montmorillonite, hectorite, and kaolinite respectively) with about 50 % decrease in the absorption cross section. The intensity of the $\pi-\pi^*$ band near 285 nm is dramatically reduced [106]. The differences in the absorption spectra have been attributed to the differences between the $[Ru(bpy)_3]^{2+}$ complex and the clay surface. Possible explanations include the distortion of the bipyridine ligands due to steric constraints and an enhancement in the quasi-metal-to-ligand charge transfer in the ground state.

In contrast to the absorption profile, the luminescence profiles are very similar. Also the excitation spectra followed essentially the absorption spectral profiles. However, there are significant differences in the relative magnitude of the luminescent quantum yields and lifetimes. After correcting for the changes in the ground-state absorption coefficients, the emission yield is about 30 % larger for $[Ru(bpy)_3]^{2+}$ in hectorite, whereas it is almost six times lower in montmorillonite. The greatly reduced yield in montmorillonite has been attributed to the quenching by Fe^{3+} in the octahedral layers. The emission decay profiles in the presence of clays are complex, but have been fitted to double exponential decays. It has been suggested

that the double exponential is due to the presence of two different adsorption sites on the clay particle: on the outer surface and intercalation between the phyllosilicate sheets. In effect, the lifetime, quantum yield, and nature of the absorption spectrum are dependent on whether $[Ru(bpy)_3]^{2+}$ is adsorbed in layers as in the natural clays or whether it is adsorbed at the surface as with laptonite [107]. At low concentrations of laptonite, $[Ru(bpy)_3]^{2+}$ is adsorbed on the outer layers and is in contact with the aqueous phase. However, at higher clay concentrations or in the presence of calcium chloride, layering of the clay occurs and the probe molecule is placed progressively between the layers where its photophysics are altered.

Spectroscopic methods using ruthenium(II) complexes as probes have also been applied to the understanding of the interior structure and dynamics of micelles and hemimicelles. This probe has been used to study the structure and evolution of anionic surfactant aggregates in solution. Shifts in frequency and enhancements in intensities of the excited-state Raman spectra of $[Ru(bpy)_3]^{2+}$ in sodium dodecyl sulphate (SDS) micelles have proven remarkable in responding to the general course of the aggregation process [108]. In addition, ruthenium polypyridyl complexes have also been used in DNA probe technology and their use as labels for proteins has also been reported [109].

Ruthenium(II) metal complexes have been incorporated into a number of natural and synthetic polymer membranes such as silk fibroin [110,111], cellulose [85,112], and indeed poly(ethyleneoxide) membranes [114]. The incorporation of ruthenium complexes into these particular matrices will be discussed in more detail in Chapters 3 and 4. Membranes and membrane surface chemistry play a key role in many biosystems and a more comprehensive understanding of their properties can be obtained through these spectroscopic techniques.

The sol-gel process is continuously gaining acknowledgement in a number of specific fields. One particularly intriguing application of the sol-gel science for solar-energy conversion materials has recently been reported by Avnir and co-workers [115-116]. This current research is oriented towards the design of efficient photoredox systems. In these studies, the donor is immobilised in a sol-gel matrix,

and the mobile acceptor is located within the intrapore region of the gel. The mobile acceptor can then shuttle redox energy to a secondary acceptor immobilised in a different location within the gel. In this manner, the back electron-transfer rate is inhibited by the long distance between the oxidised donor and the reduced acceptor. Employing this methodology, charge separated pairs which live for hours have been produced. In a particularly novel system, back-electron transfer rates of approximately 7 orders of magnitude slower than in fluid solution were established [117]. It has been proposed that the sol-gel trapping technique offers several advantages over other heterogeneous systems previously employed for the study of such photosensitised reactions: This medium is completely transparent and the method is simply applicable as compared to for example, the covalent attachment of the reactant to the glass. With respect to adsorbed systems, sol-gel trapping is free of disadvantages such as solvent-induced desorption by high ionic strengths and by low pH. Compared to micelles, the purely inorganic glass medium minimises undesirable side reactions with charge-separated species. Another area in which extensive research has been carried out is in the development of luminescence-based optical sensors involving the quenching of ruthenium complexes which have been incorporated into a sol-gel matrix [14].

However, several fundamental questions remain before the application of these advances to practical photocatalytic materials and optical sensors can be realised. For example, how and to what extent are species immobilised within a sol-gel? What fraction of immobilised species reside in regions where they can participate in reactions with reactants in the intrapore region of the gel? How do the preparation conditions of the sol-gel matrix affect immobilised species within this matrix? These questions may be better addressed when a detailed knowledge of the local environments of the dopant species is obtained. Luminescent dyes can be employed as probes of both sol-gel transformation and the accompanying chemical and matrix rigidity changes. Another interesting aspect of the dye-doped sol-gel materials is the opportunity to use this approach for matrix-isolation purposes and to investigate the fundamental spectroscopy of the molecule in the sol-gel environment.

For these purposes, the spectroscopic properties of $[Ru(bpy)_3]^{2+}$ within a sol-gel matrix have been investigated by a number of authors and compared to those of the molecule in low-temperature glasses and in water [118-121].

Reisfeld and co-workers have investigated the spectroscopic behaviour of $[Ru(bpy)_3]^{2+}$ in sol-gel glasses, heavy fluoride glasses, polyvinylalcohol films and in boric acid at room temperature. It was found that essentially the mechanism of absorption, internal conversion, and intersystem crossing was similar for all of these solids studied. All the absorption spectra show a maximum around 450 nm assigned to the ^{1}MLCT. The fluorescence spectra of all the samples, peaking at approximately 600 nm, were assigned to the Stokes-shifted emission of the ^{3}MLCT excited state to the ground state. The lifetimes and quantum yields of $[Ru(bpy)_3]^{2+}$ in polyvinyl alcohol (PVA), boric acid, tin-lead fluoride glass and sol-gel glass indicate that in dense matrices part of the quenching mechanisms, such as oxygen quenching and freedom of motion, are absent. This also conforms to the theory of four levels by van Houten and co-workers [45,46] in order to explain the high temperature behaviour of $[Ru(bpy)_3]^{2+}$ in liquids. The slightly lower lifetime of the complex in the sol-gel matrix as compared to the other fore mentioned glasses, indicates that this particular matrix is still porous, permitting both some measure of oxygen quenching and freedom of rotation. The fact that the quantum yields are still much smaller than unity can be rationalised by intersystem crossing to a quenching level, governed by Boltzmann population of this level.

The behaviour of the luminescence decay profile was similar for different types of glass, showing a double exponential dependence [118]. An increase in lifetime was found in all cases. This increase is the result of the fixation of the ruthenium complex into a rigid solid matrix where a majority of bimolecular deactivating mechanisms that can quench the excited states are removed *e.g.* concentration quenching can be neglected due to isolation of the complex molecules in the matrix. Increased lifetime of $[Ru(bpy)_3]^{2+}$ in solids at room temperature, has been attributed to decreased k^{nr}, *i.e.* decreased interaction of the lowest triplet manifold of the complex with the solid surroundings as compared to water and

alcohol. These results are consistent with the scheme proposed by van Houten and Watts [45-46].The non-radiative decay rate for the triplet level of $[Ru(bpy)_3]^{2+}$ is dependent on the nature of the material. In these studies it was also found that the more dense the material the lower the non-radiative rates. In addition, Matsui and co-workers have employed $[Ru(bpy)_3]^{2+}$ as a luminescent probe in order to follow the sol-gel reaction system of tetraethoxysilane [122]. The spectrum exhibited a blue shift during the sol-gel stage, indicating that the probe molecule became entangled by siloxane polymers and finally became tightly bound to the sol-gel silica. It was found that the relative rates of the spectral shift of $[Ru(bpy)_3]^{2+}$ differed depending on the preparation conditions thus suggesting the potential use of this complex as a photoprobe of sol-gel systems.

1.5 Scope of thesis.

This thesis is concerned with the study of ruthenium(II) complexes in a sol-gel matrix. There are two complementary goals for these studies. The first objective is to use the existing extensive knowledge on the photophysics of these complexes to probe the sol-gel-xerogel reactions and hence, the factors which determine the progress of these reactions. The second and indeed converse goal is to use the known information on the sol-gel system to examine the excited state processes under a novel environment.

In Chapters 3 and 4, particular emphasis is given to the way in which these transition metal complexes can be employed as photophysical probes of the sol-gel process. In condensed media, the solvent molecules constituting the medium (for microheterogeneous systems the medium is referred to as "the environment") can intervene in some of the excited-state processes. Usually solvents interact strongly with excited states that have higher dipole character compered to the ground state. The solute-solvent interactions can affect the relative populations at various vibrational levels of the excited state or the relative populations of the Franck-

Condon envelope of the excited state with respect to the ground state. The former manifests itself as variations in the vibronic band intensities and the latter in red or blue shifts in the emission maxima, often accompanied by changes in the fluorescence yields. The polarity and viscosity of the medium can influence the orientation and mobility of the probe molecule in the medium. In effect, these two chapters are primarily concerned with changes in the nature of the environment from an initial fluid medium to the more restricted nature of the final xerogel on both the position of the photoluminescence energy maximum and also the luminescent lifetime.

As mentioned in section 1.3.2, the lifetime of ruthenium complexes in solution is highly temperature dependent above 250 K, with the luminescence lifetime decreasing with increasing temperature. In Chapters 5 and 6, the effect of the incorporation into a solid matrix on the temperature dependent nature of a number of ruthenium(II) complexes, both monomers and dimers and also $[Os(bpy)_3]^{2+}$ have been investigated. The aim of these chapters is to further elucidate the photophysics of these complexes in a sol-gel matrix at such temperatures above which population of the ^{3}MC state is prevalent in a solution media.

Finally, Chapter 7 serves to draw all the information gathered in the thesis together and give an overview of the photophysical behaviour of these complexes in a solid environment as compared to the well documented nature of these complexes in solution media.

1.6 References.

[1] C.J. Brinker,G.W. Scherer, Sol-gel Science: The Physics and Chemistry of Sol-Gel Processing, Boston, Academic Press, **1990**.

[2] R.W. Jones, Fundamental Priniples of Sol-Gel Technology, Brookfield VT: Institute of Metals, **1989**.

[3] J.D. MacKenzie, *J. Non-Cryst. Solids*, 100, 162, **1988**.

[4] O. Lev, *Analusis*, 20, 543, **1992**.

[5] D.R. Ulrich, *J. Non-Cryst. Solids*, 100, 174, **1988**.

[6] S. Sakka, *J. Sol-Gel Sci. and Tech.*, 3, 69, **1994**.

[7] F. Salin, G. Le Saux, P. Georges, A. Brun, C. Bangall, J. Zarcycki, *Opt. Lett.* 14, 785, **1989**.

[8] A. Makishima, K. Morita, H. Inoue, T. Tani, *Riv. Stn. Sper. Vetro.*, 22, 21, **1992**.

[9] D. Avnir, D. Levy, *J. Phys. Chem.*, 92, 4734, **1988**.

[10] T. Fujii, H. Yamamoto, K. Oki, *J. Mater. Chem.*, 4, 635, **1994**.

[11] M. Nakamura, H. Nasu, K. Kamiya, *J. Non-Cryst. Solids*, 135, 1, **1991**.

[12] C. Rottman, M. Ottolenghi, R. Zusman, O. Lev, M. Smith, G. Gang, M.L. Kagan, D. Avnir, *Mater. Lett.*, 13, 293, **1992**.

[13] J. E. Lee, S.S. Saavedra, *Anal. Chim. Acta*, 285, 265, **1994**.

[14] P. Kiernan, C. McDonagh, B.D. MacCraith, K. Mongey, *J. Sol-Gel Sci. Tech.*, 2, 513, **1994**.

[15] B. Dunn, J. Zink, *J. Mater. Chem.*, 1, 903, **1991**.

[16] L.L. Hench, J.K. West, *Chem. Rev.*, 90, 33, **1990**.

[17] H. Dislich, *Angew. Chem., Inst. Ed. English*, 10, 363, **1971**.

[18] K.S. Mazdiyashni, R.T. Dolloff, J.J. Smith, *J. Am. Ceram. Soc.*, 52, 523, **1969**.

[19] J.D. Mackenzie, *J. Non-Cryst. Solids*, 48, 1, **1982**.

[20] H. Schmidt, *Structure and Bonding*, 77, 120, **1992**.

[21] J.D. MacKenzie, D.R. Ulrich, UltraStructure Processing of Advanced Ceramics, Wiley, California, **1988**.

[22] D. Ulrich, C.J. Brinker, B. Zelenski, D. Clark, Better Ceramics Through Chemistry IV, Mater. Res. Soc., California, **1990**.

[23] H. Schmidt, H. Scholze, A. Kaiser, *J. Non-Cryst. Solids*, 63, 1, **1984**.

[24] R.K. Iler, The Chemistry of Silica, Wiley, New York, **1979**.

[25] E.J. Pope, J.D. Mackenzie, *J. Non-Cryst. Solids*, 87, 185, **1986**.

[26] T.W. Zerda, I. Artaki, J. Jonas, *J. Non-Cryst. Solids*, 81, 365, **1986**.

[27] S.Y. Chang, T.A. Ring, *J. Non-Cryst. Solids*, 147/148, 56, **1992**.

[28] C.J. Brinker, *J. Non-Cryst. Solids*, 100, 31, **1988**.

[29] R.T. Morrison, R.N. Boyd, Organic Chemistry, Allyn and Bacon Inc., New York., **1990**.

[30] M.G. Vorankov, V.P. Mileshkevich, Y.A. Yuzhelevski, The Siloxane Bond. New York **1978**.

[31] I. Artaki, T.W. Zerda, J. Jonas, *J. Non-Cryst. Solids*, 81, 381, **1986**.

[32] V.R. Kaufman, D. Avnir, *Langmuir*, 2, 717, **1986**.

[33] M.W. Colby, A. Oaska, J.D. Mackenzie, *J. Non-Cryst. Solids*, 82, 37, **1986**.

[34] D. Avnir, V.R. Kaufman, R. Reisfeld, *J. Non-Cryst. Solids*, 74, 395, **1985**.

[35] K. Karyanasundaram, *Coord. Chem. Rev.*, 46, 159, **1982**.

[36] T.J. Meyer, *Pure Appl. Chem.*, 58, 1193, **1986**.

[37] A. Juris, V. Balzani, F. Barigelletti, S. Campagna, P. Belser, A. von Zelewsky, *Coord. Chem. Rev.*, 84, 85, **1988**.

[38] T.J. Meyer, *Pure Appl. Chem.*, 62, 1003, **1990**.

[39] E.M. Kober, T.J. Meyer, *Inorg. Chem.*, 23, 3877, **1984**.

[40] F.E. Lytle, D.M. Hercules, *J. Am. Chem. Soc.*, 105, 1067, **1983**.

[41] J.N. Demas, G.A. Crosby, *J. Am. Chem. Soc.*, 93, 2841, **1971**.

[42] J.N. Demas, D.G. Taylor, *Inorg. Chem.*, 18, 3177, **1979**.

[43] E.R. Carraway, J.N. Demas, B.A. Degraff, J.R. Bacon, *Anal. Chem.*, 63, 337, **1991**.

[44] S.R. Allsopp, A. Cox, T.J. Kemp, W.J. Reed, *J. Chem. Soc.; Faraday Trans.*, 1, 1275, **1978**.

[45] J. van Houten, R.J. Watts, *J. Am. Chem. Soc.*, 98, 4853, **1976**.

[46] J. van Houten, R.J. Watts, *Inorg. Chem.*, 17, 3381, **1978**.

[47] B. Durnham, J.V. Casper, J.K. Nagle, T.J. Meyer, *J. Am. Chem. Soc.*, 104, 4803, **1982**.

[48] D.V. Pinnick, B. Durham, *Inorg. Chem.*, 23, 3841, **1984**.

[49] E.A. Seddon, K.R. Seddon, The Chemistry of Ruthenium, Elsevier, Amsterdam, **1984**.

[50] R.J. Watts, *J. Chem. Ed.*, 60, 835, **1983**.

[51] J.V. Caspar, T.J. Meyer, *Inorg. Chem.*, 22, 2444, **1983**.

[52] G.D. Harrigan, G.A. Crosby, *J. Phys. Chem.*, 59, 3468, **1973**.

[53] C.D. Hagar, R.J. Watts, G.A. Crosby, *J. Am. Chem. Soc.*, 97, 7037, **1975**.

[54] G.A. Crosby, W.H. Elfring Jr., *J Phys. Chem.*, 80, 2206, **1976**.

[55] R.S. Lumpkin, E.M. Kober, L.A. Whorl, Z. Muttaza, T.J. Meyer, *J. Phys. Chem.*, 94, 239, **1990**.

[56] P. Connolly, J.H. Espenson, A. Bakas, *Inorg. Chem.*, 25, 2169, **1986**.

[57] K. Nitamaru, H.B. Kim, S. Okano, S. Tazuke, J. *Phys. Chem.*, 93, 5750, **1989**.

[58] A. Vleck, F. Bolletta, *Inorg. Chim. Acta*, 76, L227, **1983**.

[59] G. Jones II, V. Malta, *J. Org. Chem.*, 50, 5776, **1985**.

[60] G.P. Porter, *J. Chem. Ed.*, 60, 785, **1983**.

[61] V. Balzani, R. Ballardini, *Photochem. Photobiol.*, 52, 409, **1990**.

[62] J.V. Caspar, E.M. Kober, B.P. Sullivan, T.J. Meyer, *J. Am. Chem. Soc.*, 104, 630, **1982**.

[63] J.V. Caspar, E.M. Kober, B.P. Sullivan, T.J. Meyer, W.J. Dreswick, *J. Am. Chem. Soc.*, 102, 7383, **1980**.

[64] B.P Sullivan, H.D. Abruna, H.O. Finklea, D.J. Salmon, J.K. Nagle, T.J. Meyer, H. Sprintschnick, *Chem. Phys. Lett.*, 58, 389, **1978**.

[65] G.H. Allen, R.P. White, D.P Rillema, T.J. Meyer, *J. Am. Chem. Soc.*, 106, 2613, **1984**.

[66] J.N. Demas, B.A. Degraff, *Anal. Chem.*, 63, 829A, **1991**.

[67] G.D. Danzer, K.R. Kincaid, *J. Phys. Chem.*, 94, 3976, **1990**.

[68] E.V. Dose, L.J. Wilson, *Inorg. Chem.*, 17, 2660, **1978**.

[69] P.J. Steel, E.C. Constable, *J. Chem. Soc., Dalton Trans.*, 1389, **1990**.

[70] H. Hughes, Ph. D. Thesis, Dublin City University, **1993**.

[71] E. Ryan, R. Wang, J.G. Vos, *Inorg. Chem. Acta*, 208, 49, **1993**.

[72] R. Hage, A. Dijkhuis, J.G. Haasnoot, R. Prins, J. Reedijk, B.E. Buchanan, J.G. Vos, *Inorg. Chem.*, 27, 2185, **1988**.

[73] N.S. Hush, *Electrochim. Acta*, 13, 1005, **1968**.

[74] R. Sahai, L. Morgan, D.P. Rillema, *Inorg. Chem.*, 27, 3495, **1988**.

[75] M. Haga, T. Matsumura-Inoue, S. Yamabe, *Inorg. Chem.*, 26, 4148, **1987**.

[76] F. Barigelletti, L. DeCola, V. Balzani, R. Hage, J.G Haasnoot, J. Reedijk, J.G. Vos, *Inorg. Chem.*, 30, 641, **1991**.

[77] F. Barigelletti, L. DeCola, V. Balzani, R. Hage, J.G Haasnoot, J. Reedijk, J.G. Vos, *Inorg. Chem.*, 28, 4344, **1989**.

[78] R.J. Crutchley, A.B.P. Lever, *J. Am. Chem. Soc.*, 102, 7129, **1980**.

[79] R. Hage, J.G. Haasnoot, H.A. Niellwerhuis, J. Reedijk, T.L. Snoek, J.G Vos, *Inorg. Chem.*, 30, 48, **1991**.

[80] M. Kaneko, S. Hayakawa, *J. Macromol. Sci. Chem.*, 25, 125J, **1988**.

[81] K. Kalyansundaram, Photochemistry in Microheterogeneous Systems; Academic Press, New York, **1982**.

[82] E.R. Carrraway, J.N. Demas, B.A. Degraff, *Langmuir*, 7, 2991, **1991**.

[83] J.H. Fendler, *J. Phys. Chem.*, 89, 2230, **1985**.

[84] N. Sutin, *J. Photochem.*, 10, 19, **1979**.

[85] B.H. Milosavijevic, J.K. Thomas, *J. Phys. Chem.*, 87, 616, **1983**.

[86] K. Kurihara, P. Tundo, J.H. Fendler, *J. Phys, Chem.*, 87, 3777, **1983**.

[87] J.L. Colon, C.Y. Yang, A. Clearfield, C.R. Martin, *J. Phys. Chem.*, 94, 874, **1990**.

[88] J.L. Colon, C.Y. Yang, A. Clearfield, C.R. Martin, *J. Phys. Chem.*, 92, 5777, **1988**.

[89] K. Hashimoto, M. Hiramoto, T. Sakata, H Muraki, H. Takemura, M. Fujihara, *J. Phys. Chem.*, 91, 6198, **1987**.

[90] T. Kajiwora, K. Hasimoto, T. Kawai, T. Sakata, *J. Phys. Chem.*, 86, 4516, **1982**.

[91] M. Fox, M. Chanon, Photoinduced Electron Transfer, Elseveir, Amsterdam, **1988**.

[92] M. Ryan, E. Fitzgerald, J. Spitler, *J. Phys. Chem.*, 6150, 93, **1989**.

[93] B. O'Reagan, M. Grtäzel, *Nature*, 353, 737, **1991**.

[94] A. Kay, M. Grätzel, *J. Phys. Chem.*, 97, 6272, **1993**.

[95] B.A. Parkinson, M. Spitler, *Electrochim. Acta*, 37, 943, **1992**.

[96] W.T. Wu, A.J. McEvoy, M. Grätzel, *J. Electroanal. Chem.*, **1990**.

[97] T. Heimer, C. Bignozzi, G. Meyer, *J. Phys. Chem.*, 97, 11987, **1993**.

[98] N. Vlachopoulos, P. Liska, J. Augustynski, M. Grätzel, *J. Am. Chem. Soc.*, 110, 1216, **1988**.

[99] N. Vlachopoulos, P. Liska, M. Nazeeruddin, P. Compte, M. Grätzel, *J. Am. Chem. Soc.*, 110, 3686, **1988**.

[100] N. Vlachopoulos, P. Liska, M. Nazeeruddin, J. Moser, M. Grätzel, *Helv. Chim. Acta*, 73, 1788, **1990**.

[101] M. Kaneko, *J. Macromol. Sci.; Chem.*, A24, 3&4, 357, **1987**.

[102] K. Nagai, N. Takamuya, M. Kaneko, *J. Inorg. Organomet. Pol.*, 4, 391, **1994**.

[103] J. Wheeler, J.K. Thomas, in "Inorganic Reactions In Organised Media" (S.L. Holt, ed.) ACS Symposium Series, No. 177, p. 97, *Am. Chem. Soc.*, Washington, D.C., **1981**.

[104] I. Willner, J.W. Otvis, M. Calvin, *J. Am. Chem. Soc.*, 103, 3203, **1981**.

[105] A. Shimoyama, W.D. Johns, *Nature (London), Phys. Sci.*, 232, 140, **1971**.

[106] R.A. Dellaguardia, J.K. Thomas, *J. Phys. Chem.*, 87, 990, **1983**.

[107] T. Nakamura, J.K. Thomas, *J. Phys. Chem.*, 90, 641, **1986**.

[108] J.T. Kunjappu, P. Somasundarun, N.J. Turro, *J. Phys. Chem.*, 94, 8464, **1990**.

[109] A.B. Tossi, J.M. Kelly, *Photochem. Photobiol.* 49, 545, **1989**.

[110] M. Kaneko, S. Iwahata, T. Asakura, *J. Photchem. Photobiol. A;Chem.*, 61, 373, **1991**.

[111] M.N. Szentirmay, N.E. Prieto, C.R. Martin, *J. Phys. Chem.*, 89, 3017, **1985**.

[112] M. Kaneko, A. Yamada, *Photochem. Photobiol.*, 33, 793, **1981**.

[113] A. Masschelein, A. Kirsh-De Mesmaeker, C.J. Willsher, F. Wilkinson, *J. Chem. Soc., Faraday Trans.*, 87, 259, **1991**.

[114] S. Campagna, A. Bartolotta, G. DiMarco, *Chem. Phys. Lett.*, 206, 30, **1993**.

[115] A. Slama-Schwok, M. Ottolenghi, D. Avnir, *J. Phys. Chem.*, 93, 7544, **1989**.

[116] A. Slama-Schwok, M. Ottolenghi, D. Avnir, *J. Am. Chem. Soc.*, 113, 3984, **1991**.

[117] A. Slama-Schwok, M. Ottolenghi, D. Avnir, *Nature*, 355, 240, **1992**.

[118] R. Reisfeld, *J. Non-Cryst. Solids*, 121, 254, **1990**.

[119] R. Reisfeld, C. Joergensen, *Structure and Bonding*, 77, 207, **1992**.

[120] S. Modes, P Lianos, *Chem. Phys. Letters*, 4, 351, **1988**.

[121] F.N. Castellano, T.A. Heimer, M.T. Tandhasetti, G.J. Meyer, *Chem. Mater.*, 6, 1041, **1994**.

[122] K. Matsui, K. Sasaki, N. Takahashi, *Langmuir*, 7, 2866, **1991**.

Chapter 2.

Experimental Procedures.

2.1 Materials.

The synthetic procedures for the preparation of the sol-gel matrices and metal complexes used during the course of this thesis are described in the following section. All synthetic reagents and solvents were of commercial grade and no further purification was employed.

2.2 Synthesis of complexes.

The following complexes were synthesised according to general literature procedures.

	Reference.
1. $[Ru(bpy)_3](PF_6)_2$	[1]
2. $[Ru(phen)_3](PF_6)_2$	[2]
3. $[Ru(dpp)_3](PF_6)_2$	[3]
4. $[Ru(phen)_2(H3Mptr)](PF_6)_2$	[4]
5. $[Os(bpy)_3](PF_6)_2$	[5]
6. $[Ru(bpy)_2(dpp)](PF_6)_2$	[6]
7. $[Ru(dpp)_2(bpy)](PF_6)_2$	[6]
8. $[Ru(bpy)_2(biq)](PF_6)_2$	[7]
9. $[Ru(bpy)_2(bpt)]PF_6$	[8]
10. $[(Ru(bpy)_2)_2(bpt)](PF_6)_3$	[8]
11. $[Ru(bpy)_2(bpzt)]PF_6$	[9]
12. $[(Ru(bpy)_2)_2(bpzt)](PF_6)_3$	[9]

2.2.1 Synthesis of $[Ru(L\text{-}L)_3](PF_6)_2$ complexes.

The $[Ru(L\text{-}L)_3](PF_6)_2$ complexes (where L-L = 2,2'-bipyridine (bpy), 1,10'-phenanthroline (phen), or 4,7'-diphenyl,1,10-phenanthroline (dpp)) were all synthesised according to the following general procedure. 2.0 mmol of $RuCl_3.3H_2O$, 6.2 mmol of the appropriate ligand (bpy, phen or dpp) and 1.5 g of LiCl were heated under reflux in 50 ml of N,N-dimethylformamide (DMF) for 8 h. After cooling, 500 ml of acetone was added to the solution. After leaving the solution for 24 h at -20 ^{0}C, the precipitated complex, $[Ru(L\text{-}L)_3]Cl_2$, was filtered and washed with 20 ml of diethyl ether. The solid was then dissolved in 20 ml water and a few drops of a concentrated aqueous NH_4PF_6 solution were added. The precipitation ($[Ru(L\text{-}L)_3](PF_6)_2$) was filtered and dried using diethyl ether. The product was then recrystallised from 20 ml of an acetone/water (1/1 v/v) solution. Yields > 80 %.

2.2.2 Synthesis of $[Ru(bpy)_2(L\text{-}L)](PF_6)_2$ complexes

The $[Ru(bpy)_2(L\text{-}L)](PF_6)_2$ complexes (where L-L = 2,2'-biquinoline (biq), or 4,7'-diphenyl,1,10-phenanthroline (dpp)) were all synthesised according to the following general procedure. 1.0 mmol of $[Ru(bpy)_2Cl_2].2H_2O$ [10] was heated under reflux with 1.2 mmol of the appropriate ligand for 5 h in 50 ml of ethanol/water (4/1 v/v). The solvent was then removed by rotary evaporation, and the remaining solid dissolved in 10 ml water. A few drops of a concentrated aqueous NH_4PF_6 solution were added. The precipitation ($[Ru(bpy)_2(L\text{-}L)](PF_6)_2$) was filtered and dried using diethyl ether. The product was then recrystallised from 20 ml of an acetone/water (1/1 v/v) solution. Yields > 75 %.

2.2.3 Synthesis of $[Ru(dpp)_2(bpy)](PF_6)_2$ complex.

1.0 mmol of $[Ru(dpp)_2Cl_2].2H_2O$ [10], was heated under reflux with 1.2 mmol of 2,2'-bipyridine for 5 h in 50 ml of ethanol/water (4/1 v/v). The solvent was then removed by rotary evaporation, and the remaining solid dissolved in 10 ml water. A few drops of a concentrated aqueous NH_4PF_6 solution were added. The precipitation was filtered and dried using 20 ml diethyl ether. The product was then recrystallised from 20 ml of an acetone/water (1/1 v/v) solution. Yield 70 %.

2.2.4 Synthesis of $[Ru(phen)_2(H3Mptr)](PF_6)_2$ complex.

1.0 mmol $[Ru(phen)_2Cl_2].2H_2O$ and an excess of ligand 1.2 mmol of H3Mptr ligand were heated under reflux in ethanol/water (4/1 v/v) for 6 h. In order to ensure complete protonation of the bound ligand, 1-2 drops of conc. HCl were added. The solvent was then removed by rotary evaporation, and the remaining solid dissolved in 10 ml water. A few drops of a concentrated aqueous NH_4PF_6 solution were added. The precipitation was filtered and dried using 20 ml diethyl ether. The product was then recrystallised from 20 ml of an acidified acetone/water (1/1 v/v) solution.

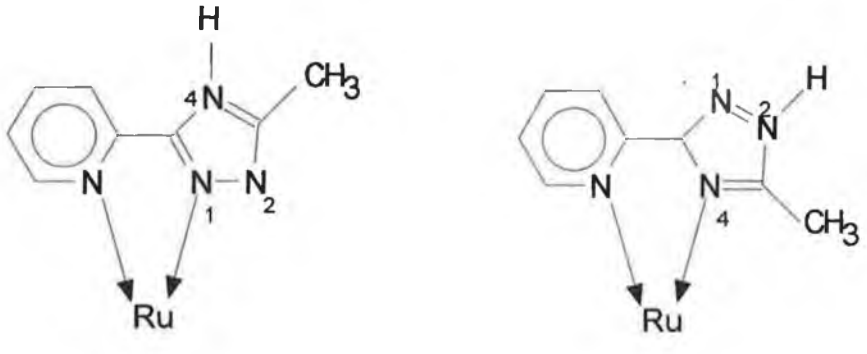

Figure 2.1 Possible coordination modes for the pyridyltriazole ligand in the two isomers of $[Ru(phen)_2(H3Mptr)]^{2+}$.

Two isomers of $[Ru(phen)_2(H3Mptr)]^{2+}$ were formed (in a ratio 5/1) during the synthesis since chelation can take place through the N1 or the N4 nitrogen atom of the triazole ring. The preferred site of coordination is anticipated to be the N1 site as the methyl ring on the triazole ring causes steric hindrance at the N4 site. The two isomers were separated using HPLC methods as described in section 2.6. The N1 coordinated isomer was used for the preparation of the of sol-gel samples in the following section.

2.2.5. Synthesis of Hbpt and Hbpzt complexes.

The following complexes $[Ru(bpy)_2(Hbpt)]^{2+}$, $[(Ru(bpy)_2)_2(bpt)]^{3+}$, $[Ru(bpy)_2(Hbpzt)]^{2+}$, and $[(Ru(bpy)_2)_2(bpzt)]^{3+}$, were synthesised by Dr. Helen Hughes, Dublin City University [8,9].

2.2.6 Synthesis of $[Os(bpy)_3](PF_6)_2$.

$[Os(bpy)_3](PF_6)_2$ was synthesised by Dr. Helen Hughes, Dublin City University using the literature procedure [5].

The purity of the complexes were established using the HPLC methods described later in this chapter and also ^1H NMR. Figure 2.2 illustrates the ^1H NMR spectra obtained for the mixed ligand complexes $[Ru(bpy)_2(dpp)]^{2+}$ in CD_3CN and $[Ru(bpy)(dpp)_2]^{2+}$ in DMSO. These NMR spectra have been previously reported [11].

The complexes were incorporated within a sol-gel matrix using initial concentrations of 10^{-5} M, unless otherwise stated. The structure, numbering, names, and abbreviations of the ligands employed in this thesis have been previously presented in Figure 1.10.

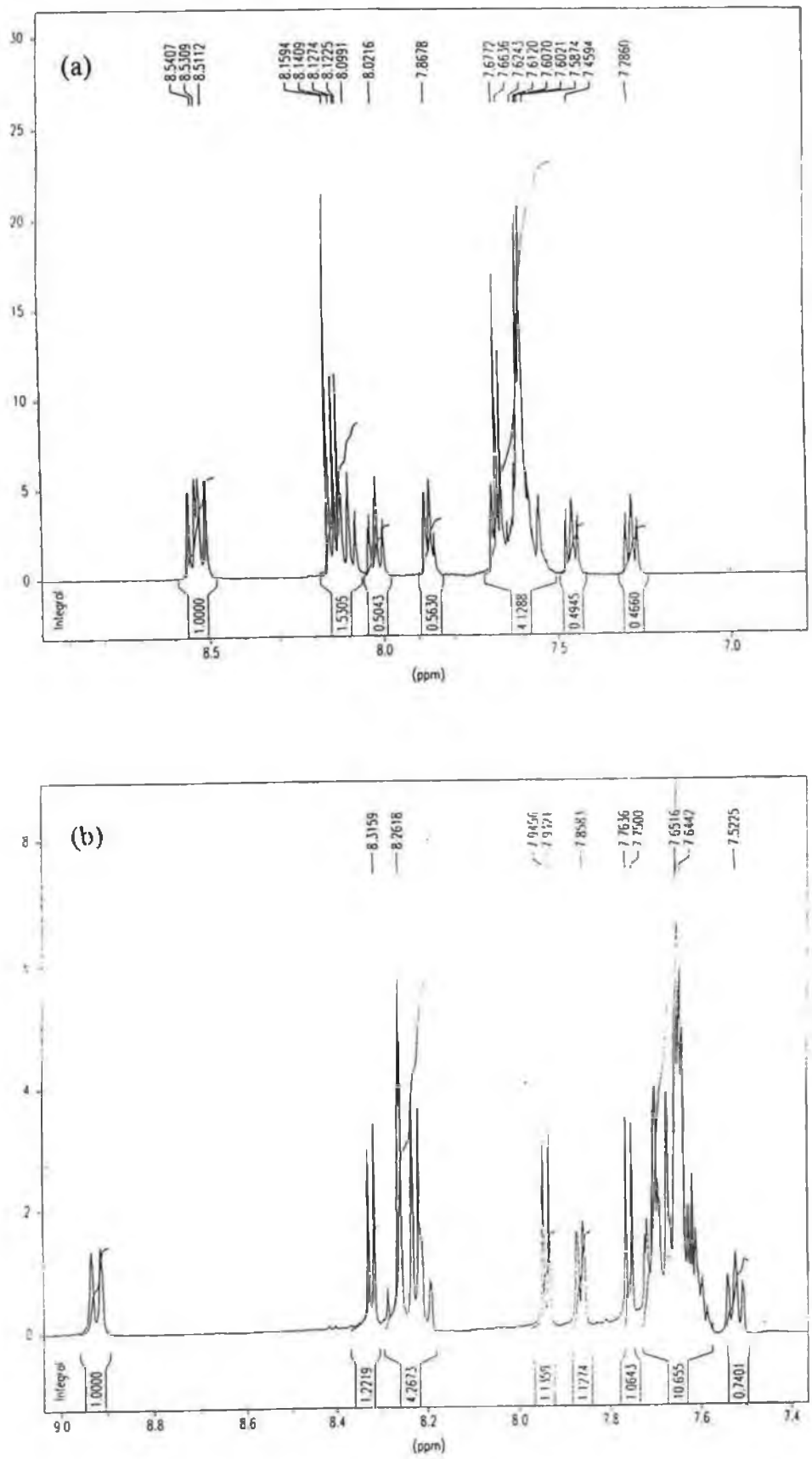

Figure 2.2 ^{1}H-NMR of (a) $[Ru(bpy)_2(dpp)]^{2-}$ and (b) $[Ru(bpy)(dpp)_2]^{2+}$.

2.3 Synthesis of sol-gel samples.

Monolithic sol-gel samples of varying water to silane ratio (R), were prepared by the hydrolysis of tetraethoxysilane (TEOS) in water-ethanol solutions. The time required to reach gel point was found to depend greatly on HCl concentration, temperature and the water to silane ratio employed. The undoped gels display high optical transparency in the visible region.

Method 1: Sample R = 2. *(1)*

To a mixture of 3.6g (0.2 moles) of water (adjusted to the appropriate pH using conc. HCl) and 13.8g (0.3 moles) of ethanol (containing the desired dopant complex), 20.8g (0.1 moles) of TEOS was added dropwise. The mixture was stirred for one hour in a sealed beaker before pouring into a plastic cell suitable for spectroscopic measurements (1cm × 0.5cm × 4cm). The plastic cell was covered to allow gelation and aging to occur in a closed environment. The initial concentration of the complexes in the sols was 10^{-5} M unless otherwise stated. The samples were aged for 500 h unless otherwise stated. The lid was then pierced to allow for the evaporation of excess solvent. All samples were stored at 50 ^{0}C unless otherwise stated.

Method 2: Sample R = 4.

These gel samples were prepared as described for *(1)* above using 3.6g (0.2 mole) water, 13.8g (0.3 mole) ethanol and 10.4g (0.05 mole) of TEOS.

Method 3: Sample R = 8.

These gel samples were prepared as described for *(1)* above using 3.6g (0.2 mole) water, 13.8g (0.3 mole) ethanol and 5.2g (0.025 mole) of TEOS.

Method 4: Sample R = 12.

These gel samples were prepared as described for *(1)* above using 3.6g (0.2 mole) water, 13.8g (0.3 mole) ethanol and 3.67g (0.017 mole) of TEOS.

Method 5: Sample R = 15.

These gel samples were prepared as described for *(1)* above using 3.6g (0.2 mole) water, 13.8g (0.3 mole) ethanol and 2.88g (0.013 mole) of TEOS.

2.4 Absorption and emission spectroscopy.

UV-vis spectra were obtained using a Shimadzu 3100 UV-vis/NIR spectrophotometer interfaced with an Elonex PC-433 personal computer or a Shimadzu UV240 instrument. The solvent used for obtaining solution absorption measurements of the metal complexes was acetonitrile, unless otherwise stated. To acquire spectra of the solid gel samples the UV-vis/NIR integrating sphere attachment was used which employs the diffuse reflectance technique [12].

Emission measurements were obtained using an LS50B spectrometer interfaced with an Elonex PC-466 personal computer which employs Fluorescence Data Manager software. Room temperature measurements of solutions were carried out in acetonitrile unless otherwise stated with excitation and emission slit widths of 10 nm. At 77K the slits were set to 5 nm and a 4/1 (v/v) ethanol/methanol mixture was employed.

Quantum yields of emission, Φ_{em} were carried out using optically dilute measurements as described by Demas and Crosby [13] and are accurate to ± 10 %. The standard employed was $[Ru(bpy)_3]^{2+}$ which has a known quantum yield of 0.028 in an air equilibrated water solution [14]. Normalisation of absorbance intensity was carried out prior to emission measurements.

Ground and excited state pK_a measurements were carried out in a Britton-Robinson buffer solution (0.04 M H_3BO_3, 0.04 M H_3PO_4, 0.04 M H_3CCOOH) using the instrumentation described above. The pH of the solutions was adjusted using concentrated H_2SO_4 or NaOH and monitored using a Phillips PW9421 pH meter. Ground state pK_a values were determined monitoring the intensity changes in absorption as a function of pH. The point of inflection of a plot of percentage change in absorbance versus pH was used to determine this value. Excited state pK_a values (pK_a^*) were determined by monitoring emission intensity at a specific wavelength as a function of pH. These emission titrations were carried out using the isobestic point (obtained from the absorption titration data) as the excitation wavelength. The pK_a^* value was calculated using the pH_i (point of inflection on percentage change in emission intensity versus pH plot) in the Forster cycle equation [15].

Temperature dependent emission studies were carried out in a custom built quartz sample holder using a variable temperature liquid nitrogen cryostat PE1704 equipped with a Thor 3030 temperature controller. The absolute error on the temperature is estimated at ± 2 K. Excitation and emission slit widths of 5 nm were employed for these studies. Samples were degassed for 30 minutes under nitrogen prior to analysis.

2.5 Luminescent lifetime and temperature dependent luminescent lifetime measurements.

The lifetime measurements were carried out using a Q-switched Nd-YAG spectrum laser system. Room temperature measurements of solution samples were carried out in ethanol, unless otherwise stated. Temperature dependent studies of solutions were carried out in 4/1 (v/v) ethanol/methanol using samples of low concentration (*i.e.* < 10^{-4} M). No solvent was employed for the gel samples. Samples (both solution and solid sol-gel samples) were degassed for 30 minutes under nitrogen prior to temperature dependent studies. A custom built quartz sample holder was employed

inside a Thor C600 nitrogen flow cryostat equipped with a Thor 3030 temperature controller. The absolute error on the temperature is estimated at ± 2 K.

2.5.1 Data Analysis.

The fluorescence lifetime of a substance usually represents the average amount of time the molecule remains in the excited state prior to its return to the ground state. The fluorescence lifetime is generally equated with the time required for the intensity to decay to $1/e$ of its initial value. One of the commonly accepted rules is the exponential decay of isolated fluorescent molecules with lifetime τ :

$$\Phi(t) = \exp(-t/\tau) \qquad (2.1)$$

However, the luminescence of molecules emitting from heterogeneous systems frequently depart from first order kinetics. Thus, a plot of the logarithm of emission intensity versus time is non-linear. In kinetic studies of these systems the non-linear semi-logarithmic plot can be fitted to a multi-exponential decay model. For the delta function excitation (*i.e.* zero duration) with independently emitting noninteracting species the detector response is:

$$\Phi(t) = {}^{N}\sum_{i=1} K_i \exp(-t/\tau_i) \qquad (2.2)$$

$$\tau_i = 1/k_i \qquad (2.3)$$

where N is the number of emitting components. For the ith component, τ_i is the lifetime and K_i is the preexponential factor contributing to the signal at zero time. The K_i are functions of the spectral response of the detector, the concentration,

emission and absorption characteristics of each component, the spectral transmission properties of the filters and the spectral distribution of the exciting light [16].

For the studies reported in this thesis two different models were used to calculate the emission lifetimes. The first was a simple monoexponential decay law used to analyse those lifetimes conforming to single exponential decay behaviour:

$$\Phi(t) = A_1(1 - \exp(-k_1 t)) \qquad (2.4)$$

where A_1 is the pre-exponential factor and k_1 is the decay rate constant.

A multi- exponential decay expression was used to analyse the data for the gelled samples:

$$\Phi(t) = [(A_1(1 - \exp(-k_1 t)) + (A_2(1 - \exp(-k_2 t))] \qquad (2.5)$$

where A_1 and A_2 are the components pre-exponential factors, k_1 and k_2 are the decay rate constants. This model above assumes two populations of emitters, one which decays with a rate constant k_1 and another which decays with rate constant k_2. It was possible to add on more terms for higher exponential fit .

In order to ascertain which decay behaviour is indeed observed, it was important to be able to judge the quality of the fit. From the best fit parameters, the expected curve was calculated. Even for the correct model, the theoretical and observed decays differed slightly due to noise. In order to visualise these discrepancies, a plot of the weighted residuals (as percentage errors) versus time was made.

$$\% \text{ error} = [(F(t_i) - D(t_i)) / D(t_i)] \times 100 \qquad (2.7)$$

where $D(t_i)$ and $F(t_i)$ are the calculated best fit and observed decay data, respectively. For a good fit, the differences were small with a low % range (< 5 %) and randomly distributed plot whereas a bad fit yielded a cosine wave distribution. As mentioned earlier, the pre-exponential factors values depend on the experimental set-up. However, changes in the ratio of these factors A_1 and A_2 throughout an experiment may be deemed as significant so long as the experimental conditions remain constant throughout.

2.6 Chromatographic Techniques.

High performance liquid chromatography (HPLC) cation exchange experiments were carried out using a Waters 990 photo-diode array HPLC system, equipped with an NEC PAC III computer, a Waters pump model 6000 A, a 20 μl injector loop and a Partisil SCX radial PAK cartridge. The detection wavelength used was 280 nm. The mobile phase used 80:20 CH_3CN : H_2O containing 0.08 M lithium perchlorate, unless otherwise stated. A flow rate of 2 ml/min was employed.

Semi-preparative HPLC was carried out using an Applied Chromatography service pump (model RR066) and ACS detector (model 353 / UV/vis) fitted with a 1 ml injection loop and a Magnum 9 Partisil cation exchange column (10 mm / 25 cm). The mobile phase employed was 80:20 CH_3CN : H_2O containing 1 M KNO_3. the flow rate used was 2-3 ml/min depending on the elution of the complexes.

2.7 Molecular modelling.

Basic modelling of complexes and ligands was carried out using Hyperchem software. Molecular mechanics optimisation of ligand and complex structures was carried out employing the Hyperchem Polak-Ribier algorithm.

2.8 Nuclear Magnetic Resonance Spectroscopy.

Proton nuclear magnetic resonance (NMR) spectra were obtained using a Bruker AC 400 MHz spectrometer. Measurements were carried out in deuterated acetonitrile or DMSO.

2.9 References.

[1] J. Caspar, T.J. Meyer, *J. Am. Chem. Soc.*, 105, 5583, **1983**.

[2] C.T. Lin, W. Bottcher, M. Chou, C. Creutz, N. Sutin, *J. Am. Chem. Soc.*, 98, 6536, **1976**.

[3] R.J. Watts, G.A. Crosby, *J. Am. Chem. Soc.*, 93, 3184, **1971**.

[4] E. Ryan, R. Wang, J.G. Vos, R. Hage, J.G. Haasnoot, *Inorg. Chim. Acta*, 208, 49, **1993**.

[5] F. Burstall, F. Dwyer, E. Gyarfas, *J. Chem. Soc.*, 953, **1950**.

[6] G.A. Crosby, W. Elfring, *J. Phys. Chem.*, 80, 2206, **1976**.

[7] P. Belser, A. Von Zelewsky, *Helv. Chim. Acta*, 63, 1675, **1980**.

[8] R. Hage, A. Dijkhuis, J.G Haasnoot, R. Prins, J. Reedijk, B. Buchanan, J.G.Vos, *Inorg. Chem*, 27, 2185, **1988**.

[9] H. Hughes, Ph. D. Thesis, Dublin City University, **1993**.

[10] B.P. Sullivan, D.J. Salmon, T.J. Meyer, *Inorg. Chem.*, 17, 3334, **1978**.

[11] J. Baggot, G. Gregory, M. Piling, S. Anderson, K. Seddon, J. Turp, *J. Chem. Soc., Faradays Trans. II*, 79, 195, **1983**.

[12] H. Willard, Instrumental Methods of Analysis: 7th ed., Wadsworth, California, **1988**.

[13] J. N. Demas; G. A. Crosby; *J. Phys. Chem.*, 75, 991, **1971**.

[14] K. Makamura; *Bull. Chem. Soc. Japn.*, 55, 2697, **1982**.

[15] J.F. Ireland, P.A.H. Wyatt, *Adv. Phys. Org. Chem.*, 12, 131, **1976**.

[16] J.N. Demas, Excited State Lifetime Measurements, Academic Press, New York, **1983**.

Chapter 3.

The influence of the sol-gel matrix on the emission maxima of Ru(II) polypyridyl complexes.

3.1 Introduction.

Luminescence has been commonly used as a probe of porous materials for over a decade. Luminescence methods are very sensitive and can also be quite selective. By proper choice of excitation wavelength it is possible to selectively excite one species present in a complicated system. Transient methods can also be used to obtain information concerning luminescent solids. These lifetimes measurements can yield information concerning the number and type of excited state species, kinetic rate laws for the luminescence decay process, details of energy transfer mechanisms, effects of impurity additives (quenchers), distances between absorbers and emitters, and other kinds of information.

The basic concept of excited state techniques to characterise polymer systems is to use the photophysical and photochemical properties exhibited by a single probe molecule in the system to comment on its environment, its ease of movement, and on access of other molecules to the probe. In section 1.4 the capacity of ruthenium polypyridyl complexes to be employed as probes of their microenvironment was described. In particular, section 1.4.3 deals with the incorporation of such complexes in a sol-gel matrix. For the most part, these investigations have involved the spectroscopic behaviour of the archetype, $[Ru(bpy)_3]^{2+}$. In this chapter we have extended these studies to investigate the various parameters affecting the sol-gel transition by incorporating three tris ruthenium polypyridyl complexes $[Ru(L\text{-}L)_3]^{2+}$, where L-L represents one of the bidentate ligands 2-2'-bipyridine, 1,10-phenanthroline, or 4,7-diphenyl,1,10-phenanthroline. In addition, the sol-gel-xerogel transition is followed as a function of time and pH using the acid-base properties of $[Ru(phen)_2(H3Mptr)]^{2+}$. The purpose of these investigations is to gain improved understanding of the reactions which lead to the final glass structure, and the parameters which affect these reactions.

3.1.1 Understanding the sol-gel process.

An understanding of sol-gel processing has become increasingly important as the number of applications have grown. The sol-gel process offers a number of distinct advantages in many specific areas [1]. Among the advantages which sol-gel matrix offers in the area of laser material technology for example, include the photostability of the glass matrix, trapping of the dye molecule and its isolation from undesired interactions with its neighbouring dye molecules, impurities, and photodecompostition products; nonleachability of the dye; the ability to reach stable very high concentrations of the dye; reduction of translational, rotational, and vibrational degrees of freedom of the trapped dye [2]. The importance of the solid matrix which hosts the laser dye cannot be over emphasised since the nature of this matrix affects virtually all characteristics of the dye, *i.e.* it may cause spectral shifts of both absorption and emission of the incorporated dopant, it can affect photostability, and it may also alter the distribution between processes that the excited state may undergo, such as intersystem crossing, collisional energy loss, and consequently also the fluorescence lifetime. Developments in this area require a detailed knowledge of the overall reactions involved in the sol-gel process and how alterations in the various parameters affect the structural evolution and hence the form of the final gel.

Despite the numerous advantages this technology offers, the sol-gel process is not without problems. The process has a number of disadvantages from the standpoint of preparation of inorganic materials. Some of the disadvantages, such as the large shrinkage associated with the gelation process and shattering of gelled samples during drying have been outlined by Mackenzie and co-workers [3]. The most serious problem in any application of the sol-gel process at the present time, is the lack of scientific understanding of many complexities associated with the process. Thus, although numerous potential applications in the area of doped glasses exist [4], the development of these applications requires a good understanding of the structure of the doped sol-gel matrices, the properties of the matrices on a molecular

level, and the conditions that the oxide network imposes on the optical properties of the dopant. Little is known thus far concerning the fundamental aspects of the interaction between guest molecules and the inorganic host matrix, (whether for example, the molecules are truly entrapped and not merely adsorbed on the surface of the exterior of the pores), or about the parameters that control the luminescence the luminescence of molecules embedded in these inorganic systems. Molecular mobility, solvation, and reorientation processes have a dominant effect on electronically excited states. As such, the fluorescent dye is likely to behave differently in a solid matrix than in solution. Another interesting aspect is that the sensitivity of dyes to chemical environment suggests the potential for using luminescent probes during polymerisation, gelation and drying of the gels to investigate the sol-gel chemistry and/or structural development. The following two sections briefly reviews the use of spectroscopic probes employed to follow the gelation process through its various stages.

3.1.2 Probing the sol-gel chemistry.

Understanding the reactivity of doped sol-gel glasses is intimately linked with understanding the nature of the entrapment and the cage properties. Various spectroscopic techniques have been employed to study the dopant cage properties and their evolution with time along the sol→gel→xerogel transition. The chemical changes that occur during the polymerisation reactions are an important aspect of the gelation process which has been studied using molecular probes. A particular change which has been used to follow the rate of gelation is the change in the water:alcohol ratio (R). As the hydrolysis reaction proceeds, alcohol is continuously being produced and the amount of water to the amount of alcohol is steadfastly decreasing. Perhaps one of the earliest investigations in optical probing of the sol-gel process was that work carried out by Kaufman and co-workers [5]. In these studies the proton transfer from the excited state of pyranine, (8-hydroxy-1,3,6-trisulphonated

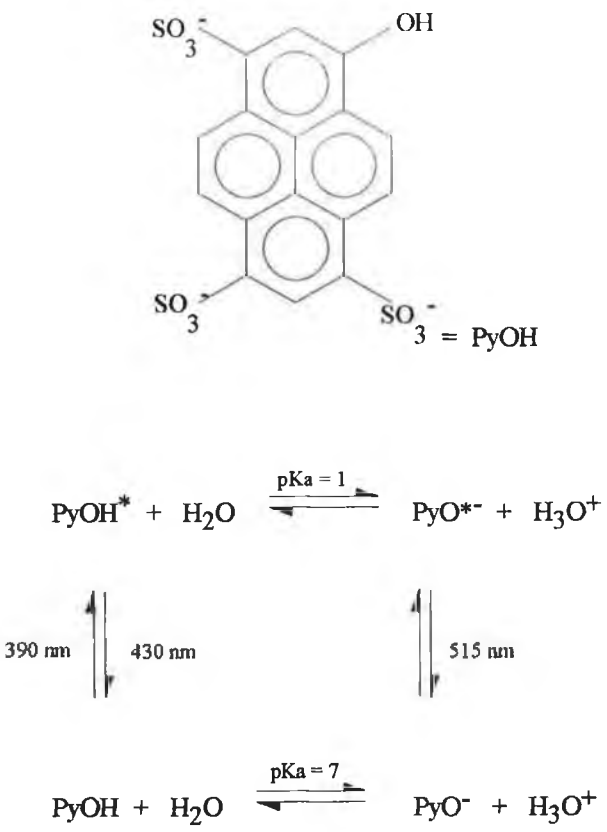

Figure 3.1 Chemical structure of pyranine and its absorption-emission processes.

pyrene), to surrounding water molecules was used as a sensitive fluorometric method for following directly and in detail the kinetics of water consumption during the early stages of the tetramethoxysilane sol-gel polymerisation process. Absorption and fluorescence spectra of pyranine are very sensitive to the proton-transfer phenomena. In an ionic medium, the SO_3-Na^+ groups are believed to be fully dissociated. In the ground state, the protonated molecule PyOH is reported to be a weak acid with a pK_a of about 7.5. In the excited state, however, it is a more acidic molecule, PyOH*, with a pK_a of about 1. The protonated ground-state form is stabilised in acidic solution (pH < 7.5) while the deprotonated form of the molecule PyO^- is present in basic conditions (pH > 10). The two forms present a maximum absorption at 400 and 450 nm, respectively.

After excitation by light, the competition between the kinetics of the protonation-deprotonation and the deactivation processes of the two forms controls the relative intensity of the green emission peak at 515 nm (due to the PyO^- form) and of the blue emission peak at 430 nm (due to the PyOH*) form). In water solution, the excited states have a fluorescence lifetime of approximately 10^{-10} s^{-1} and 3×10^{-7} s^{-1}, respectively. The relative intensities of the blue and green emission are affected by the proton donor-acceptor ability of the surrounding medium or by large changes in the pH from neutral to very acidic conditions.

The studies carried out by McKiernan and co-workers using this photoprobe revealed that alterations in water/silane ratio and in pH markedly effected the kinetic behaviour of water consumption [5]. Since then, Pouxviel and co-workers have extended these investigations to the emission and excitation of aluminosilicate sols and gels by the hydrolytic condensation of a double alkoxide, $(BuO)_2Al\text{-}O\text{-}Si(OEt)_3$ doped with the pyranine probe [6]. The sensitivity of pyranine to the internal solvent chemistry and to the ambient acceptor/donor proton characteristics of the surrounding matrix environment was further established. The chemical structure of pyranine and the absorption and emission processes are given in Figure 3.1.

In water rich environments the green emission band dominates because water acts as a proton acceptor. In alcoholic environments (specifically propanol rich environments) the blue band is dominant, because the pyranine remains protonated. The changes in the ratio of the intensity of the blue peak to that of the green that accompany aging and drying of the pyranine-doped aluminosilicate gels are shown in Figure 3.2. From the point of view of molecular scale structural characteristics, the gelation point emerged as a relatively unimportant point compared to the overall picture. These results are an indication that the changes in gel chemistry continue well beyond the gelation period. The macroscopic rigidity observed at the gel point does not mean that the reactive entities are immobile at the microscopic level.

The initial increase in F, was assigned to the consumption of water and production of alcohol which occurred during hydrolysis. Ultimately an equilibrium was established as the aging process continued. The changes in emission which

occurred during the drying of the gels can be explained as follows; Of the two solvents, water and propanol, present in the pore system at this time, propanol is the most abundant. The first step of drying corresponded to the vaporisation of propanol (propanol has a higher vapour pressure than water) which gave rise to an increase in the relative concentration of water in the remaining solvent. F decreased accordingly.

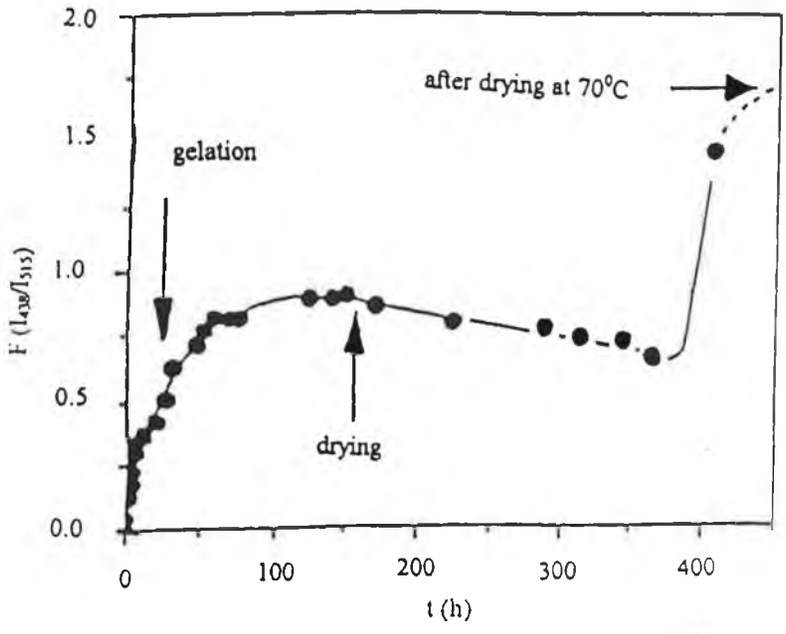

Figure 3.2 Evolution of the emission intensity ratio (F) of pyranine during gelation, aging and drying processes [6].

Later, as the drying continued, the free water content approached zero and F increased sharply. The most important result of these studies was the demonstration that there is a slower decrease in water content at the higher pH values. This conclusion was explained in terms of the gradual changes in the rates of the opposing processes of water consumption and water release with pH [6].

In recent years, coumarin dyes have been used to probe the effects of pH on sol-gel processing. In particular, the luminescence of coumarin 4 (7-hydroxy-4-methylcoumarin) in aged and dried gels has been examined in detail [7].

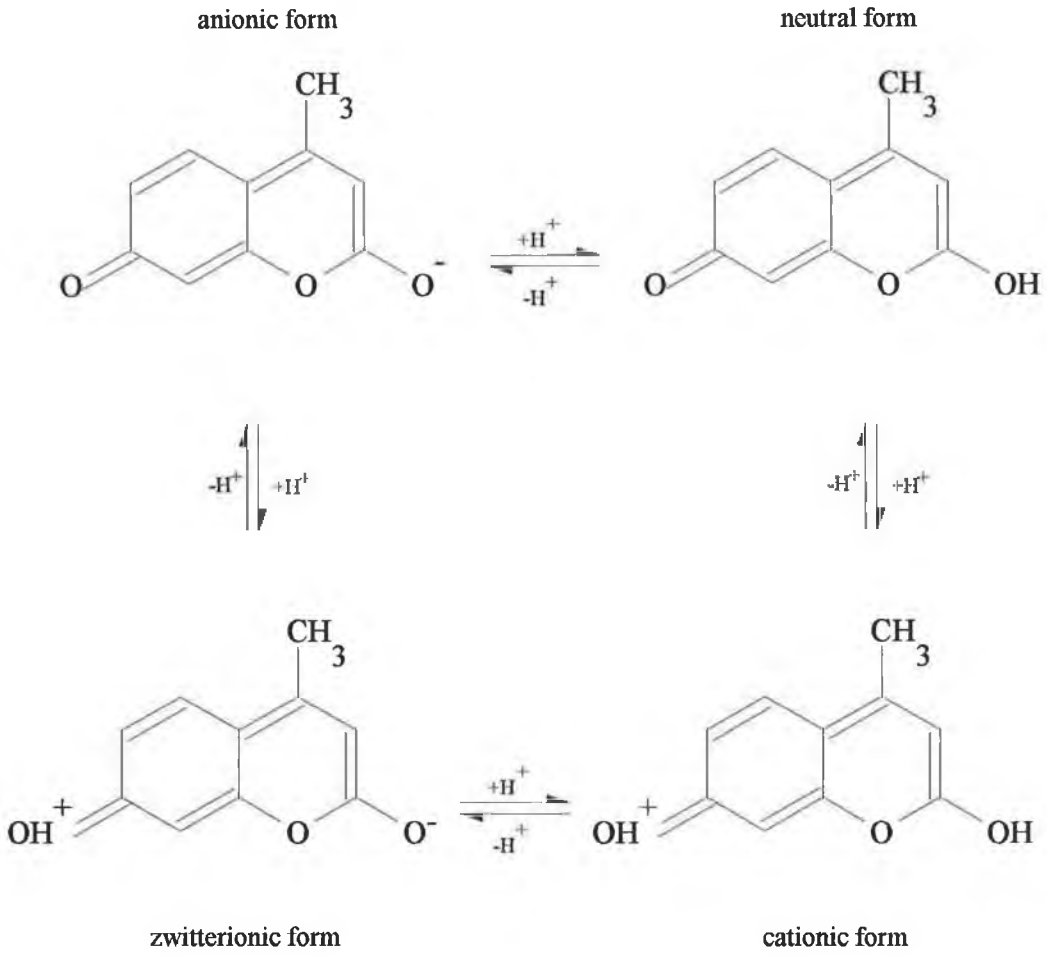

Figure 3.3 Molecular structure of different forms of Coumarin 4 and the corresponding acid-base equilibria.

The neutral form of coumarin 4 is the dominant species in aqueous alcoholic solutions for a wide range of pH and water contents. The various reactions leading to the different species responsible for the varying fluorescence energies are shown in Figure 3.3.

The luminescence spectra of coumarin 4 in the gels were found to be different from those in solutions. The differences suggested that the dye was not simply dissolved in solvent-filled pores in the gel. Consequently, changes in the surface composition of the gel led to changes in the interactions between coumarin 4

and the gel matrix and subsequently caused the luminescence of aged and dried gels to differ substantially from the luminescence in solution. In these studies, it was found that the luminescence of xerogels differs substantially from that of aged gels in two important respects. Firstly, the luminescence intensity from xerogels was much greater because gel shrinkage produced an increase in dopant concentration. The second important spectral difference was that the relative intensities of specific emission bands, caused by the formation of the different coumarin 4 species, exhibited substantial changes as drying occurred. Drying the gels synthesised under the most acidic conditions led to an increase in the intensity of the band from the protic form of coumarin 4. Drying the gels synthesised under less acidic conditions caused an increase in the intensity of the bands from the neutral and the anionic forms.

Pyranine and coumarin 4 are only two examples of the numerous photoprobes which have been employed in recent years to study the chemistry involved in the sol-gel process. The effect of varying the preparation parameters on the final xerogel has also been studied using such spectroscopic probes as oxazine-170 [8-9], thymol blue [10], and fluorescein [11] to name but a few.

3.1.3 Probing the sol-gel rigidity.

The question of rigidity of the sol-gel cage is one which has been addressed since the potential use of sol-gel materials was realised. One class of probes which have been used for monitoring the rigidity changes during the transformation from the sol to the dried glass are the 'rigidochromic' molecules $[ReCl(CO)_3L\text{-}L]$, where L-L represents a bidentate diimine. The emission energy position of these complexes depends substantially on the nature of L-L, and is associated with the lowest lying metal to ligand absorption band [12]. The emissive state is thought to possess a substantial degree of triplet character . The luminescence of these molecules changes markedly with changes in the rigidity of the medium into which they are

incorporated. Specifically, the wavelength of the emission shifts to the blue (*i.e.* higher energy), and the quantum yield increases in rigid media compared to the values of these properties in fluid solutions [12]. The term "luminescence rigidochromism" has been used to describe the substantial dependence of the emission maxima on environmental rigidity. This rigidochromic effect has been employed by McKiernan and co-workers as a sensitive means of probing the structural changes that occur in two sol-gel systems, namely, tetraethoxysilane (TEOS), and a mixed aluminosilicate system [13-14]. The idea behind these studies is that if the internal changes which occur during gelation are enough to produce measurable shifts in the emission energy of a rigidochromic molecule, then the luminescence spectra could provide a direct measure of the rigidity of the system on the molecular level. The magnitudes of the shifts of the luminescence maximum of the rigidochromic probe molecule were established in relevant test systems by using fluid and frozen solid ethanol and TEOS as test matrices. Large spectral shifts of approximately 2500 cm^{-1} in these systems were found. The changes in the luminescence were then followed during the sol-gel-xerogel transformation of the aluminosilicate and TEOS systems. In the former system, the emission maximum monitored the initial partial rigidification during aging and further followed the subsequent rigidification which occurred during drying. In the TEOS system, it was found that the emission energy of the probe did not shift during aging but exhibited a large change during drying. These contrasting results show that on a molecular level the two systems have quite different structural properties. The aluminosilicate gel contains small pores that trap the dye molecules and large pores that enable the solvent to diffuse. The small pores partially contract during aging without macroscopic changes of the gel. Further shrinkage occurs during drying. In contrast, in the TEOS system the $[ReCl(CO)_3bpy]$ molecules are not encapsulated into the gel and instead remain in the interstitial liquid phase of the system. The molecules adsorb onto the silica surface of the pore walls at the very last stage of drying.

This rigidochromic probe has also been used in fluorescence depolarisation experiments to probe the gelation, aging, and drying of silica and aluminosilicate sol-

gel derived materials. The fluorescence depolarisation technique uses polarised light to excite a fluorescent probe molecule. The probe molecules in the proper orientation will absorb the light and then luminesce at a later time which is dependent on their emission lifetime. If the molecule is held rigidly, the emission of these probes is polarised. If the molecule rapidly tumbles, emission from many orientations is observed and the polarisation is scrambled. The depolarisation provides a relative measure of the microscopic viscosity if the probe interacts with its environment. This scrambling of the emission polarisation is expressed as P, the degree of polarisation,

$$P = (I_{\Uparrow} - I_{\perp}) / (I_{\Uparrow} + I_{\perp}) \qquad (3.1)$$

where $I_{\Uparrow}$ and $I_{\perp}$ are the emission intensities parallel and perpendicular to the polarisation of the exciting light. When the probe is free to tumble, $I_{\Uparrow} = I_{\perp}$ and P therefore equals zero. When the emitter is immobilised P can have a value up to 0.5. The rigidochromic properties of the probe $[ReCl(CO)_3bpy]$ have been used in probing the contribution of rigid and fluid environments to the total P in a sol-gel matrix [15]. These studies follow both the microviscosity of the matrix and the restriction of the probe rotation due to pore collapse. They indicate that the local environment of the probe is fluid until well after gelation has occurred. The aluminosilicate gels experience large depolarisation changes in two distinct regions, one after gelation and the second after drying had begun. During the aging stage the gel is an open network filled with a viscous fluid phase. On the other hand, TEOS-derived silica materials were also found to have a network which does not restrict the probe motion, but the interstitial fluid is of lower viscosity. Upon drying these gels display an increased interstitial viscosity which restricts the motion of the probe. In both cases however, the changes in the degree of polarisation as a function of gelation, aging and drying for each system follow the same trend as the changes in the emission energy which occur with rigidity.

The use of the sensitivity of photochromism to environmental parameters has also been exploited in order to follow the structural and chemical changes that occur along the formation of the trapping glass. Photochromism is defined as the reversible light-induced colour change caused by absorption of a photon. The photochromic molecules which have been doped into sol-gel glasses undergo large structural changes after absorption of a photon. The rates of both the light-driven structural changes and of the back reactions are sensitive to the environment in the matrix. Both the rigidity and polarity of the sol-gel cage can be altered by changing the monomer, by the incorporation of suitable additives, and by copolymerisation. Investigations have recently been carried out by Levy and co-workers involving a series of photochromic spiropyrans [16]. When the entrapment was in pure SiO_2, the photochromism was observable only up to the wet-gel stage. Beyond this stage, the cage became so rigid that the isomerisation between the closed spiro form (colourless) and the open coloured zwitterion form stopped at the final dried xerogel stage. A straight forward method to relax the rigidity is to use a three-dentate monomer, rather than the normal tetraalkoxy monomer, thus reducing the degree of cross-linking. Indeed, entrapment of the spiropyrans in a sol-gel matrix prepared from ethyltriethoxysilane provided the needed flexibility for lasting photochromism. These observations were rationalised in terms of a gradual change in the environment of the photochromic molecule from solution environment encapsulated in a small cage to adsorption on the surface of the gradually forming silica surface, and in terms of the accompanying changes in the environmental polarity. In effect, a change in the environment of the spiropyran from solution to surface adsorption occurred.

Finally, the chemical and physical changes that occur during the sol-gel-xerogel transitions have been studied by using pyrene as a photophysical probe in both TEOS and TMOS systems [17]. This probe is a convenient and popular probe employed for studies in colloids and surface science by virtue of three characteristics:

(a) The ability to form an excimer, *i.e.* a complex between an excited-state molecule and one in the ground state. The excimer has a characteristic emission distinctive from the emission of a lone excited-state molecule.

(b) The luminescence spectrum of this molecule exhibits vibronic structure. The ratio of the intensities of the first to fifth peaks in the spectrum (I_1/I_5) is sensitive to the polarity of the environment. The ratio increases with increase in polarity.

(c) The singlet lifetimes of both monomer and excimer are usually long, exceeding in many instances 100 ns.

In the case of the TMOS gels, two general patterns were observed depending on the water to silane ratio. At low ratios, geometric irregularity and porosity built up gradually along the whole process, resulting first in an increase in excimer emission intensity as aggregation became more pronounced, followed by a decrease in excimer intensity (but an increase in the monomer band) as pyrene molecules became isolated. At high water to silane ratios, a smooth surface was formed. These results suggests that polymerisation-gelation occurs at low water to silane ratios whereas formation of a colloid followed by its gelation occurs at high water to silane ratios. Ethoxy groups slowed down the polymerisation reactions in comparison with methoxy groups, but the reaction rates coincided once all of the alkoxy groups were hydrolysed. Thus, the gel-xerogel transitions in both TEOS and TMOS systems proceed at the same rate. The pyrene excimer disappeared at the final xerogel state, proving that the sol-gel process is an effective method for isolating organic molecules. This matrix isolation feature has also been demonstrated with the use of the organic sulphorhodamine 640 [18].

The investigations carried out in this thesis involve a sol-gel system produced by employment of tetraethoxysilane in an aqueous-alcoholic environment. Because water and TEOS are immiscible, a mutual solvent such as alcohol, in this case

ethanol, was employed as a homogenising agent. In the studies presented here, it was important to choose a monomer which formed upon polymerisation Si-O-Si bonds, with reaction by-products which could be easily removed from the system. The sol-gel process consists of two main steps, the first of which falls into the domain of surface science. During this first step, a high surface area microporous glass is formed at room temperature by a complex sequence of polymerisation, sol formation, gelation and gel desiccation. The second step consists of annealing the porous glass at elevated temperatures, in order to close the pores. This results in a shrunken nonporous glass. The porous glass obtained at the first stage is the precursor to the second stage and, as such, determines not only the properties of the final glass but also the transition conditions from one to the other. This chapter is concerned only with the porous glass formed, and the structural evolution of the glass from its precursors, namely TEOS and water. The analytical approach employed here is the use of a variety of Ru(II) polypyridyl complexes as photoprobes of the sol-gel transition. The structures of the Ru(II) polypyridyl complexes cited in this chapter are given in Figure 3.4. The gels discussed in this and subsequent chapters have been prepared according to those appropriate methods described in Chapter 2 (*e.g.* A "Method 1 (5)" gel has been prepared according to method 1 as described in Section 2.2, *i.e.* R = 2, the number in parentheses indicates the pH of the water employed in the preparation of the gel. The temperature at which these samples are stored is 50^0C).

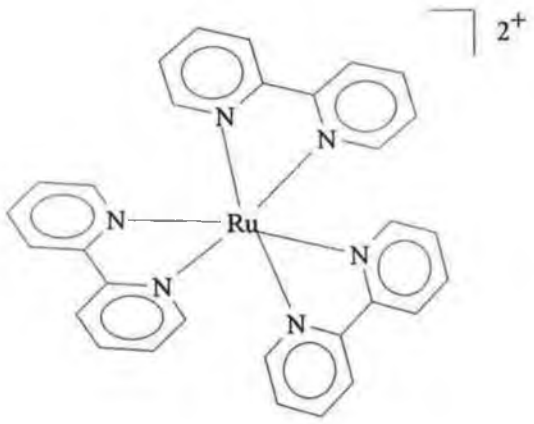

$[Ru(bpy)_3]^{2+}$

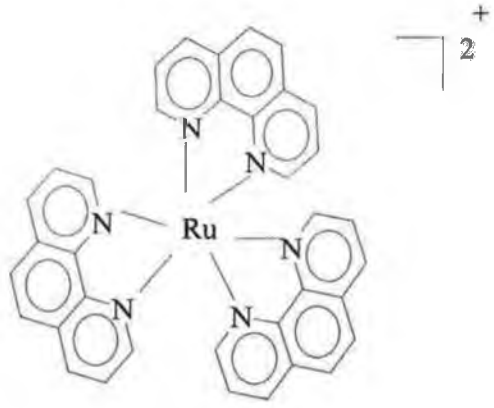

$[Ru(phen)_3]^{2+}$

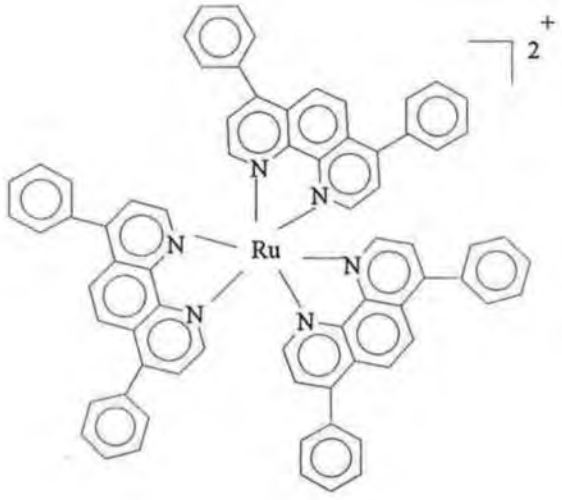

$[Ru(dpp)_3]^{2+}$

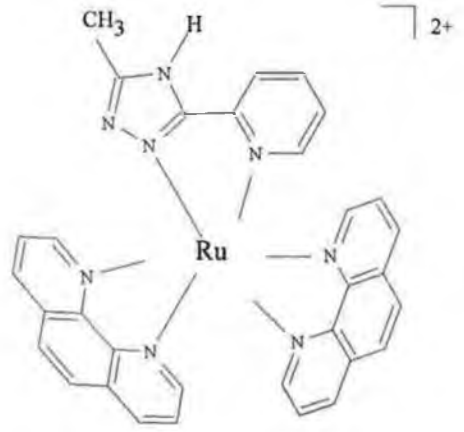

$[Ru(phen)_2(H3Mptr)]^{2+}$

Figure 3.4(a) The structures of the Ru(II) polypyridyl complexes cited in this chapter.

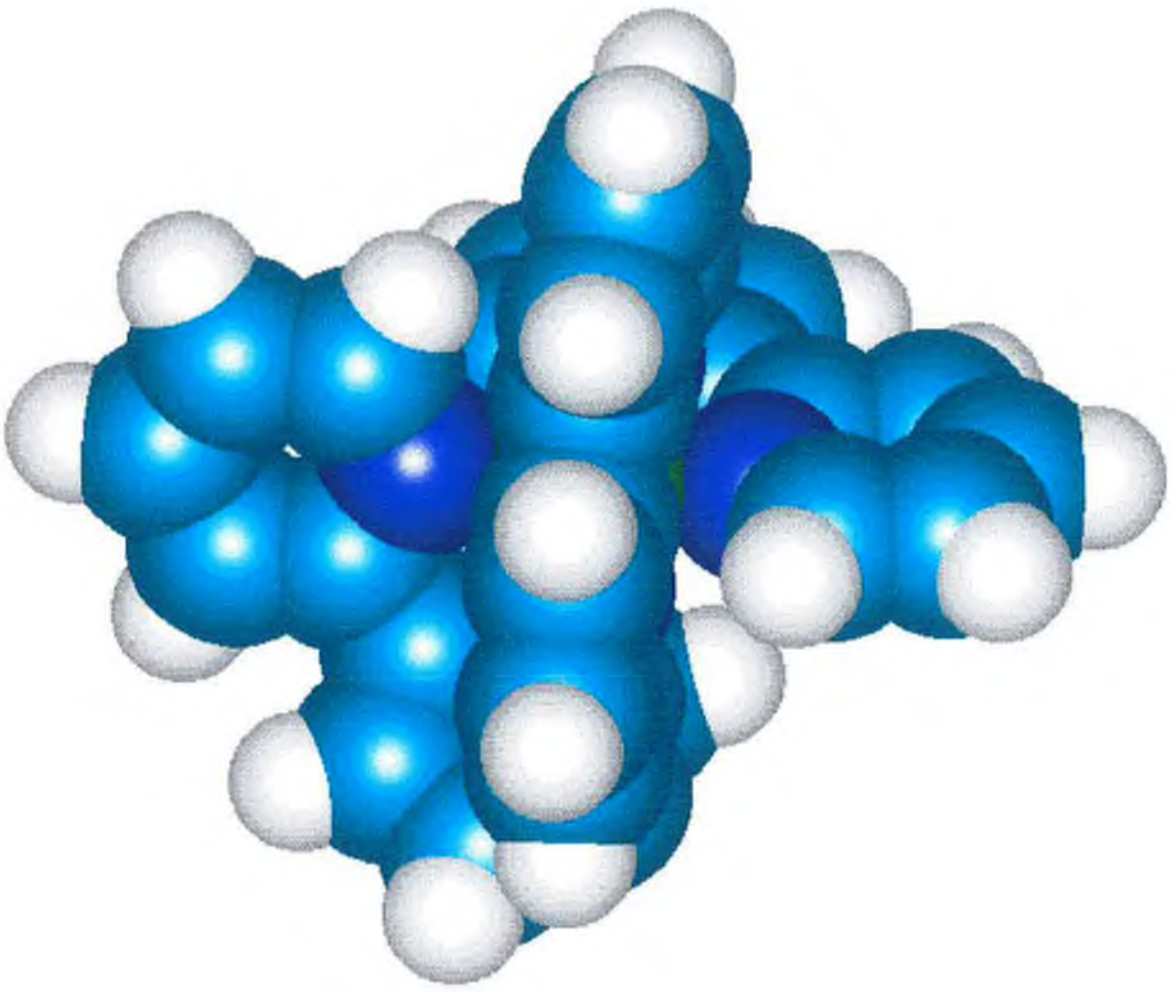

Figure 3.4(b) Computational model of $[Ru(bpy)_3]^{2+}$, where pale blue = carbon, dark blue = nitrogen, white = hydrogen and green = ruthenium.

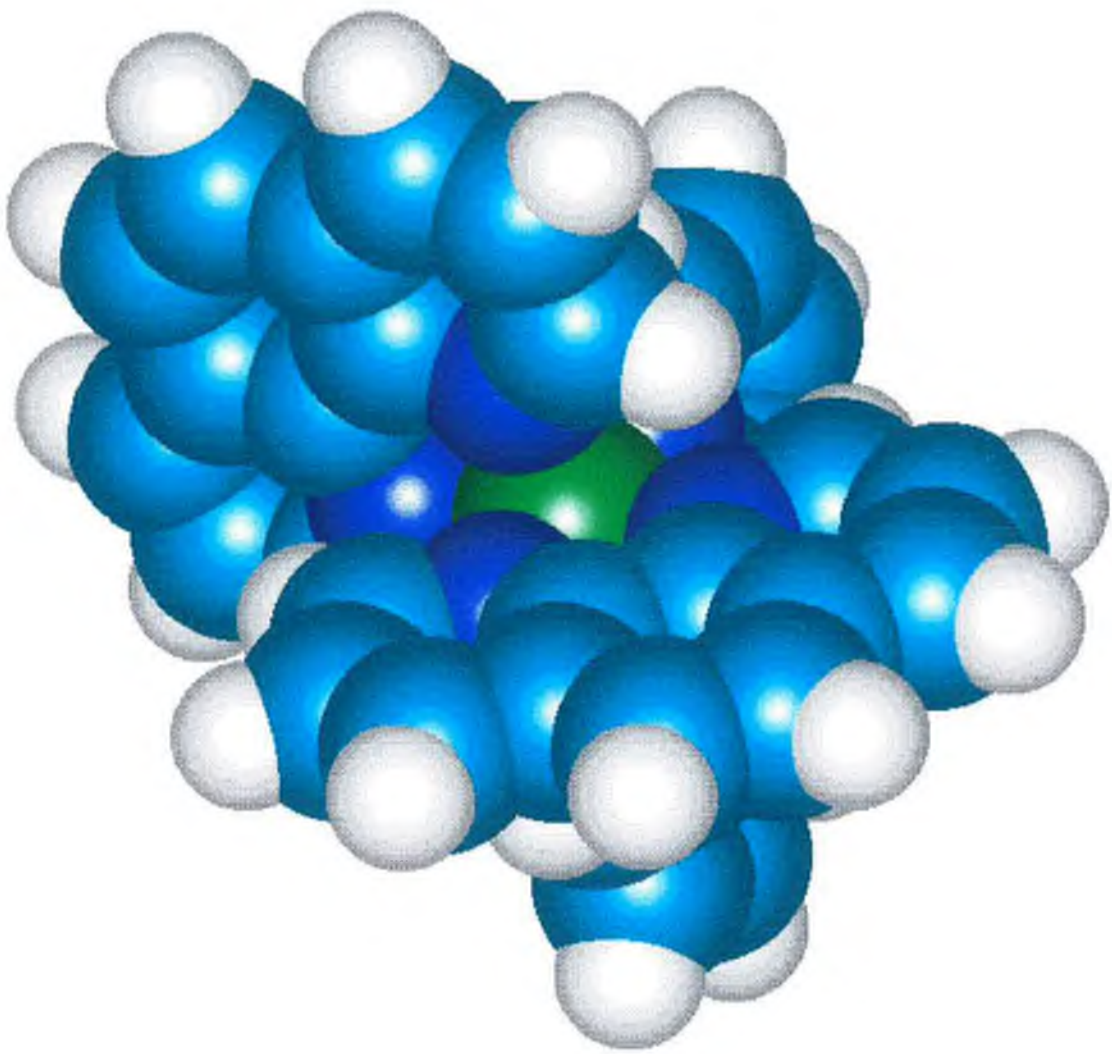

Figure 3.4(c) Computational model of $[Ru(phen)_3]^{2+}$, where pale blue = carbon, dark blue = nitrogen, white = hydrogen and green = ruthenium.

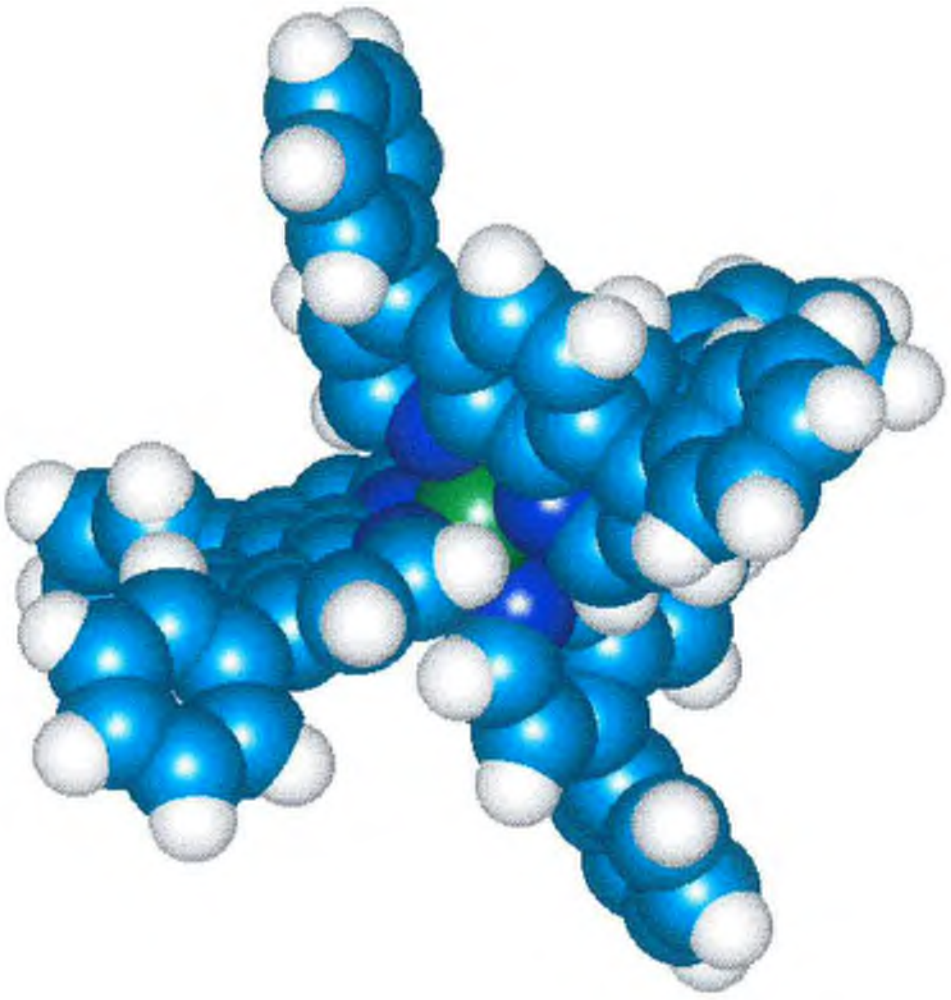

Figure 3.4(d) Computational model of $[Ru(dpp)_3]^{2+}$, where pale blue = carbon, dark blue = nitrogen, white = hydrogen and green = ruthenium.

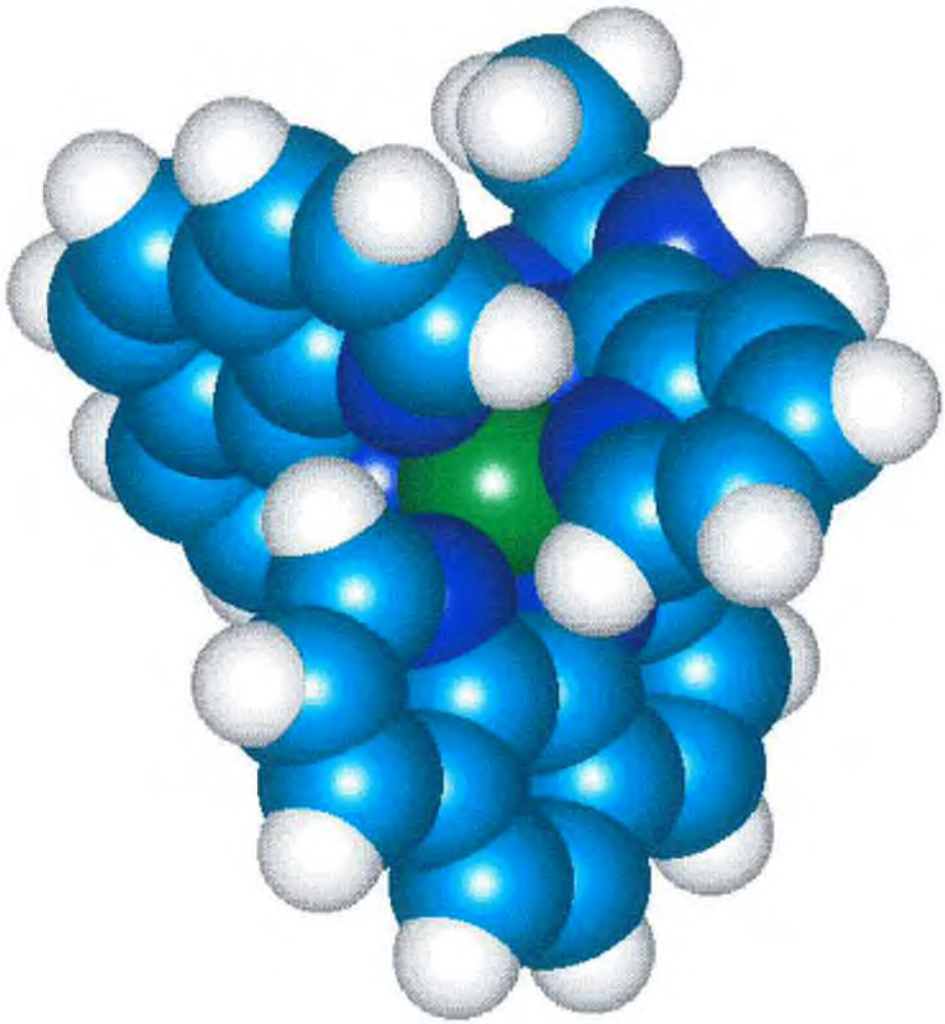

Figure 3.4(e) Computational model of $[Ru(phen)_2(H3Mptr)]^{2+}$, where pale blue = carbon, dark blue = nitrogen, white = hydrogen and green = ruthenium.

3.2 Results and discussion.

3.2.1 Electronic properties of $[Ru(L\text{-}L)_3]^{2+}$ in solution, (L-L = bpy, phen, dpp).

As mentioned in Chapter 1, the electronic properties of these ruthenium complexes are governed by charge transfer states which involve both the organic ligand and the metal. Metal-to-ligand charge-transfer involves promoting an electron from a metal orbital to a ligand orbital. Taking $[Ru(bpy)_3]^{2+}$ as an example, photoexcitation of the complex generates the charge-separated excited state:

$$[Ru^{II}(bpy)_3]^{2+} + h\nu \longrightarrow {}^{*}[Ru^{III}(bpy^{-})(bpy)_2]^{2+} \qquad (3.2)$$

The absorption spectra of these $[Ru(L\text{-}L)_3]^{2+}$ complexes in solution are dominated by a strong band at approximately 450 nm [20-21]. In the UV region, very intense ligand centred transitions are observed, most commonly π–π^* transitions. In the ^{3}MLCT excited state, an excited state electron is localised on one bpy ligand so that the dipole moment is much larger than that in the ground state. The solution electronic properties of the $[Ru(L\text{-}L)_3]^{2+}$ complexes employed in this chapter are given in Table 3.1.

Temperature influences the emission properties of the $[Ru(L\text{-}L)_3]^{2+}$ complexes in solution, particularly around the solvent's glass-to-fluid transition temperature, T_g. When the medium is cooled below T_g the intensity increases dramatically, the emission maximum shifts to higher energy, and the spectral peaks sharpen (see Figure 3.5). Luminescence energy shifts with changes in environment have been previously observed in MLCT excited states, and the effect was originally termed "rigidochromism" [22]. Detailed studies since that time have shown this to be a general phenomenon due to dipole reorientation time scales [23].

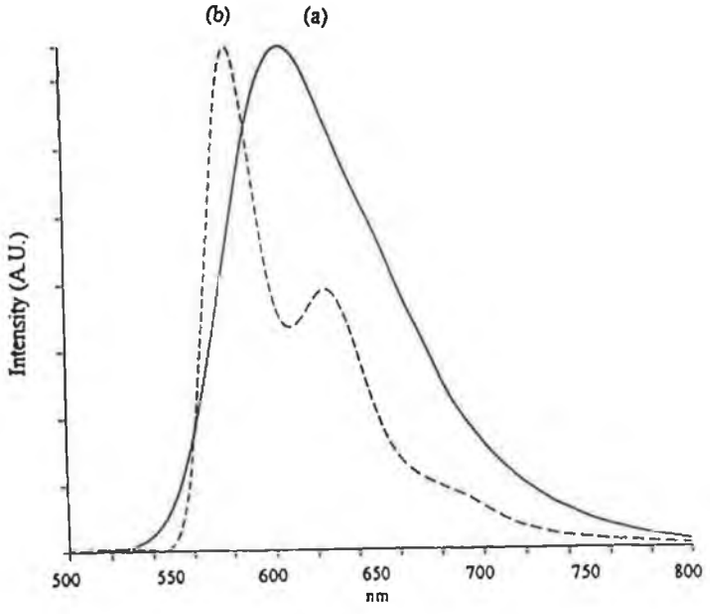

Figure 3.5 Emission spectra of $[Ru(bpy)_3]^{2+}$ measured in 4/1 ethanol/methanol (v/v) at (a) room temperature and at (b) 77K.

Table 3.1 Absorption and emission data of $[Ru(L\text{-}L)_3]^{2+}$ complexes in ethanol solution.[d]

Complex	Abs. λ_{max} (nm)[a]	Emission (nm)		Lifetimes (ns)		Φ_{em}[c]
		RT[a]	77K[b]	RT[a]	77K[b]	
$[Ru(bpy)_3]^{2+}$	452 (452)	609 (610)	580 (581)	700 (720)	4500 (5000)	0.016
$[Ru(phen)_3]^{2+}$	445 (446)	590 (589)	568 (567)	301 (290)	9100 (9800)	0.010
$[Ru(dpp)_3]^{2+}$	465 (465)	612 (610)	597 (595)	4200 (4680)	8900 (9580)	0.015

[a] For lifetime measurements at room temperature, samples were degassed by purging with argon.

[b] At 77K the solvent employed was ethanol/methanol 4:1 v/v.

[c] Quantum yields measured in ethanol. [d] All measurements carried out in our laboratory.

Values in parentheses indicate literature values (from [20] and references therein)

In alcohol glasses formed at 77 K the solvent dipoles are "frozen" in averaged orientations appropriate to the ground state electronic configuration of the complex. In fluid solution the dipole orientation times are (usually) short on the scale of the lifetime of the excited state. Whereas, in frozen matrix solvent dipoles reorient very slowly with respect to the excited state, and may not reach equilibrium with the electronic distribution of the polar excited state, $[Ru^{III}(bpy^{-})(bpy)_2]^{2+}$, within its lifetime. The result is an increase in the energy of the transition as manifested by the blue shift observed in the emission. For $[Ru(bpy)_3]^{2+}$ a shift in emission wavelength from 609 nm (16420 cm^{-1}) at room temperature to 580 nm (17240 cm^{-1}) at 77 K was observed in 4/1 ethanol/methanol. In comparison, the changes in the emission spectrum of $[ReCl(CO)_3bpy]$ in ethanol as a function of temperature exhibits a similar, though more pronounced rigidochromic shift [14]. At room temperature the emission maximum was found to be 612 nm (16340 cm^{-1}) while at 77 K the emission maximum was 529 nm (18900 cm^{-1}). The overall shift in emission energy is greater for $[ReCl(CO)_3bpy]$ than for $[Ru(bpy)_3]^{2+}$ (~2500 cm^{-1} versus ~800 cm^{-1}). The more the polarity of the excited state molecule is different from the polarity of the ground state molecule, the more the reorganisation process is effective in stabilising the excited state. This suggests that $[ReCl(CO)_3bpy]$ experiences a greater change in polarity upon excitation than $[Ru(bpy)_3]^{2+}$.

A second important influence of low temperature on the emission spectra of $[Ru(bpy)_3]^{2+}$ is the increase in the intensity and lifetime of the emission observed. This is associated with two factors, the first is solvent dependent. At low temperature the complex and its surroundings are rigid, making it less susceptible to vibronic coupling to low frequency, high amplitude Ru-N vibrations, which contribute to k^{nr}. Solvent interactions which may also contribute to k^{nr} are also reduced considerably in frozen matrix, as is oxygen quenching since diffusion of O_2 to the excited sites is restricted. The second factor is related to the ^{3}MLCT-^{3}MC transition. This transition is thermally activated. At 77K there will not be sufficient thermal energy to populate ^{3}MC, and as a result intensity and lifetime are observed to increase. The blue shift in emission energy which accompanies the solution to

glass transition in the alcohol glass for $[Ru(dpp)_3]^{2+}$ is less pronounced than for $[Ru(bpy)_3]^{2+}$ and $[Ru(phen)_3]^{2+}$ suggesting that this particular complex is less sensitive to its environment. This is discussed in greater detail in the following sections.

3.2.2 Electronic properties of $[Ru(L\text{-}L)_3]^{2+}$ in the sol-gel matrix.

3.2.2.1 General electronic properties of $[Ru(bpy)_3]^{2+}$ in a sol-gel matrix.

Incorporation of $[Ru(bpy)_3]^{2+}$ into silica gels shows that the inorganic sol-gel matrix has an effect on the photophysical properties of the cation as compared to that of alcoholic or water solutions. The emission from fluorophores generally occurs at wavelengths which are longer than those of light absorption. This loss of energy between absorption and reemission of light, or Stokes' shift, is a result of several dynamic processes. These processes include energy losses due to the dissipation of vibrational energy, redistribution of electrons in the surrounding solvent molecules induced by the altered dipole moment of the excited fluorophore and the solvent. Specific interactions include hydrogen bonding and formation of charge transfer complexes. Absorption of light occurs in about 10^{-15} s, a time scale too short for significant displacement of nuclei (Franck-Condon principle), but evidently adequate for the redistribution of electrons. Generally, the electronically excited states of transition metal complexes possess dipole moments which are larger than in the ground state. As a result, the absorption of a photon by the fluorophore results in essentially instantaneous creation of a dipole, which perturbs the environment surrounding the fluorophore. Subsequent to excitation, the solvent responds by a reorganisation of the solvent cage around the fluorophore. This process is called solvent relaxation, the timescale of which is dependent on the physical and chemical properties of the solvent. In most cases, spectral shifts in fluorescence maxima observed are associated with the effects of solvent molecules having insufficient time

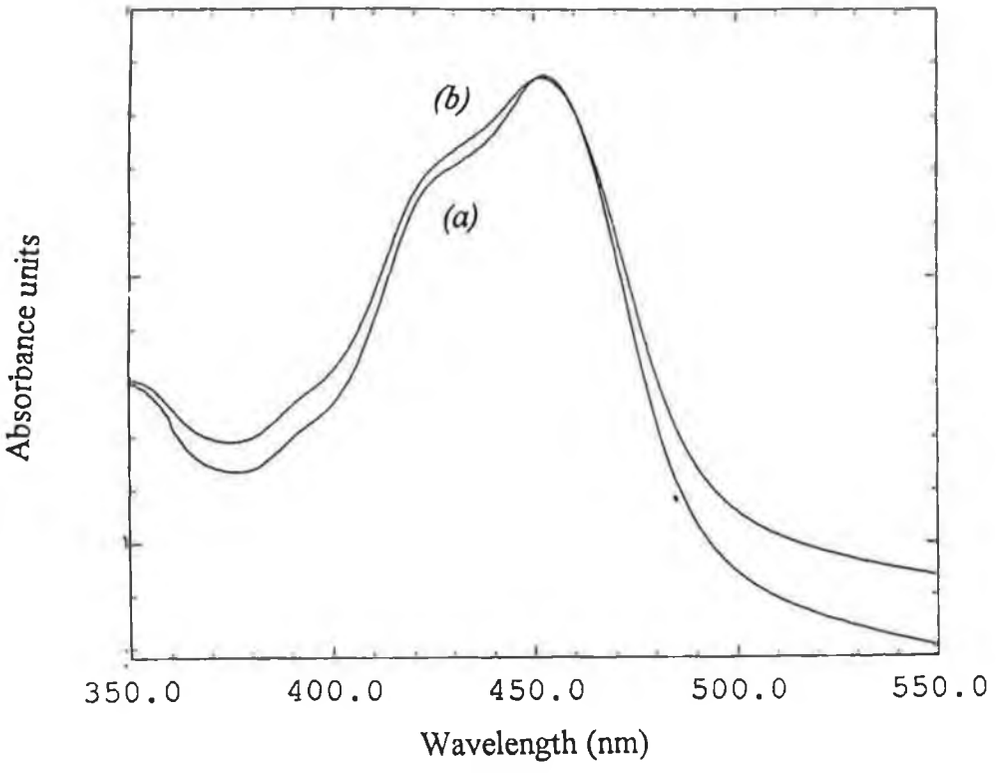

Figure 3.6 Normalised absorption spectra of $[Ru(bpy)_3]^{2+}$ in (a) the initial sol and (b) the final xerogel.

to reorient themselves around an equilibrium excited state [23] The absorption spectrum of $[Ru(bpy)_3]^{2+}$ incorporated into a sol-gel matrix immediately after preparation and in the xerogel is given in Figure 3.6. As can be seen from this diagram, the position of the ^{1}MLCT band is unaffected by the gel matrix, and remains unperturbed even after a period of 6 months. The π–π^* transitions of the bipyridine ligands are obscured by gel absorption. However, while the absorption spectra of this ruthenium complex is largely preserved before and after gelation, the photoluminescence properties are dramatically altered by the gel matrix. This perturbation manifests itself in higher emission intensities, blue shifted emission maxima, and the appearance of nonexponential emission decays with long average lifetimes.

It was noticed that as the reactions from the initial sol to the aging gel proceed, the $[Ru(bpy)_3]^{2+}$ emission intensity from any given sample increased. During the gelation stages, the most drastic chemical and physical changes of the sol-

During the gelation stages, the most drastic chemical and physical changes of the sol-gel system occur. The initial sol, which is completely fluid, is transformed into a solid and brittle material. The augmentation of intensity which takes place during this time is most likely due to the isolation of the trapped molecules from deactivating bimolecular processes (specifically oxygen quenching). In addition, the luminescence intensity from xerogels is much greater than that observed from the corresponding aging gel. This is because of the massive gel shrinkage which accompanies the drying stage as excess solvent is allowed to evaporate. Effectively, an increase in dopant concentration and thus luminescence intensity is brought about. The isolation of the guest molecules and the rigidity of the surroundings are also reflected in the luminescence lifetime [24].

The emission spectrum of a luminescent species, provides a convenient method of determining whether or not the molecule remains intact in the glass. As mentioned previously, a blue shift in the emission of $[Ru(bpy)_3]^{2+}$ is induced when the motion of the solvent molecules surrounding the excited state molecule is restricted. Thus, incorporation of $[Ru(bpy)_3]^{2+}$ into a sol-gel matrix causes the position of the photoluminescence peak to move to a shorter wavelength. This phenomena has been previously reported by Matsui and co-workers [25] and it has been suggested that it is caused by the destabilisation of the ^{3}MLCT excited state. In effect, this excited state is not completely stabilised within its lifetime. As a direct result of this, the energy gap between it and the ground state is widened, and a corresponding increase in the emission energy is observed. Recent electrochemical measurements of $[Ru(bpy)_3]^{2+}$ doped sol-gel processed SiO_2 films demonstrate that the ground state potential is unchanged from its solution value [26]. This result together with the unperturbed absorption spectra rule out the possibility of the blue shift in emission being caused by a stabilisation of the ground state. Figure 3.7 shows the emission spectra of $[Ru(bpy)_3]^{2+}$ as measured in the initial sol immediately after preparation (Method 2 (5)), and in the final xerogel.

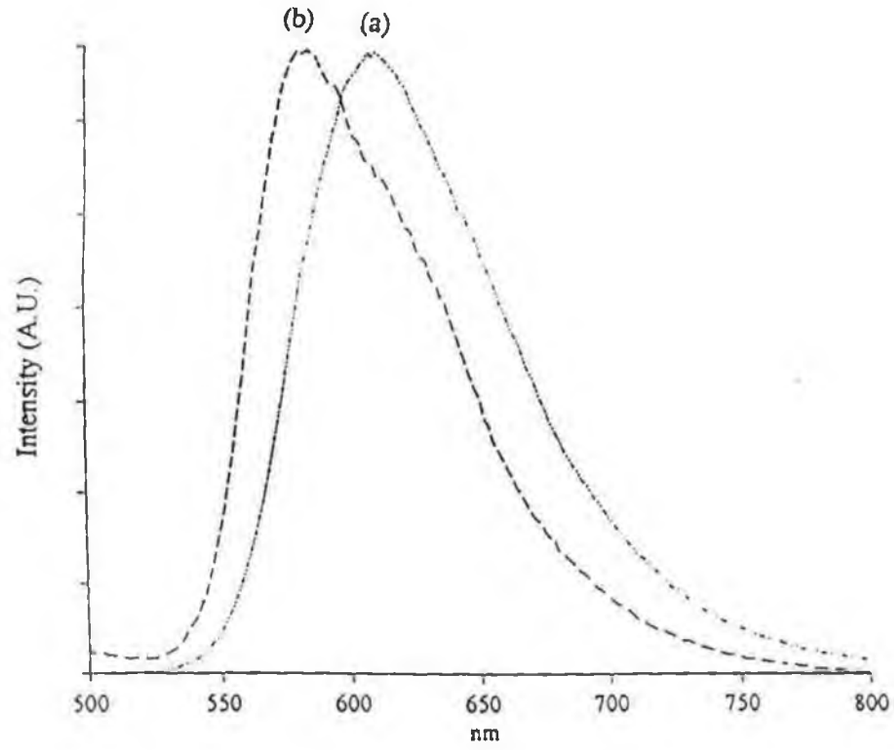

Figure 3.7 Normalised emission spectra of $[Ru(bpy)_3]^{2+}$ in (a) the initial sol and (b) the final xerogel, prepared at pH 5, R=4.

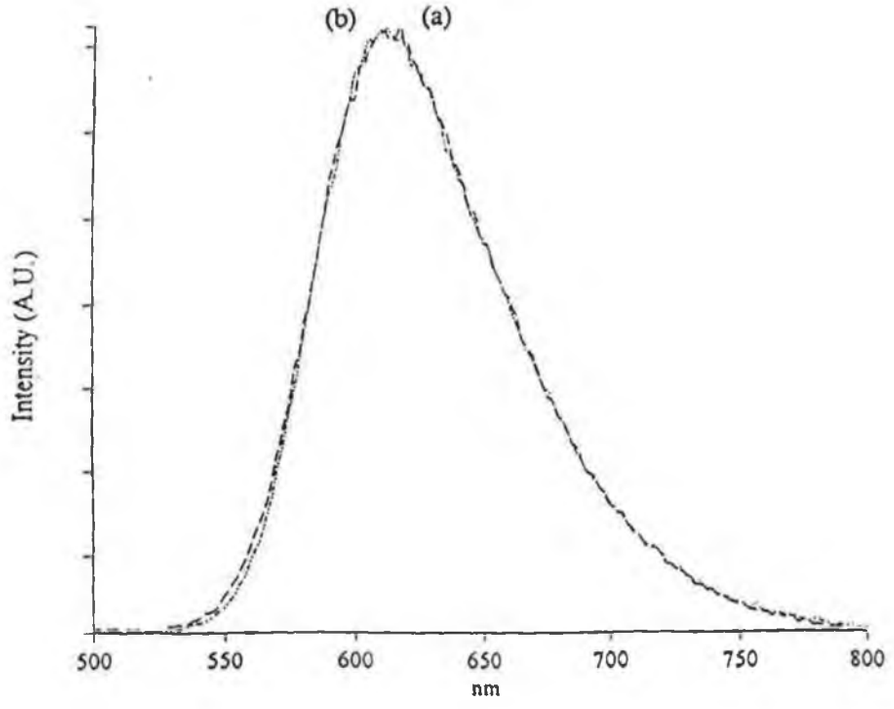

Figure 3.8 Normalised emission spectra of $[Ru(dpp)_3]^{2+}$ in (a) the initial sol and (b) the final xerogel, prepared at pH 5, R=4.

The emission maximum shifted from 609 nm in the solution to 588 nm in the xerogel (*i.e.* a total shift of ~ 590 cm^{-1}). This shift in emission energy is similar to that observed upon going from room temperature to 77K for an alcoholic solution of $[Ru(bpy)_3]^{2+}$ (*i.e.* 609 to 580 nm ~ 800 cm^{-1} shift).

3.2.2.2 The effect of pH on the gel matrix.

It is this inability of the ^{3}MLCT excited-state of $[Ru(bpy)_3]^{2+}$ to fully relax within its lifetime which forms the basis of the investigations described in the following sections of this chapter. The sensitivity of the fore mentioned shift in emission energy which occurs as the sol-gel-xerogel can be employed to relay information as to the environment of the luminescent probe. Both the extent of this shift and the rate at which it occurs provide information as to the final structure of the xerogel and the parameters which effect the reaction mechanisms involved in its formation.

As can be seen from Table 3.2, the photoluminescence properties of $[Ru(phen)_3]^{2+}$ doped gels behave similarly to those doped with $[Ru(bpy)_3]^{2+}$, specifically a blue shift in the emission energy is observed in all cases along the sol-gel transition. For both of these complexes, the initial pH of the solution strongly influences the position of the final λ_{max}. In this regard, it is important to recognise that the effect of the variation of the initial pH on gel formation is essentially to change the kinetics of polymerisation and to produce charging of the gel surface.

Table 3.2 Emission data for $[Ru(L\text{-}L)_3]^{2+}$ in sol-gel matrix.

Complex	Method 2 (1)[$] Initial λ_{max}(nm)	Method 2 (5)[$] Initial λ_{max}(nm)	Method 2 (1)[$] Final λ_{max}(nm)	Method 2 (5)[$] Final λ_{max}(nm)
$[Ru(bpy)_3]^{2+}$	610	610	597	588
$[Ru(phen)]^{2+}$	597	596	582	574
$[Ru(dpp)_3]^{2+}$	612	611	611	611

[$] Values in parentheses indicates pH of water used in the sol-gel preparation.

Colloidal silica has an isoelectric point of pH 2.2 [27]. Above this pH, the surface charge of the silica is negative owing to the presence of $\equiv Si\text{-}O^-$ groups on the surface, while at pH less than 2.2 a positive charge is induced on the silica surface by $\equiv SiOH_2^+$. These surface charges are potential adsorption sites for ionic forms of guest molecules as well as for water molecules [28]. The results in Table 3.2 suggest that the $[Ru(bpy)_3]^{2+}$ and $[Ru(phen)_3]^{2+}$ dications are more rigidly held to the negatively charged silica polymers than to those which are positively charged, through electrostatic interaction. Thus a more pronounced shift in photoluminescence maximum is observed for those gels prepared at higher pH. On comparison of the data observed in Tables 3.1 and 3.2, one can see that for these two particular complexes, a rigidochromic effect is observed on passing from a sol to a xerogel similar to that which was observed on passing from an alcoholic solution at room temperature to a glass at 77K. However, the higher energy of the emission energy peak observed at 77K suggests that the environment experienced by the complex in this glass matrix is more restricted than that of the final xerogel at room temperature.

While these two Ru(II) polypyridyl complexes exhibit shifts in emission energy during the initial sol-gel stages of this TEOS system, the emission maximum of the $[ReCl(CO)_3bpy]$ complex employed by McKiernan and co-workers remained fixed at approximately 600 nm from the initial liquid state to almost the end of drying

[14]. A blue shift for this Re(I) complex in a TEOS system only occurs with the final removal of the alcohol. The authors suggest that during the gelation and aging phase, the Re(I) probe molecules are confined in the interstitial liquid phase and are not incorporated into the silica polymer network. The adsorption of the of the active dyes onto the surface of a pore once the water and ethanol are almost completely evaporated may account for the evolution of the $[ReCl(CO)_3bpy]$ fluorescence toward the characteristic blue shift of the rigidified state. This stage is also accompanied by the shrinkage of pores. Therefore, while the Re(I) probe molecules are unconstrained in a solvent-like environment until the drying phase, the emission energy of $[Ru(bpy)_3]^{2+}$ and $[Ru(phen)_3]^{2+}$ molecules suggest that these complexes are more immediately affected by the initial sol-gel reactions. These differences reflect the different nature of the Ru(II) and Re(I) probes. While the Ru(II) dopants are positively charged, the rhenium probe is a neutral molecule.

In contrast to $[Ru(bpy)_3]^{2+}$ and $[Ru(phen)_3]^{2+}$, no shift of the emission energy peak is observed for those gels doped with $[Ru(dpp)_3]^{2+}$. The photoluminescence maximum remains at approximately 612 nm and appears indifferent to the surface charge of the silica sol-gel matrix (Figure 3.8). As mentioned earlier, on excitation a molecule may no longer be in its most stable configuration. Because of electronic rearrangement and especially because of changes in dipole moment, the organisation of solvent molecules around the ground state molecule is not necessarily the most stable one for the excited state. If the excited state lifetime is long enough, the solvent and the excited state molecules can rearrange and acquire a more stable configuration for the excited state. With respect to $[Ru(dpp)_3]^{2+}$, a possible explanation for the unchanging photoluminescence is that upon excitation, the excited state electron is localised on the phenanthroline moiety of one of the ligands [29], the bulk of the two phenyl groups shielding the excited state from 'experiencing' the influence of the solvent. The polarity of the excited state may have the same magnitude as the other two complexes studied, but the effect of solvent reorientation is not as significant because the polar excited state is in effect

internalised and hence shielded within the molecule. Therefore, the excited state electronic distribution of the complex as seen by its surroundings does not differ that much from the ground state and no shift in λ_{max} is observed. Another possibility is that the $[Ru(dpp)_3]^{2+}$ molecules may be trapped in, or create, bigger pores. In this thesis, the ruthenium dopants are introduced at the initial mixing stage. When polymerisation is completed, the dopant molecules are entangled in the inorganic network. It is possible that as the polymer network forms, it surrounds the dopant molecules and, due to the large size of the $[Ru(dpp)_3]^{2+}$ molecules, larger pores may be formed.

It still remains uncertain as to what holds the Ru(II) dopants within the final sol-gel matrix. The nature and mechanism for such encapsulation are of considerable interest because of the potential application of Ru(II) doped glasses [24,30,31]. It is significant to note that these ruthenium dopants are dications. Above the isoelectric point, when the silica surface is negatively charged, it could be argued that incorporation of these guest molecules is primarily electrostatic in nature. However, it is more likely that a number of factors are responsible for holding these guest molecules within the matrix. For those gels doped with $[Ru(dpp)_3]^{2+}$, a concentration gradient was noticed in the final xerogel with the surface which had been closest to the external atmosphere being darker in colour. For the other Ru(II) complexes employed here, the colour of the entire xerogel appeared uniform. As the excess alcohol and water molecules evaporate during the drying process, they are drawn up through the gel towards the pierced lid through which they escape. $[Ru(dpp)_3]^{2+}$ molecules are more hydrophobic relative to those of $[Ru(bpy)_3]^{2+}$ and $[Ru(phen)_3]^{2+}$. Because the $[Ru(dpp)_3]^{2+}$ dopant molecules are less affected by electrostatic interaction, it is likely that a proportion of these dopants will be drawn along with the solvent, in which they are dissolved, to the exposed surface, thus leaving a greater concentration at this surface. This suggests that, as was the case for $[ReCl(CO)_3bpy]$, the $[Ru(dpp)_3]^{2+}$ molecules may remain dissolved in the interstitial liquid phase of the TEOS derived silica gel until the final removal of the solvent. It is

possible that the $[Ru(dpp)_3]^{2+}$ molecules which remain behind as the solvent evaporates are physically entrapped or immobilised in pores within the inorganic matrix.

In order to shed some further light on this subject, crude leaching experiments were carried out. An aged sample, (Method 2 samples), of each complex at the two extreme pH's of 1 and 5 was placed into separate 5 cm^3 scintillation vials containing deionised water which were then sealed and left to stand for three days. The luminescence spectra of the surrounding solution was then measured. Firstly, it should be noted, that in all cases only a small proportion of the dye molecules leached out, with the vast majority remaining in the gel matrix. Secondly, it was noticed for those samples containing $[Ru(bpy)_3]^{2+}$ and $[Ru(phen)_3]^{2+}$ that the luminescence intensity of the solution surrounding those gels prepared at pH 1 was significantly stronger (by a factor of 5 for $[Ru(bpy)_3]^{2+}$ and almost 7 for $[Ru(phen)_3]^{2+}$) than those prepared at pH 5. No notable difference between pH 1 and 5 was observed for $[Ru(dpp)_3]^{2+}$ samples, the photoluminescence intensity of both solution being almost equal. These results further suggest that the effect of electrostatic interactions of $[Ru(dpp)_3]^{2+}$ within the gel matrix is less pronounced than for the gels doped with $[Ru(bpy)_3]^{2+}$ or $[Ru(phen)_3]^{2+}$. Contrary to what was expected, the concentration of the leached $[Ru(dpp)_3]^{2+}$ did not appear substantially greater than the other two Ru(II) complexes, suggesting that these molecules are somehow immobilised within the gel. While the concentration gradient of these samples appeared faded to the naked eye, it still remained present to a large extent. These results indicate that electrostatics alone cannot explain dopant binding, and that more than likely a combination of such interactions and different types of physical immobilisation are responsible for dye incorporation.

Figures 3.9 and 3.10 show the changes in the emission maximum for $[Ru(bpy)_3]^{2+}$ and also $[Ru(phen)_3]^{2+}$ (Method 2 samples) during the sol-gel-xerogel transition prepared under different pH conditions. The arrowheads in these diagrams indicate the gel time (t_g) for each particular sample.

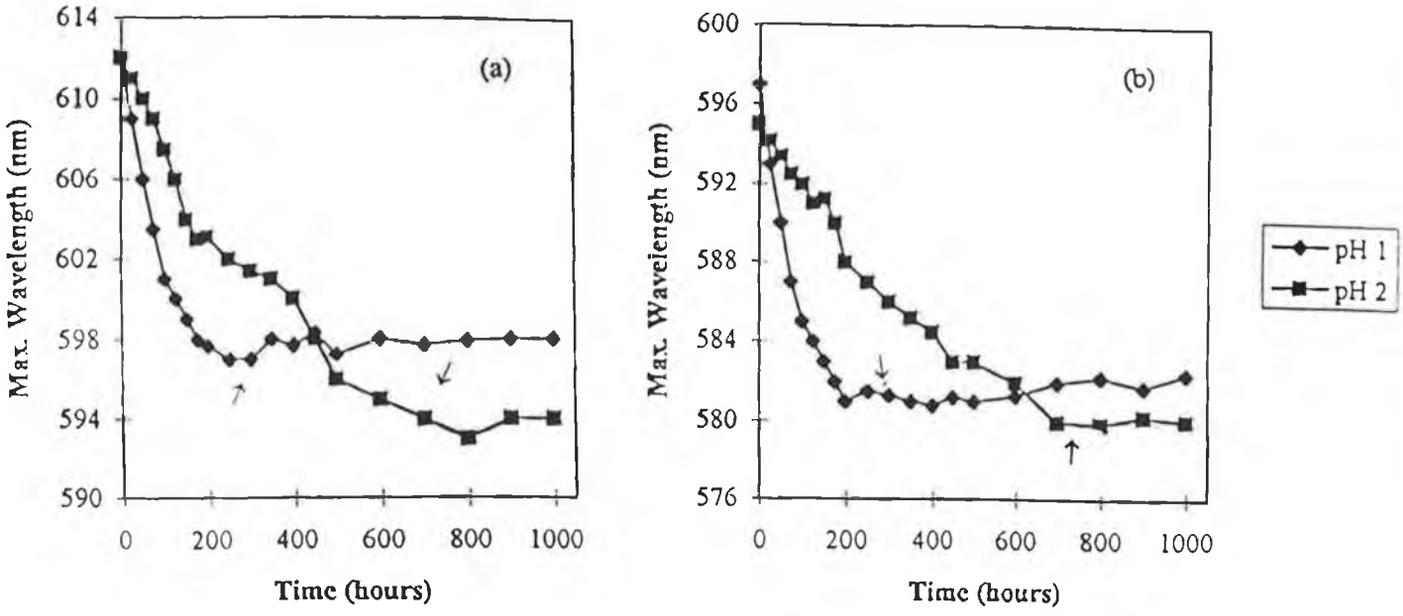

Figure 3.9 Maximum emission wavelength of (a) $[Ru(bpy)_3]^{2+}$ and (b) $[Ru(phen)_3]^{2+}$ over time during the sol-gel process at pH 1 and pH 2 (where R = 4).

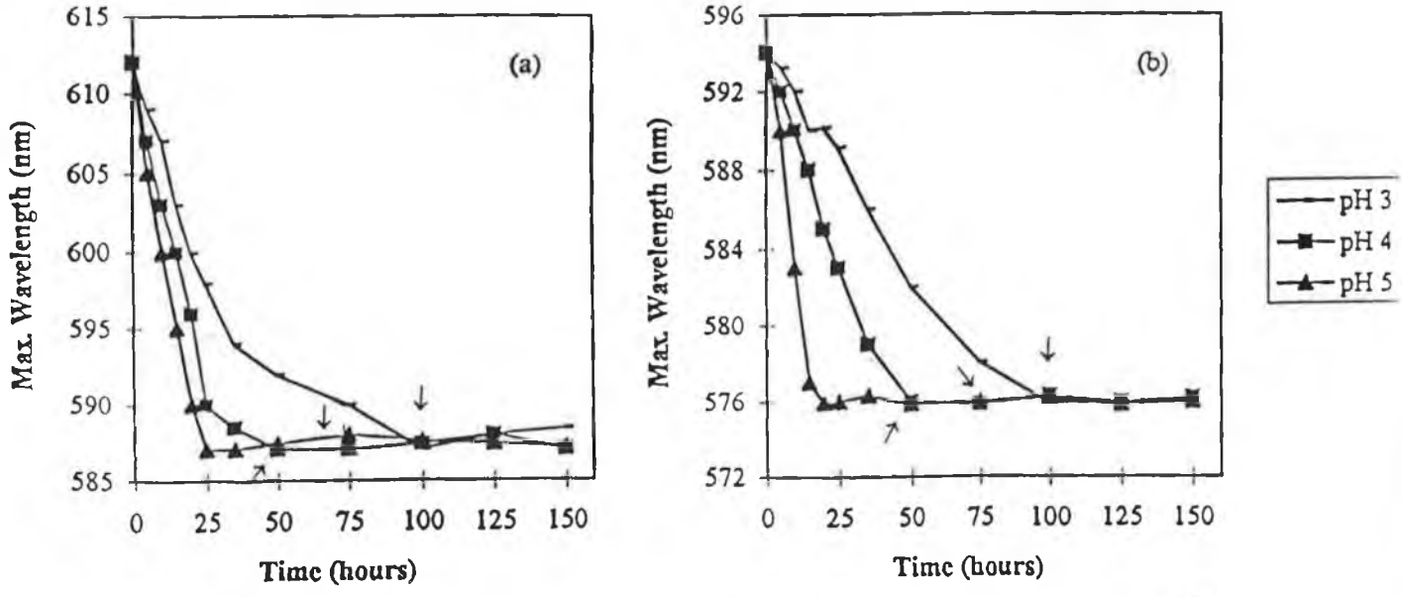

Figure 3.10 Maximum emission wavelength of (a) $[Ru(bpy)_3]^{2+}$ and (b) $[Ru(phen)_3]^{2+}$ over time during the sol-gel process at pH 3, pH 4 and pH 5 (where R = 4).

The observations in these studies can be rationalised in terms of changes in the kinetics of the hydrolysis and polycondensation reactions which accompany different pH regimes [32-33]. The structure of the sol-gel glass evolves sequentially as the product of successive hydrolysis and condensation reactions (and the reverse reactions: esterification and alcoholic or hydrolytic depolymerisation). In the case of $Si(OEt)_4$ which was employed in these studies presented here, the entire sol-gel reaction is written as follows:

$$m\text{Si(OEt)}_4 + 2m\text{H}_2\text{O} \longrightarrow (\text{-O-Si-O-})_m + 4m\text{EtOH} \qquad (3.3)$$

During the hydrolysis reaction, the water molecules are consumed by the hydrolysis of the silicon alkoxide, and simultaneously, alcohol and silanol groups are generated. The hydrolysis and condensation reactions for the sol-gel process can be written as shown in the following equations:

$$\text{Si(OEt)}_4 + m\text{H}_2\text{O} \xrightarrow{k_h} \text{Si(OH)}_m\text{(OEt)}_{4-m} + m\text{EtOH} \qquad (3.4)$$

$$2(\equiv\text{SiOH}) \xrightarrow{k_{cw}} \equiv\text{SiOSi}\equiv + \text{H}_2\text{O} \qquad (3.5)$$

$$\equiv\text{SiOH} + \equiv\text{SiOR} \xrightarrow{k_{ca}} \equiv\text{SiOSi}\equiv + \text{ROH} \qquad (3.6)$$

where k_h, k_{cw}, and k_{ca} are the hydrolysis rate constant, the water producing condensation and the alcohol producing condensation rates respectively [34-36]. Each alkoxy functional group is first hydrolysed to a silanol group and one alcohol molecule is produced for each water molecule consumed. If condensation is completed, an ≡Si-O-Si≡ linkage and two alcohol molecules are produced for each water molecule consumed. The hydrolysis reaction forms silicic acid (m = 4) or partially hydroxylated silicate intermediates (Equation 3.4), and is followed by

condensation reactions (Equations 3.5 and 3.6). According to Iler, polymerisation occurs in three stages:

(a) Polymerisation of monomer to form particles,
(b) Growth of particles,
(c) Linking of particles into chains, then networks that extend throughout the liquid medium, thickening it into a gel [27].

The degree of the sol-gel reaction most likely determines the position of the photoluminescence peak. The effect of pH is complicated. At low pH the hydrolysis rate is fast, producing monosilicic and disilicic acids which act as potential nuclei for further particle growth [37]. Due to the large number of equivalent nucleation centres, the particles formed are large in number but small in size. At high pH, the rate of hydrolysis is diminished and therefore far fewer nucleation centres are produced. Since the condensation and hydrolysis reactions proceed on nearly the same time scale, newly hydrolysed molecules, rather than nucleating into new particles, attach to pre-existing polymer structures, and as a result, fewer but significantly larger particles are formed. The total rate of gelation is a function of both the hydrolysis and the polymerisation reactions. Iler has divided the polymerisation process into three approximate domains: < pH 2, pH 2-7, and > pH 7. In the case of silica, pH 2 appears as a boundary, since the point of zero charge (PZC), where the surface charge is zero, and the isoelectric point (IEP), where the electrical mobility of the silica particles is zero, both occur at a pH quite close to 2. In this respect, pH 2 represents a metastable region where the observed gel times are quite long. Silanols become more acidic with the extent of condensation of the siloxane network to which they are attached [27].

The influence of the initial preparation pH on the sol-gel process is reflected both in the position of the photoluminescence peak and also the relative gel time, t_g, of the sample. Under acidic conditions the rate of hydrolysis is large compared to the

rate of condensation. Firstly, below pH 2, the polymerisation rate is proportional to the concentration of H^+ [27,36]. In this respect, increasing the acidity causes an increase in the rate of change of emission maximum (see Figure 3.9). It is not surprising therefore, that the rate of change of emission and indeed the time to gelation (as indicated by the arrowheads) is faster for the sample prepared at pH 1 than that at pH 2. The gel point of the solution was defined as the time at which the solution loses its fluidity as determined by visual observation upon inverting the sample. A prolonged gel time of approximately 700 hours was obtained for samples prepared at pH 2 further indicating the slow nature of the sol-gel reactions at this pH. However, the final change in the position of the emission maximum for the gel prepared at pH 1 is less than that observed at pH 2, reflecting the positive charge of the surface silanols at the lower pH.

As can be seen in Figure 3.10, above the isoelectric point, as the pH was increased, the rate of change in the emission maximum also increased. This observation is consistent with the predicted behaviour of hydrolysis and condensation as a function of pH [36]. As mentioned in the introduction, the relative gel time of a given sample is minimised at neutral pH (see Figure 1.6). Above the isoelectric point, the polymerisation process is catalysed by the hydroxyl ions and proceeds by an entirely different mechanism. Depending upon the pH of the medium, an ionisation equilibrium is established to produce deprotonated silicon anions, ≡Si-O^-, which subsequently condense by reacting with silanol groups. The condensation reaction is maximised near neutral pH, thus explaining the increased rate of change of emission maxima on changing the pH from 3 to 5.

$$\equiv\text{Si-OH} + OH^- \xrightarrow{fast} \equiv\text{Si-}O^- + H_2O \qquad (3.7)$$

$$\equiv\text{Si-}O^- + \text{HO-Si} \xrightarrow{slow} \equiv\text{Si-O-Si}\equiv + OH^- \qquad (3.8)$$

Therefore, it would be expected that a continuous decline in gelation time with increasing OH concentration. A decrease in gelation time was observed for these samples with t_g of the sample prepared at pH 3 > pH 4 > pH 5. Above pH 7, polymerisation occurs by the same nucleophilic mechanism (Equations 3.7 and 3.8). However, because all the condensed species are more likely to be ionised and therefore mutually repulsive, growth occurs primarily by the addition of monomers to more highly condensed particles rather than particle aggregation. In this pH regime, particles are formed that, after reaching a critical size, become stable towards gelation due to mutual repulsion effects. As pH is increased beyond this point (> pH 7), the size of the sol particles must correspondingly increase in order to overcome this repulsive charge effect.

The $[Ru(bpy)_3]^{2+}$ and $[Ru(phen)_3]^{2+}$ molecules probe the microviscosity of the microenvironment around the polymers onto which they are adsorbed [38]. As can be seen from Figure 3.10, the result of increasing the pH from 3 to 5 is effectively, to increase the rate at which the position of the emission maximum of the particular incorporated ruthenium complex changes occurs. The emission maximum does not differ significantly beyond the gelation point, indicating $[Ru(bpy)_3]^{2+}$ to be so rigidly held to the polysiloxane polymers that further decrease in the energy gap between the ^{3}MLCT state and the ground state does not occur [25].

As mentioned previously, these two Ru(II) polypyridyl complexes behave dissimilarly to those rigidochromic probes employed by McKiernan and co-workers [14]. While the $[Ru(bpy)_3]^{2+}$ and $[Ru(phen)_3]^{2+}$ molecules probe the initial reactions of the sol-gel process, the Re(I) probe monitors changes in the rigid nature of the gel matrix during drying in a TEOS sol-gel system. This further implicates the importance of electrostatic interaction as opposed to the trapping of the Ru(II) complex within pores as a reason for the shift in emission maximum. The Ru(II) complexes are dications, possessing a 2^+ charge and as such they become involved in electrostatic interactions early on in the sol-gel reaction. In effect the ionised silanols produced in the early stages of the sol-gel process may act as potential adsorption

sites for the $[Ru(bpy)_3]^{2+}$ and $[Ru(phen)_3]^{2+}$ cations. The $[ReCl(CO)_3bpy]$ is a neutral molecule and remains dissolved in the solvent phase until the drying stage at which time it is brought into direct contact with the surrounding sol-gel network. As such, the Re(I) probe will be less sensitive to the initial sol-gel reactions. Our observations are also in contrast to those investigations carried out using pyrene where spectral changes of this particular probe molecule occur mainly after gelation. It is known that although gelation has occurred and the sample appears rigid on a macroscopic level, a fairly fluid-like micro-environment with an open structure still exists [17]. These differences can be ascribed to the different nature of these probe molecules. Thus, through judicious choice of the spectroscopic probe, various aspects of the sol-gel-xerogel transition can be investigated.

3.2.2.3 The effect of temperature on the sol-gel matrix.

In the previous section, all the samples were stored at 50 ^{0}C, as described in Chapter 2. Most chemical reactions, especially those occurring in liquid solution are dependent on temperature. Frequently, the gelation process of a sol-gel system requires very long times at room temperature. The effect of increasing temperature is to effectively speed up the rate of hydrolysis and condensation, which reduces the gelling time t_g [39]. This is reflected in Figure 3.11, where the effect of three different temperature conditions on the shift in emission maximum for $[Ru(bpy)_3]^{2+}$, of otherwise identically prepared gels is displayed (Method 2 (1) samples). Again, the arrowheads indicate the t_g of each particular sample. It can be seen here that the rate of change of the emission λ_{max} is much faster at the higher storage temperature of 50^{0}C than at room temperature or 4 ^{0}C. The change in the photoluminescence energy of the sample stored at 4 ^{0}C does not conclude until approximately 2000 hours, and is not shown in this diagram.

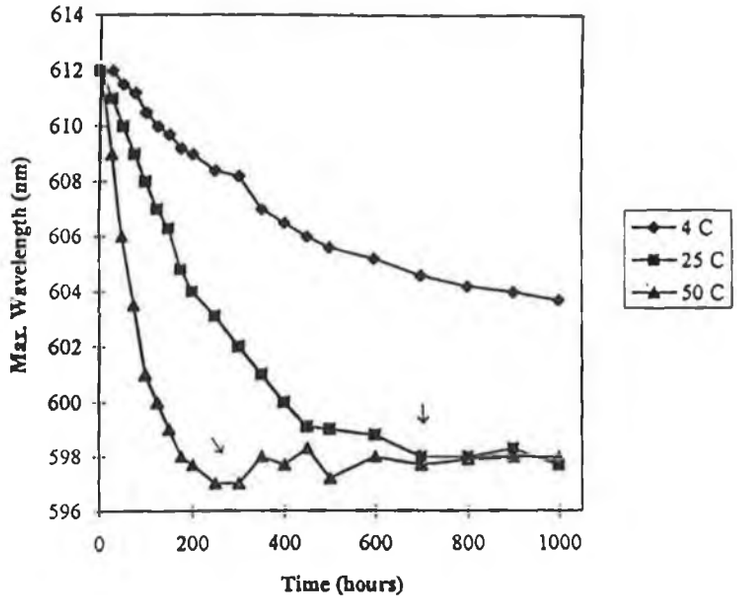

Figure 3.11 Position of the maximum emission wavelength of $[Ru(bpy)_3]^{2+}$ over time during the sol-gel process at 3 different storage temperatures (where R = 4)

Importantly however, the final λ_{max} observed for each of the three gels prepared is identical, which suggests that the final structure, as probed by $[Ru(bpy)_3]^{2+}$, of each of the gels is the same. Similar results were obtained for those gels doped with $[Ru(phen)_3]^{2+}$ Gels doped with $[Ru(dpp)_3]^{2+}$ prepared under identical conditions and stored under these various temperatures showed no change in the position of the photoluminescence peak.

3.2.2.4 The effect of water to silane ratio (R) on the sol-gel matrix

As can be seen from Figure 3.12, the rate of change in emission maximum is increased as the water to silane ratio is increased from 2 to 8, all other parameters kept constant The samples shown in these figures were all prepared according to Method 1(1), Method 2(1) and Method 3(1), and stored at 50^0C. Again, the number

in brackets indicates the pH at which the sample was prepared. Attempted preparation of gels with over-stoichiometric R ratios (R > 4) at pH 5 failed. It was found that under these high pH conditions, phase separation occurred. A possible explanation is that alone, TEOS and water are immiscible. The function of ethanol in the initial reaction vessel is to act as a mutual solvent for both of these reactants. At pH 1, the rate of hydrolysis is very fast [27]. Therefore, under these acidic conditions, as the TEOS is added dropwise to the reaction vessel, it is at once hydrolysed, with the result that water is immediately consumed with ethanol being produced according to Equation 3.4. Therefore the R ratio decreases instantly, and the ethanol concentration increases. This increase in ethanol concentration which occurs almost instantaneously at low pH, ensures that sufficient alcohol is present and prevents phase separation at these high R values. At pH 5 however, the rate of hydrolysis is slow. In order for phase separation to be avoided at high R values, the initial concentration of ethanol would have to be increased to an amount sufficient to ensure homogenisation of the TEOS and water. Interestingly, on preparation of a gel at pH 5 with an intermediate R value of 6, the initially immiscible solution became clearly miscible after approximately 2 hours of vigorous stirring. This suggests that adequate ethanol has been evolved only after this time. The sol-gel transition for different starting compositions of TEOS, ethanol, and water mixtures under acidic conditions has recently been reported by Chang and co-workers [40].

Because water is produced as a by-product of the condensation reaction, an R value of 2 is theoretically sufficient for complete hydrolysis and condensation to yield anhydrous silica as shown by the net reaction in Equation 3.3. However, even when excess water is employed (R>>2), the reaction does not go to completion. Instead, a spectrum of intermediate species is generated.

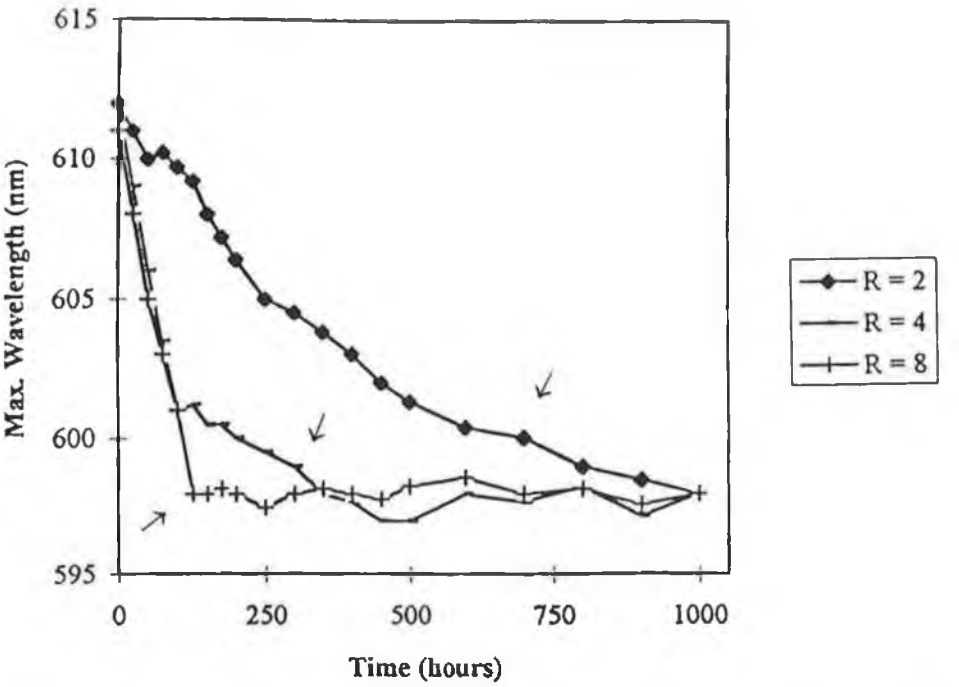

Figure 3.12 Position of the maximum emission wavelength of $[Ru(bpy)_3]^{2+}$ over time during the sol-gel process at 3 water/silane ratios, R = 2, R = 4, R = 8 (where pH = 1).

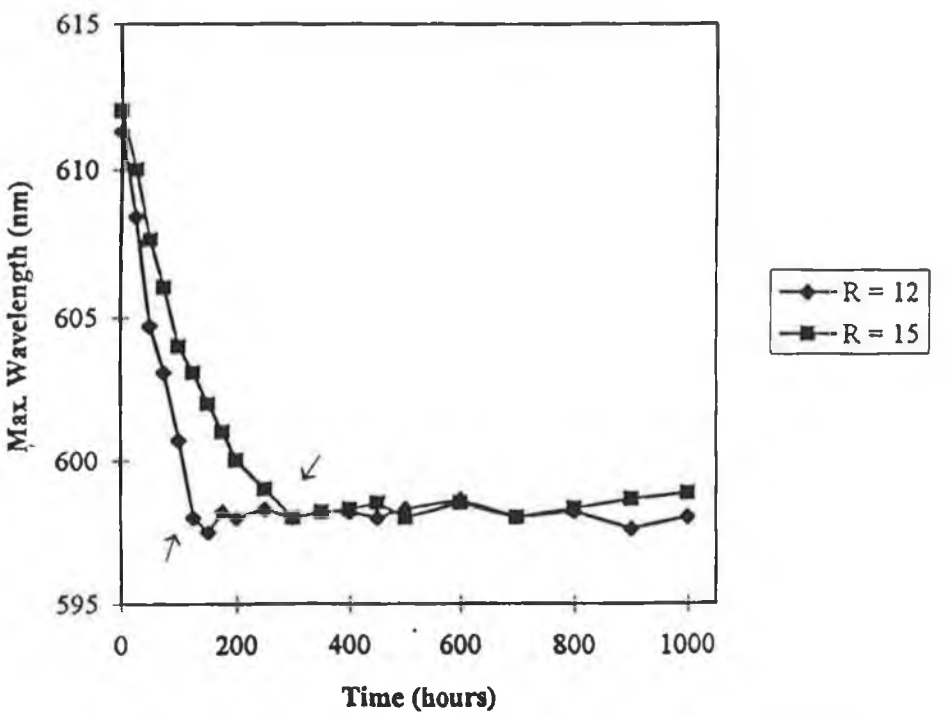

Figure 3.13 Position of the maximum emission wavelength of $[Ru(bpy)_3]^{2+}$ over time during the sol-gel process at 2 water/silane ratios, R = 12 and R = 15 (where pH = 1).

When a water to silane ratio of 2 is employed, the rate of change in the emission maximum of either $[Ru(bpy)_3]^{2+}$ or $[Ru(phen)_3]^{2+}$ is extremely slow. From Equation 3.9, an increased value of R is expected to promote the hydrolysis reaction. Theoretically increasing the water content will increase the hydrolysis rate to a point after which Le Chatelier's principle suggests that the reaction rate will slow down *i.e.* after the water concentration has exceeded the equilibrium value, since water is also a product of the condensation reaction.

$$n\mathrm{Si(OR)_4} + 4n\mathrm{H_2O} \rightleftharpoons n\mathrm{Si(OH)_4} + 4n\mathrm{ROH} \qquad (3.9)$$

The gelation time decreases as R is varied from 2 to 8, with the rate of change of λ_{max} increasing with increasing R. Employing a water to silane ratio of 12 results in a gel which does not significantly differ from that prepared using a ratio of 8. Curiously, when R is increased from 12 to 15, the rate of change of emission decreases (see Figure 3.13). This may be explained by assuming that although increased values of R generally promote hydrolysis, when R is increased while maintaining a constant solvent:silicate ratio, the silicate concentration is reduced (a dilution effect). This in turn reduces the hydrolysis and condensation rates, causing an increase in gel time. However, in all cases the position of the final emission maximum is the same, 597 nm for $[Ru(bpy)_3]^{2+}$ doped gels and 582 nm for those doped with $[Ru(phen)_3]^{2+}$.

The spectral behaviour of those gels doped with $[Ru(phen)_3]^{2+}$ is similar in many respects to those observations seen for $[Ru(bpy)_3]^{2+}$. The results outlined in the previous sections, demonstrate how these two Ru(II) polypyridyl complexes can be used as photophysical probes for studying the sol-gel-xerogel transition. Essentially, they provide distinctive information about the matrix and the various effects of altering specific parameters involved in gel growth, according to the excited state electronic properties of the complexes.

3.2.3 $[Ru(phen)_2(H3Mptr)]^{2+}$ as a luminescent probe of the sol-gel process.

The triazole ring of this complex can be deprotonated and this leads to an extensive ground-state and excited-state acid-base chemistry [19,41]. Significant changes in the absorption and luminescence spectra of this complex brought about by protonation/deprotonation allows it to be employed as a spectroscopic probe in order to monitor changes in the acidity of the surrounding environment, in this case the sol-gel system. This complex is likely to behave differently in a solid matrix as compared to solution because molecular mobility, solvation and reorientation processes have the dominant effect on its electronic excited states.

3.2.3.1 Spectroscopic behaviour of $[Ru(phen)_2(H3Mptr)]^{2+}$ in solution.

The electronic properties of this complex are given in Table 3.3. Deprotonation of the compound causes profound changes in its absorption. The negative charge that can be introduced on the triazole ring by deprotonation results in the destabilisation of the metal d orbitals. This destabilisation causes the $d\pi-\pi^*$ energy gap to decrease, and therefore the ^{1}MLCT is shifted to lower energy. This complex exhibits room temperature emission in acetonitrile at neutral pH associated with decay from the ^{3}MLCT state. Again, as with the absorption spectra, the emission λ_{max} is blue shifted by protonation of the triazole ring, and for the same reasons. This blue shift is associated with a marked decrease in emission intensity. Again, this is a result of the lower σ-donation of the ligand. The ligand field splitting ($10Dq$) is decreased with lower σ-donation, resulting in thermal population of the ^{3}MC state, and faster radiationless decay. Redox properties of this complex indicate that the π^* levels for the pyridyltriazole ligand are at higher energy than those of the phenanthroline, and therefore this ligand is harder to reduce [19]. This implies that the phenanthroline ligand acts as the emitting ligand while the pyridyltriazole acts as a spectator ligand.

As was described for the $[Ru(L\text{-}L)_3]^{2+}$ complexes, at low temperature in an alcohol glass the emission is further blue shifted, in both the protonated and deprotonated species. However, the protonated complex exhibited a radiative lifetime which was considerably increased with respect to the deprotonated complex. This peculiarity is a result of the energy gap law [42]. Protonation leads to a stabilisation of the t_{2g} level and hence an increase in the t_{2g} - ^{3}MLCT gap. According to the energy gap law, the smaller the energy gap, the faster the rate of decay between the two states. This implies that in the absence of sufficient thermal energy to populate the ^{3}MC state, the lifetime of the protonated complex is longer than that of the deprotonated complex.

Table 3.3 Electronic properties of pyridyltriazole complex in ethanol solution.

	Abs.	**Emission**		**τ**		**Φ_{em}**
	λ_{max} (nm)[A]	**(nm)[A]**		**(ns)**		
	RT	**RT**	**77K**	**RT[A]**	**77K**	**RT**
$[Ru(phen)_2(H3Mptr)]^{2+}$	418	606(610)[c]	568(568)[c]	----[B]	9800	3.39×10^{-4}
$[Ru(phen)_2(3Mptr)]^{1+}$	425	654(651)[c]	606(608)[c]	90	7200	1.21×10^{-3}

[A] RT measurements were carried out in ethanol degassed by purging with argon. At 77K the solvent employed was ethanol/methanol 4/1.

[B] This value is outside the range of the instrumentation (*i.e.* < 20 ns). [c] From reference [47].

Considerable electronic redistribution occurs between protonation and deprotonation of pyridyltriazole complexes, which is reflected in the absorption and emission spectroscopy of the complexes. As described, protonation/deprotonation alters the σ-donor and π-acceptor properties of the ligand. In Ru-polypyridyl complexes the Ru-N bond is mainly σ in nature, but is stabilised by backbonding between t_{2g} and π^* of metal and ligand. Determination of the pK_a of a complex yields

information about the extent of backbonding from the metal and σ-donor and π-acceptor properties of the ligands [43,44]. For most ruthenium complexes, the pK_a value of the ligand decreases on coordination, which is an electrostatic effect caused by the Ru(II) centre. Comparison of the pK_a and pK_a^* for the one complex usually reveal large differences. If in the excited state the pK_a of the complex is lower, *i.e.* more acidic, than in the ground state, this implies that the source of the protonation site is a spectator ligand which is not directly involved in the excited state. Alternatively, if the complex is more basic in the excited state, and the $pK_a^* > pK_a$, this implies that the site of protonation contains the LUMO.

(i) Ground state behaviour: The ground state acid-base behaviour of $[Ru(phen)_2(H3Mptr)]^{2+}$ is shown in Figure 3.14. The titration was carried out in Britton Robinson buffer over the pH range 1 to 10. All changes are fully reversible and independent of the direction of the pH change. Using the titration values obtained, a graphical analysis was carried out by plotting percentage change in absorbance versus pH. The observed behaviour can be explained by deprotonation of the pyridyltriazole ligand at higher pH to form $[Ru(phen)_2(3Mptr)]^+$. The pK_a was determined from the point of inflection of the curve as 5.03.

(ii) Excited state behaviour: The effect of pH on the emission properties of this complex was also investigated (Figure 3.15). The spectral changes observed are typical of these type of complexes, with the emission intensity increasing with pH and the λ_{max} of emission shifting to lower energy upon deprotonation. The excited state pK_a was obtained using the Forster cycle as in Equation 3.10 [45], whereby the excited state pK_a^* may be calculated from its ground state properties.

$$pK_a^* = pK_a + 0.625(\nu_b - \nu_a)/T \qquad (3.10)$$

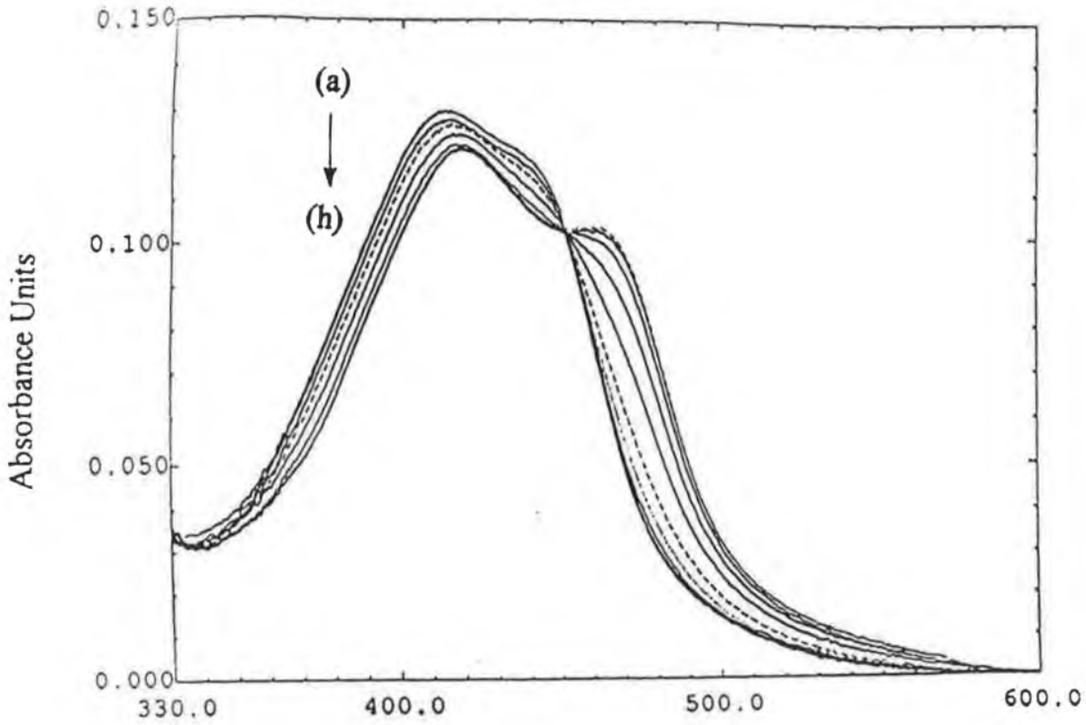

Figure 3.14 Absorbance of $[Ru(phen)_2(H3Mptr)]^{4+}$ solution (5×10^{-5}M) in Britton-Robinson buffer at pH: (a)-(h): 2.7, 3.8, 4.2, 4.6, 5.1, 5.6, 6.3, 7.2.

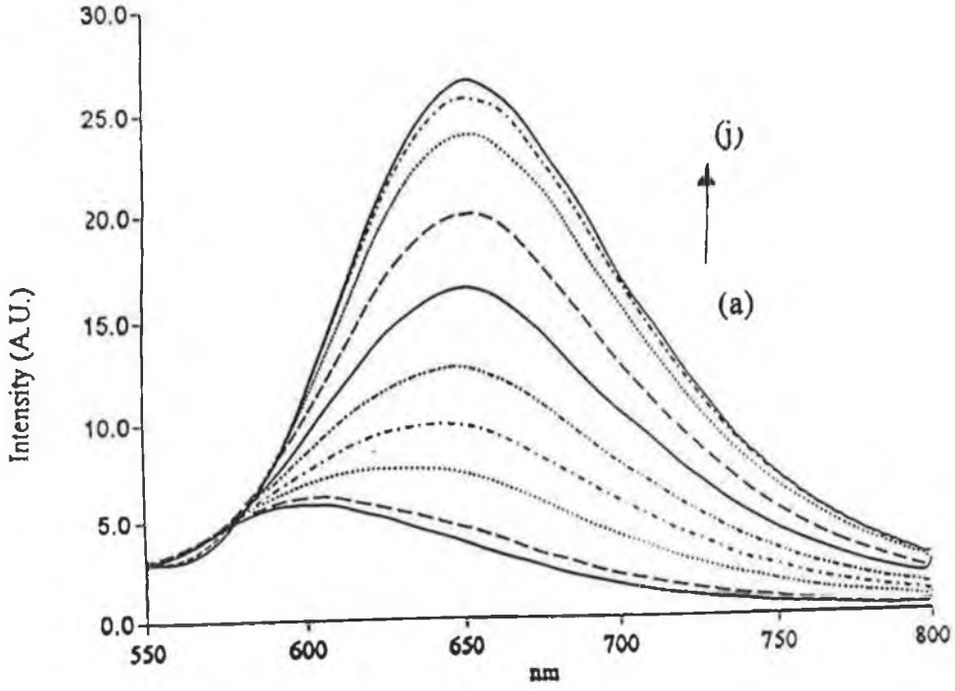

Figure 3.15 Emission of $[Ru(phen)_2(H3Mptr)]^{2+}$ solution (5×10^{-5}M) in Britton-Robinson buffer at pH: (a)-(j): 2.2, 2.5, 3.1, 3.4, 3.7, 4.2, 4.7, 5.2, 5.9, 6.5.

where ν_a and ν_b are the energies of the (0-0) transition involved in the deprotonation equilibrium, for the protonated and deprotonated forms, respectively, obtained using the λ_{max} emission values measured at 77K, and pK_a is the ground state pK_a value. From this equation a pK_a^* of 2.7 was obtained. The pK_a^* value is more acidic than the ground state value. This indicates that the triazole is a spectator ligand and does not become directly involved in the excited state. In other words, the ^{3}MLCT is a phenanthroline based state.

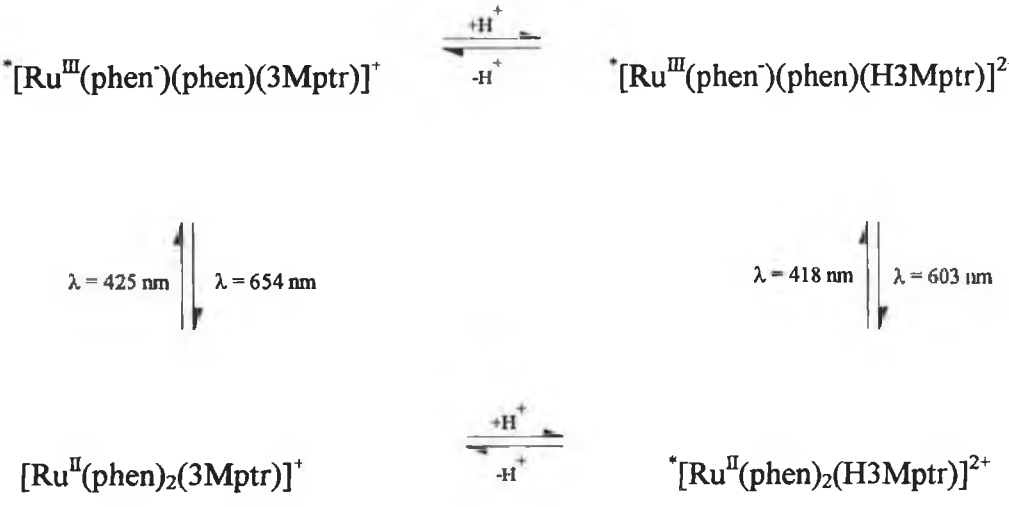

Figure 3.16. Schematic of the acid-base absorption and emission properties of $[Ru(phen)_2(H3Mptr)]^{2+}$

3.2.3.2 Spectroscopic behaviour of $[Ru(phen)_2(H3Mptr)]^{2+}$ in sol-gel matrix.

The fluorescence spectrum of the doped Ru(II) polypyridyl complex changes significantly during the progress of the sol-gel-xerogel reaction of the TEOS system.

The effect of pH in the starting solution on the fluorescence of the sol-gel sample was investigated on a series of Method 2 gels doped with this pyridyltriazole complex. As in solution, the pH of the surrounding sol strongly influences the position of the absorption and fluorescence peaks of the complex. Table 3.4 shows the initial photoluminescence maximum of the doped gels directly after their preparation.

Table 3.4 Initial electronic properties of $[Ru(phen)_2H3Mptr]^{2+}$ in sol-gel after 1 hour of stirring.

Sol-gel Sample*	Absorption λ_{max} (nm)	Emission λ_{max} (nm)
Method 2 (1)	417	606
Method 2 (2)	418	621
Method 2 (3)	423	654
Method 2 (4)	425	655
Method 2 (5)	425	655

* The value in parentheses indicates the pH at which the sample was prepared. These samples were all prepared at room temperature.

The values obtained in the table above correspond well with the values obtained for the pyridyltriazole complex in solution. The absorption maxima of 417 nm and the emission maxima of 606 nm found for those gels prepared at pH 1 are indicative of the protonated form, while at pH > 3 the deprotonated species, identified by an absorption maxima of 425 nm and an emission maxima of 655 nm, is present. At pH 2, an emission maximum with an intermediate value of 620 nm is observed testifying to a substantial presence of both the protonated and deprotonated species. This is to be expected since the pK_a^* of the complex in Britton-Robinson buffer is 2.7. These results therefore indicate that the absorption spectrum of the fluorescent state in the

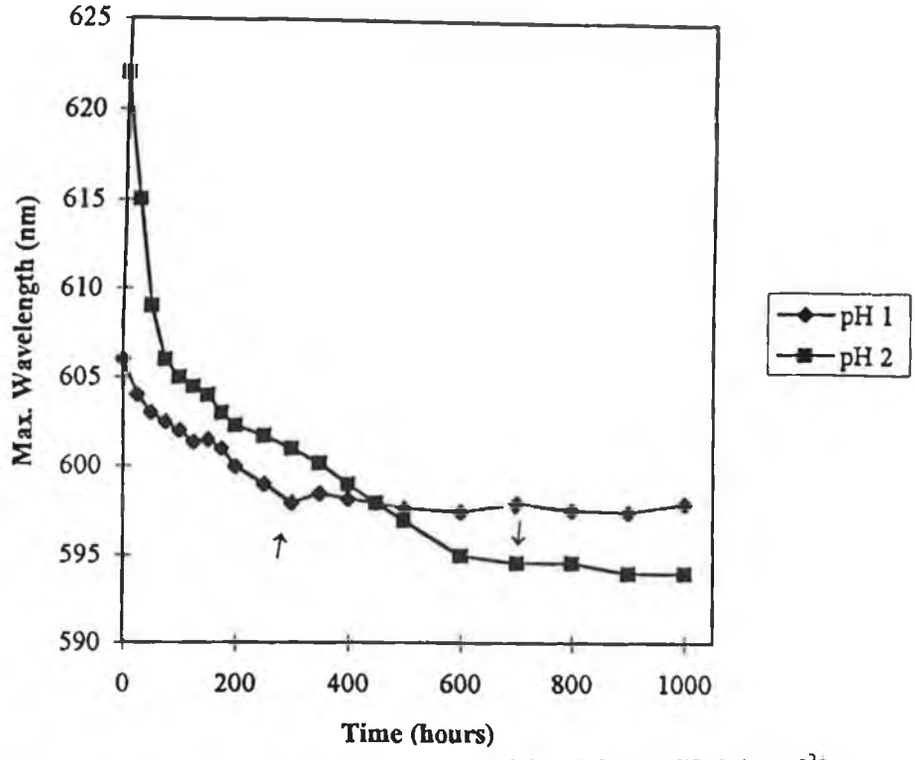

Figure 3.17 Maximum emission wavelength of $[Ru(phen)_2(H3Mptr)]^{2+}$ over time during the sol-gel process at pH 1 and pH 2 (where R = 4).

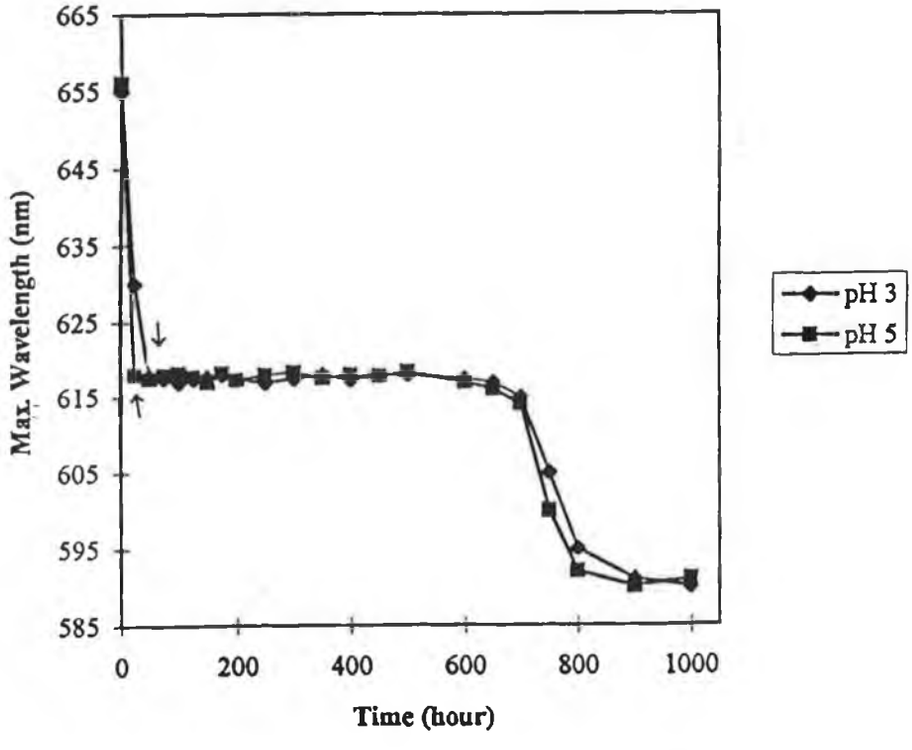

Figure 3.18 Maximum emission wavelength of $[Ru(phen)_2(H3Mptr)]^{2+}$ over time during the sol-gel process at pH 3 and pH 5 (where R = 4).

initial sol-gel is similar to that in solution. Essentially, upon initial incorporation, no substantial difference in the acid-base properties of the pyridyltriazole complex is observed in the sol-gel.

Figures 3.17 and 3.18 illustrate the effect of time on the position of the fluorescence maximum of this ruthenium complex in sol-gels prepared at different pH values (where the arrowheads indicate t_g). When considering the change in emission energy which occurs during the sol-gel-xerogel reactions for these pyridyltriazole doped samples two factors should be taken into account. The first effect is that of increased rigidity leading to a destabilisation of the ^{3}MLCT state. The second effect involves the pH at which the sample was prepared and consequently the protonation/deprotonation of this ruthenium complex. As mentioned previously, protonation of the pyridyltriazole ligand results in a stabilisation of the metal d orbitals and thus an increase in emission energy is observed. Gels prepared at pH < pKa* of the pyridyltriazole, *i.e.* those gels prepared at a pH of 1 and 2, exhibit a continuous blue shift in the luminescence emission until gelation is reached. It is likely that this change to higher energy for these samples is again due to the destabilisation of the ^{3}MLCT state resulting in an increase in the ^{3}MLCT-ground state energy gap. It has been previously established that for $[Ru(bpy)_3]^{2+}$ and indeed $[Ru(phen)_3]^{2+}$ doped gels, the extent of the sol-gel reaction most likely determines the position of the photoluminescence peak. The sample doped with $[Ru(phen)_2(H3Mptr)]^{2+}$ and prepared at pH 2 exhibited a significantly longer time to gelation and hence, a slower rate of change in emission maxima than the sample prepared at pH 1. This is in agreement with those results obtained for $[Ru(bpy)_3]^{2+}$ and $[Ru(phen)_3]^{2+}$ and again, it reflects that below pH 2, the rate of polymerisation is proportional to the hydrogen ion concentration [27,36] *i.e.* increasing the acidity in this range, increases the kinetics of the sol-gel reactions.

For those gels prepared at pH > pK_a^*, the band maximum of the emission exhibits large shifts at various stages of the gelation and drying processes (see Figure 3.18). This evolution of emission energy as a function of time is composed of two steps. While the emission band in the liquid state just after the mixing of the

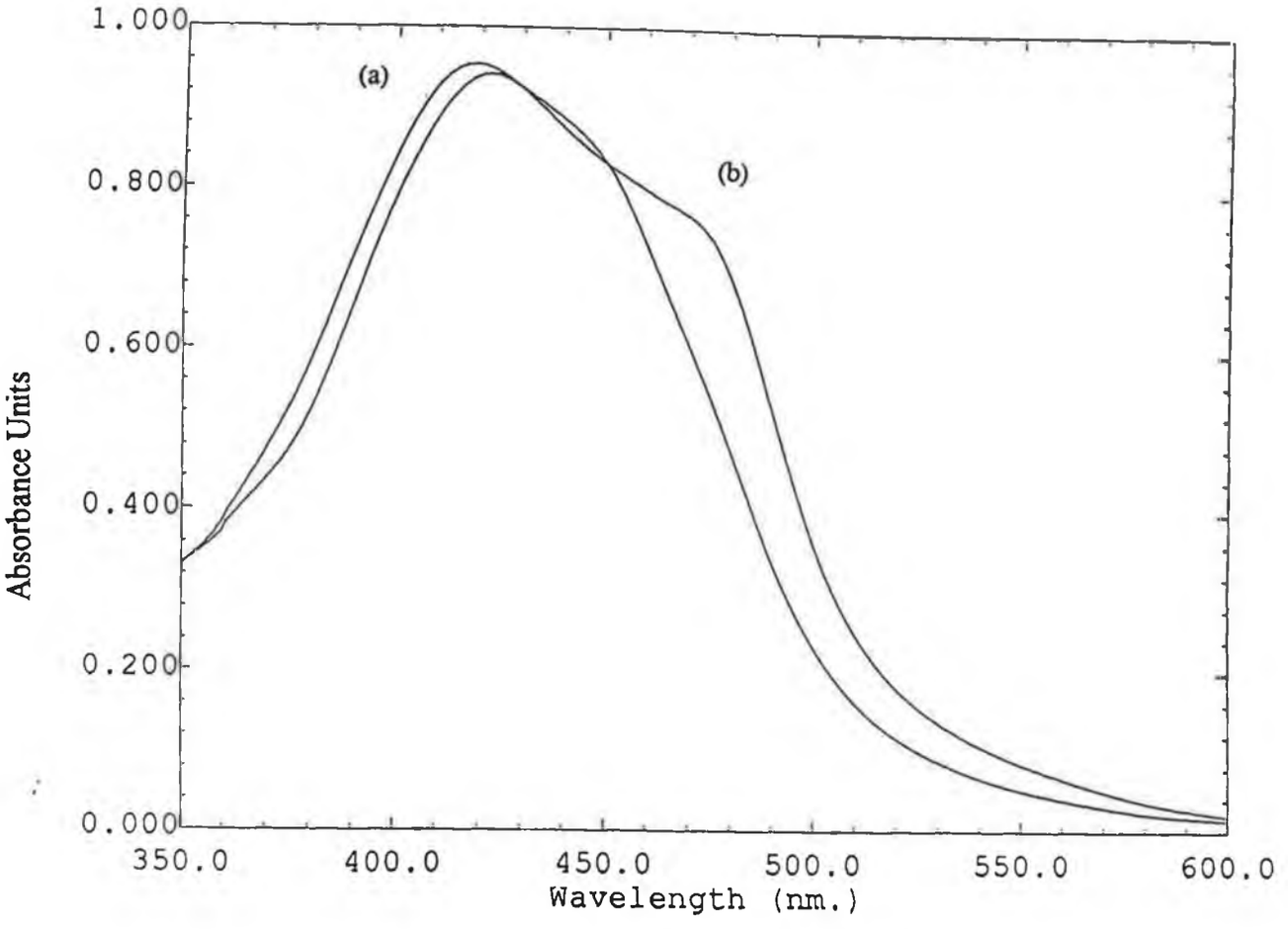

Figure 3.19 Absorption profile of $[Ru(phen)_2(H3Mptr)]^{2+}$ over time during the sol-gel process at (a) zero time and (b) after 25 hours (where R = 4, pH = 5).

components is broad and centred at 655 nm, a significant decrease in wavelength is noticed during the first 25 hours of the reaction. Figure 3.19 shows the change in absorption profile of a gel doped with this pyridyltriazole complex prepared at pH 5, measured during this time. The emission plateau value of 618 nm is maintained throughout the gelling/aging processes even though the solution has turned to a solid amorphous material that does not flow when the container is tilted. For the remaining discussion, the term "aging" reflects changes in the structure and properties of the sol-gel matrix after gelation. "Drying" denotes the removal of solvent molecules from the sol-gel network. However, because aging and drying normally occur simultaneously and are accompanied by shrinkage of the gel, they are

somewhat difficult to decouple [36]. After a long period of aging (approximately 500 hours) in a closed container, a small hole was pierced in the lid to allow slow evaporation of alcohol and water. A further decrease in the emission λ_{max} was noticed during the final stages of the drying process.

The evolution of the Ru(II) pyridyltriazole luminescence prepared at pH > pKa* can be separated into three distinct regions, each of them related to a specific sequential step of the sol-gel transformation: gelation, aging and drying. During the first stages of the sol-gel reaction, the emission jumps from 655 nm for a gel prepared at pH 5 to 618 nm. In order to explain this initial decrease, the following mechanisms were considered;

1. As discussed previously, relaxation of the solvent molecules around the excited molecules, which have an increased dipole moment with respect to the ground state, results in stabilisation of the excited state. In the case of $[Ru(bpy)_3]^{2+}$, the blue shift in emission energy which occurs during the initial stage of the sol-gel process is associated with a destabilisation of the ^{3}MLCT state, which thereby increases the t_{2g}-^{3}MLCT energy gap. In the case of this pyridyltriazole complex, the ^{3}MLCT state is a phenanthroline based state. The change in the absorption profile which accompanies the blue shift in emission energy of this pyridyltriazole complex during this initial stage of the sol-gel reaction, suggests that destabilisation of the ^{3}MLCT state with respect to the ground state alone cannot explain this phenomena. (if this were the case, the UV profile would remain unaffected since the absorption only involves the ground state and the ^{1}MLCT state).

2. Secondly, it is possible that the initial blue shift of the photoluminescence λ_{max} is due to the deprotonated complex accepting a proton rather than the destabilisation of the ^{3}MLCT state as was observed for the $[Ru(L\text{-}L)_3]^{2+}$ complexes. The change in the absorption profile which occurs during this time is consistent with this theory. This indicates an initial increase in the

acidity of the overall system or that the surrounding matrix tends to be more acidic than the pyridyltriazole complex.

During this time, much of the water will be consumed in hydrolysis. The environment surrounding the doped luminescent molecules is expected to become more polar during the progress of the hydrolysis step because the -OH group is more polar than the -OR group and the former tends to form hydrogen bonds. At pH above 2.2, the isoelectric point, silanols formed through the hydrolysis reaction of TEOS will be present as SiO^- [27]. The pK_a of the pyridyltriazole complex is approximately 5. It is possible that it is these protons which are accepted by the deprotonated complex causing the observed blue shift in both the absorption and emission maxima. In other words, the surface of the gel particles acts as a base toward the pyridyltriazole complex at this reaction stage [10]. These surface charges are potential adsorption sites for the Ru(II) polypyridyl complex molecules. It is reasonable to suggest that the protonated form of this complex which has a net charge of 2^+ would be stabilised to a greater extent by the electrostatic interaction with SiO^- groups present on the polymer network than the deprotonated form, which has a net charge of 1^+. Therefore, under the initial reactions of the sol-gel process at higher pH, the majority, but not all the deprotonated species revert to the protonated form as indicated by an emission maximum of 618 nm. The effect of the sol-gel matrix on the lifetime of these samples is discussed in detail in Chapter 4.

Once reached, the plateau remains level until after the drying process has begun. During this time, the polymerisation reactions proceed in sealed container increasing the connectivity of the network and decreasing the porosity [32]. In aged gels it is important to recognise that the ethanol/water solvent system is still present and little if any shrinkage occurs. Unlike pyranine in aluminosilicate gels, this probe molecule is insensitive to changes of water and ethanol content during the polymerisation process [6]. Despite the increasing rigidity of the silica cage known to accompany aging, no further increase in the emission energy of the pyridyltriazole complex is observed during this time. One possible explanation for this observation

could be that the complex experiences a screening effect due to the presence of the interstitial liquid phase. One of the most significant features of gels kept in a closed environment is that they continue to evolve structurally, long after gelation. As probed by the luminescence of this particular Ru(II) complex, the evolution of the oxide network during drying is as important as during the gelation process itself. At the gel point the solution is macroscopically rigid due to interconnection of large clusters. However, at a microscopic level, there is a likelihood for structural changes which could be promoted by some flexibility and by possible condensation reactions. Water is also able to diffuse in the gel, thus promoting further hydrolytic reactions. These structural changes are expected to continue until the structure has reached a stable state. Unlike the $[Ru(L\text{-}L)_3]^{2+}$ dopants, the gelation point does not correspond to the maximum blue shift of the pyridyltriazole complex. This indicates that the microenvironment as experienced by the $[Ru(phen)_2(H3Mptr)]^{2+}$ dopant complex molecules does not remain constant after the gelation point.

The third stage of the process, which is related to the final changes of the Ru(II) pyridyltriazole emission, is the drying of the gel. As indicated by the further blue emission, this step is accompanied by the complete protonation of all the complex molecules, and a progressive increase in electrostatic interaction between the complex cations and the silica surface. Irrespective of the pH employed in the preparation of these sol-gel samples (*i.e.* pH 1→5) it is the protonated form of the complex which appears to exist in the final xerogel. When the solvents are removed, the gel structure collapses and the gel shrinks continuously [28]. From a surface which is initially smooth on a molecular scale and partially reversed phase, there is a gradual increase in irregularity, accompanied by an increase in the number of pores and a decrease in their size [46]. Both the increase in surface energy due to modification of the interface between the oxide polymers and the liquid and the capillary forces of the solvents provide the driving force for this partial densification. The solvent which fills up the network and the cages changes its composition through condensation from rich alcoholic aqueous solution (shortly after hydrolysis it

is virtually pure alcohol) to a water interface and finally, through slow evaporation, to a dry xerogel in which only a few water molecules may be trapped. This change in the relative ethanol contents is an outcome of the different rates by which ethanol and water leave the system. This in turn is due to three factors: first, ethanol evaporates more quickly as it has a lower boiling point than water; second, water molecules are held to the matrix silanols by more and stronger hydrogen bonds than ethanol molecules [46], and thirdly, whereas the fast alcohol production stops at a relatively early stage of the sol-gel process, water is released continuously by the slower condensation reaction $2Si\text{-}OH \rightarrow Si\text{-}O\text{-}Si + H_2O$, which takes place well into the xerogel stage. New condensation reactions occur because some reactive groups are in closer proximity. As a result, the oxide network becomes more compact. Its flexibility drastically decreases with the departure of the solvating species. In effect, the removal of the liquid phase ensures that the pyridyltriazole molecules loose their solvation shell and therefore are forced into increased contact with the gel surface, and the screening effect of the solvent is diminished. As a result of this, the remaining deprotonated species of the complex appear to revert to the protonated form, and a further blue shift in emission is observed. In addition, a final λ_{max} of 585 nm (as opposed to 605 nm for the protonated $[Ru(phen)_2(H3Mptr)]^{2+}$ in solution) suggests a destabilisation of the ^{3}MLCT state. In this respect, the position of the photoluminescence maximum of this complex is a sensitive probe of the structural changes which occur during the sol-gel reaction. These observations can be rationalised in terms of;

(a) creation of interfacial properties which induce strong adsorption onto the polymer surface,

(b) elimination of solvent molecules (water and ethanol) from the immediate environment of the trapped molecule, and

(c) an increase in the rigidity of the trapping matrix.

3.3 Conclusion.

Sol-gels have been prepared by the hydrolysis and condensation of TEOS and doped with a number of ruthenium polypyridyl complexes. The incorporation of luminescent molecules into a liquid sol and subsequently, into an oxide gel can modify the photophysical behaviour of the guest molecule. Because of their ionic character, the Ru(II) polypyridyl complexes tend to adsorb onto the surface of the oxide network. Consequently, the photophysics of the molecule is influenced by the characteristics of this surface and by the changes that occur to this surface during the sol-gel transformation. From emission and absorption spectroscopy during the sol-gel process, it was established that the blue shift noted for $[Ru(bpy)_3]^{2+}$ and $[Ru(phen)_3]^{2+}$, indicates that the relaxation process which leads to an equilibrium excited state configuration is prevented at a molecular level and hence the emission energy increases. The ionic nature of these two ruthenium complexes keeps them in intimate contact with the surface of the polymeric oxide network. An increase in the microviscosity of the matrix around these dopant molecules is required for the prevention of the possible electronic relaxation process from a Franck-Condon state to an equilibrium state during the fluorescence lifetime. This phenomenon observed for both of these complexes has been employed successfully as an analytical tool in probing not only the factors which effect the kinetics of the sol-gel process but also the charging of the surface. The introduction of two bulky phenyl groups on each of the phenanthroline ligands ensures that $[Ru(dpp)_3]^{2+}$ within the sol-gel matrix sustains a "screening effect". As a result, the polar excited state is internalised within the molecule and the excited state electronic distribution of the complex as seen by its surroundings does not differ that much from the ground state, leading to no shift in the emission energy.

Above its excited state pK_a, $[Ru(phen)_2(H3Mptr)]^{2+}$ exhibits interesting emission behaviour in the sol-gel matrix. The deprotonated complex reverted to the protonated form during the initial stages of the sol-gel reactions, suggesting the

proton-donating nature of the sol-gel environment. During the drying of these gels, the Ru(II) complex was brought into increased contact with the sol-gel surface, and a final increase in emission energy was observed.

3.4 References.

[1] S. Sakka, *J. Sol-Gel Sci. and Tech.*, 3, 69, **1994**.

[2] D. Avnir, D. Levy, R. Reisfeld, *J. Phys. Chem.*, 88, 5956, **1984**.

[3] J.D. Mackenzie, *J. Non-Cryst. Solids*, 100, 162, **1988**.

[4] O. Lev, *Analusis*, 20, 543, **1992**.

[5] V.R. Kaufman, D. Avnir, D. Pines-Rojanski, D. Huppert, *J. Non-Cryst. Solids*, 99, 379, **1988**.

[6] J.C. Pouxviel, B. Dunn, J.I. Zink, *J. Phys. Chem.*, 93, 2134, **1989**.

[7] J. M^{c}Kiernan, S. Yamanaka, E. Knobbe, J.C. Pouxviel, S. Parveneh, B. Dunn, J. Zink, *J. Inorg. Organomet. Polym.*, 1, 87, **1991**.

[8] E. Eyal, R. Gvishi, R. Reisfeld, *J. De Physique*, C7-471, **1987**.

[9] R. Gvishi, R. Reisfeld, *J. Non-Cryst. Solids*, 128, 69, **1991**.

[10] T. Fujii, K. Toriumi, *J Chem. Soc., Faraday Trans.*, 89 (18), 3437, **1993**.

[11] T. Fujii, A. Ishii, Y. Kurihara, *Res. Chem. Inter.*, 19, 4, 333, **1993**.

[12] P.J. Giordano, M.S. Wrighton, *J. Am. Chem. Soc.*, 101, 2888, **1979**.

[13] B. Dunn, E. Knobbe, J. M^{c}Kiernan, J.C. Pouxviel, J. Zink, *Mat. Res. Soc. Symp. Proc.*, 121, 331, **1988**.

[14] B. Dunn, J. M^{c}Kiernan, J.C. Pouxviel, J. Zink, *J. Phys. Chem.*,93, 2129, **1989**.

[15] B. Dunn, J. M^{c}Kiernan, J. Zink, Sol-Gel Optics II, SPIE, Vol. 1758, 381, **1992**.

[16] D. Levy, D. Avnir, *J. Phys. Chem.*, 92, 4734, **1988**.

[17] V.R. Kaufman, D. Avnir, *Langmuir*, 2, 717, **1986**.

[18] M. Canva, P. Georges, G. Le Saux, A. Brun, D. Larrue, J. Zarzycki, *J. Mater. Sci. Lett.*, 10, 615, **1991**.

[19] E. Ryan, R. Wang, J.G. Vos, R. Hage, J.G. Haasnoot, *Inorg. Chim. Acta*, 208, 49, **1993**.

[20] A. Juris, V. Balzani, F. Barigelletti, S. Campagna, P. Belser, A. Von Zelewsky, *Coord. Chem. Rev.*, 84, 85, **1988**.

[21] J.N. Demas, G.A. Crosby, *J. Am. Chem. Soc.*, 93, 2841, **1971**.

[22] M. Wrighton, D.L. Morse, *J. Am. Chem Soc.*,96, 996, **1974**.

[23] R. A. Marcus, *J. Phys. Chem.*, 94, 4963, **1990**.

[24] R. Reisfeld, *J. Non-Cryst. Solids*, 121, 254, **1990**.

[25] K. Matsui, K. Sasaki, N. Takahashi, *Langmuir*, 7, 2866, **1991**.

[26] O. Dvorak, M.K. DeArmond, *J. Phys. Chem.*, 97, 2646, **1993**.

[27] R.K. Iler, The Chemistry of Silica, Wiley, New York, **1979**.

[28] L.L. Hench, J.K West, *Chem. Rev.*, 90, 33, **1990**.

[29] W.P. Krug, J.N. Demas, *J. Am. Chem. Soc.*, 101, 4394, **1979**.

[30] P. Kiernan, C. McDonagh, B.D. MacCraith, K. Mongey, *J. Sol-Gel Sci. Tech.*, 2, 513, **1994**.

[31] B.D. MacCraith, C. McDonagh, G. O'Keeffe, E.T. Keyes, J.G. Vos, B. O'Kelly, J.F. McGilp, *Analyst*, 118, 385, **1993**.

[32] C.J. Brinker, *J. Non-Cryst. Solids*, 100, 31, **1988**.

[33] E.J. Pope, J.D. MacKenzie, , *J. Non-Cryst. Solids*, 87, 185, **1986**.

[34] R.A. Assink, B.D. Kay, *J. Non-Cryst. Solids*, 107, 35, **1988**.

[35] R.A. Assink, B.D. Kay, Better Ceramics Through Chemistry III, Pittsburgh: Materials Research Society, 25, **1988**.

[36] C.J. Brinker, G. W. Scherer, Sol-Gel Science, Academic Press, Boston, **1990**.

[37] T, Zerda, I Artaki, J. Jonas, *J. Non-Crys. Solids*, 81, 365, **1986**.

[38] F.N. Castellano, T.A. Heimer, M.T. Tandhasetti, G.J. Meyer, *Chem. Mater.*, 6, 1041, **1994**.

[39] M.W. Colby, A. Osaka, J.D. MacKenzie, *J. Non-Crys. Solids*, 82, 37, **1986**.

[40] S.Y. Chang, T.A. Ring, *J. Non-Crys. Solids*, 147/148, 56, **1992**.

[41] R. Wang, J.G. Vos, R.H. Schmehl, R. Hage, *J. Am. Chem. Soc.*,114, 1964, **1992**.

[42] T. J. Meyer, *Prog. Inorg. Chem.*, 30, 389, **1983**.

[43] R.J. Crutchley, N. Kress, A.P.B. Lever, *J. Am. Chem. Soc.*, 105, 1170, **1983**.

[44] C. Long, J.G. Vos, *Inorg. Chem.*, 125, 131, **1984**.

[45] B.E. Buchanan, J.G. Vos, M. Kaneko, W.J.M. Van der Putter, J.M. Kelly, R. Hage, R. Prins, J.G. Haasnoot, J. Reedijk, *J. Chem. Soc., Dalton Trans.*, 2425, **1992**.

[46] D. Avnir, D. Levy, *J. Phys. Chem.*, 92, 4743, **1988**.

[47] E. Ryan, Ph D. Thesis, Dublin City University, **1991**.

Chapter 4.

The effect of the sol-gel matrix on the luminescent lifetimes of Ru(II) polypyridyl complexes.

4.1 Introduction.

Organometallic dyes, like transition metal complexes, can be used as photosensitisers in photochemical conversion of solar energy, and their incorporation into solid matrices may be advantageous. Fluorescence and phosphorescence spectroscopy provide a broad spectrum of tools for studying morphology and dynamics, and these have obvious applications in the study of polymer interfaces and interphases. The objective is to introduce a foreign element into a particular environment, hopefully unobtrusively, to gather and report specific kinds of information about this environment. Several different kinds of luminescence measurements are possible with these tagged systems. Each of these various luminescence measurements provide different information about the system, potentially offering information about structure, local molecular order, interfacial characteristics and transport phenomena [1]. The most powerful information comes from applying a variety of techniques to each system. In the previous chapter, useful information as to the environment of the ruthenium complexes of the form $[Ru(L\text{-}L)_3]^{2+}$ was obtained from the position of the emission maximum wavelength for L-L = phen or bpy. For L-L = dpp, no change in the photoluminescence peak was observed. This chapter deals with the emission lifetime decay of these complexes in the sol-gel matrix. The information reported here, when coupled with that in the previous chapter, serves to provide a more detailed account of the sol-gel process and also reinforces the previous findings with regards to the nature of the final xerogel.

A common kinetic problem arises when several species with different lifetimes emit simultaneously and independently. The luminescence of molecules emitting from heterogeneous systems frequently depart from first order kinetics. In this chapter, the emission lifetime of ruthenium polypyridyl complexes of the form $[Ru(L\text{-}L)_3]^{2+}$ is studied with respect to the sol-gel-xerogel transition. In all cases, the emission decay lifetime in the final xerogel was greater than that in the initial sol. For $[Ru(bpy)_3]^{2+}$ and $[Ru(phen)_3]^{2+}$ doped samples the luminescence decay could be described by a single exponential model only in the early stages of gel formation,

after which time a double exponential model had to be employed. The introduction of a second lifetime component was noticed much later for those samples doped with $[Ru(dpp)_3]^{2+}$. In addition, the initial pH of the samples effects these complexes in a contrasting manner.

4.1.1 Resolution of fluorescence from micro-heterogeneous systems.

On a molecular scale, the ensemble of chromophore sites in any doped system may be described as a distribution of site properties. Property distributions exist in all unordered systems, but there is in this respect, a fundamental difference between fluids and solids: in fluids, time averaging ensures the approximate constancy of the distribution, so that these systems can be treated as if they consisted of identical molecules of unchanging average properties. In solids, by contrast, the distribution of site properties becomes evident due to the rigid nature of the medium.

Fluorescence spectroscopy has been widely used to provide detailed information in regard to the structure and the nature of interactions between molecules in the solid state [1]. One of the commonly excepted rules is the exponential decay of isolated fluorescent molecules with lifetime τ :

$$\Phi(t) = \exp(-t/\tau) \qquad (4.1)$$

However, as mentioned in section 2.4, this is not always the case. The relaxation of fluorescent species embedded in a solid medium can be subject to spatial disorder. Heterogeneous media frequently give rise to complex decay kinetics that can be characterised as the sum of several exponentials or as the sum of distribution functions of exponentials [2-4]. Since decay data can frequently be fit equally well by several widely different decay models, mechanistic interpretation is often hampered by the lack of a unique solution. It has been proposed that fluorescence decay profiles of isolated fluorescent species can be described by:

$$\Phi(t) = {}^{n}\Sigma_{m=1}\, a_m \exp(-t/\tau_m) \qquad (4.2)$$

where a_m is the preexponential factor associated with the lifetime τ_m. Equation 4.2 has been used to account for the differences in the local environments of which interaction with fluorescent molecules could lead to different decay properties as given by τ_m [4]. For the purpose of this thesis, this equation has been employed in fitting the emission decay data for Ru(II) doped sol-gel samples reported here.

Although a satisfactory agreement of Equation 4.2 has been reported here, and by other authors [2,3,5,6], it is important to recognise the physical limitations of this approximation. The main issue associated with Equation 4.2 is that it neglects the fact that the measured fluorescence decay profile is an average signal from all molecules excited by the light. Thus, if a fluorescent molecule is embedded in the nonuniform medium, one has to calculate the decay profile of fluorescence as an average over the distribution of relaxation rates. A number of authors have addressed this issue [4,7,8], but for the studies related here, a double exponential equation was found to suffice.

This inherent complexity in dealing with multicomponent emission decay from heterogeneous environments is carried over in the application of transition metal complexes doped in solid matrices for use as optical sensors. Determination of oxygen is most important in various fields of clinical analysis and environmental monitoring, and is usually performed amperometrically using Clark-type electrodes. Recently, optical sensors based on luminescence measurements have gained much interest because of their high sensitivity and specificity [9-10]. Various authors have suggested the use of transition metal complexes, especially Ru(II), Os(II), and Re(I), in developing oxygen sensors, since the luminescence of these complexes is strongly quenched by oxygen [11-13]. Another advantage is their relatively long luminescence decay time, ranging from several hundreds of nanoseconds up to 10 μs.

For molecules embedded in a polymer matrix the decay is influenced by interactions between the fluorophores and the polymer. Most polymers are nonuniform media in the sense that there is no long-range structural order. In homogeneous media with only a single-component exponential decay, and under circumstances of purely dynamic quenching, the variation in luminescence intensity (I), or luminescence decay time (τ), with externally applied oxygen partial pressure p_{O_2} is described by the Stern-Volmer equation:

$$I_0/I = \tau_0/\tau = 1 + k_{sv} p_{O_2} \qquad (4.3)$$

with $$k_{sv} = k\tau_0 \qquad (4.4)$$

where I_0 is the luminescence intensity and τ_0 the lifetime of the excited state in the absence of oxygen, k_{sv} is the Stern-Volmer quenching constant, and k is the bimolecular quenching constant. When dye molecules are incorporated into a polymer matrix, deviations from linear intensity-based Stern-Volmer plot are frequently encountered. In these micro-heterogeneous systems, the multiexponentiality of the decay curves and the uncertainty of the fitting model preclude evaluating a single exponential lifetime for use in Equations 4.3 and 4.4. The plots of I_0/I versus quencher concentration are downward curved, which makes accurate calibration difficult. In addition, the question of the relative contributions of static and dynamic quenching is difficult to address. In effect, a single time constant is no longer sufficient to describe the luminescence decay. Since the Stern-Volmer constant is the product of a bimolecular quenching constant and a lifetime, any lifetime distribution is also reflected by a distribution of Stern-Volmer constants. In essence, this micro-heterogeneity gives rise to complex decay kinetics and obscure sensor performances.

The downward curvature of the Stern-Volmer plots necessitates a model more complex than a single species quenched bimolecularly. A number of

mechanistic models have been proposed in order to deal with this deviation. Among the most widely accepted are:

(1) The complex exists in two distinctly different environments, with one being quenchable and the other being unquenched.
(2) The complex exists in two distinctly different environments, with both being quenchable but with different quenching rate constants.

Model 1 assumes two independent sites with only one site having significant sensitivity to oxygen quenching. Model 2 is a two-site model that includes quenching of both sites. MacCraith and co-workers have successfully employed Model 1 in order to describe the luminescent quenching behaviour of $[Ru(bpy)_3]^{2+}$ or $[Ru(dpp)_3]^{2+}$ in sol-gel silica thin films [14]. For each complex ruthenium fluorescence was quenched in the presence of oxygen. The optical decay times were analysed in terms of one quenched and one unquenched component, the latter arising from the fraction of complex molecules which are inaccessible to oxygen. In the absence of oxygen, the decay was found to be single exponential. In the presence of oxygen, plotting the extracted fast quenched decay (from the constant unquenched background) versus oxygen pressure, yielded good Stern-Volmer plots.

In the case of Ru(II) complexes in silicone rubber [11], model 1 gave distinctly inferior fits compared to model 2 with chi-square values (χ^2) that were 50-100% larger than for Model 2. The basic equation for Model 2 is:

$$I_0/I = (f_{01}/(1 + k_{sv1}[Q]) + f_{02}/(1 + k_{sv2}[Q]))^{-1} \qquad (4.5)$$

where the f_{0i}'s are the fraction of the total emission from each component under unquenched conditions and the k_{svi}'s are the associated Stern-Volmer quenching constants for each component. Model 1 is therefore a special case of Model 2 where k_{sv2} equals 0.

Recently Wolfbeis and co-workers carried out luminescence and decay time measurements of ruthenium complexes in a number of different polymers [15]. As expected, these measurements resulted in multicomponent luminescence decays and non-linear Stern-Volmer plots. This work includes a new model for describing the nonexponential luminescence decay, which takes into consideration the interaction of the fluorophore with the nonuniform environment provided by the polymer. This theory suggests that the luminescence decay profiles of molecules in a nonuniform medium can be assumed as being an average over a distribution of relaxation rates. The relaxation probability of a single fluorophore molecule is determined by interactions with the neighbouring regions of the polymer. The influence of these interactions on the decay time can be assumed to depend on the distance between the fluorophore and the nearest interacting polymer site. The excited state of the fluorophore then relaxes with a distance-dependent rate.

By taking into account the interactions with the medium, these studies revealed that the luminescence decay profile of molecules embedded in a nonuniform medium even in the absence of any quencher deviated from the usual exponential form where the exponent is a linear function of time. The luminescence decay curves were fitted by trial functions consisting of a sum of two or three exponentials. In addition a preexponential weighted mean lifetime τ_m was shown for each membrane. All the fits were of good quality, as judged by usual mathematical criteria (χ^2, and residuals). However, the preexponential factors exhibited a dependence on the oxygen pressure which could not be described by any reasonable physical model. This suggested that the decay was due to a distribution of decay rates. The model relating this distribution to a distribution of distances between fluorophores and interaction sites on the polymer proved to be well-suited to describe the relaxation of luminophores in nonuniform environments. Quenching of a luminophore by oxygen proved to be a more difficult case. In principle a single quenching parameter is sufficient for a full description, and in favourable conditions, this quenching parameter varies linearly with oxygen pressure. These favourable conditions were

found to prevail only in certain polymer matrices, while a non-linear dependence of the quenching parameter on oxygen pressure was found in others.

4.1.2 Heterogeneity in sol-gel systems.

The excited-state properties of Ru(II) polypyridyl-doped sol-gels are complex. Specifically, multicomponent emission decays are routinely observed [16-19]. Only in the early stages of gel formation can the temporal optical properties be modelled by a single exponential. Previous studies carried out by Reisfeld and co-workers describe the luminescence decay profile of $[Ru(bpy)_3]^{2+}$ in the final xerogel as a double exponential. In these studies, it was concluded that the increase in lifetime of $[Ru(bpy)_3]^{2+}$ in the glass was a result of the fixation of the ruthenium complex into a rigid solid matrix, where a majority of the mechanisms that can quench the excited states are removed. In addition, it was assumed that concentration quenching could be neglected due to the isolation of the complex molecules in the matrix [17]. In this chapter, the lifetimes given for the immobilised complexes are those obtained for the aerated samples. However, for these particular complexes, degassing the sol-gel samples did not alter the lifetime data in any way.

Again, the fundamental question is, are the nonexponentials decays a result of several discrete rates or is there an underlying distribution of rates. Castellano and co-workers addressed this question [19] by fitting data, obtained from Ru(II) doped sol-gels, to a sum of two discrete rates and also to the Kohlrausch-Williams-Watts model which can be derived from a distribution of rates. Statistically, however, it was impossible to distinguish which model more accurately described the observed data. In order to gain more insight into the fundamental nature of the complex decay kinetics, the exponential series method was implemented. This method directly recovers distributions of rates from complex fluorescence decays. Evidence for a bimodal distribution of dopant sites was obtained from modelling the emission decays with this series [19,20].

In order to develop those optical sensors described in the previous section, or indeed any sol-gel based device in general, it becomes important to understand the effects of the surrounding sol-gel matrix on the photophysics and the dynamics of the entrapped dopant. In particular the viscosity of a sol-gel material is an important practical parameter because it dictates firstly the ability to cast thin films and draw fibres and secondly the mobility and accessibility of chemically selective dopants within the matrix. Thus, information on the local microviscosity surrounding a dopant trapped within a sol-gel matrix becomes important to a material's ultimate end use. Several research groups have reported on the viscosity of sol-gel materials during the early stages of the sol-gel transformation [21,22,23]. Recently, Jonas and co-workers carried out steady-state fluorescence anisotropy experiments with three probes and concluded that gelation led to relatively small changes in the fluorophores [23]. This was attributed to the pore in the wet gel allowing substantial mobility of the fluorescent probe even though the bulk viscosity remained quite high.

Unfortunately, much of the work in this field, including that of Jonas, has been carried out just past gelation and does not explore the gel as it ages further. Therefore, although there is some information on the microviscosity within a sol-gel matrix versus ageing, it does not extend far into the ageing cycle. There is also little direct information on how the ageing cycle influences the photophysics of inorganic dopants within the sol-gel matrix. This latter issue is of especial importance as one attempts to understand sol-gels in general and the chemistry of dopants entrapped in a sol-gel matrix. In a recent paper by Narang and co-workers [24], this issue was addressed by employing the static and dynamic fluorescence spectroscopy of rhodamine 6G (R6G, Figure 4.1(a)), in a sol-gel matrix. The steady-state and time-resolved fluorescence results for R6G in a tetramethoxysilane (TMOS) sol-gel were reported as a function of ageing and pH.

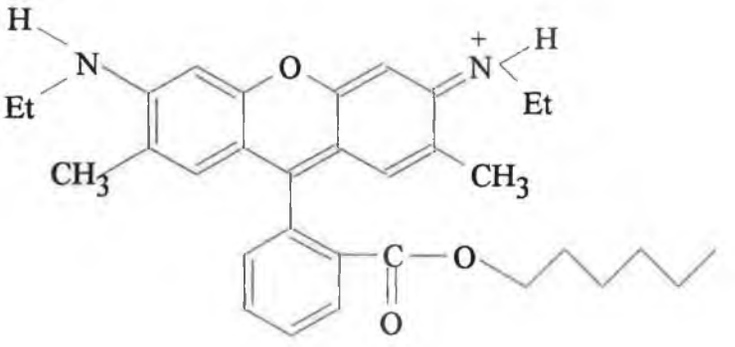

Figure 4.1(a) Chemical structure of rhodamine 6G.

Upon excitation with polarised light the emission from fluorescent samples is also polarised. This polarisation is a result of the photoselection of fluorophores according to their orientation relative to the direction of the polarised excitation. Rotational diffusion of fluorophores is one common cause of depolarisation of the emission. The anisotropy measurements reveal the average angular displacement of the fluorophore which occurs between absorption and subsequent emission of a photon. This angular displacement is dependent upon the rate and extent of rotational diffusion during the lifetime of the excited state. These diffusive motions in turn depend upon the viscosity of the solvent and the size and shape of the diffusing species. For example, for a fluorophore dissolved in a solvent, the rotational rate of the fluorophore is dependent upon the viscous drag imposed on the fluorophore by the solvent. As a result, a change in solvent viscosity will result in a change in fluorescence anisotropy [24].

Fluorescent anisotropy experiments provide insight into the mobility of the fluorescent probe within a given microdomain. The steady-state results indicated four distinct regions in the ageing cycle (as shown in Figure 4.1(b)). The initial stage represented the liquid to gel region which was found to be strongly pH dependent. After gelation had taken place, the mean anisotropy plateaued and the sol-gel began to age.

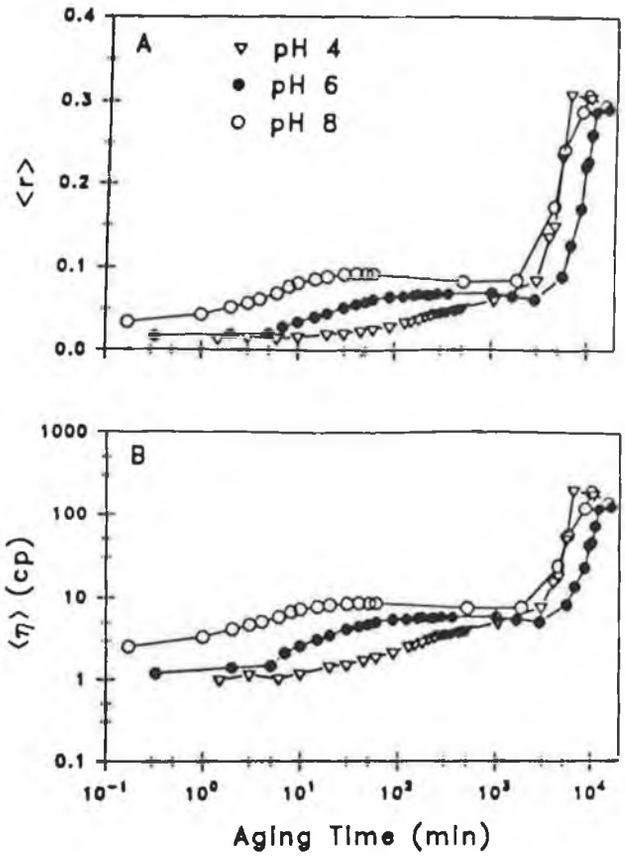

Figure 4.1(b) Recovered steady-state anisotropy (A) and average microviscosity (B) for R6G in a TMOS sol-gel as a function of time [24].

This result was consistent with the average dopant (R6G) having significant reorientational mobility even after gelation with the mean pore size remaining large and solvent still filling these pores. Thus it appeared that at this stage, the majority of the R6G molecules were in a wet, low-viscosity environment. The third stage noticed in the ageing cycle, was denoted by a fast increase in the anisotropy and corresponded to the initial stages of sol-gel drying. During this time the solvent was expelled from the siloxane network. In the final stage the anisotropy levelled off as the sol-gel was dried.

The time-resolved anisotropy experiments revealed that the observed anisotropy resulted from two distinct reorientational motions throughout the entire sol-gel ageing cycle. One of the rotational correlation times remained constant throughout the sol-gel ageing cycle and the other varied with the ageing time. The rotational correlation time data was transformed into microviscosity data and the results were interpreted in terms of a two-microdomain model. One of the rotational motions (the fastest component) remained constant throughout the sol-gel process and was assigned to R6G in a wet sol-gel pore. The longer rotational reorientation time increased substantially with ageing time. The fractional contribution of the faster component was high during the initial stages of the sol-gel ageing process and dominated even after gelation. However, its contribution decreased dramatically during the drying process.

Figure 4.2 presents the simple model employed in this report by Narang and co-workers, which is consistent with the microenvironments sensed by R6G during the TMOS sol-gel ageing cycle. The key points noticed in these studies are as follows. First, as mentioned, the R6G probed simultaneously two distinct microdomains during the sol-gel ageing process. Second, one rotational reorientation time was invariant and the other changed with the sol-gel ageing process. For a freshly prepared sol-gel solution the "constant" domain, corresponding to the faster reorientation time, dominated the decay of anisotropy (upper panel in Figure 4.2). The "variable" domain also contributed, but the average microviscosity sensed by R6G was low, as most of the R6G molecules were in low viscosity constant domain. Third, as the sol-gel ageing cycle proceeded to the gelation stage (central panel), the variable domain about the R6G became more viscous, but its contribution to the total decay of anisotropy still did not increase significantly. This suggested that a fixed number of "free" R6G molecules, that rotationally diffuse independently, were being observed as the pores were not yet emptied of solvent. Finally, during the drying stage (lower panel), the number of constant domains decreased significantly, the variable domain became extremely viscous, and the majority of the observed R6G rotational reorientations were now from a highly viscous microevironment.

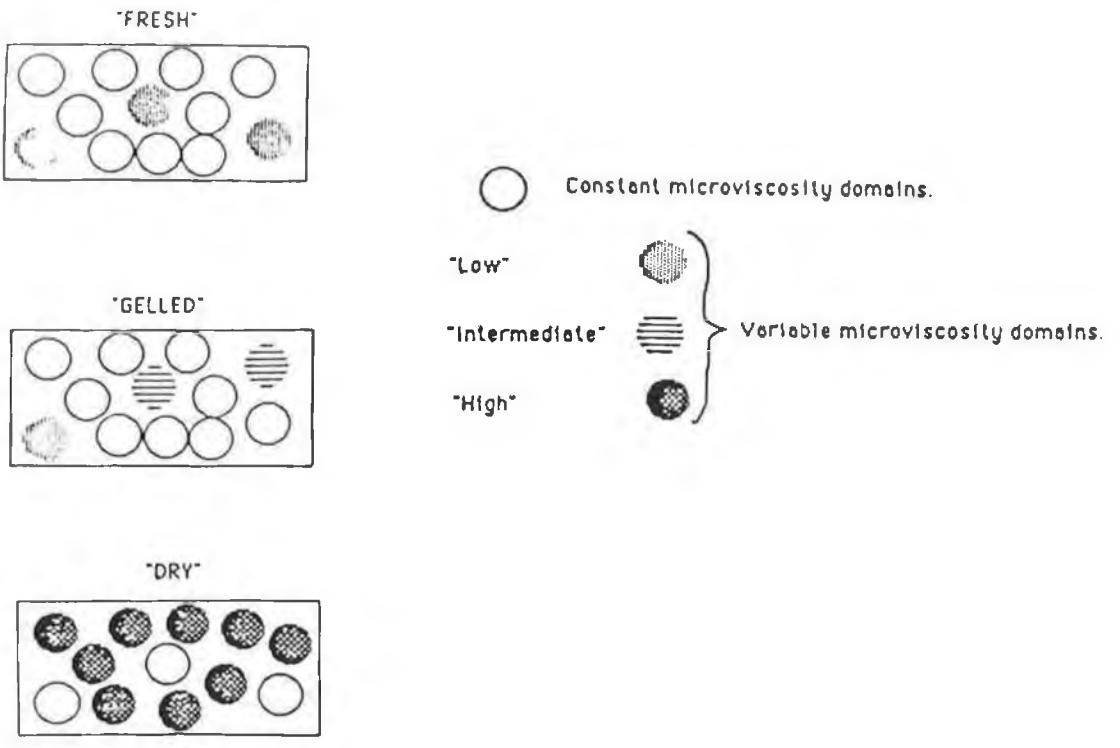

Figure 4.2 Model to describe the observed rotational kinetics of R6G in a TMOS gel [25] The circles represent sol-gel domains probed by the R6G, and the level of shading corresponds to the magnitude of the microviscosity (light, low: dark, high).

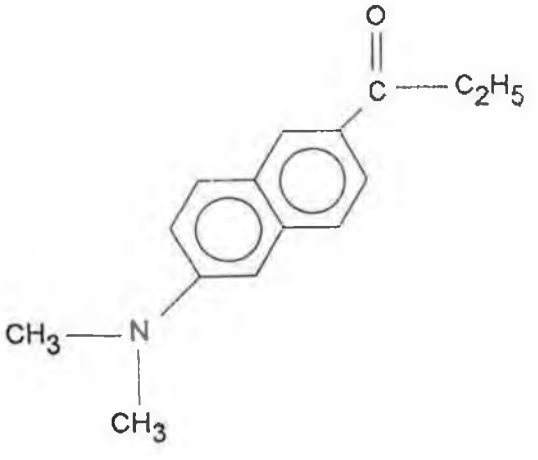

Figure 4.3 Chemical structure of PRODAN.

This is consistent with the expulsion of solvent and shrinkage of the sol-gel pores about the R6G probe which occurs at this final stage. This picture is further consistent with bimodal distribution of rates obtained by Castellano and co-workers mentioned earlier [19]. This work suggests that there was substantial mobility of R6G dopants within a sol-gel matrix up to the drying stage. Beyond this point, the contribution of the mobile species plummeted. These results indicate that, if mobility of reagents is important to a sol-gel based device, it is critical that one control or arrest the ageing process prior to drying.

Further work carried out by this particular research group includes probing the microenvironment of the neutral molecule PRODAN (6-Propionyl-2-(dimethylamino)naphthalene) in TMOS derived sol-gels. PRODAN (see Figure 4.3) was chosen because it is a probe which is highly sensitive to the physicochemical properties of its local environment (with emission ranging from 401 nm in cyclohexane to 530 nm in water) [25]. In addition, its excited-state decay kinetics are a strong function of its local environment. The steady-state results of these particular studies suggested that the microenvironment about the dopant remained constant well beyond the gelation point. The interpretation of the recovered intensity decay data which was suggested by the authors was a corresponding distribution of microviscosities. The fluorescence emission characteristics of PRODAN indicated that the expulsion of solvent was a stepwise process, in which the removal of ethanol was followed by that of water. The studies carried out with R6G did not observe this phenomenon because this probe was not nearly as sensitive to the sol-gel environment compared to PRODAN. Significant rotational freedom of the entrapped PRODAN was found even after the sol-gel was dried under ambient conditions. The excited state decay was found to be best described by a unimodal continuous Gaussian distribution throughout the entire sol-gel process. The width of the Gaussian distribution was employed as a qualitative measure of the heterogeneity of the microenvironment in the system. The expulsion of solvent was followed by changes in the PRODAN lifetime distribution. The microenvironment of the sol-gels was found to be heterogeneous immediately after the onset of gelation. The width of

this distribution increased concurrently with the removal of ethanol This increase in heterogeneity was attributed to the random removal of ethanol from the more accessible domains, with varying amounts of water remaining. These domains, containing different amounts of water and ethanol, accounted for the increased matrix heterogeneity and, as a result, the increased width of the Gaussian distribution. Upon the removal of water, the width of the distribution decreased as the system became more homogeneous.

4.2 Results and discussion.

4.2.1 The emission lifetime of $[Ru(bpy)_3]^{2+}$ in solids as compared to solution.

Upon incorporation of $[Ru(bpy)_3]^{2+}$ into a solid matrix, the observed lifetime is seen to increase due to the elimination of a number of factors which in solution, serve to quench the excited state. A double exponential model has been employed by a number of authors to fit the luminescence decay of $[Ru(bpy)_3]^{2+}$ in solid matrices including silk fibroin membranes [26], cellulose [27], zirconium phosphate sulfophenylphosphonate [6] and indeed in previous studies involving sol-gels [17]. Table 4.1 shows the emission lifetimes of excited $[Ru(bpy)_3]^{2+}$ in various media or matrices. In a liquid medium (*i.e.* a solution system), $[Ru(bpy)_3]^{2+}$ shows single exponential decay according to Equation 4.1, and the lifetime seems to depend on the affinity of the medium for the hydrophobic bpy ligand. When the affinity between the medium and the ligand is high, molecular motion of the complex is reduced, the emission lifetime increases (*e.g.* 980 ns in *N,N*-dimethylformamide (DMF) while 600 ns in water) by suppressing the non-radiative rate. Therefore, the emission lifetime can be employed as an indicator of molecular motion [26].

The $[Ru(bpy)_3]^{2+}$ incorporated into a silk fibroin membrane exhibited, under argon, a very long lifetime component of 1700 ns. It has been suggested by Kaneko [26], that the shorter component of the $[Ru(bpy)_3]^{2+}$ of this particular emission decay profile, which has a lifetime of 433 ns, is due to the so-called concentration quenching of the neighbouring excited state molecules since the value is shorter than in aqueous solution. A similar double exponential behaviour was obtained in the work of this thesis for those sol-gels doped with $[Ru(bpy)_3]^{2+}$ at pH 1, with a longer lifetime component of 1100 ns and a shorter component of 470 ns. It would seem unlikely that the shorter component observed here is due to concentration quenching, as the concentration of these samples is still quite low despite the shrinking which accompanies ageing of the gel to form the xerogel.

Table 4.1 Lifetime of the excited state of $[Ru(bpy)_3]^{2+}$ in various media at room temperature under argon.

Phase	Sample	Lifetime (ns) (% fraction)
liquid	$[Ru(bpy)_3]^{2+}$ solution (H_2O)[c]	600 (100)
	$[Ru(bpy)_3]^{2+}$ solution (EtOH)[c]	710 (100)
	$[Ru(bpy)_3]^{2+}$ solution (DMF)[c]	980 (100)
solid	$[Ru(bpy)_3]^{2+}$ in silk fibroin [26]	1700(94), 433(6)
	$[Ru(bpy)_3]^{2+}$ in nafion [26]	1340(80), 480(20)
	$[Ru(bpy)_3]^{2+}$ in cellulose [26]	1010(80), 458(20)
	$[Ru(bpy)_3]^{2+}$ in polyethylene oxide [27]	1020(100)
	$[Ru(bpy)_3]^{2+}$ in sol-gel [19][a]	1680(69), 580(39)
	$[Ru(bpy)_3]^{2+}$ in sol-gel [18][b]	1600(10), 610(90)
	$[Ru(bpy)_3]^{2+}$ in sol-gel pH 1[c]	1100(70), 470(30)
	$[Ru(bpy)_3]^{2+}$ in sol-gel pH 5[c]	2100(70), 660(20)

[a] Acid catalysed TMOS gel from reference 19. [b] Acid catalysed sol-gel from reference 18.
[c] Present work.

Furthermore, several research groups have reported on the matrix isolation properties of sol-gel doped with $[Ru(bpy)_3]^{2+}$ [17]. With the low concentrations employed in this thesis (estimated final concentrations of approximately 6×10^{-5} M), it is expected that the majority, if not all of these Ru(II) complex molecules will be surrounded by the silicon oxide matrix, *i.e.* they are isolated within the pores of the sol-gel. In support of this, Avnir and co-workers also found that, upon transition from gel→xerogel, the presence of pyrene eximers is diminished due to the isolation of the pyrene molecules within individual pores [28]. Again, it must be emphasised that the number of exponentials extracted from the experimental fluorescence raw-data by means of multiexponential fitting procedures is very strongly determined by the quality of the data and also by the given time domain over which the collection of fluorescence photons is done. On the one hand, a certain degree of scepticism must be maintained, and one cannot consider the values of the decay lifetime recovered

through employing this double exponential model to be exact. However, since the experimental conditions remain constant throughout each experiment, it is possible to compare values within an experiment as an indication of the changing environmental properties of the surrounding sol-gel matrix (see Section 4.2.3).

One interesting feature concerning Table 4.1, is that the emission decay from all of the solid phases, with the exception of polyethylene oxide (PEO), is best described by a double exponential model. This contrasting behaviour of $[Ru(bpy)_3]^{2+}$ in PEO has been largely explained by considering the microheterogeneous nature of this matrix. PEO-600000 is a semicrystalline matrix, having both crystalline and amorphous sites [27]. It has been suggested that the crystalline sites cannot reorganise around the excited state molecules within the timescale of the radiative relaxation. On the contrary, a fast reorganisation process of the matrix around the excited molecule could be possible for the amorphous sites. If the complexes were statistically distributed between crystalline and amorphous sites, a double exponential would have appeared. Because the observed decay could be fitted by a single exponential model, it was assumed that all the $[Ru(bpy)_3]^{2+}$ molecules immobilised in the PEO matrix experienced the same environment, and were exclusively placed in the amorphous sites. In essence, the amorphous region of solid PEO has the ability to stabilise the polar excited species within the timescale of radiative relaxation.

In order to explain the spectroscopic behaviour of $[Ru(bpy)_3]^{2+}$ in sol-gel glasses, Reisfeld and co-workers have adopted the four-level model proposed by Van Houten and Watts, and by Demas and Crosby [16,17,29,30]. As mentioned previously, the luminescent first excited state of $[Ru(bpy)_3]^{2+}$ is attributed to triplet metal-to-ligand charge-transfer (^{3}MLCT) states, having one of the six 4d-electrons in the ground state transferred to the lowest empty orbital of a single bipyridyl ligand. Weak interligand interactions seem to permit the migration of the excited state electron from one ligand to another on a nanosecond timescale. The lifetime reveals the quantum efficiency and nonradiative relaxation of the excited state due to triplet-triplet quenching by atmospheric oxygen and temperature dependent interactions with the solvent (or solid surroundings). The results and explanations outlined in

these papers indicate that at low temperatures the lifetimes are dependent on the Boltzmann population of three adjacent triplet levels, of which transitions to the singlet level are spin forbidden [29,30]. Each of these triplet levels is characterised by different temperature independent radiative and nonradiative decay constants. At higher temperatures (above 77 K) these levels can be dealt with as a single level. Following the population of the ^{3}MLCT state, three deactivating processes can occur: by radiative decay (k^r) and radiationless decay (k^{nr}), both of which return the excited state complex to its ground state, or by thermal activation to a spectroscopically unobservable ligand field (LF) excited state ($A_i\exp(-\Delta E_i/RT)$). A_i is an Arrhenius-type frequency factor which contains kinetic terms involving the formation and subsequent decay of the LF excited state (see subsequent chapters). Once formed, the LF excited state may undergo radiationless decay to the ground state under nonphotochemical conditions. The simple schematic representation of the model used to interpret the photophysics of Ru(II) complexes has been previously given in Chapter 1, Figure 1.7. The additional manifold of d-parentage is believed to be placed at about 3600 cm^{-1} above the first manifold and has a non-radiative decay rate of the order 10^{13} s^{-1}. At 77 K its contribution to the total decay is negligible but at room temperature it contributes significantly.

The radiative rate of the d-π^* triplet state is almost constant in different media of the same refractive index as is reported in numerous works and equals about 14-15 μs when thermal equilibrium between the three components of the triplet state exists [30]. The radiationless rate constant k^{nr} is strongly dependent on the local environment [30]. In addition, k^{nr} generally increases with decreasing excited-state energy, as expected on the basis of the energy gap law [31,32]. The quantum efficiency from the d-π^* states at temperature T is the ratio of the thermalised radiative rate (k^r) and the sum $[k^r + k^{nr} + A_i(\exp(-\Delta E_i/RT)]$ where ΔE_i is the average energy difference between the ^{3}(d-π^*) state and the ^{3}(d-d) states. Thus comparing different hosts at the same temperature where all parameters are equal with the exception of k^{nr}, one may estimate the role of triplet quenching by atmospheric oxygen and by the surroundings. It has been suggested by Reisfeld [17],

that one would expect that part of the quenching mechanisms present in solution would be eliminated in sol-gels, and that the quantum yield should increase.

As mentioned in Chapter 3, it was found that while the position of the emission maximum wavelength of $[Ru(bpy)_3]^{2+}$ was altered in the gel, the mechanism of absorption, intersystem crossing, followed by emission is essentially the same as in solution [16-19]. The absorption spectra of the doped xerogels show a maximum around the 450 nm region assigned to the ^{1}MLCT. The fluorescence spectra of all the samples, peaking in the 600 nm region were assigned to the Stokes-shifted emission of the ^{3}MLCT excited state to the ground state, as in solution. An increase in lifetime of $[Ru(bpy)_3]^{2+}$ upon incorporation into a sol-gel was found in all of these studies [16-19]. Previous reports have suggested that this increase is the result of the fixation of the ruthenium complex into a rigid solid sol-gel matrix where a majority of bimolecular deactivating mechanisms that can quench the excited states (such as oxygen quenching) are removed. Increased lifetime of $[Ru(bpy)_3]^{2+}$ in solids at room temperature, has also been attributed to decreased k^{nr}, *i.e.* decreased interaction of the lowest triplet manifold of the complex with the solid surroundings as compared to water and alcohol. These results are consistent with the scheme proposed by van Houten and Watts [30] in their study of temperature dependence of the luminescence lifetimes of $[Ru(bpy)_3]^{2+}$ in water and with low temperature measurements. Our lifetime results for $[Ru(bpy)_3]^{2+}$ in the sol-gel matrix are consistent with those previously reported in sol-gels [18,19], in so far as an increase in lifetime was observed, and a double exponential was required to fit the data (see Table 3.1). An important point to note here is that, the lifetimes of the sol-gel samples studied in this chapter, were not affected by degassing.

In addition to the exclusion of oxygen and decreased interaction of the lowest triplet manifold with the solid surroundings, the increase in lifetime observed in the gel matrix is consistent with a decrease in the nonradiative rate constant of $[Ru(bpy)_3]^{2+}$ due to the energy gap law. The energy gap law predicts an exponential decrease in the nonradiative rate constant with increasing energy gap. As discussed in Chapter 3, the incorporation of $[Ru(bpy)_3]^{2+}$ within a sol-gel induces a blue shift in

the emission energy of the excited state complex. Again, this blue shift in emission wavelength corresponds to an increase in the energy gap between the ^{3}MLCT state and the ground state, caused by the destabilisation of this excited state. This is caused by the lack of mobility of the solvent dipoles on the timescale of the lifetime of the excited state which as a result, cannot respond to the change in electronic structure between the ground and the excited state.

Another possible cause for the detected increase in lifetime may be a result of the term $A_i\exp(-\Delta E_i/RT)$. Previous studies have revealed, that for $[Ru(bpy)_3]^{2+}$, a profound change occurs in the kinetic decay parameters between a cellulose acetate matrix and solution [33]. It has been suggested that, in the solid matrix, the MLCT→dd transition is inhibited. A similar effect has been noticed in sol-gel matrices doped with $[Ru(bpy)_3]^{2+}$ in this thesis and will discussed in greater detail in the following chapters. With the loss of this temperature dependence, decay *via* an additional fourth MLCT state [34,35] becomes apparent in the temperature dependent lifetime data.

In summary, at this stage, there appear to be four possible causes for the observed increase in lifetime of $[Ru(bpy)_3]^{2+}$ upon incorporation within the sol-gel matrix:

(1) the absence of quenching due to molecular oxygen and other bimolecular quenching reactions.
(2) a decrease in k^{nr} due to the inhibition of the molecular motion of the complex caused by the rigid nature of the surrounding sol-gel matrix.
(3) a decrease in k^{nr} *via* the energy gap law.
(4) a change in the term $A_i\exp(-\Delta E_i/RT)$ which describes the population of the anti-bonding d-d state.

The contribution of each of these factors will be discussed throughout the following sections of this chapter.

4.2.2 Luminescent decay as a probe of the sol-gel process.

4.2.2.1 Luminescent decay of $[Ru(bpy)_3]^{2+}$ and $[Ru(phen)_3]^{2+}$ in the sol-gel matrix.

In this section, a comparison is made between the complexes of the form $[Ru(L\text{-}L)_3]^{2+}$, where L-L = bpy or phen, doped in sol-gel matrices (prepared by Method 2, Chapter 2) prepared at different pH values (in the pH range 1-5). The data for this section are presented in Tables 4.2 and 4.3. As in Chapter 3, similarities between the interaction of the immobilised $[Ru(bpy)_3]^{2+}$ and $[Ru(phen)_3]^{2+}$ molecules with the host matrix were observed.

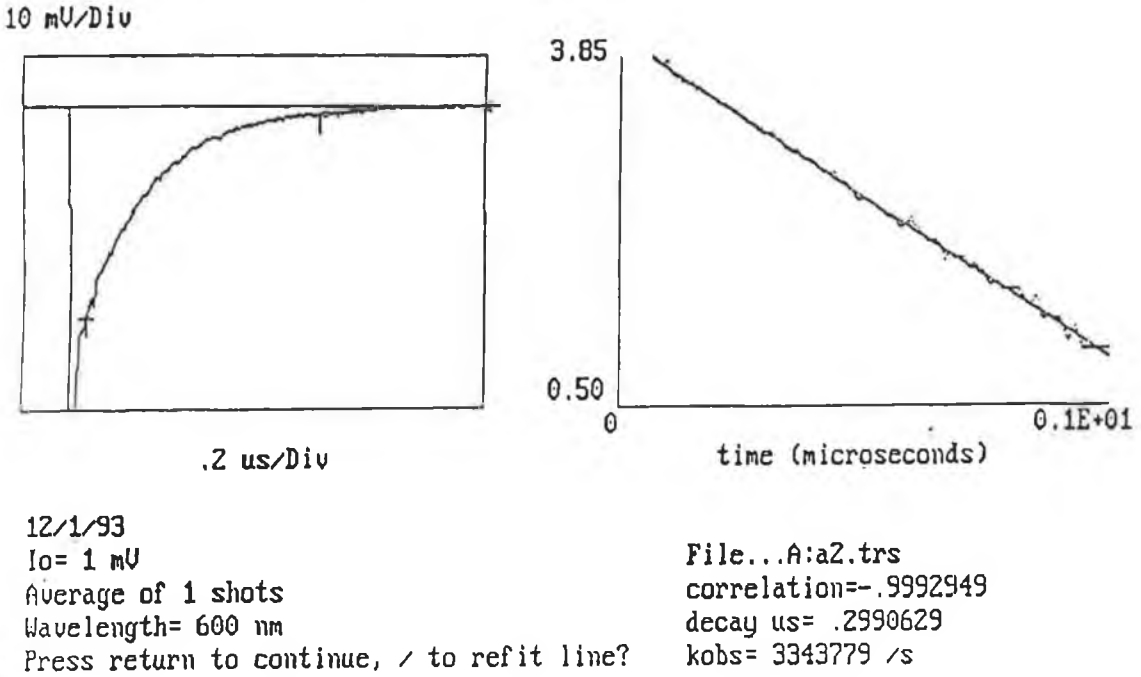

Figure 4.4 The emission decay profile of a $[Ru(bpy)_3]^{2+}$ doped sol-gel (Method 2(1)) directly after preparation.

Table 4.2 Luminescent decay data for $[Ru(bpy)_3]^{2+}$ doped sol-gel samples prepared at various initial pH values.

Time (h)	$[Ru(bpy)_3]^{2+}$ Method 2 (1)[a] τ_1,τ_2 (ns)[b]	$[Ru(bpy)_3]^{2+}$ Method 2 (2)[a] τ_1,τ_2 (ns)[b]	$[Ru(bpy)_3]^{2+}$ Method 2 (3)[a] τ_1,τ_2 (ns)[b]	$[Ru(bpy)_3]^{2+}$ Method 2 (5)[a] τ_1,τ_2 (ns)[b]
0	295(100)	280(100)	270(100)	260(100)
5	300(100)	300(100)	95(10),320(90)	280(80),400(20)
10	310(100)	325(100)	105(15),450(85)	300(70),505(30)
20	360(100)	340(100)	150(30),700(70)	330(65),620(35)
50	480(100)	380(100)	250(40),1050(60)	400(65),620(35)[$]
100	450(70),800(30)	385(100)	300(55),1400(45)[$]	455(30),1900(70)
150	485(25),1100(75)	400(85),200(15)	320(50),1450(50)	555(40),2000(60)
300	465(30),1100(70)[$]	380(55),600(45)	310(40),1500(60)	700(35),2100(65)
400	480(30),1100(70)[*]	380(50),720(50)	300(35),1480(65)[*]	680(35),2100(65)[*]
500	460(25),1120(75)	370(55),840(45)	315(40),1520(60)	650(20),2110(80)
600	440(30),1125(70)	390(50),950(50)	320(35),1500(65)	630(25),2150(75)
700	450(30),1100(70)	365(55),970(45)[$]	330(30),1550(70)	650(20),2120(80)
800	460(30),1100(70)	360(40),1110(60)[*]	320(25),1500(75)	660(20),2150(80)
1000	470(30),1100(70)	370(35),1080(65)	310(20),1500(80)	660(20),2100(80)

[$] Indicates gel time ($t_g$) of the sample. [*] Sample top pierced to allow for evaporation of solvent. [a] Indicates the pH at which the gel was prepared. [b] Values in parentheses are the components pre-exponential factors given in percent. Accuracy of measurements is ± 10 %. Excitation wavelength of 355 nm.

Firstly, the rate of increase in the overall lifetime of these two Ru(II) complexes is faster at pH 5 than at pH 1. This is consistent with those results observed for the rate of change in the emission maximum at these two pHs, with the rate being notably faster at pH 5 than at pH 1 (see Section 3.2.2.2). Again it is most likely caused by changes in the kinetics of the polycondensation which are maximised around neutral pH. We will return to this point shortly.

Table 4.3 Luminescent decay data for $[Ru(phen)_3]^{2+}$ doped sol-gel samples prepared at various initial pH values.

Time (h)	$[Ru(phen)_3]^{2+}$ Method 2 (1)[a] τ_1,τ_2 (ns)[b]	$[Ru(phen)_3]^{2+}$ Method 2 (2)[a] τ_1,τ_2 (ns)[b]	$[Ru(phen)_3]^{2+}$ Method 2 (3)[a] τ_1,τ_2 (ns)[b]	$[Ru(phen)_3]^{2+}$ Method 2 (5)[a] τ_1,τ_2 (ns)[b]
0	190(100)	170(100)	160(100)	150(100)
5	210(100)	175(100)	215(100)	1800(80),250(20)
10	220(100)	185(100)	265(100)	2400(60),300(40)
20	250(100)	205(100)	50(20),360(80)	2800(55),340(45)
50	270(100)	200(100)	180(65),700(35)	660(30),4200(70)[$]
100	90(20),430(80)	230(100)	240(60),1050(40)[$]	720(25),4200(75)
150	270(55),680(45)	180(30),440(70)	300(55),1400(45)	800(20),4200(80)
300	260(45),730(55)[$]	250(40),550(60)	455(45),1950(55)	920(20),4250(80)
400	250(45),690(55)[*]	240(50),690(50)	500(50),2050(50)[*]	990(25),4300(75)[*]
500	280(40),700(60)	220(40),750(60)	540(40),2100(60)	1050(20),4250(80)
600	260(35),720(65)	250(30),900(70)	535(35),2150(65)	1100(20),4300(80)
700	250(30),740(70)	240(50),1100(50)[$]	540(30),2100(70)	1100(25),4280(75)
800	255(35),730(65)	245(35),1115(65)[*]	535(35),2150(65)	1100(20),4300(80)
1000	240(40),720(60)	250(30),1110(70)	550(35),2200(65)	1100(20),4300(80)

[$] Indicates gel time ($t_g$) of the sample. [*] Sample top pierced to allow for evaporation of solvent.

[a] Indicates the pH at which the gel was prepared. [b] Values in parentheses are the components pre-exponential factors given in percent. Accuracy of measurements is ± 10 %. Excitation wavelength of 355 nm.

Secondly, as mentioned previously, while the sol-gel reactions proceed the decay data can be more accurately described by a double exponential model. Deviation from first-order decay for these complexes is due to the heterogeneity of the sol-gel environment. For the lifetime studies of the ruthenium(II) complexes reported here, two separate models were used to fit the decay data. The first was a simple monoexponential equation, the second a double exponential decay expression. This approach was chosen for its simplicity, and because it had been used previously to

describe the decay profile of Ru(II) polypyridyl complexes in a sol-gel matrix [17]. Figure 4.4 shows the emission decay profile of a $[Ru(bpy)_3]^{2+}$ doped sol-gel directly after preparation, *i.e.* at zero time. This sample, prepared at pH 1 obeys a single exponential expression having a lifetime of 299 ns. This value is comparable to that of $[Ru(bpy)_3]^{2+}$ in an aerated ethanol solution. This suggests that directly after preparation, the $[Ru(bpy)_3]^{2+}$ molecules experience no significant change in their environment. After 100 hours, the luminescent decay profile of this sample is best described by a double exponential model. The final lifetime values of the xerogel in this case when fit to this double exponential model, are 470 ns,(30%) and 1100 ns, (70%). Figure 4.5(a) shows the final observed and theoretical (as obtained from the double exponential model) decay profiles for this particular sample. Having generated the best-fit parameters, it was then necessary to judge the quality of the fit. From the best fit parameters the expected curve was calculated. Even for the correct model, the theoretical and observed decay profiles will differ because of noise. As can be seen from Figure 4.5(b), an excellent fit was obtained, with the points being randomly distributed above and below the X axis.

The introduction of a second lifetime component is noticed earlier for those gels prepared at pH 5 than those at pH 1, and it would seem that the ruthenium probe molecules partition themselves into two different environments. It would appear from Tables 4.2 and 4.3, that for $[Ru(bpy)_3]^{2+}$ and $[Ru(phen)_3]^{2+}$ the lifetime of these complexes probes the sol-gel reactions, from the initial sol up until gelation of the sample. After gelation, no significant increase in lifetime was observed for either of these Ru(II) polypyridyl complexes. The lifetime of these two complexes can therefore be used in conjunction with the shift in the photoluminescence peak in order to probe the sol-gel formation in the early stages of these reactions. With respect to the initial pH of the samples, similar trends were observed for the change in lifetime as were observed for the change in emission energy. In particular, the rate of growth in lifetime for each of these two complexes increased in the following order pH 5 > pH 3 > pH 1 > pH 2. The reasons for these different rates with respect to the shift in emission energy as related to the sol-gel reactions has been previously

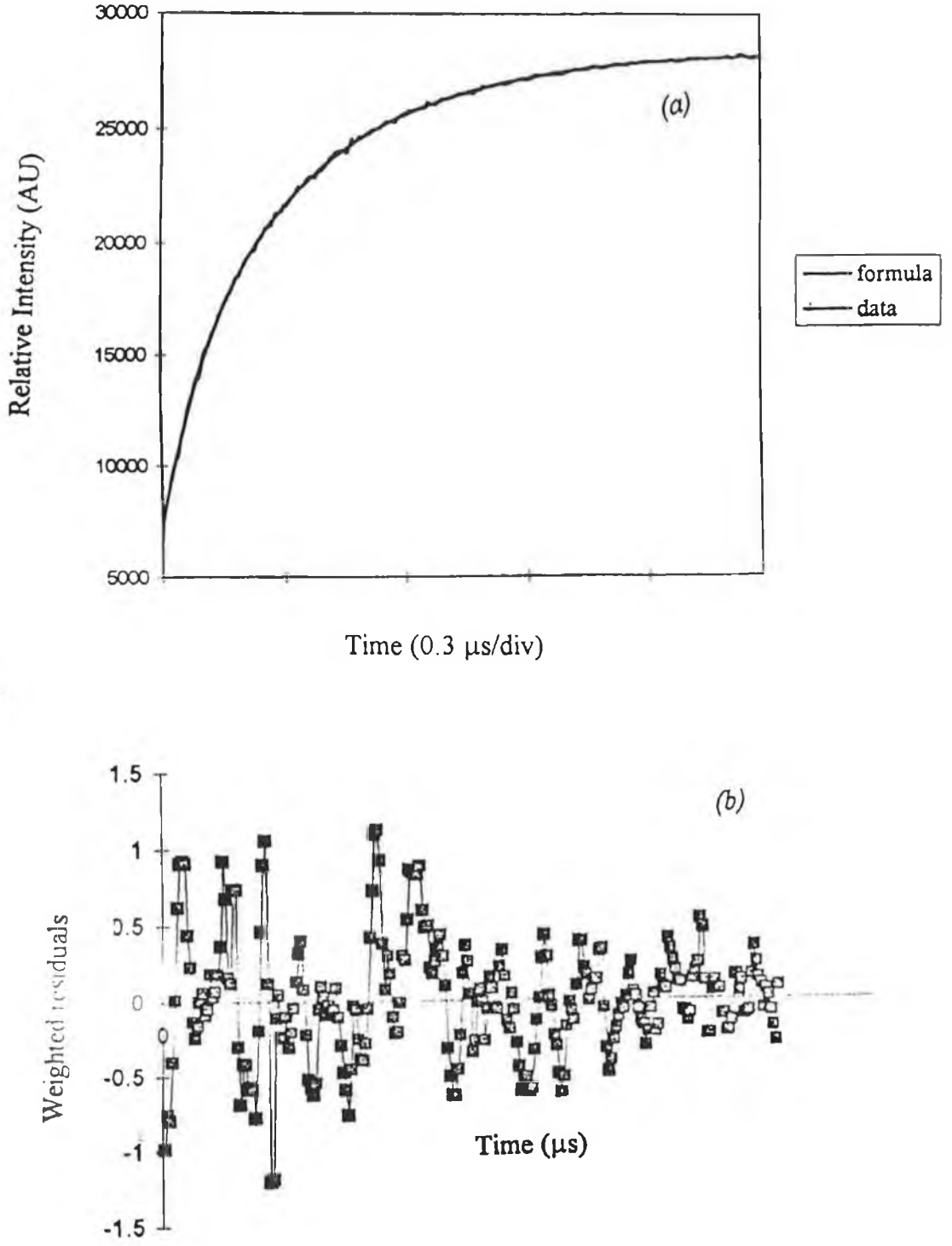

Figure 4.5 (a) Emission decay profile of $[Ru(bpy)_3]^{2+}$ doped xerogel (R = 4, pH = 1).
(b) Weighted residual plot for this double exponential fit.

discussed in Section 3.3.2.2. It seems likely that the same arguments hold here. Again, the kinetics of the sol-gel reactions most likely determines the lifetime of these complexes. The dramatic increase in lifetime during the early stages of the sol-gel reactions, which is specifically evident for those samples prepared at high pH (*i.e.* pH 5), suggests that a specific interaction between the matrix and the complex. This is presumably caused by the electrostatic interaction between the negatively charged silanols and the positively charged complex.

The introduction of a second component in order to fit the decay profile of these samples suggests the existence of a heterogeneous environment as seen by both of these complexes, $[Ru(bpy)_3]^{2+}$ and $[Ru(phen)_3]^{2+}$, even before gelation has occurred. As mentioned in the introduction, the heterogeneity observed by rhodamine 6G has been attributed to this probe molecule reporting simultaneously from two discrete microdomains, each having a different microviscosity [24].

It is possible that the ruthenium complexes are also experiencing the effect of domains of varied viscosity, resulting in different k^{nr} values. The greater the viscosity of the domain, the lower the nonradiative decay rate for the ruthenium polypyridyl complex in that domain will be. Therefore, a longer lifetime would be observed from the domain of higher microviscosity. In all the above cases, the fractional contribution to the total decay of the longest lived constituent is greater than for the shorter component. In this respect, these results are consistent with the model used to describe the observed rotational reorientation kinetics of R6G in a TMOS sol-gel, the high microviscosity domain being dominant in the final xerogel. Unfortunately, little information as regards the ageing and drying stages of the sol-gel process can be deduced from the lifetimes data displayed in Tables 4.2 and 4.3.

When considering the consequence of pH on the final lifetimes of the doped gels, two effects should be taken into account. The first effect is that of surface charge, with the negatively charged surface impeding vibrational deactivation of the excited state complex by electrostatic interaction to a greater extent than the positively charged surface [21]. The ruthenium polypyridyl complexes employed here are dications and it seems likely that electrostatic interactions play an important

role in their encapsulation. The second effect involves the density of the host gel. The nonradiative decay rate (k^{nr}) for the triplet level of Ru(II) complexes is dependent on the nature of the host material, where there is an indication that the more dense the material, the lower the nonradiative rates [17]. It is known that increasing the initial pH of the sol forms gels which are less dense and with increased porosity [36]. This would give rise to higher k^{nr} values and thus the observed lifetime would decrease. Therefore the lifetimes observed at pH 5 would be smaller than those observed at pH 1. For gels doped with $[Ru(bpy)_3]^{2+}$ and $[Ru(phen)_3]^{2+}$, the eventual lifetimes of the gels prepared at pH 5 are larger than those prepared at pH 1. This is in agreement with the fluorescent data obtained for these samples. and it suggests that the extended lifetime results from the rigid microenvironment, with the surface charge being the dominant factor in determining the final lifetime values.

4.2.2.2 Luminescent decay of $[Ru(dpp)_3]^{2+}$ in the sol-gel matrix.

Significant differences were observed in the behaviour of the decay profile for those gels doped with $[Ru(dpp)_3]^{2+}$ as compared to the two complexes discussed in the previous section. Table 4.4 displays the lifetime components of the sol-gel samples prepared at various pH values for this complex as a function of time. Firstly, the decay profile of both $[Ru(dpp)_3]^{2+}$ samples could be fit to a single exponential model even after 300 hours, regardless of the initial pH of the gel. It is likely that the small increase in lifetime that occurs during this period is due to the slowing down of diffusion controlled oxygen as the viscosity of the surrounding solution increases, rather than the actual fixation of the dye molecules to the silicon polymer chains. A second lifetime component arises only after approximately 600 hours of initial preparation. At this stage, the plastic caps have been pierced and much of the excess solvent has evaporated, causing the gel to shrink by an appreciable amount. We believe that the jump in lifetime which occurs at this time may be caused by the

increased exclusion of oxygen from the gel as the pores decrease in size [36]. Finally, the gels prepared at higher pH show a smaller increase in lifetime than those prepared at low pH values. This is again in contrast to those results obtained for $[Ru(bpy)_3]^{2+}$ and $[Ru(phen)_3]^{2+}$ doped gels. This suggests that the effect of electrostatic interaction is less significant for $[Ru(dpp)_3]^{2+}$ doped gels, and that the final lifetime of the gels is dominated by the density of the host material as mentioned previously.

The results outlined above suggest that in the case of $[Ru(dpp)_3]^{2+}$, the excited state electron is localised on the phenanthroline component of one of the ligands, the bulk of the two phenyl groups shielding the solvent from experiencing the influence of the excited state. In effect, the polar excited state is internalised within the molecule and the excited state electronic distribution of the complex as seen by the surroundings does not differ that much from the ground state, leading to no shift in the emission energy. A more detailed account of the behaviour of the emission properties of $[Ru(dpp)_3]^{2+}$ as a function of temperature will be presented in Chapter 5.

We have mentioned previously that the decay lifetime of the $[Ru(dpp)_3]^{2+}$ dopant increases only after gelation has occurred. Therefore, an important aspect of this particular system is its potential use as a photophysical probe for studying the final gel-xerogel transition and the structural changes which accompanies this transition. It would appear that it is the final stages of the trapping of $[Ru(dpp)_3]^{2+}$ molecules within the matrix which is responsible for this increase in lifetime. Therefore, this ruthenium complex when introduced into the sol-gel matrix can be exploited to provide distinctive information about the ageing and drying procedures according to the lifetime decay profile.

Table 4.4 Luminescent decay data for $[Ru(dpp)_3]^{2+}$ doped sol-gel samples prepared at various initial pH values.

Time (h)	$[Ru(dpp)_3]^{2+}$ Method 2 (1)[a] τ_1,τ_2 (ns)[b]	$[Ru(dpp)_3]^{2+}$ Method 2 (3)[a] τ_1,τ_2 (ns)[b]	$[Ru(dpp)_3]^{2+}$ Method 2 (5)[a] τ_1,τ_2 (ns)[b]
0	295(100)	295(100)	290(100)
50	310(100)	340(100)	370(100)[$]
100	335(100)	380(100)[$]	380(100)
300	355(100)[$]	385(100)	385(100)
800[*]	360(100)	380(100)	500(100)
850	380(100)	420(100)	700(100)
900	640(100)	620(100)	100(20),920(80)
950	300(35),820(80)	170(10),710(90)	250(15),1200(85)
1000	420(40),1150(60)	225(15),805(85)	280(20),1250(80)
1100	480(35),1500(65)	250(20),940(80)	290(15),1180(85)
1200	490(40),1800(60)	275(15),1100(85)	285(20),1200(80)
1300	470(30),2100(70)	280(20),1200(80)	290(25),1250(750
1400	490(35),2150(65)	290(25),1200(75)	300(30),1200(70)
1500	500(40),2100(60)	280(25),1250(75)	300(30),1200(70)

[$] Indicates gel time ($t_g$) of the sample. [*] Sample top pierced to allow for evaporation of solvent.

[a] Indicates the pH at which the gel was prepared. [b] Values in parentheses are the components pre-exponential factors given in percent. Accuracy of measurements is ± 10 %. Excitation wavelength of 355 nm.

Previous studies [37] have shown that no drastic change in structure occurs at the gelation threshold of the sol-gel system. On the one hand, macroscopic properties, like the viscosity exhibit drastic changes during gelation. The viscosity is known to diverge at the gel point [38], which shows that the solution is macroscopically rigid at this point due to the interconnection of large polymer clusters. However, at the molecular level, the rigidification of the gel is not accompanied by rigidity at the microscopic level.

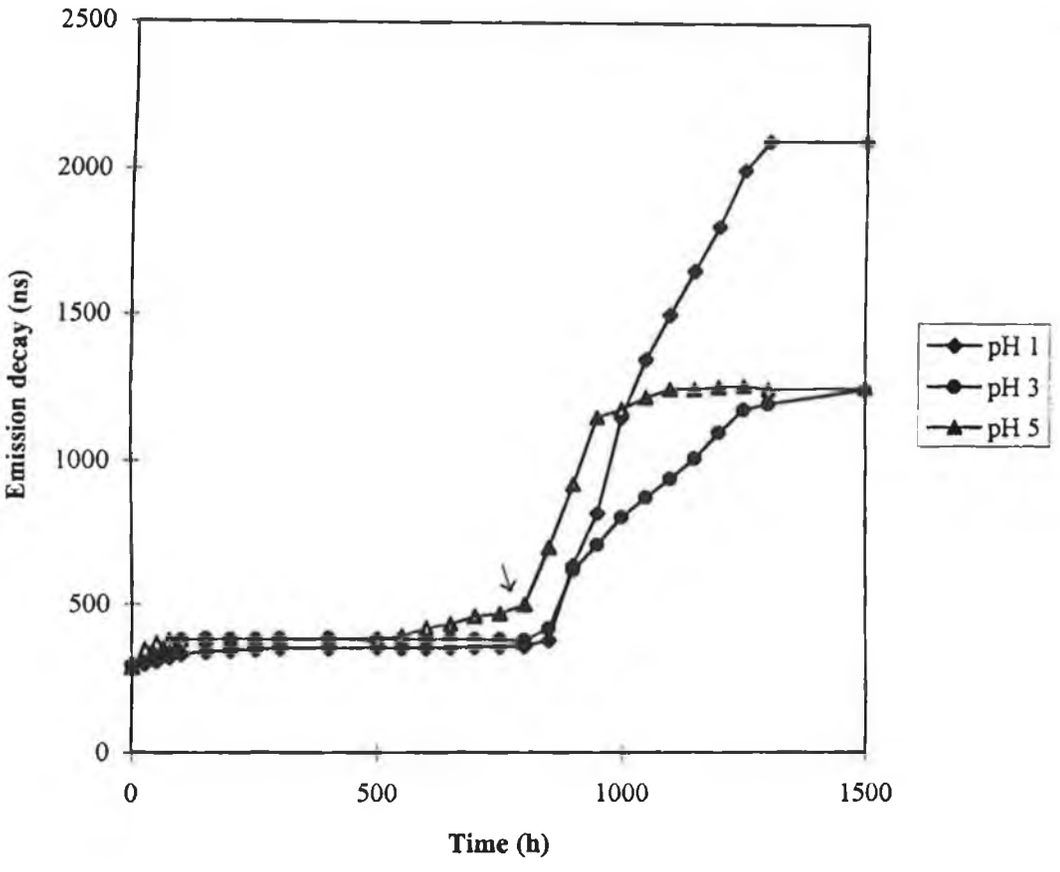

Figure 4.6 Change of the emission lifetime of $[Ru(dpp)_3]^{2+}$ sol-gels with time, prepared according to Method 2, at various pH's.

Similarly, while the overall viscosity increases dramatically at the gel point, the microviscosity does not. At this point, a relatively open structure is still evident.

Figure 4.6 illustrates the changes in the emission lifetime of $[Ru(dpp)_3]^{2+}$ doped samples prepared at a number of different pHs as a function of time while Table 4.4 shows the accompanying emission decay data for this diagram. For clarity, only the longer lifetime component is displayed in this figure. The gels were allowed to age for an extended period of time in order to ascertain any increase in lifetime which may have occurred during this interval. The arrowhead indicates the time at which the sample lids were pierced in order to allow for the evaporation of the solvent molecules. Several features merit additional discussion at this point.

First, a very slight increase in the emission lifetime is observed. This initial stage represents the liquid to gel region which, as discussed in Chapter 3, is strongly pH dependent. For example, although not clearly evident from Figure 4.6, the rise in emission lifetime is more gradual at pH 5 than pH 1 and 3. This result is consistent with previous work in Chapter 3. A possible explanation for this increase in lifetime during this time, is the slowing down of diffusion-controlled oxygen quenching which is not favoured when the oncoming gelation increases the apparent viscosity [18].

After gelation takes place, the lifetime plateaus and the sol-gel begins to age as polycondensation and networking continue. This suggests that the microenvironment as experienced by the $[Ru(dpp)_3]^{2+}$ molecules remains more or less constant throughout this period despite the on-going change in structure caused by the continuing reactions of the ageing process. During this stage, the mean pore size remains large and solvent fills these pores; the gel is considered "wet". Water is thought to be almost freely diffusing even in the gel state, thus promoting the possibility for further hydrolytic reactions so that the structural changes are expected to continue until the gel has reached a final stable state. Thus, it appears that while ageing occurs the $[Ru(dpp)_3]^{2+}$ molecules are in a wet, low-viscosity environment. The lifetime of the complex at this stage suggests that there is little, if any, electrostatic interaction between the complex molecules and the surface of the gel. Throughout the ageing process, the emission decay profile of the $[Ru(dpp)_3]^{2+}$ molecules is best described by a single exponential model which suggests that this dopant is not capable of distinguishing between those different microdomains experienced by $[Ru(bpy)_3]^{2+}$ and $[Ru(phen)_3]^{2+}$ during the early stages of the sol-gel process. This can be attributed to the different sensitivities of these complexes to the nature of the surrounding medium. The small increase in lifetime which occurs prior to piercing the lid of the sample prepared at pH 5 can be attributed to synerisis. As mentioned in the introduction, syneresis is the shrinking of the gel caused by formation of new bonds through condensation reactions. Towards the end of the

ageing process, the increase in bridging bonds causes contraction of the gel network [38].

The third stage of the ageing process, is denoted by a rapid increase in the emission lifetime and represents the initial stages of sol-gel drying. During this stage, the solvent is expelled from the siloxane network of the sol-gel and the volume of the monolith decreases significantly. The lifetime of the $[Ru(dpp)_3]^{2+}$ dopants changes dramatically during this stage as the pores collapse and are emptied of solvent. The relative rate of drying is different for the different pH suggesting that the drying rate is also pH dependent. Thus, it appears that the increase in lifetime at this time, is due to the partial expulsion of ethanol from the matrix followed by the removal of water. As drying of the monolith proceeds, constriction of the pores results in the $[Ru(dpp)_3]^{2+}$ molecules being brought into closer contact with the solid surroundings. Consequently, the observed sequence of an increase in lifetime could simply be explained by the shrinkage of the solid medium, leading to the constriction of the chromophores within the pores, which would decrease their vibrational degrees of freedom and thus the nonradiative rate constant. Another interesting feature of this particular system is that the introduction of a second lifetime component for the emission decay profile of the $[Ru(dpp)_3]^{2+}$ molecules only becomes apparent during the drying procedure. This again demonstrates that this particular ruthenium polypyridyl complex is not sensitive to the changes which occur during the gelation and ageing of the sol-gel. It does not sense the heterogeneous nature of the sol-gel matrix until the solvent is expelled from the system. In the final stage, the sol-gel is dried, the majority of the solvent is removed, and the lifetime levels off. As mentioned, the emission lifetime is now better described by a double exponential model.

In all cases, the longer lived component of the luminescence decay profile exhibits the greatest fractional contribution. This is consistent with the model proposed by Narang and co-workers [24], which suggest that a highly viscous microenvironment exists after the drying procedure has taken place. One possible interpretation of the luminescent decay data is that the $[Ru(dpp)_3]^{2+}$ dopants sense

two local microenvironments, one which allows a substantial degree of rotational vibration resulting in a short lived component ("wet pores"), the second longer lived component arising from a more compact environment ("dry pores").

4.2.2.3 Luminescent decay of $[Ru(phen)_2(H3Mptr)]^{2+}$ in the sol-gel matrix.

For $[Ru(bpy)_3]^{2+}$, relaxation of the emissive metal-to-ligand charge-transfer (^{3}MLCT) state exhibits a temperature dependence in the 150-300 K range which has been ascribed to the thermally activated population of a metal-centred excited state (^{3}MC) which decays more rapidly than the ^{3}MLCT state [32]. The relative energies of the ^{3}MLCT and ^{3}MC states can be controlled to some degree by the making of mixed ligand complexes in which there is a single weak σ-donor diimine ligand with a relatively low π^* level and the remaining ligands are strong σ donors [39,40]. The result is to increase the ^{3}MLCT-^{3}MC splitting, thereby removing the thermally activated nonradiative decay pathway and inhibiting the photoanation of the complex.

A wide body of literature exists demonstrating the effects of solution acidity on molecular luminescence. In general excited states of photoactive acids have excited state pK_as which differ from those in the ground state. Table 4.5 shows the emission decay behaviour of $[Ru(phen)_2(H3Mptr)]^{2+}$ in the sol-gel prepared at the two extreme pH values (*i.e.* 1 and 5) as a function of time. The emission energies and indeed the emission lifetimes of the protonated and dissociated forms differ immensely. In metal diimine complexes where the lowest energy MLCT state involves charge-transfer to the ligand exhibiting acid-base behaviour, the excited state becomes more basic than the ground state. When the MLCT state is localised on the spectator ligand, the pK_a decreases upon excitation of the complex. In the case of $[Ru(phen)_2(H3Mptr)]^{2+}$, the ground state has a pK_a of 5.03, while the excited

Table 4.5 Luminescent decay data for $[Ru(phen)_2(H3Mptr)]^{2+}$ doped sol-gel samples.

Time after preparation (h)	Method 2 (1) τ_1,τ_2 (ns)[b]	Method 2 (5) τ_1,τ_2 (ns)[b]
0	----[a]	70(100)
50	----[a]	400(90),50(10)[$]
100	60(100)	800(40),200(60)
300	300(55),35(45)[$]	1850(45),380(55)
600	320(65),50(35)[*]	1900(40),450(60)[*]
650	345(70),55(30)	1900(55),480(45)
700	350(85),65(15)	1880(85),470(15)
850	355(85),60(15)	1900(85),475(15)
1000	350(85),60(15)	1920(90),480(10)

[$] Indicates gel time ($t_g$) of the sample. [*] Sample top pierced to allow for evaporation of solvent.

[a] This value is outside the range of the instrumentation (i.e. < 20 ns). [b] Values in parentheses are the components pre-exponential factors given in percent. Accuracy of measurements is ± 10 %. Excitation wavelength of 355 nm.

state pK_a has a value of 2.7 (see Chapter 3). Protonation of this complex results in a much shorter lifetime than that of the deprotonated form. This is evident from the data given in Table 4.5 whereby the initial lifetime of the pyridyltriazole doped sol-gel prepared at pH 1, was too short lived to be measured. The gel prepared at pH 5 on the other hand exhibits an initial lifetime of 70 ns which corresponds to the lifetime of the dissociated complex in solution (see Table 3.3). As such, the lifetime measurements obtained for these pyridyltriazole doped sol-gel samples directly after preparation (*i.e.* at zero time) coincide well with the solution values The origin of this much shorter luminescence lifetime for the protonated complex and subsequently the increase in emission energy is associated with the ^{3}MLCT-^{3}MC energy gap. $3Mptr^-$ is a stronger σ-donating ligand than H3Mptr due to the negative charge induced on the deprotonated ligand. Assuming an averaged ligand field environment for both protonated and deprotonated complexes the $Ru(d\pi)\rightarrow Ru(e_g^*)$ energy should

be larger for the deprotonated complex. So, the ^{3}MLCT-^{3}MC energy gap is larger making the ^{3}MC state more difficult to populate, and this is reflected in the longer emission lifetimes.

At the lower pH of 1, the lifetime remained too short to be measured accurately until approximately 48 hours after the initial preparation. As was observed for those gels doped with $[Ru(bpy)_3]^{2+}$, the proceeding sol-gel reactions result in an increase in the lifetime of the pyridyltriazole complex of these doped gels. With the oncoming gelation, the lifetime of this sample was fitted to a double exponential model. From section 3.2.3.2, it was suggested that the increase in emission energy maximum which occurs during this time for the sample prepared at pH 1 was associated with a destabilisation of the ^{3}MLCT state. Again, this destabilisation results in a subsequent increase in the t_{2g}-^{3}MLCT energy gap and as such an increase in the lifetime of the immobilised complex is expected on the basis of the energy gap law [31,32]. It is also likely that the increase in lifetime for this sample is partly caused by the decrease in the molecular motion of the complex as it is restricted by the sol-gel matrix.

As mentioned previously, it was possible to measure the initial lifetime of the pyridyltriazole doped gel prepared at the higher pH of 5. Directly after preparation, the deprotonated form of the complex is known to be present. In the preceding chapter it was deemed that for this sample, $[Ru(phen)_2(3Mptr)]^+$ accepts a proton to become $[Ru(phen)_2(H3Mptr)]^{2+}$ during the initial sol-gel reactions from the position of the emission maximum and also the absorption profile (see Section 3.2.3.2). As such, one would expect a decrease in the lifetime of the complex due to the formation of the protonated complex. However, this was not the case. Instead the lifetime of the doped sol-gel was observed to increase continuously. Again, the reason for this increase is as yet unclear, but most likely the same factors as were mentioned for $[Ru(bpy)_3]^{2+}$ contribute here (*i.e.* a decrease in k^{nr} and accessibility of the dd level). Therefore, it is possible that any decrease in lifetime which may occur upon formation of the protonated complex during the initial sol-gel reactions would be masked by these opposing factors.

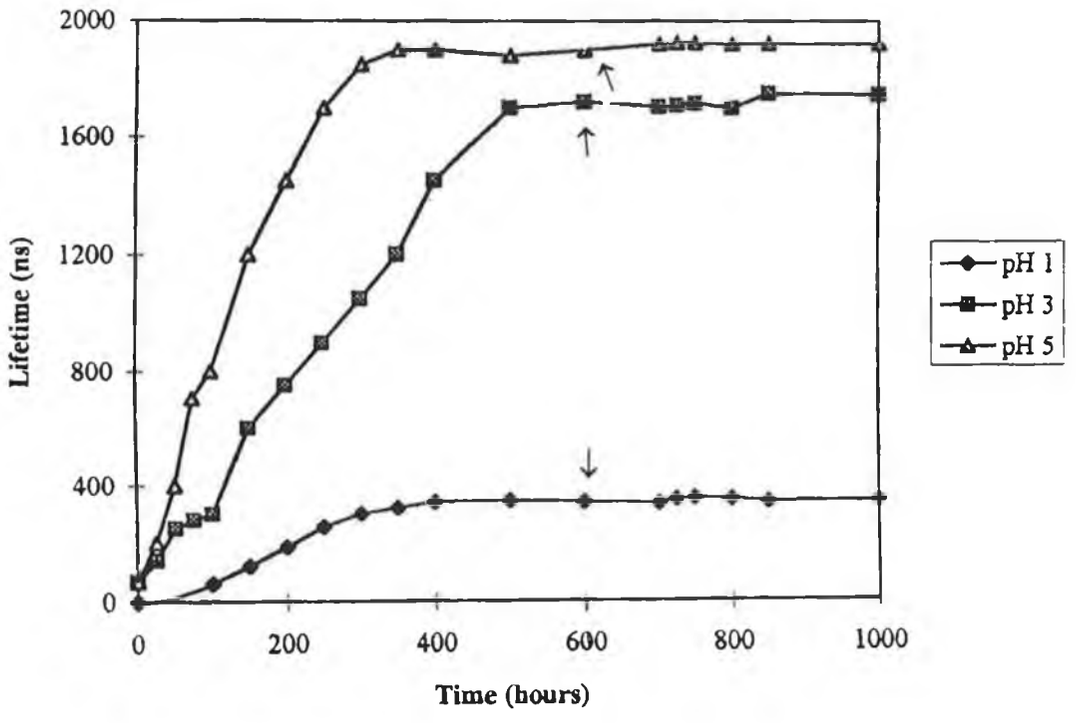

Figure 4.7 Change of the emission lifetime of $[Ru(phen)_2(H3Mptr)]^{2+}$ sol-gels with time, prepared according to Method 2, at various pH's.

In the preceding chapter, the final emission maximum of the gel prepared at pH 5 was ascribed to the presence of the protonated form of the complex.

Figure 4.7 illustrates the increase in lifetime of this Ru(II) complex during the sol-gel process prepared at three different pH values. A number of features should be mentioned here. Firstly, in the low pH regime, the lifetime of the gel prepared at pH 1 shows a significantly smaller increase than those gels prepared at the higher pH values. This effect was noticed previously for those gels doped with $[Ru(bpy)_3]^{2+}$ and $[Ru(phen)_3]^{2+}$. Although the protonated pyridyltriazole complex is thought to be present in each of the final xerogels, the lifetimes differ immensely. This suggests that the extent of interaction between the complex and the surrounding matrix is different at the low and high pH. Again, this is most likely caused by the charge of the sol-gel surface. As mentioned previously, a negatively charged surface would

diminish the nonradiative decay of the Ru(II) pyridyltriazole cation to a greater extent than a positively charged one. In effect, the SiO^- groups would inhibit the molecular motion of the dopant more effectively than the positively charged $SiOH_2^+$ surface groups. In addition, a negatively charged surface may be successful in distorting the dopant such that the ^3MC may no longer be populated. This possibility will be addressed in greater detail in the following two chapters. Another important feature of this diagram is that the lifetime of each of the samples continues to increase after the gel time, t_g. This is more pronounced for the sample prepared at higher pH values. Furthermore, the rate of increase of the lifetime of the gel prepared at pH 5 is faster than that prepared at pH 3. This is consistent with the theory that above pH 2, the rate of the sol-gel reaction depends on the concentration of OH^-. It is interesting to compare this figure with Figure 3.17 (which shows the shift in emission maxima of this complex with time). From Figure 3.17, for the gels prepared above pH 2, a further blue shift in the emission energy was observed during the drying stage of the gel. During this stage, the sol-gel is dried and the majority of the solvent is removed. However, this was not accompanied by an increase in the lifetime of the $[Ru(phen)_2(H3Mptr)]^{2+}$ dopant. Nevertheless, from Table 4.5 it can be seen that, while the lifetimes remain relatively constant during the drying phase, the contribution of the longer lifetime increases significantly during this stage. This suggests that upon drying, the number of molecules which experience a restricted environment increases. This result is consistent with the expulsion of solvent and the overall shrinkage of the sol-gel.

4.3 Conclusion.

The photophysical properties of sol-gel matrices doped with the Ru(II) complexes $[Ru(bpy)_3]^{2+}$, $[Ru(phen)_3]^{2+}$ and $[Ru(dpp)_3]^{2+}$ were explored further in this chapter. The excited state lifetime of these complexes are dramatically altered by the sol-gel matrix. In particular, an increase in the lifetime of all of these complexes was noticed in the xerogel stage. This increase in excited state lifetime is dependent on nature of the dopant and also the sol-gel processing conditions (*i.e.* the pH at which the gel was prepared). The introduction of a second lifetime component for all of these complexes is strong evidence for the heterogeneous nature of the sol-gel matrix.

The excited state lifetimes of $[Ru(bpy)_3]^{2+}$ and $[Ru(phen)_3]^{2+}$ were found to probe the initial sol-gel reactions. The rate at which the lifetime of these complexes increases depends greatly on the pH at which the gel was prepared (*i.e.* the rate of the sol-gel reactions). $[Ru(dpp)_3]^{2+}$ successfully probed the final stages of the sol-gel process. For this complex an increase in lifetime was only observed at the drying stage, during which most of the excess solvent evaporated. It is important to note here that at the storage temperatures used in this thesis (*i.e.* 50 ^{0}C) it is likely that a fraction of residual solvent molecules will remain within the pore system. Finally, the emission decay profile of $[Ru(phen)_2(H3Mptr)]^{2+}$ was studied as the sol-gel reactions proceeded. The results reported for this complex suggest that the extent of electrostatic interaction is much greater when the surface of the silicon network is negatively charged.

The results in this chapter suggest that both the size of the dopant and also the nature of the surface charge of the silica network are important in determining the magnitude of the excited state lifetime of the immobilised/encapsulated Ru(II) polypyridyl complex. The following chapter addresses these issues further.

4.4 References.

[1] J.F. Rabek, Photochemistry and Photophysics Volume 1, CRC Press, **1990**.

[2] A. Siemiarczuk, W.R. Ware, *J. Phys. Chem.*, 91, 3677, **1987**.

[3] A. Siemiarczuk, W.R. Ware, *J. Phys. Chem.*, 93, 7609, **1989**.

[4] K. Sienicki, S. Blonski, G. Durocher, *J. Phys. Chem.*, 95, 1576, **1991**.

[5] K. Hashimoto, m. Hiramoto, T. Sakata, H. Muraki, H. Takemura, M. Fujihira, *J. Phys. Chem.*, 91, 6198, **1987**.

[6] J. Colon, C. Yang, A. Clearfield, C. Charles, *J. Phys. Chem.*, 94, 874, **1990**.

[7] Y. Liu, W. Ware, *J. Phys. Chem.*, 97, 5980, **1993**.

[8] K. Kemnitz, N. Tamai, I. Yamazaki, N. Nakashima, K. Yoshihara, *J. Phys. Chem.*, 91, 1423, **1987**.

[9] W.R. Seitz, *Anal. Chem.*, 56, 16A, **1984**.

[10] J. Janata, J. Bezagh, *Anal. Chem.*, 60, 63R, **1988**.

[11] E.R. Carraway, J.N. Demas, B.A. DeGraff, J.R. Bacon, *Anal. Chem.*, 63, 337, **1991**.

[12] X. Li, K. Wong, *Anal. Chim. Acta*, 262, 27, **1992**.

[13] J.N. Demas, B.A. DeGraff, *Anal. Chem.*, 63, 17, 829A, **1991**.

[14] P. Kiernan, C. McDonagh, B.D. MacCraith, K. Mongey, *J. Sol-Gel Sci. Tech.*, 2, 513, **1994**.

[15] S. Draxler, M. Lippitsch, I. Klimant, H. Kraus, O. Wolfbeis, *J. Phys. Chem.*, 99, 3162, **1995**.

[16] R. Reisfeld, J. Non-Cryst. Solids, 121, 254, **1990**.

[17] R. Reisfeld, C.K. Jorgenson, *Structure and Bonding*, 77, 208, **1992**.

[18] S. Modes, P. Lianos, *Chem. Phys. Lett.*, 153, 351, **1988**.

[19] F.N. Castellano, T.A. Heimer, M.T. Tandhasetti, G.J. Meyer, *Chem. Mater.*, 6, 1041, **1994**.

[20] A. Siemiarczuk, B.D. Wagner, *J. Phys. Chem.*, 94, 1661, **1990**.

[21] K. Matsui, K. Sasaki, N. Takahashi, *Langmuir*, 7, 2866, **1991**.

[22] B. Dunn, J. Zink, *J. Mater. Chem.*, 1, 903, **1991**.

[23] R. Winter, D. Hua, X. Song, W. Mantulin, J. Jonas, *J. Phys. Chem.*, 94, 2706, **1990**.

[24] U. Narang, R. Wang, P. Prasad, F. Bright, *J. Phys. Chem.*, 98, 17, **1994**.

[25] U. Narang, J. Jordan, F. Bright, P. Prasad, *J. Phys. Chem.*, 98, 8101, **1994**.

[26] M. Kaneko, *J. Photochem. Photobiol. A,: Chem.*, 61, 373, **1991**.

[27] S. Campagna, A. Bartolotta, G. Di Marco, *Chem. Phys. Lett.*, 206, 30, **1993**.

[28] D, Avnir, V.R. Kaufman, *Langmuir*, 2, 717, **1986**.

[29] J.N. Demas, G.A. Crosby, *J. Am. Chem. Soc.*, 93, 2841, **1971**.

[30] J. van Houten, R.J. Watts, *J. Am. Chem. Soc.*, 98, 4853, **1976**.

[31] R. Lumpkin, T.J. Meyer, *J. Phys. Chem.*, 90, 5307, **1986**.

[32] A. Juris, V. Balzani, F. Barigelletti, S. Campagna, P. Belser, A. Von Zelewsky, *Coord. Chem. Rev.* 84, 85, **1988**.

[33] S. Allsopp, A. Cox, T. Kemp, W. Reed, *J. Chem. Soc., Faraday Trans. I*, 74, 1275, **1977**.

[34] S. Lumpkin, E. Kober, L. Whorl, Z. Murtaza, T. Meyer, *J. Phys. Chem.*, 94, 239, **1990**.

[35] M. Fetterolf, H. Offen, *J. Phys. Chem.*, 89, 3320, **1985**.

[36] C. J. Brinker, *J. Non-Cryst. Solids*, 31, 100, **1988**.

[37] J.C. Pouxviel, B. Dunn, J. Zink, *J. Phys. Chem.*, 93, 2134, **1989**.

[38] L. Hench, J. West, *Chem. Rev.*, 90, 33, **1990**.

[39] E. Ryan, R. Wang, J.G. Vos, R. Hage, J.G. Haasnoot, *Inorg. Chim. Acta*, 208, 49, **1993**.

[40] G.H. Allen, R.P. White, D.P. Rillema, T.J. Meyer, *J. Am. Chem. Soc.*, 106, 2613, **1984**.

Chapter 5.

The temperature dependence of the emission properties of Ru(II) and Os(II) polypyridyl complexes immobilised in a sol-gel matrix.

5.1 Introduction.

The results of extensive studies on the photochemical and photophysical properties of polypyridyl complexes of Ru(II) and Os(II) are now available [1-3]. At temperatures below 77 K Crosby and co-workers found that the temperature dependencies of excited-state lifetimes and indeed emission quantum yields for $[Ru(bpy)_3]^{2+}$ and related tris-chelates could be reasonably well described by the presence of three low-lying metal-to-ligand charge-transfer (MLCT) excited states [4]. At or above 77 K, all three states are essentially equally populated, and hence, this state may be considered an "average state". Besides the processes of radiative and radiationless decay, a third, thermally activated process may deactivate this triplet state. By evaluating either the luminescent lifetime or quantum yield as a function of temperature, the activation energy for this process was determined to be approximately 3600 cm^{-1} [5]. This process has been identified as the population of a non-luminescent, metal-centred d-d state (or states). It has been suggested that population of these states leads to the photoinduced ligand loss chemistry that is observed for many polypyridyl complexes of ruthenium(II) [6-11]. For such complexes, lifetimes in fluid solution are generally highly temperature dependent. In addition, evidence for the presence of a fourth MLCT state lying approximately 800 cm^{-1} above the lowest lying ^{3}MLCT level has been reported [10]. These latter processes play an important role in determining excited-state properties under ambient conditions, and their origins are the subject of this chapter.

In this chapter we report the study of the luminescence properties of a number of transition metal complexes as a function of temperature. These experiments were carried out both in alcohol solution and in a rigid sol-gel matrix. The purpose of these studies was to investigate the effect of the gel on the photophysical properties of the complex. The polypyridine complexes were selected to represent complexes which have different metals and ligands involved in the ^{3}MLCT excited-state responsible for the luminescence properties [12,13]. Comparison with literature data, where available, concerning the photophysical properties of these polypyridine complexes in other rigid matrices have also been

made. In addition, evidence is presented which supports the existence of a thermally accessible, higher lying MLCT state for polypyridyl complexes of Ru(II) and Os(II).

5.1.1 General photophysical properties of excited-state molecules.

An electron can be promoted from the ground state to an electronically excited state by the absorption of a photon of light. The necessary condition is that the photon energy, *hν*, matches the energy gap between the ground state and the excited state. This energy gap, for low energy states of common organic and inorganic molecules, corresponds to light in the visible and near ultraviolet regions. Light absorption often generates the excited state in a high vibrational level because of the Frank-Condon principle (*i.e.* the nuclei cannot change either their position or their kinetic energy during the electronic absorption transition). The newly formed electronically excited state molecules can thus be regarded as an "energetic" species with respect to the surrounding ground state molecules that have a Boltzmann equilibrium distribution largely centred on the zero vibrational level. The vibrationally excited molecules will tend to dissipate their excess vibrational energy by interactions (collisions) with surrounding molecules. This process is called "vibrational relaxation". In general, vibrational relaxation occurs in the picosecond time scale. Much of the consequential photophysical aspects of electronically excited state molecules occurs on a much longer timescale, thermally equilibrated excited states should be considered the only relevant photophysical species, regardless of the initial amount of vibrational excitation with which they may have been created.

Electronically excited molecules can return to the ground state *via* the emission of a photon of light *hν'*. This radiative transition is the reverse process of light absorption and is often referred to as "spontaneous emission". In radiative deactivation, energy conservation is provided by this emission. If an excited state is to be converted into the ground state (or a lower excited state) without emission of radiation, a two-step mechanism must operate:

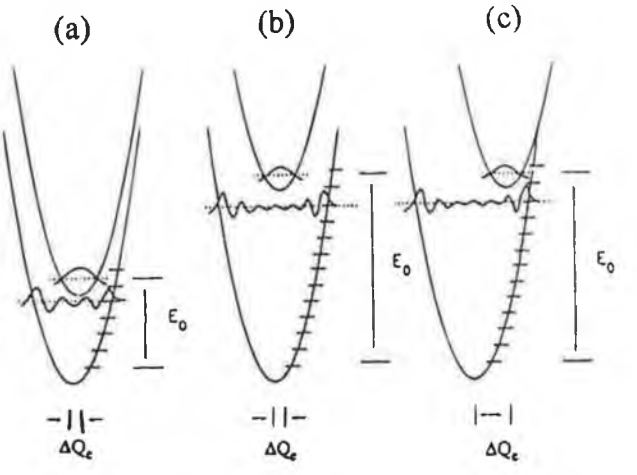

Figure 5.1 The potential energy diagram and associated vibrational wave functions (a) illustrating the effects of the energy gap (b) and changes in the equilibrium displacement (c) on vibrational wave function overlaps [17].

(a) isoenergetic conversion of the electronic energy of the upper state into vibrational energy of the lower state (radiationless transition),

(b) vibrational relaxation of the lower excited state.

Step (b) is known to be very fast, making step (a) the rate determining process [14]. Radiationless transitions between states of different or equal spin multiplicity are called "intersystem crossing" and "internal conversion" respectively.

The decay of metal-to-ligand charge transfer excited states of polypyridyl complexes of Ru(II) and Os(II) at room temperature are typically dominated by nonradiative processes [1,12,15-18]. Their rate constants typically increase as the energy gap between the ground and excited states decrease, consistent with the energy gap law [15]. Because of this effect, complexes with low energy

absorption bands normally are weak emitters and have short-lived excited states. The decreased lifetimes limit their use as sensitisers in photoinduced electron and energy transfer [18,19].

It is important to recognise that it is both the energy gap between the excited and ground state and also the change in equilibrium displacement (ΔQ_e) which influence vibrational overlap and hence the nonradiative rate k^{nr}. Figure 5.1(b) illustrates the situation of 'nested' surfaces [17,18]. In this case, the vibrational overlap tends to be poor because of the oscillatory behaviour of the wavefunction of the high vibrational level of the ground state. In this situation, ΔQ_e is very small, the probability of radiationless deactivation is low, and the two states are "weakly coupled". For a given ground state vibrational frequency, this probability decreases exponentially with the energy gap between the states (energy gap law), since the higher the energy gap, the higher the vibrational quantum number of the isoenergetic level of the ground state, and the smaller the overlap. At a constant energy gap, the probability depends on the vibrational spacings of the ground state, since the smaller is the energy spacing, the higher is the vibrational quantum number of the isoenergetic level of the ground state, and the smaller is the overlap. Therefore, high energy vibrations are more effective than low-frequency ones as energy accepting modes. For this reason, deuteration can be employed to reduce the rate of radiationless deactivation.

The case depicted in Figure 5.1(c) is that of potential energy surfaces crossing in the vicinity of the excited-state minimum. In this situation, where ΔQ_e is large (*i.e.* strong coupling), there is relatively good vibrational overlap, independent of the vibrational quantum number of the ground-state level. The probability of radiationless transition tends to be high, insensitive to the energy gap, and independent of the vibrational frequency of the accepting mode. Therefore, a low emission lifetime caused by a low energy gap could be overcome by decreasing ΔQ_e and structural distortion in the excited state.

In principle, radiationless transitions can occur between excited states as well as between an excited state and the ground state. Generally speaking, electronically excited states are relatively closely spaced with respect to the large energy separations occurring between the excited state and the ground state. In

addition, the higher excited states are more likely to have distorted geometries than the lowest excited states. Both of these factors favour radiationless transitions among excited states (small energy gaps and frequent crossing) with respect to those between the lowest excited state and the ground-state (large energy gap and often nested surfaces). The unimolecular excited state processes described in this section do not cause any chemical change in the light-absorbing molecule and thus can be classified as "photophysical" processes. Excited states can, however, achieve deactivation to the ground-state species by a variety of chemical processes. Because excited states are "energy rich" with respect to the ground state species, they are expected to be more reactive than the corresponding ground state. In order to compete with photophysical processes, these photochemical reactions of the excited state must be very fast on the conventional chemical timescale.

As mentioned previously, the photochemical and photophysical behaviour of a given molecule depends on the relative efficiencies of luminescence, radiationless decay, and chemical reaction, and on the excited state lifetime which, in effect, controls the interactions with other species. These quantities are determined by the rate constants of the various decay processes. In turn, such rate constants are controlled by symmetry and spin properties and by the relative positions and shapes of the potential energy curves that describe the various excited states [16]. Much research has been carried out involving the examination of the relationship between the MLCT energies of a series of complexes and the corresponding photophysical properties [7-14]. As regards the photochemical lability of these systems, the literature suggests photosubstitution results from the population of low-energy ligand field states (^{3}MC) that are not spectroscopically observed. For a series of complexes which have been studied, such as $[Ru(NH_3)_5(pyX)]^{2+}$, where pyX is a series of substituted pyridines, the quantum yield for ligand loss decreases as substituents are added that decrease the energy of the ^{3}MLCT state [17]. The decrease in the substitution yield occurs as the ^{3}MLCT state becomes isolated from the ligand field states which are actually responsible for substitution.

The photophysics and photochemistry of numerous ruthenium(II) polypyridyl complexes have been examined in solution [1]. Because of its prominence in transition metal chemistry, extensive work has been carried out in order to establish in detail the photochemical and photophysical properties of $[Ru(bpy)_3]^{2+}$. The complication for complexes of Ru(II) associated with the interconversion of a low-lying d-d state or states has proved to be a challenge for photophysicists. Evidence for the d-d state has come from temperature-dependent lifetime and photochemical and ligand loss experiments. An obvious extension of the ruthenium polypyridyl chemistry is to that of analogous complexes of osmium, where similarities in chemical properties have been observed. A very important feature of Os(II) complexes is that the metal-nitrogen distances are very similar to those found for the analogous ruthenium(II) compounds [18] and the two can be easily compared. These Os(II) polypyridyl complexes have similar properties to those of Ru(II), in that their oxidation processes are metal-centred, their reduction processes are ligand-centred and the lowest excited state is a triplet metal-to-ligand charge-transfer (^{3}MLCT) level. They also exhibit excellent absorption properties in the visible region, stability in their oxidised and reduced forms and relatively long-lived luminescent excited-states.

Despite the similarites outlined above, differences in the electronic structure of the analogous complexes of the two metals exist. The luminescence of the Os(II) complexes are at lower energy than their Ru(II) analogues due to the reduced energy gap between the ^{3}MLCT state and the ground state. This results in very short lifetimes for ^{3}MLCT emission of Os(II) complexes. In equivalent polypyridyl ligand environments, dd states do not appear to play an important role for complexes of Os(II) as compared to Ru(II). A larger value of $10Dq$ for Os results in dd states which occur at higher energies (and which are well removed from the emitting MLCT states) than those of analogous Ru(II) complexes [6]. Another major difference between ruthenium and osmium is spin-orbit coupling, which is much larger for third-row transition elements than second-row metals. This results in extensive mixing of excited states of different spin-multiplicities.

5.1.2 Temperature dependent lifetime data.

The excited-state electronic structures of $[Ru(bpy)_3]^{2+}$ and related complexes have been investigated by spectroscopic studies [19], low-temperature emission and lifetime measurements [4], and theoretical studies [20]. As mentioned in the preceding chapters, excitation is followed by rapid intersystem crossing from the initially formed ^{1}MLCT to a ^{3}MLCT state which is believed to occur with nearly unit efficiency for $[Ru(bpy)_3]^{2+}$ [21]. The triplet charge-transfer state decays via both temperature-dependent and temperature-independent processes [5,7,22]. The thermally activated decay mode has been ascribed to the internal conversion from this ^{3}MLCT state to a triplet metal-centred state, ^{3}MC [11]. The energy of the ^{3}MC state will be influenced principally by the σ-donating strength of the ligands and the ^{3}MLCT state depends principally on the energy of the lowest ligand π^* orbitals. Preparation of complexes having bipyridine with a low-energy π^* level and more basic bipyridines filling the remaining coordination sites may result in ruthenium polypyridine complexes having ^{3}MC states thermally inaccessible from the ^{3}MLCT level. Since most polypyridyl complexes of ruthenium exhibit fluorescence at room temperature, it is possible to monitor the ^{3}MLCT to ^{3}MC internal conversion as a function of systematic structural variations associated with the surrounding ligands.

A number of tris chelate and mixed-ligand ruthenium (II) complexes have been prepared and their spectroscopic and electrochemical properties have been investigated. Initially, the ligands employed were bpy and phen, or their methyl, phenyl, carboxyl derivatives and so forth [3,23]. Such minor modifications of ligands do not bring about large changes in the redox and the excited-state properties of these complexes in solution. In contrast to these complexes, tris chelate complexes containing for example the 2,2'-biquinoline (biq) ligand, exhibit greatly different spectroscopic and redox properties in comparison to those of $[Ru(bpy)_3]^{2+}$ [24,25]. Temperature-dependence studies of the luminescence behaviour can yield important information concerning the energy, electronic nature, and deactivation rate of the luminescent and reactive excited states [25,26]. When such studies are performed over a sufficiently large

temperature range, a rigid-fluid transformation of the matrix (assuming the matrix is solution at room temperature) takes place which may cause luminescence rigidochromism and discontinuity in the ln $1/\tau$ vs. $1/T$ plots. A better knowledge of the parameters which govern the photophysical properties of transition-metal complexes is fundamental for the progress of photochemistry and essential for the design of new photosensitisers [27,28]. These temperature dependence studies of the luminescence behaviour can yield important information concerning the energy ordering of the various excited states and the dynamics of interstate conversion. In this chapter, a detailed study of the temperature dependence of the luminescence emission (both emission energy and lifetime) of a number of transition-metal complexes are reported both in an alcoholic solution and in the sol-gel matrix, over a wide range of temperatures. As such, a review of the literature methods which are currently employed to analyse the temperature dependent lifetime of such complexes in solution follows.

5.1.2.1 Analysis of temperature dependent lifetime data.

As mentioned previously, the relatively long-lived luminescent excited state of $[Ru(bpy)_3]^{2+}$ is metal-to-ligand charge-transfer (MLCT) in character. Excitation of $[Ru(bpy)_3]^{2+}$ leads to a luminescence emission whose intensity, lifetime and energy position are temperature dependent. From the results of low-temperature lifetime (< 77K) and emission-yield experiments on polypyridyl complexes of Ru(II) and Os(II), there is direct evidence for contributions to the excited state decay from 3 low-lying metal-to-ligand charge-transfer (^{3}MLCT) excited states [4,29]. These ^{3}MLCT levels (ΔE 10-100 cm^{-1}) are in Boltzmann equilibrium, each having its own radiative and non-radiative temperature independent rate constant. Theoretical treatments propose that the states have the same orbital parentage and are largely triplet in character, but mix to differing degrees with low-lying, largely singlet states of MLCT origin through the effect of spin-orbit coupling [4,29]. These studies also suggest that a fourth state should exist at slightly higher energies [20]. At the temperatures employed in this thesis (*i.e.* >

77K) the Boltzmann factors relating the three states are such that emission from them is essentially temperature independent and can be viewed as occurring from a single state, namely ^{3}MLCT. The effect of spin-orbit coupling is to mix singlet character into the triplet states and vice versa, but the lowest lying excited states responsible for emission remain largely triplet in character. The efficiency of population of the ^{3}MLCT state following light-absorption throughout the very-near-UV and visible spectral regions is known to be approximately 1 [21].

Again, for polypyridyl complexes of Ru(II) there is the added complexity at higher temperature due to the appearance of thermally accessible d-d states that contribute to, and can dominate, the excited state decay [7,8,11]. Experimentally, establishing such details has required temperature measurements from well above room temperature to that at liquid helium by a number of research groups. Figure 5.2 illustrates a plot of $\ln(1/\tau)$ of 10^{-5} M solution of $[Ru(bpy)_3]^{2+}$ in 4/1 ethanol/methanol (v/v) as a function of temperature in the range of 77-310 K, carried out in our laboratory. The lifetime of the excited state is determined by rate terms for three separate processes from two different states:

(1) radiative decay (k^r) and non-radiative decay (k^{nr}), from a low-lying ^{3}MLCT state or states to the ground state, and

(2) thermal activation to a d-d state or states which subsequently undergo non-radiative decay to the ground state or photochemistry *via* ligand loss.

The excited-state lifetime of $[Ru(bpy)_3]^{2+}$ and related compounds is known to be strongly temperature dependent [4,5,7,8,11] To account for this behaviour, $1/\tau$ can be expressed as the sum of a temperature independent and a temperature dependent terms as given in the equation given below.

$$1/\tau = k_0 + A_i \exp(-\Delta E_i/RT) \qquad (5.1)$$

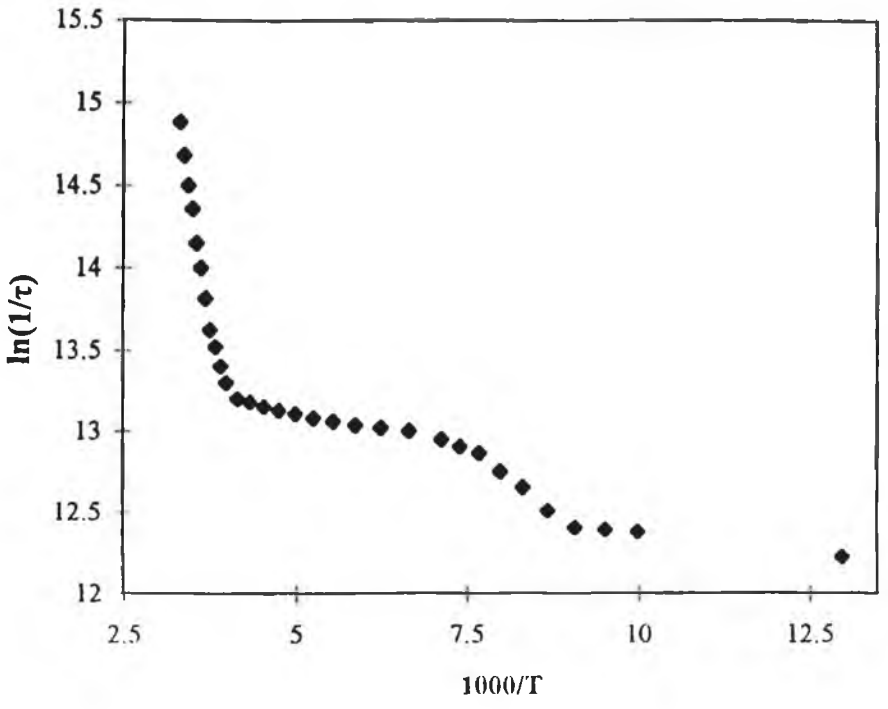

Figure 5.2 Temperature dependence for the luminescence lifetime of $[Ru(bpy)_3]^{2+}$ *in ethanol/methanol 4/1 v/v.*

where $k_0 = k^r + k^{nr}$ (the sum of the temperature independent radiative and non-radiative decays), A_i the frequency factor and ΔE_i the activation energy for surface crossing between states. While the rate of the radiative transition is essentially governed by spin and symmetry factors [30], the radiationless rate constant generally increases with decreasing excited state energy, as expected on the basis of the energy gap law [31].

There is general agreement in the literature that the Arrhenius type term given below (Equation 5.2) which accounts for the temperature dependence of the luminescence lifetime at high temperatures (> 250 K) is related to an activated surface crossing from the ^{3}MLCT manifold to a ^{3}MC level (Equation 5.3) which undergoes photochemical and/or photophysical deactivation (Equation 5.4).

$$k_e = A_e \exp(-\Delta E_e/RT) \qquad (5.2)$$

$$^3\text{MLCT} \underset{k_b}{\overset{k_a}{\rightleftharpoons}} {}^3\text{MC} \qquad (5.3)$$

$$^3\text{MC} \xrightarrow{k_c} \text{ground state and/or products} \qquad (5.4)$$

The ^{3}MC-state energies cannot be determined directly, but the gap between ^{3}MLCT and ^{3}MC states can be approximated from activation parameters obtained from temperature-dependent luminescence lifetimes [13]. In Equation 5.4, k_c represents the sum of all the rate constants of the processes that deactivate ^{3}MC, with the exception of the back surface crossing to the ^{3}MLCT. The experimental deactivation rate constant that comes into play at high temperature can be expressed as follows [22]:

$$k_e = k_a[k_c/(k_b + k_c)] \qquad (5.5)$$

Equation 5.5 leads to two limiting cases as shown in Figure 5.2.

(a) When $k_c >> k_b$, the decay of ^{3}MC is rapid and Equation 5.5 becomes

$$k_e = k_a \qquad (5.6)$$

From this, one can deduce:

$$A_e\exp(-\Delta E_e/RT) = A_a\exp(-\Delta E_a/RT) \qquad (5.7)$$

In this limiting case, the ^{3}MLCT-^{3}MC transition becomes an irreversible crossing, as the subsequent decay from the ^{3}MC state is probably very fast. In this limit, the A_e and the ΔE_e parameters obtained from the fitting correspond to the pre-exponential factor and the activation energy for the ^{3}MLCT$\rightarrow$^{3}MC surface crossing shown in Figure 5.3(a). It follows that for complexes whose ^{3}MC excited state undergoes a very fast decay, the only way to maintain a long excited state lifetime in fluid solution at room temperature is to have a large activation

energy for the ^{3}MLCT→^{3}MC surface crossing. The energy barrier for this surface crossing is presumably related to the energy gap between the zero-zero energies of the two states [22]. Thus, in principle, activation energy can be tuned by tuning the energy of the ^{3}MLCT and ^{3}MC excited states as mentioned in Section 1.3.4.

(b) The second limiting case occurs when $k_b >> k_c$, the decay of ^{3}MC is slow compared to the back surface crossing to the ^{3}MLCT. In such a case, the two states are in equilibrium and Equation 5.5 becomes

$$k_e = (k_a/k_b)k_c \qquad (5.8)$$

Since $k_a/k_b = K = \exp(-\Delta E/RT)\exp(\Delta S/R)$, where ΔE and ΔS are the internal energy and entropy differences between the ^{3}MLCT and ^{3}MC, it follows that;

$$A_e\exp(-\Delta E_e/RT) = k_c\exp[-\Delta E/RT]\exp[\Delta S/R] \qquad (5.9)$$

Since the entropic difference between the two states is expected to be small, Equation 5.9 can be rewritten as;

$$A_e\exp(-\Delta E_e/RT) = k_c\exp[-\Delta E/RT] \qquad (5.10)$$

The meaning of the experimental quantities A_e and ΔE_e depends on the nature of the processes that contribute to k_c. The following limiting cases have been observed;

(b-i) When the major contribution to k_c comes from a chemical reaction or a deactivation process that can be described by an Arrhenius-type equation, Equation 5.10 can be written as;

$$A_e\exp(-\Delta E_e/RT) = A_c\exp[-(\Delta E_c + \Delta E)/RT] \qquad (5.11)$$

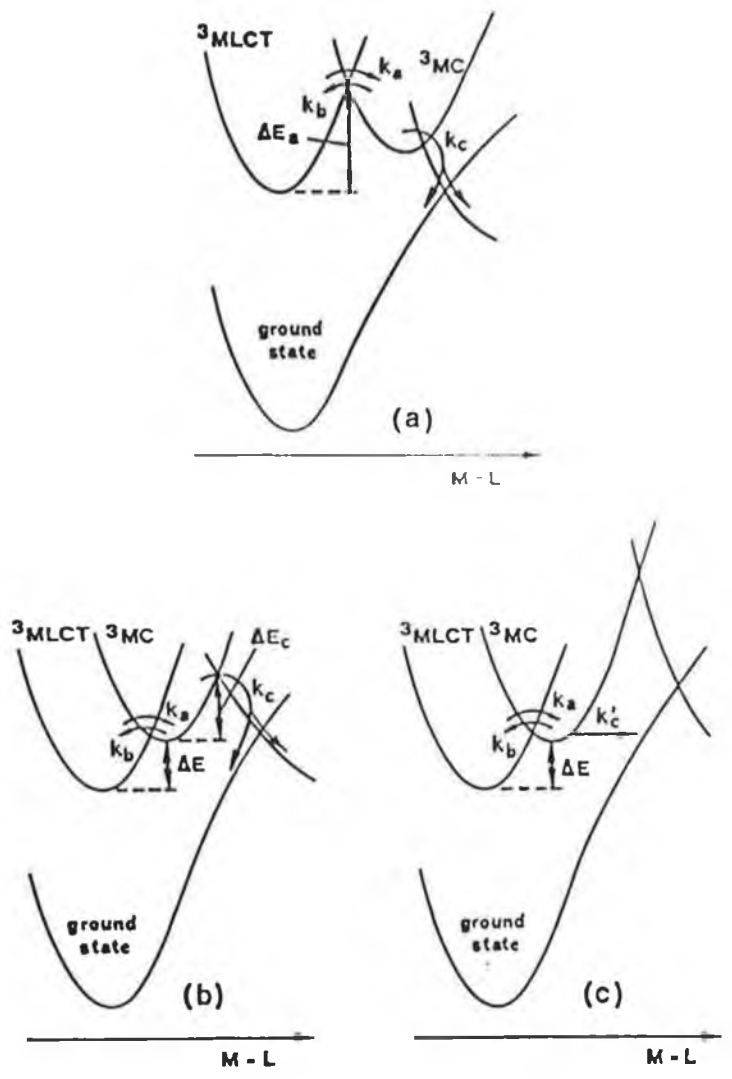

Figure 5.3 Schematic representation of the situation of the potential energy surfaces for the three limiting cases described in text [22].

In such a case, the A_e and ΔE_e parameters obtained from the fitting of the data to Equation 5.1 correspond to the sum of the ^{3}MLCT-^{3}MC energy gap and the activation energy of the decay process of ^{3}MC (Figure 5.3(b)).

(b-ii) When the major contribution comes to k_c comes from a non-activated process k_c', from Equation 5.10 it follows that the pre-exponential factor A_e corresponds to the rate of the non-activated ^{3}MC decay, k_c', and the activation energy ΔE_e corresponds to the ^{3}MC-^{3}MLCT energy gap, ΔE (Figure 5.3(c)).

Activation parameters obtained for the ^{3}MLCT emission of complexes usually fall into one of two categories [13,22,31-42]:

(a) small activation energies (<1000 cm^{-1}) and low pre-factors (< 10^9 s^{-1})

or

(b) large activation energies (>2000 cm^{-1}) and high pre-factors (> 10^{11} s^{-1})

In the second case, the activated process has been ascribed to the population of the ^{3}MC state. If relaxation of the ^{3}MC state is rapid relative to crossover from the ^{3}MC state back to the ^{3}MLCT state, the measured E_a represents the activation energy for ^{3}MLCT$\rightarrow$^{3}MC internal conversion (Figure 5.3a). Since the process is viewed as an electron transfer in a strongly coupled system, the prefactor is expected to be large (10^{13}-10^{14} s^{-1}).

When both the activation barrier and prefactor are small, (case a), interpretation of the data is less clear. Complexes exhibiting this behaviour are typically unreactive towards substitution and as a result, it is unlikely that population of the ^{3}MC state occurs [11,13,14]. The low prefactor also suggests the process involves population of a state only weakly coupled to the ^{3}MLCT state. Kober and Meyer have postulated that this activated process corresponds to the population of an MLCT state of largely singlet character [20,42].

5.2 Results and Discussion.

The results of this chapter are presented in two sections. The first section deals with the photophysical properties of the $[Ru(bpy)_{3-n}(dpp)_n]^{2+}$ series in solution in comparison with that in a sol-gel environment. The temperature dependent emission energy and lifetime of these complexes, both in solution and in a gel matrix, will be given and discussed. These measurements were carried out in order to examine the degree of shielding which the phenyl-substituted ligand extends to the incorporated complex. The second section deals with the incorporation of $[Os(bpy)_3]^{2+}$ and $[Ru(bpy)_2(biq)]^{2+}$ into the sol-gel matrix.

In the previous two chapters, the heterogeneous nature of the sol-gel matrix was reported. The excited state lifetime of all of the immobilised Ru(II) polypyridyl complexes employed in this thesis were fit to a double exponential equation. As such, two emitting components of varied lifetimes were obtained for each Ru(II) polypyridyl doped xerogel. In general, the longer lived component contributes to > 75% of the total decay, while the shorter lived component contributes < 25%. In this chapter, the excited state lifetime of a number of immobilised complexes are studied as a function of temperature. Figures 5.4 and 5.5 illustrate the temperature dependence of the two lifetime components of $[Ru(bpy)_3]^{2+}$ in two different xerogels. These diagrams suggest that the temperature dependent behaviour of both of the lifetime components for each sample show a similar trend. In addition, the relative contribution of each lifetime component remains essentially unchanged throughout the experiment. Therefore, in this chapter, analysis of the temperature dependent lifetime of the immobilised complexes was restricted to only the longer lived, most dominant lifetime component.

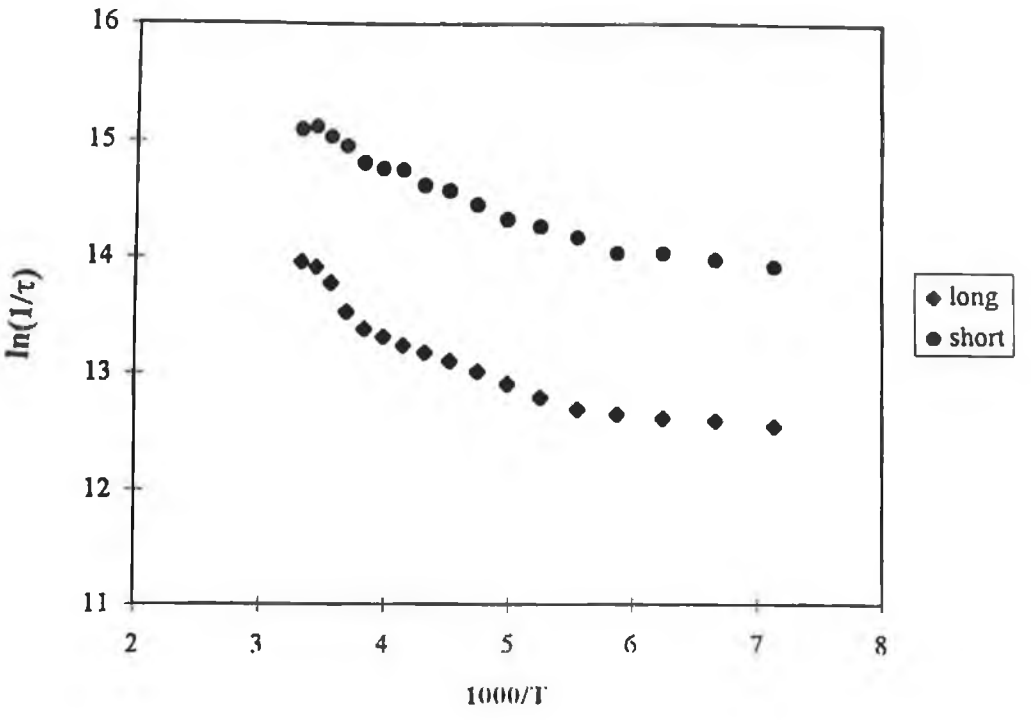

Figure 5.4 Temperature dependence of both of the lifetime components of $[Ru(bpy)_3]^{2+}$ in xerogel (prepared according to Method 2 (1)).

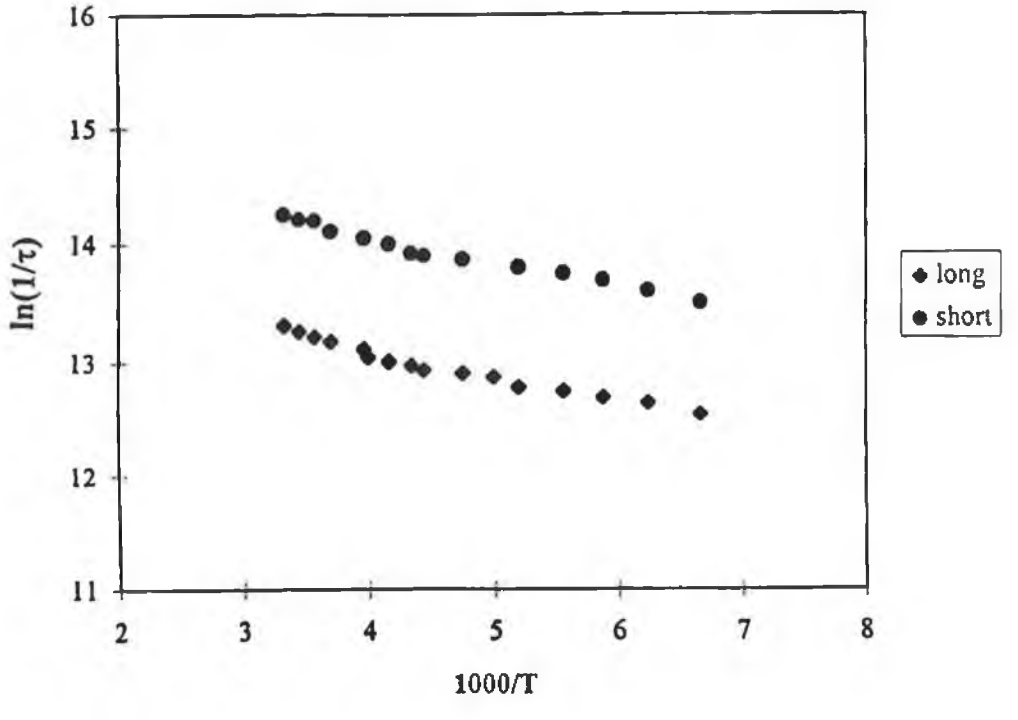

Figure 5.5 Temperature dependence of both of the lifetime components of $[Ru(bpy)_3]^{2+}$ in xerogel (prepared according to Method 2 (5)).

5.2.1 The $[Ru(bpy)_{3-n}(dpp)_n]^{2+}$ series.

Like $[Ru(bpy)_3]^{2+}$, all of the complexes are, upon excitation, emissive in fluid solution as is expected for the modest variations in the ligand systems. Likewise, the optical absorption spectra for all of the complexes are similar, showing a visible maximum in the vicinity of 450 nm. The UV-visible absorption spectra of each member of this series in ethanol is given in Figure 5.6. The two mixed ligand complexes, $[Ru(bpy)_2(dpp)]^{2+}$ and $[Ru(bpy)(dpp)_2]^{2+}$ appear to be composites of the two homo-tris chelate complexes. The lowest excited state is an MLCT state and in the case of $[Ru(bpy)_3]^{2+}$, the excited state electron is localised on one of the three bipyridyl ligands [43,44]. In mixed ligand complexes of the type $[Ru(bpy)_2(dpp)]^{2+}$, two such states might be expected to be present: one, in which the excited-state electron is localised on a bpy ligand and the other, in which the electron is localised on the second ligand, in this case dpp [45-47]. These states may exist in rapid thermal equilibrium, leading to an effective averaging of the excited state properties [46]. Time-resolved resonance Raman (TR) spectroscopy has proven to be a powerful tool in the characterisation of electron localisation in the MLCT excited state of Ru(II) diimine complexes [46,48]. In water the TR spectrum of $[Ru(bpy)_2(dpp)]^{2+}$ contains contributions from both reduced bpy and dpp, indicating that on the vibrational time scale the promoted electron is localised on the π^* orbital of either the bpy or dpp ligands. Typically a small energy difference between ligands leads to localisation on both ligands whereas localisation on only the lowest energy ligand is observed when the energy gap is large. In a recent study by Kumar and co-workers [46], the excited state absorption and resonance Raman spectra of the mixed ligand complex $[Ru(bpy)_2(dpp)]^{2+}$ were reported. The excited state spectra of this mixed-ligand complex showed that the excited state electron was localised on the individual ligands but exhibited nonstatistical contributions from states corresponding to each of the ligands present in the coordination sphere. On the basis of the excited-state absorption spectra, the contribution of dpp^* is much greater than that of bpy^*.

Table 5.1 Electronic properties of $[Ru(bpy)_{3-n}(dpp)_n]^{2+}$ in ethanol solution and in the final xerogel.

Complex	Medium	λ_{max} (nm)[a]	λ_{max} (nm)[b]	τ (ns)[a]	τ (ns)[b]
$[Ru(bpy)_3]^{2+}$	Solution	611	580	700 (280)[c]	4500
	Method 2 (1)	597	579	1110(70), 470(30)[d]	4490(75), 1590(25)[d]
	Method 2 (5)	588	576	2100(80), 660(20)[d]	4450(85), 1800(15)[d]
$[Ru(bpy)_2(dpp)]^{2+}$	Solution	612	588	1970 (290)[c]	8830
	Method 2 (1)	600	585	920(70), 220(30)[d]	8750(65), 2770(35)[d]
	Method 2 (5)	590	582	2780(80), 800(20)[d]	8600(80), 2590(20)[d]
$[Ru(bpy)(dpp)_2]^{2+}$	Solution	613	592	4100 (295)[c]	9420
	Method 2 (1)	604	594	720(75), 180(25)[d]	9500(70), 2900(30)[d]
	Method 2 (5)	598	597	3000(70), 600(30)[d]	9550(80), 2705(20)[d]
$[Ru(dpp)_3]^{2+}$	Solution	612	597	4890 (290)[c]	9640
	Method 2 (1)	611	596	2100(65), 520(35)[d]	9750(70), 2005(30)[d]
	Method 2 (5)	612	597	1200(70), 300(30)[d]	9800(80), 2435(20)[d]

[a] RT. solution measurements were degassed by purging with argon. The sol-gel samples are not degassed. The values in parentheses indicate the lifetime of the complex in aerated ethanol solution. [b] These measurements were carried out at 77 K. For solution values, the solvent employed was ethanol/methanol 4/1 v/v. [c] Value in parentheses is the lifetime of the complex in aerated solution. [d] Values in parentheses are the lifetime components pre-exponential factor given in percent.

Thus, the equilibrium distribution favours the population of dpp^* over bpy^*, in spite of the fact that there are two bpy ligands for every one dpp ligand in the coordination sphere. These observation have been explained in terms of rapid intramolecular energy redistribution. Irrespective of the initial state which are populated, excitation energy is redistributed rapidly among the ligands, favouring the ligand that can provide the lowest energy state. Furthermore, the excited-state resonance Raman spectrum of $[Ru(bpy)_2(dpp)]^{2+}$ was dominated by features characteristic of the dpp ligand. In effect, phenyl substitution shifts the excited state to slightly lower energy.

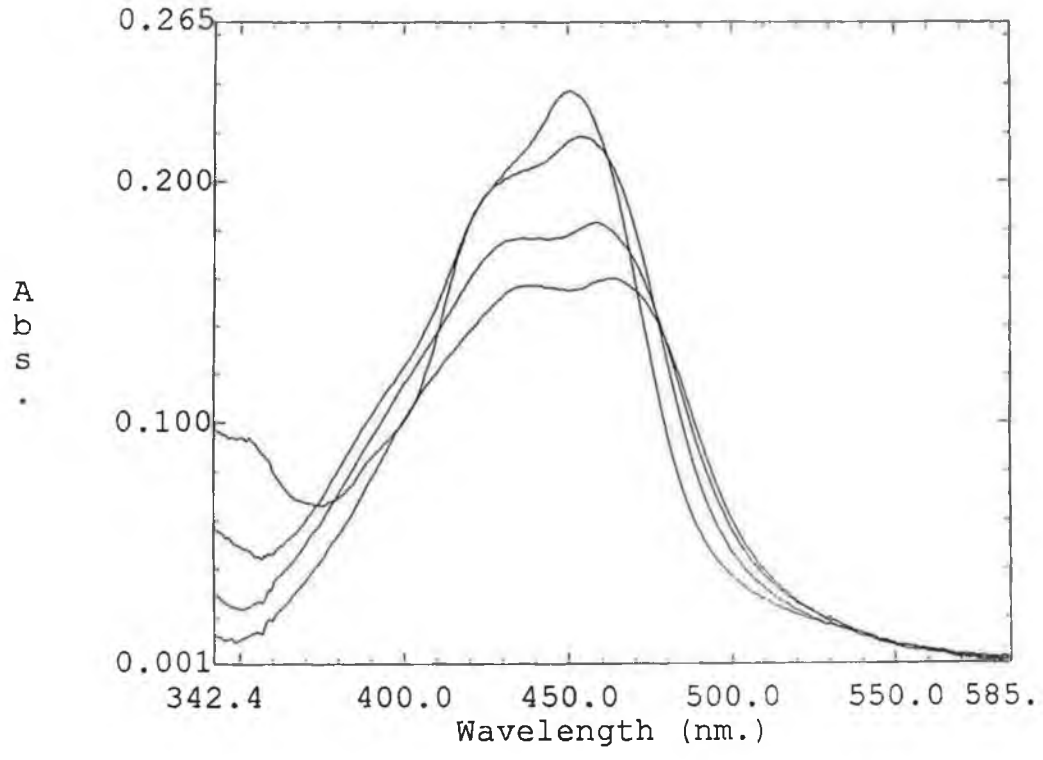

Figure 5.6 UV-Vis spectra of (a) $[Ru(bpy)_3]^{2+}$ (b) $[Ru(bpy)_2(dpp)]^{2+}$ (c) $[Ru(bpy)(dpp)_2]^{2+}$ and (d) $[Ru(dpp)_3]^{2+}$ in ethanol (arbitrary concentrations).

All the sol-gel samples were luminescent at room temperature and at 77K, displaying the typical ^{3}MLCT emission of Ru(II) polypyridyl complexes. As was found for $[Ru(bpy)_3]^{2+}$, the UV-absorption profile of all the complexes in the final xerogel remained unaltered from that in the initial sol-gel. This suggests that no change in the energy gap between the ground state and the ^{1}MLCT state occurs upon incorporation into the sol-gel matrix. In general, the emission maxima of a particular complex at 77K in solution is very similar to that at 77K in a sol-gel (for sol-gels prepared at pH 1 or pH 5). Also, the observed lifetimes in either gel for each complex at 77K are similar to each other and to the value obtained for the particular complex in 4/1 ethanol/methanol at 77K. Emission decays for all of the immobilised complexes reported here were found to be double exponential. From this table a number of trends are evident. Perhaps the most obvious trend is the gradual decrease in blue shift (caused by a decrease in the ^{3}MLCT-ground state energy gap) of the complexes upon incorporation into a sol-gel as the number of dpp ligands (n) increases from zero to three. Figure 5.7 illustrates the

position of the photoluminescence energy peaks of this series of complexes in (a) alcohol solution at 77 K, and (b) in the final xerogel at room temperature. In condensed media, the solvent molecules constituting the medium (in microheterogeneous systems such as sol-gel, the medium is referred to, more loosely as "the environment") can intervene in the excited-state processes [49]. Usually solvents interact strongly with excited states that have a higher dipole character compared to the ground state. The solute-solvent interactions can affect the relative positions of the excited-state with respect to the ground state. For the Ru(II) polypyridyl complexes studied here the rigid nature nature of the sol-gel matrix manifests itself as a blue shift in the emission maxima [50,51]. We have mentioned in the previous chapter, the phenyl moieties of $[Ru(dpp)_3]^{2+}$ serve to shield the polar excited state from the surrounding microenvironment. With respect to the series of complexes reported in this chapter, it was found that as the number of dpp ligands (n) was increased from 0→3, the energy difference between the solution and the sol-gel emissions decreased (see Figure 5.7(a)). The emission energies of the bpy complexes vary with the nature of the sol-gel and are substantially higher than in aerated solution. A similar trend was observed for the energy difference between the low- and room temperature emissions for this series. Again, no blue shift in the emission energies was observed for the immobilised $[Ru(dpp)_3]^{2+}$ complex.

As can be seen from Table 5.1, the observed excited-state decay lifetime of all four complexes of this series increases upon incorporation into the sol-gel (as compared to the room temperature solution value), the extent of which, appears to depend very much on the complex in question. Of the first three complexes in this series, the very small change in emission energy observed in the sol-gel media is not nearly sufficient to account for the magnitude of the changes in lifetime. It is expected that the rigid nature of the sol-gel matrix causes a decrease in the nonradiative decay k^{nr} by restricting the molecular motion of the immobilised complex.

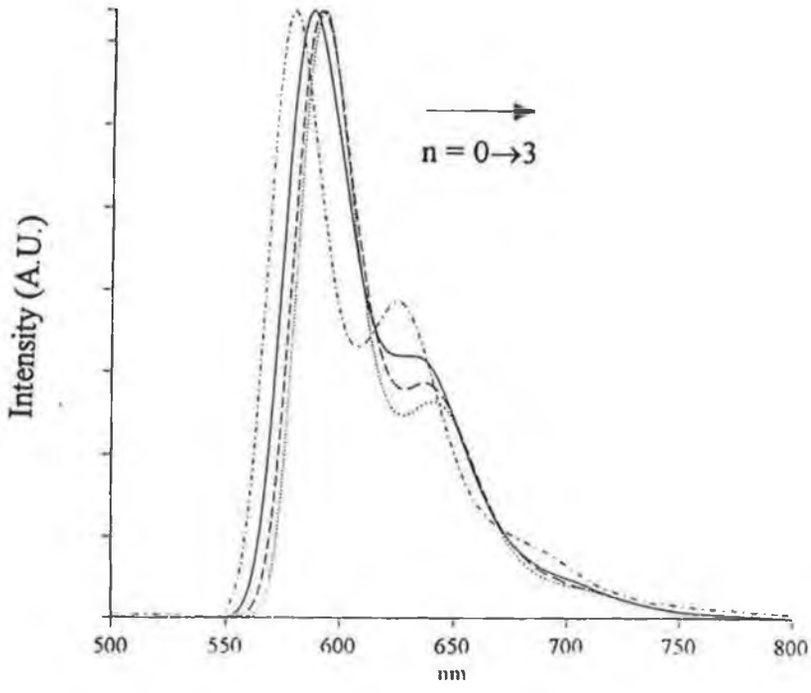

Figure 5.7(a) Normalised emission spectra of $[Ru(bpy)_{3-n}(dpp)_n]^{2}$, n = 0→3, at 77 K in ethanol/methanol 4/1 v/v.

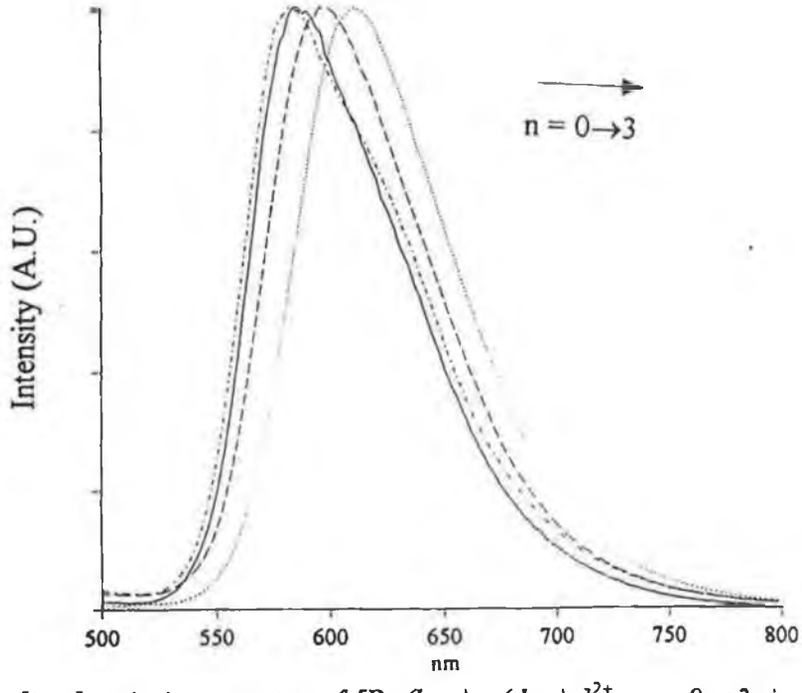

Figure 5.7(b) Normalised emission spectra of $[Ru(bpy)_{3-n}(dpp)_n]^{2+}$, n = 0→3, in xerogel (Method 2(5)) at room temperature.

The temperature-dependent lifetimes of all of these complexes were first carried out in 4/1 ethanol/methanol. These data were analysed by assuming that the excited state decay consists of a temperature independent intrinsic decay from the ^{3}MLCT state and a single thermally activated non-radiative decay process according to the Equation 5.1. From the values of Φ, and Equations 1.11 and 1.12, k_0 can be also be obtained from its components k^r and k^{nr}. Results of these calculations are given in Tables 5.2 and 5.3. Because the quantum yields for the immobilised complexes were not calculated, Table 5.2 only displays the excited state parameters of the complexes in 4/1 ethanol/methanol. Variations between parameters displayed in Table 5.3 and those in the literature probably reflect the limitations imposed by fitting a restricted number of data points over a small temperature range. These limitations restrict the numerical significance of the kinetic parameters, and their absolute values should be treated with some circumspection. Other approaches have been used in treating temperature dependent lifetimes of related Ru(II) diimine complexes. In particular, additional parameters are frequently included to fit data obtained in the solvent-glass transition region. For the solvent system employed here (*i.e.* 4/1 ethanol/methanol v/v), this transition occurs in the 100-120 K temperature region. To avoid such complexities, the kinetic parameters were procured by fitting data obtained at temperatures above this transition region.

Table 5.2 Excited state decay parameters of $[Ru(bpy)_{3-n}(dpp)_n]^{2+}$ series in ethanol solution.

Complex	k^r (s^{-1})	k^{nr} (s^{-1})	k_0 (s^{-1})	Φ
$[Ru(bpy)_3]^{2+}$ [a]	2.3×10^4 (8.0×10^4)	2.0×10^5 (1.3×10^5)	2.2×10^5 (2.1×10^5)	1.60×10^{-2}
$[Ru(bpy)_2(dpp)]^{2+}$	7.1×10^3 (----[b])	1.1×10^5 (----[b])	1.1×10^5 (----[b])	1.40×10^{-2}
$[Ru(bpy)(dpp)_2]^{2+}$	3.5×10^3 (----[b])	1.0×10^5 (----[b])	1.1×10^5 (----[b])	1.50×10^{-2}
$[Ru(dpp)_3]^{2+}$ [c]	3.1×10^3 (5.7×10^3)	1.0×10^5 (9.9×10^4)	1.0×10^5 (1.04×10^5)	1.51×10^{-2}

The parameters displayed here were obtained from the data given in Table 5.1 and Equations 1.11 and 1.12. [a] Values in parentheses are from reference [52] (solvent employed was 4/5 propionitrile/butrionitrile). [b] Literature values unavailable. [c] Values in parentheses from reference [53] (solvent employed was ethanol/methanol 4/1 v/v).

Table 5.3 Kinetic parameters k_0, A_i and ΔE_i, for the decay of the MLCT states of the complexes in 4/1 ethanol/methanol (v/v) solution and in the sol-gel matrix.

Complex	Matrix	k_0 (s^{-1})	A_i (s^{-1})	ΔE_i (cm^{-1})
$[Ru(bpy)_3]^{2+}$	EtOH/MeOH[a]	4.5×10^5	1.4×10^{14} (1.3×10^{14})	3900 (3960)
	Cellulose acetate[b]	1.00×10^7	1.70×10^7	810
	Method 2 (1)	2.3×10^5	1.2×10^7	740
	Method 2 (5)	3.0×10^5	9.1×10^6	660
$[Ru(bpy)_2(dpp)]^{2+}$	EtOH/MeOH[c]	3.4×10^5	0.70×10^{13}	2900
	Method 2 (1)	1.59×10^5	2.75×10^8	995
	Method 2 (5)	1.9×10^5	1.79×10^7	940
$[Ru(bpy)(dpp)_2]^{2+}$	EtOH/MeOH[c]	1.6×10^5	0.65×10^{13}	2950
	Method 2 (1)	3.34×10^5	3.4×10^7	800
	Method 2 (5)	1.5×10^5	2.6×10^6	660
$[Ru(dpp)_3]^{2+}$	EtOH/MeOH[c]	1.4×10^5	3.2×10^{12}	2675
	Method 2 (1)	1.27×10^5	3.0×10^{12}	2700
	Method 2 (5)	1.1×10^5	1.3×10^{12}	2520

All the parameters in this table were obtained from fitting the data to Equation 5.1. [a] Values in parentheses are from reference [52] (solvent employed was 4/5 v/v propionitrile/butrionitrile). [b] From reference [5]. [c] Literature values unavailable.

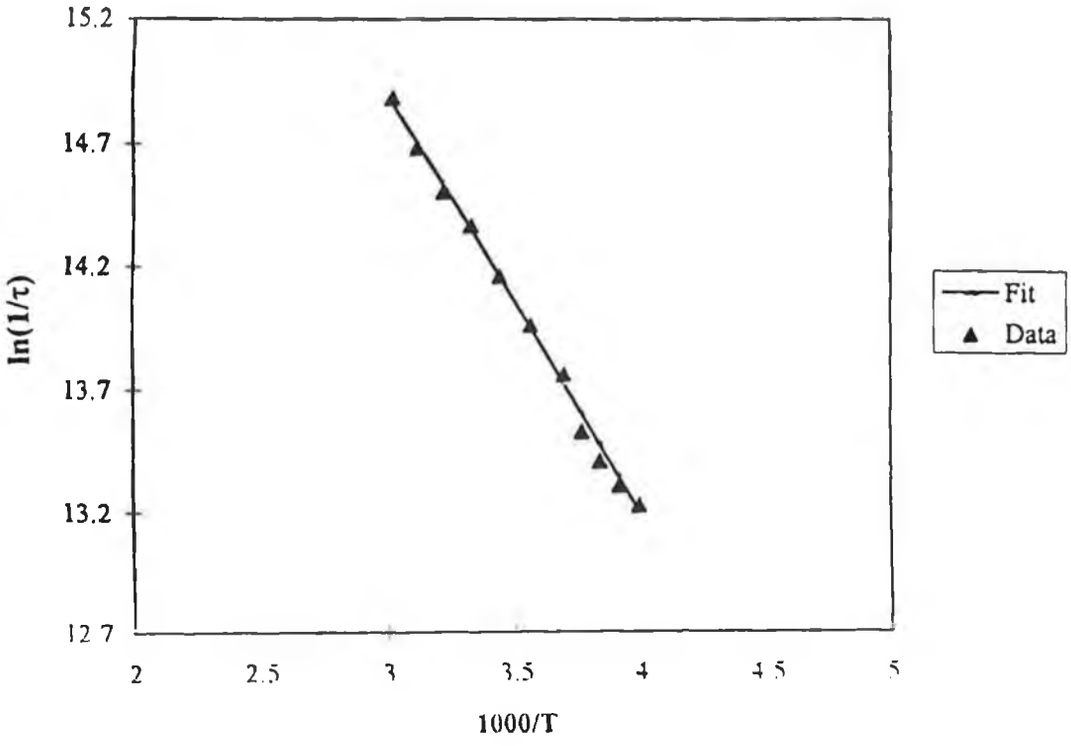

Figure 5.8 Temperature dependence of the luminescence lifetime of $[Ru(bpy)_3]^{2+}$ in ethanol/methanol (4/1 v/v) and the calculated fit from Equation 5.1, in the temperature range 250-300 K.

An example of a typical data set and the resulting theoretical fit are shown in Figure 5.8, where ln (1/τ) vs. 1000/T is shown plotted for $[Ru(bpy)_3]^{2+}$ in an alcoholic solution in the range 250-300 K. Values for the parameters k_o, A_i and ΔE_i obtained from the fits are summarised in Table 5.3. Also included in this table are the kinetic parameters obtained for the immobilised complexes. These values are dramatically altered upon incorporation into the sol-gel matrix and will be discussed in further detail in section 5.2.2.2.

Of the entries in Table 5.3, $[Ru(bpy)_3]^{2+}$ in 4/1 EtOH/MeOH is a characteristic example of the behaviour observed for a series of polypyridyl complexes of Ru(II) in solution where relatively efficient photochemically induced ligand loss photochemistry exists [30,31]. The temperature dependence of the luminescence decay of $[Ru(bpy)_3]^{2+}$ has been reported previously by a number of authors [5,22] and the kinetic parameters obtained in our laboratory for the excited state of this complex are in accordance with the literature values. The values of the kinetic parameters derived from the temperature-dependent

lifetimes fall in the range of, the frequency factor ~ 10^{12}-10^{14} s^{-1} and the activation energy ~ 2500-4500 cm^{-1}. The measured ΔE_i represents the activation energy for the ^{3}MLCT-^{3}MC internal conversion. Temperature dependent ligand loss photochemistry for this complex is observed which is associated kinetically with the temperature-dependent term $A_i\exp(-\Delta E_i/RT)$ [7,8,11,12]. Following this thermally activated ^{3}MLCT-^{3}MC transition, the d-d state may subsequently undergo ligand loss or nonradiative decay. The magnitudes of A_i and ΔE_i depend to a large extent upon the solvent [35] and the surrounding ligands [12].

5.2.1.1 The effect of the rigid nature of the sol-gel matrix on the temperature dependent emission behaviour of the $[Ru(bpy)_{3-n}(dpp)_n]^{2+}$ series.

The purpose of this chapter is to investigate how the sol-gel matrix affects the temperature dependent luminescent properties of the complexes in comparison to solution and indeed other solid matrices. As mentioned previously, the results of a parameterised theoretical analysis show that the three low-lying emitting states are largely triplet in character but can acquire singlet character through the effect of spin-orbit coupling. The state that is highest in energy of the three has the greatest singlet character and is expected to dominate both radiative and nonradiative decay. Since all of the ^{3}MLCT states of $[Ru(bpy)_3]^{2+}$ have the same basic configuration, $d\pi^5(Ru)\pi^*(bpy)$, there is no reason to believe that changes in the solvent should change the ordering of the states. The luminescent MLCT excited states formed upon light excitation deactivate following nonactivated and activated paths in which the solvent plays an important but not yet fully elucidated role. Investigations carried out by Barigelletti and co-workers suggest that the viscosity of the solvent may substantially affect the emission behaviour [24]. Temperature-dependent emission energy measurements in solution are complicated by the effects of the fluid-glass transition at intermediate temperatures. For polypyridyl complexes of both Ru(II) and Os(II), a discontinuity exists in the emission properties of the MLCT excited states between the fully fluid and glassy states. For a 4/1 ethanol/methanol solution, this

is known to occur normally at 100-120 K. A related but more dramatic effect has been observed for polypyridyl-tricarbonyl complexes of Re(I), where a large red-shift in the emission energy (rigidochromic phenomenon) is accompanied by a dramatic decrease in the excited-state lifetime upon passing through the glass-to-fluid transition [54].

The emission energy and lifetime characteristics of ^{3}MLCT excited states, most notably for $[Ru(bpy)_3]^{2+}$, have been investigated in a variety of media ranging from crystals to glasses and polymeric films [5,33,55,56]. In media where dipole reorientations in the surrounding medium are restricted and different chemical environments may exist for the excited state decay, non-exponential decay kinetics are often observed. An important contributor to such effects is, no doubt, the fact that in a rigid environment, dipole reorientation times are long on the time scale for the excited state. Dipole orientations surrounding the molecule are necessarily constrained to be those appropriate to the electronic configuration of the ground state. By contrast, in solution solvent dipole reorientation timescales are, in general, shorter than excited state lifetimes. The solvent dipoles have the opportunity to reorient to configurations appropriate to the electronic configuration of the excited state before it decays. Consequently, the excited state is stabilised in fluid solution compared to a rigid medium.

Figure 5.9 shows the temperature dependence of the emission energy of $[Ru(bpy)_3]^{2+}$ both in alcohol solution and in a sol-gel matrix in the temperature range of 77-300 K. The location of the excited electron, *i.e.* whether the excited electron, transferred from the metal, is localised on one ligand or if it is delocalised through all the bpy ligands, has been the subject of much debate [43,57,58] There is now a great deal of information which shows that in room temperature fluid solution, the transferred electron in the MLCT state is localised on one ligand [57]. Evidence includes the observation of bpy^- bands in the excited-state resonance Raman spectrum [44] and evidence of bpy^- type bands in the excited-state absorption spectrum [59,60]. As a consequence of charge localisation, there is an appreciable intramolecular charge-transfer component that exists for the excited state decay which provides the basis for solvent effects.

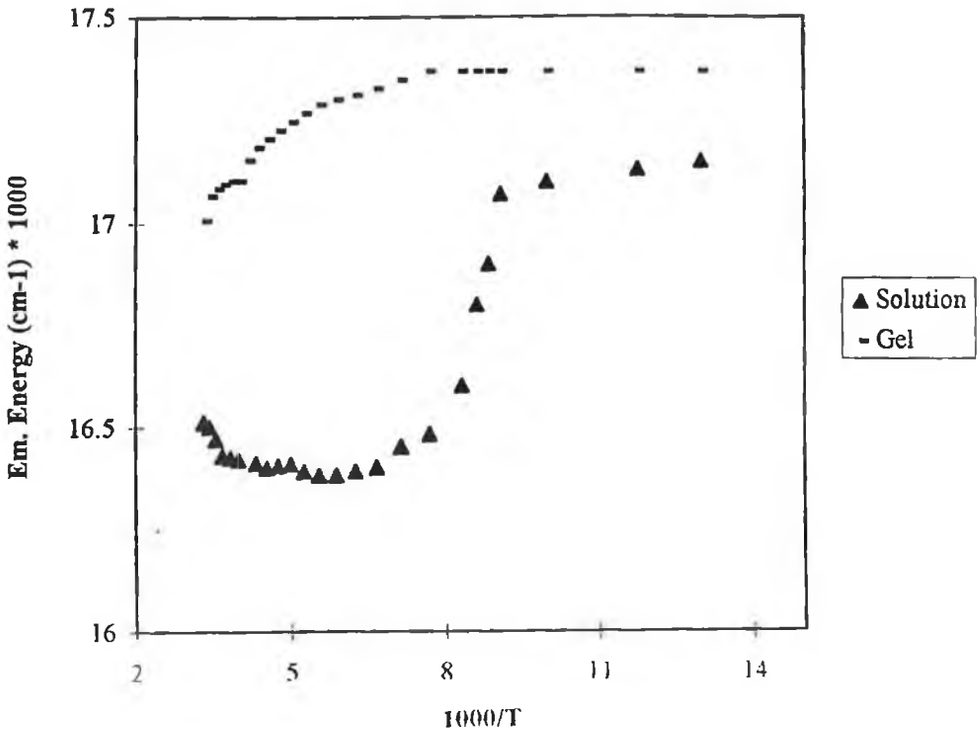

Figure 5.9 Shift of the emission maxima with temperature for $[Ru(bpy)_3]^{2+}$ in solution and in a sol-gel (Method 2 (5)), in the temperature range 77-300 K.

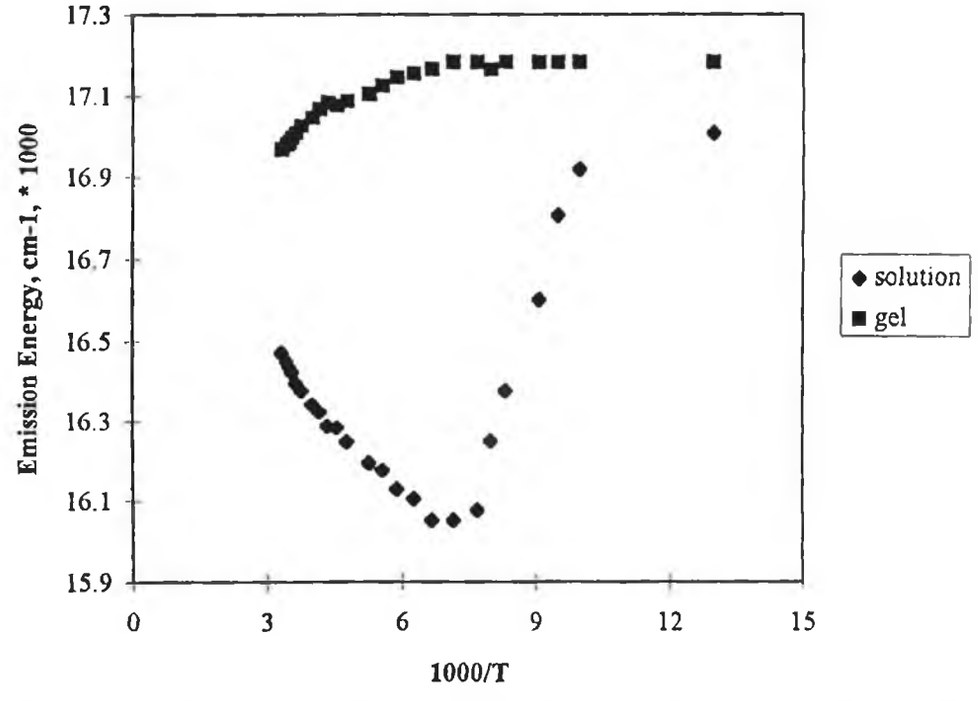

Figure 5.10 Shift of the emission maxima with temperature for $[Ru(bpy)_2(dpp)]^{2+}$ in solution and in a sol-gel (Method 2 (5)), in the temperature range 77-300 K.

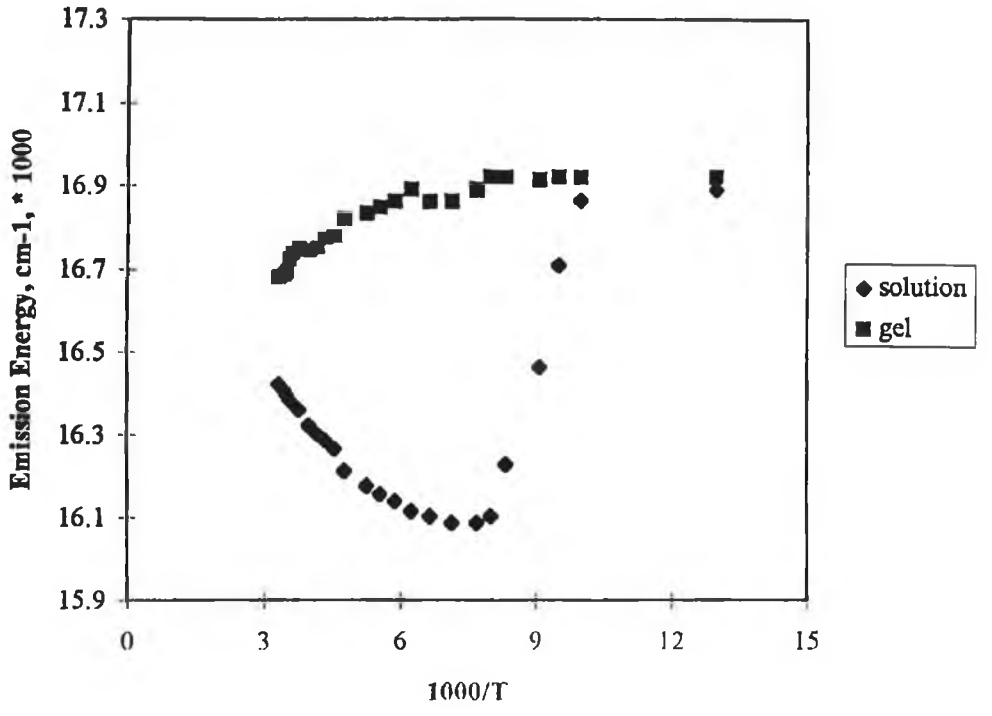

Figure 5.11 Shift of the emission maxima with temperature for $[Ru(bpy)(dpp)_2]^{2+}$ *in solution and in a sol-gel (Method 2 (5)), in the temperature range 77-300 K.*

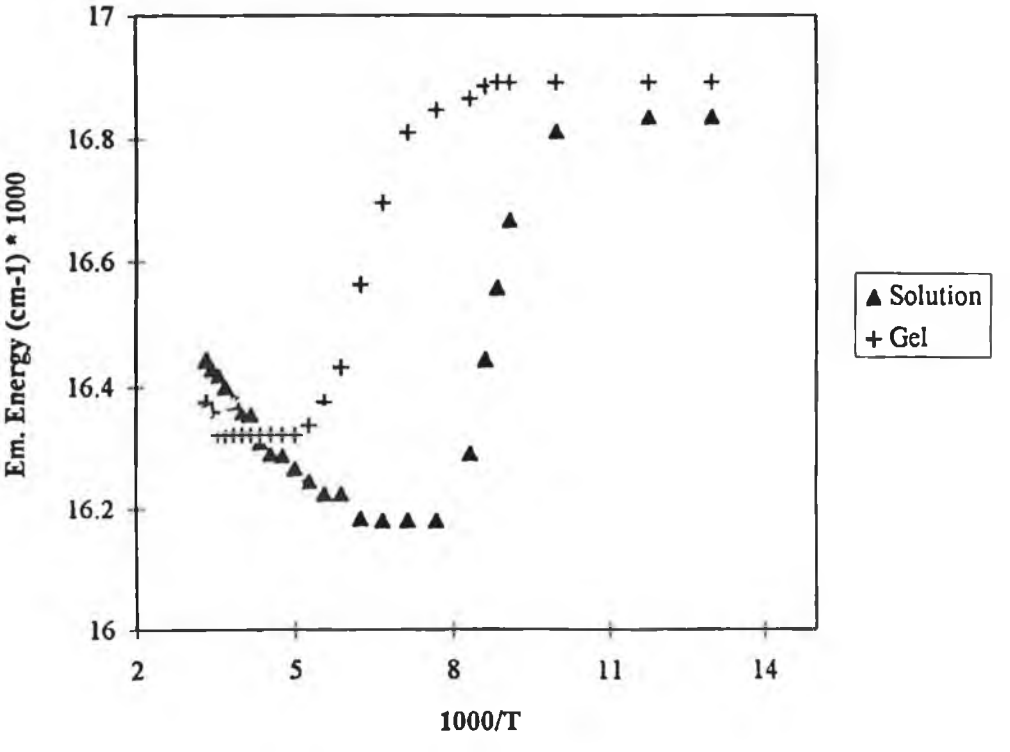

Figure 5.12 Shift of the emission maxima with temperature for $[Ru(dpp)_3]^{2+}$ *in solution and in a sol-gel (Method 2 (5)), in the temperature range 77-300 K.*

As shown in Figure 5.9, during the melting of the 4/1 ethanol/methanol solvent, the emission maximum of $[Ru(bpy)_3]^{2+}$ moved towards lower energies. The microscopic origin for such effects can be explained as follows. After optical excitation, which is a vertical process in the Franck-Condon sense, the change in electronic structure in the excited state creates an electrostatic perturbation in the solvent. The excited state strongly interacts with solvents *via* dipole-dipole, donor-acceptor, and hydrogen-bonding interactions. Therefore, solvent molecules around the excited-state ion must reorganise through orientational and translational motions, rearrangement of hydrogen-bonding, and other specific interactions. In fluid solution, correlation times for solvent reorientation are short and emission occurs from excited states whose surrounding solvent dipoles are at equilibrium with the electronic distribution of the excited state. Near the glass-to-fluid transition, solvent dipole reorientation times lengthen and become experimentally observable as a red shift in the emission spectrum. For the alcohol solvent system employed here, this glass-to-fluid transition occurs between 100-120 K. As expected, upon incorporation into the sol-gel matrix the glass-to-fluid transition is effectively removed since the solvent has been replaced by a silica polymer network. Between 77 K and 100 K the 'solvent' dipoles appear immobile on the timescale of the lifetime of the excited state and therefore cannot respond to the change in electronic structure between the ground and the excited states. As the temperature is raised beyond this point, the rigid sol-gel structure appears to soften somewhat and the emission energy decreases although not to the same extent as in solution. Small changes in the internuclear distances (particularly in the low-frequency, large-amplitude Ru-N vibrations) may take place, causing a relaxation in the $[Ru(bpy)_3]^{2+}$ excited state and a consequent red shift of the emission maxima. Even in the xerogel stage, the sol-gel matrix is thought to retain a small proportion of solvent molecules (in this case ethanol and water). An alternative explanation for the decrease in emission energy may be an enhanced stabilisation of the excited state possibly by partial dipole reorientation of these solvent molecules and perhaps rearrangement of hydrogen-bonding. In solution, a blue shift in the emission energy occurs at higher temperatures. It is not clear why such a shift occurs, but it is thought to be associated with the

population of higher lying higher lying ^{3}MLCT levels which are higher in energy than the lowest lying ^{3}MLCT level.

A similar behaviour was observed for the immobilised $[Ru(bpy)_2(dpp)]^{2+}$ and $[Ru(bpy)(dpp)_2]^{2+}$ complexes (see Figures 5.10 and 5.11) as was observed for $[Ru(bpy)_3]^{2+}$ *i.e.* a significantly reduced red shift of the emission energy in the gel matrix as compared to that obtained in solution. Figure 5.12 illustrates the temperature dependence of the emission energy of $[Ru(dpp)_3]^{2+}$ both in alcohol solution (4/1 ethanol/methanol) and in a sol-gel matrix in the temperature range of 77-300 K. For the $[Ru(dpp)_3]^{2+}$ immobilised complex, the temperature dependence of emission energy is not as significantly altered as the other complexes in this particular series. A number of important points should be noted from this diagram. Firstly, the temperature at which the initial decrease in emission energy of $[Ru(dpp)_3]^{2+}$ occurs is higher in the sol-gel (~140 K) than in ethanol/methanol (~110 K). Secondly, a significant decrease in the emission energy of the immobilised complex was observed as the temperature was increased (from approximately 16830 cm^{-1} at 140 K to 16320 cm^{-1} at 250 K). Although not as pronounced as the decrease which was observed for this complex in solution, the shift of the emission energy is nevertheless much greater than that observed for any of the other three complexes in this series (*i.e.* $[Ru(bpy)_3]^{2+}$, $[Ru(bpy)_2(dpp)]^{2+}$ and $[Ru(bpy)(dpp)_2]^{2+}$). The temperature dependent behaviour of the emission energy of the immobilised $[Ru(dpp)_3]^{2+}$ suggests that even in the xerogel state, sufficient solvent molecules remain in the pore, and that the $[Ru(dpp)_3]^{2+}$ molecules are in fact solvated to a large extent. This in turn suggests that 140 K corresponds to the melting point of the solvent within the sol-gel pores (*i.e.* water/ethanol). This again suggests a relatively shielded polar excited state for this complex. While the electronic properties of the immobilised $[Ru(bpy)_3]^{2+}$, $[Ru(bpy)_2(dpp)]^{2+}$ and $[Ru(bpy)(dpp)_2]^{2+}$ complexes appear modified by the electrostatic interaction between the complex and the surface silanols, the $[Ru(dpp)_3]^{2+}$ complex appears to be relatively unaffected by the sol-gel cage.

5.2.1.2 The effect of the rigid sol-gel matrix on the temperature dependent lifetime behaviour of the $[Ru(bpy)_{3-n}(dpp)_n]^{2+}$ series.

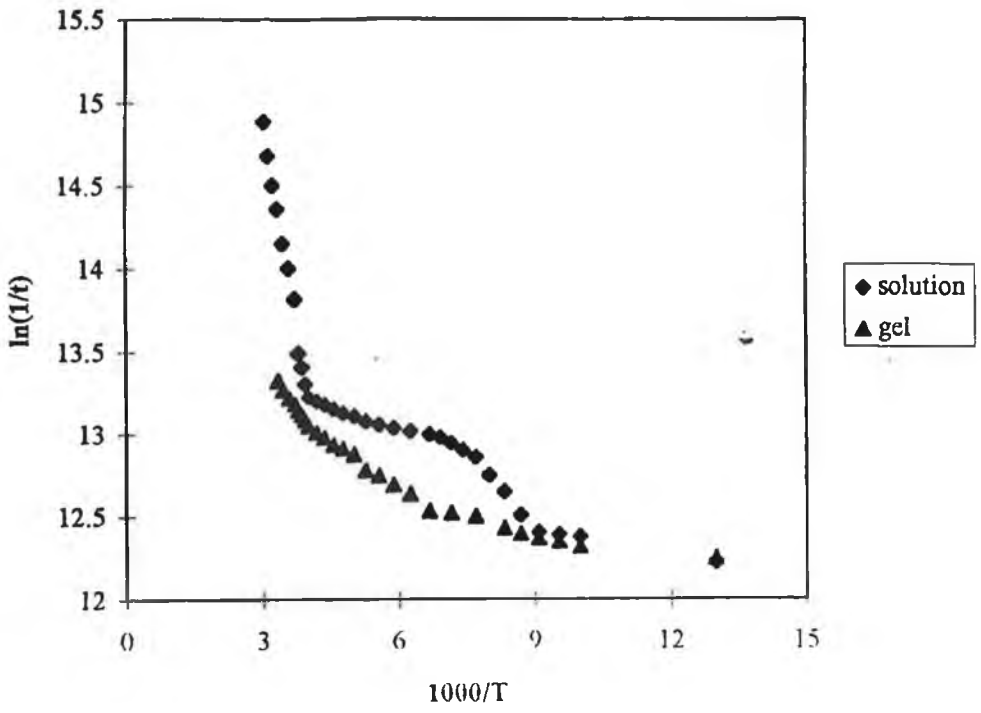

Figure 5.13 Temperature dependence of the luminescence lifetime of $[Ru(bpy)_3]^{2+}$ in ethanol/methanol 4/1 v/v, and in a xerogel (Method 2(5)) in the temperature range 77-300K

Temperature-dependent excited state decay measurements in solution are also complicated by the effects of the fluid-to-glass transition at intermediate temperatures. Figure 5.13 illustrates the temperature dependency of the lifetime of $[Ru(bpy)_3]^{2+}$ both in an alcoholic solution and in a sol-gel matrix. Again, a discontinuity can be seen to occur in the $\ln(1/\tau)$ vs. 1000/T plot for the solution at the rigid-fluid transition. Balzani and co-workers have treated the variations in emission lifetimes induced by the glass-fluid transition empirically based on the Equation 1.10 (Chapter 1) [22,24,25]. These authors have reported that the decrease in lifetime in the rigid-fluid transition is accompanied by a similar decrease in the emission intensity. It was apparent from these studies that the contribution of the nonradiative rate k^{nr} to the lifetime of the complex increased

as the viscosity decreased. This means that there is a radiationless deactivation pathway which is to some extent 'frozen' when the solvent matrix is rigid which begins to be important only as the solvent matrix becomes fluid. Such a behaviour can be accounted for by using the concept of intramolecular perturbation of molecular potentials discussed in detail by Dellinger and Kasha [61,62] and previously used to explain rigid matrix effects in spectroscopy [63]. The viscosity of the rigid matrix may be thought to make steeper the vibrational potential well and/or smaller the equilibrium nuclear distances. Large-amplitude (low frequency) vibrational modes are expected to be particularly sensitive to the presence of such a rigid matrix perturbation. It follows that the Ru-N stretching and bending vibrations may be strongly affected by the rigid-fluid transition. These vibrations possess the right symmetry requisites to promote radiationless deactivation of 'forbidden' excited states. It follows that, when the rigid matrix 'freezes' such Ru-N vibrations the complex may exhibit, to some extent, a 'vibrationally deficient' behaviour with a consequent increase in the luminescent intensity and lifetime [64]. From Figure 5.13, it is evident that no such discontinuity occurs which would correspond to a glass-fluid transition for the $[Ru(bpy)_3]^{2+}$ doped sol-gel sample. In this respect, it is possible to fit the lifetime data obtained in the entire temperature range (*i.e.* 100-300 K) to Equation 5.1.

As early as 1977, Allsopp and co-workers reported the temperature dependence of the decay processes in the luminescence of $[Ru(bpy)_3]^{2+}$ and $[Ru(phen)_3]^{2+}$ cations in a variety of media [5]. In order to fit the temperature dependent data of these complexes immobilised in cellulose acetate, the authors employed Equation 5.12 given below.

$$1/\tau = k_0 + k_1\exp(-\Delta E_1/RT) + k_2\exp(-\Delta E_2/RT) \qquad (5.12)$$

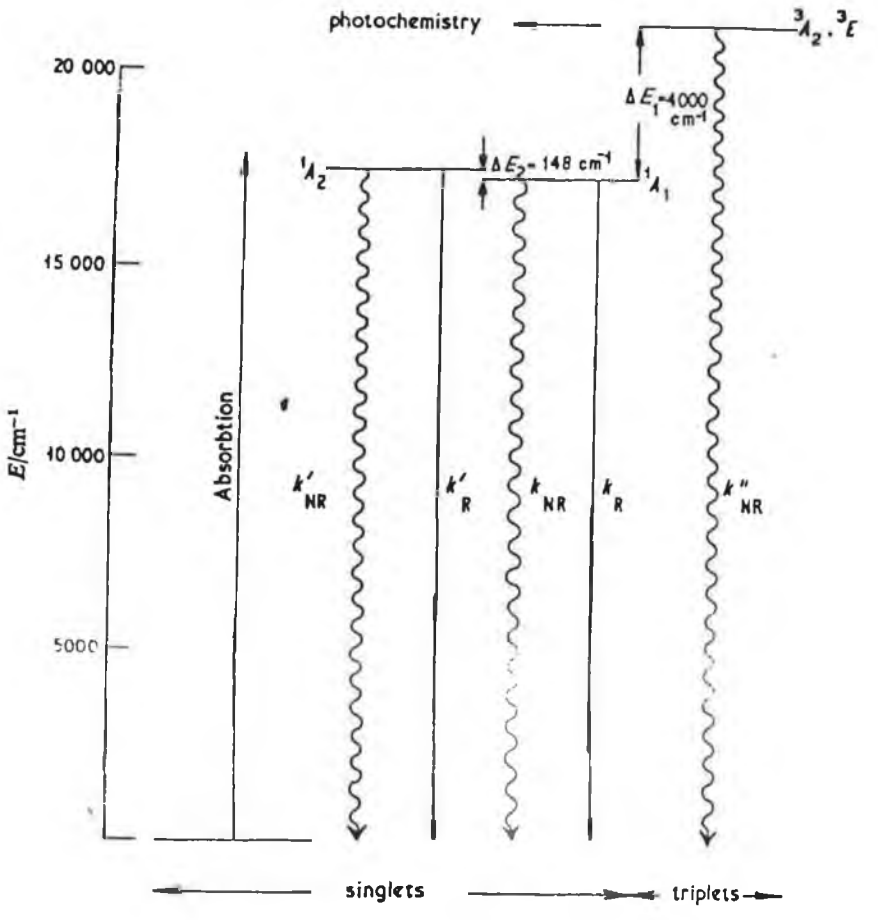

Figure 5.14 Simplified term diagram for $[Ru(bpy)_3]^{2+}$ solutions in aqueous LiCl at T > 178 K [5].

This three-term rate expression possesses two temperature dependent terms. The results published by Allsopp and co-workers, indicate that the deactivation of the luminescent state of both of these complexes proceeds through two temperature activated pathways. Figure 5.14 shows the energy-level model proposed by Allsopp and co-workers to cover the luminescence behaviour of these complexes from cryogenic to ambient temperatures in solution. The exact location of these routes was found to be dependent on the individual media. The activation energy (ΔE_i), was found to be greatly reduced in cellulose acetate film, and this decrease in ΔE_i was found to be accompanied by a 10^7 fold reduction in the frequency factor (see Table 5.3). In cellulose acetate, one term was characterised by a comparatively large energy of 810 cm^{-1}, whilst the other term involved a small activation energy, approximately 60 cm^{-1}.

We have mentioned previously that the observed excited-state decay lifetime of all four complexes of the $[Ru(bpy)_{3-n}(dpp)_n]^{2+}$ series increases upon

incorporation into the sol-gel (as compared to the room temperature aerated solution value), the extent of which, appears to depend very much on the complex in question. A number of factors should be considered here. It has been determined, that the rate of the radiative transition, k^r, is essentially governed by spin and symmetry [31,34]. The radiationless rate content, k^{nr}, generally increases with decreasing excited-state energy as expected on the basis of the energy gap law. It is also strongly dependent on the local environment [31,35]. As mentioned earlier, the effect of phenyl substitution is that it shifts the excited state to lower energy [65]. However, the longer lifetime of $[Ru(dpp)_3]^{2+}$ is thought to be due to this complex having a high degree of triplet character. Previously, the increase in emission lifetime of $[Ru(bpy)_3]^{2+}$ in a sol-gel matrix has been reported by Reisfeld and co-workers, as being caused by the relative rigidity of the glass matrix which inhibits some motions of the complex, as well as the relatively weak vibronic coupling between the complex and the polymer [66]. However, in these reported studies, an increase in k^{nr} *via* the $A_i\exp(-\Delta E_i/RT)$ term was not considered. To our knowledge, no temperature dependent lifetime studies of Ru(II) polypyridyl complexes in sol-gels have been reported.

In order to further establish the contributing factors to the changes in lifetime for each of the complexes at room temperature, the emission lifetimes of the immobilised species were studied as a function of temperature (in the temperature range 150-300 K). Figure 5.15 illustrates the $\ln(1/\tau)$ vs. 1000/T plots for this particular series of complexes in a sol-gel matrix. Only those gels prepared at pH 5 are displayed in this diagram. The kinetic emission parameters obtained for these immobilised ruthenium compounds (in gels prepared at pH 1 and at pH 5) have been listed previously in Table 5.3. The parameters displayed in this table were obtained by using Equation 5.1. From this table, a number of important points should be noted.

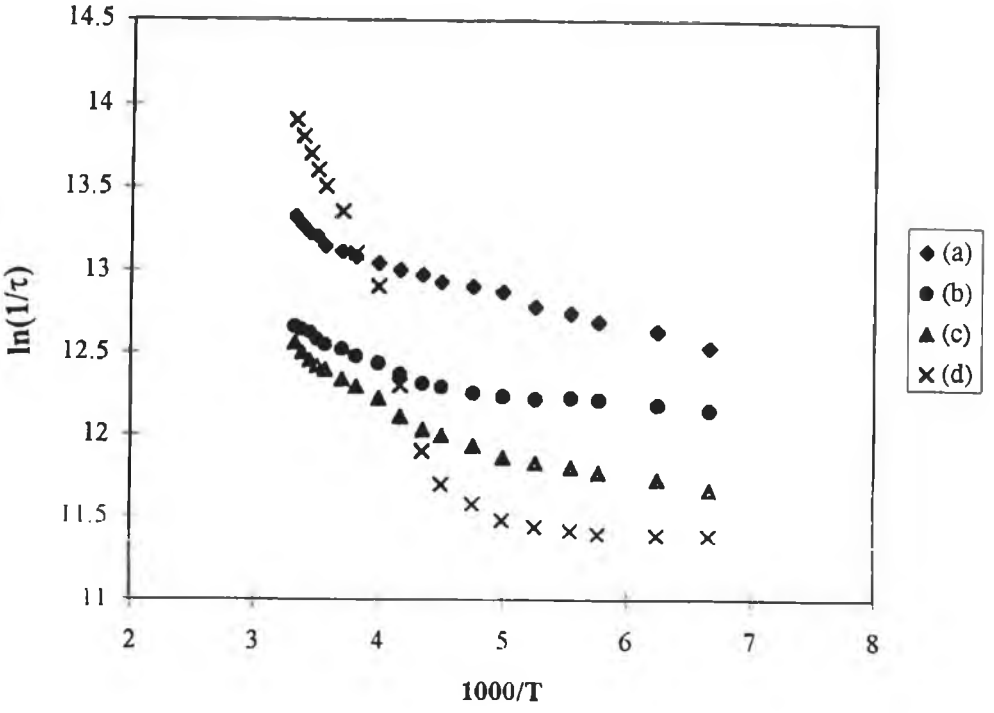

Figure 5.15 Temperature dependence for the luminescence lifetime of (a) $[Ru(bpy)_3]^{2+}$ (b) $[Ru(bpy)_2(dpp)]^{2+}$, (c) $[Ru(bpy)(dpp)_2]^{2+}$ and (d) $[Ru(dpp)_3]^{2+}$ in sol-gel (Method 2(5)).

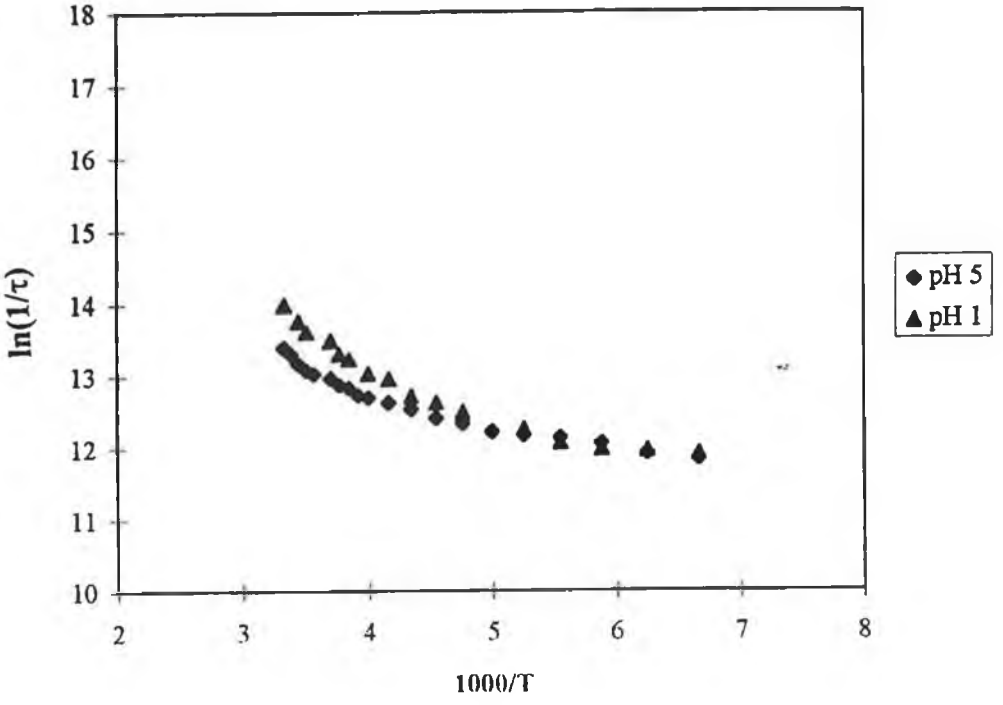

Figure 5.16 Temperature dependence for the luminescence lifetime of $[Ru(bpy)_3]^{2+}$ in xerogels prepared according to Method 2, at pH 1 and pH 5.

1. As mentioned previously, k_0 is comprised of contributions from k^r and k^{nr}, both of which are assumed to be temperature independent to a large extent. All of the k_0 values reported in Table 5.3 for both the complexes in solution and in sol-gel were determined from Equation 5.1. It was not possible to use Equations 1.11 and 1.12 to determine k_0 in the sol-gel matrix. With respect to the temperature dependent lifetime plots, the major source of error in the fits is in properly defining the plateau region at low temperatures. That region must be reasonably well defined experimentally in order to set a reasonable value for k_0. The contribution of k^{nr} to k_0 is expected to decrease as a result of the rigid nature of the sol-gel impeding molecular vibrations of the complex. In effect, a fraction of vibrational modes which in solution would enhance the rate of radiationless deactivation processes are absent in the sol-gel matrix.

2. The excited state kinetic parameters for the first three members of this series (namely $[Ru(bpy)_3]^{2+}$, $[Ru(bpy)_2(dpp)]^{2+}$ and $[Ru(bpy)(dpp)_2]^{2+}$) in the sol-gel matrix are obviously very different from the parameters in solution. This suggests a change in the excited state behaviour for these three complexes upon immobilisation. Figure 5.16 illustrates this reduced temperature dependence for $[Ru(bpy)_3]^{2+}$ in a sol-gel matrix prepared at two different pH values. No steep rise in $\ln(1/\tau)$ occurs with increased temperature for $[Ru(bpy)_3]^{2+}$ in the sol-gel matrix, irrespective of the pH at which the gel was prepared.

Of particular relevence to our study is the case of $[Ru(bpy)_3]^{2+}$ in a rigid cellulose acetate matrix [5]. While in fluid solution, the temperature dependent lifetime for this complex are apparently dominated by participation of the ^{3}MC state ($A_i = 1.4 \times 10^{14}$ s^{-1}, $\Delta E_i = 3900$ cm^{-1}), upon incorporation into the rigid matrix the data yielded values of $A_i = 1.7 \times 10^7$ s^{-1} and $\Delta E_i = 810$ ($\pm$ 120 cm^{-1}). In temperature-dependent single crystal polarised emission spectra of $[Ru(bpy)_3](PF_6)_2$, an emissive state appears at ~650 ($\pm$ 130) cm^{-1} above the low-lying MLCT states [67-70]. This behaviour was reasonably interpreted by Meyer and co-workers to indicate that the ^{3}MC is destabilised by the rigid matrix to the extent that it becomes inaccessible over the temperature range investigated. It has been suggested that this matrix effect can be attributed to the metal-to-ligand

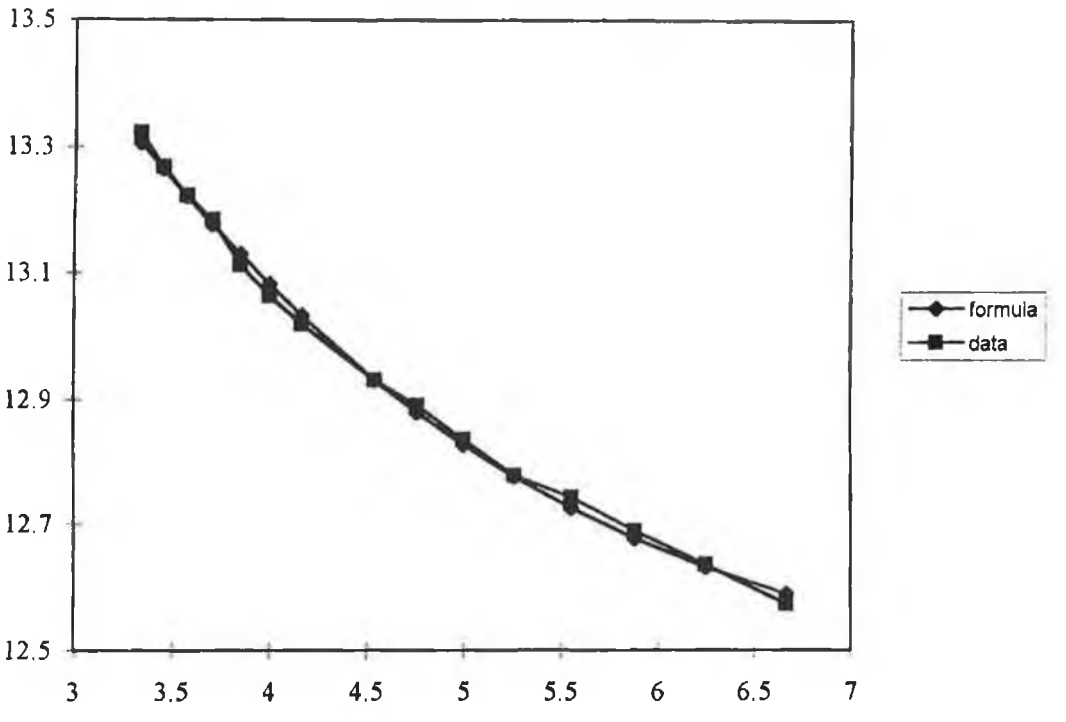

Figure 5.17 Temperature dependence of the luminescence lifetime of $[Ru(bpy)_3]^{2+}$ in a Method 2(5) xerogel in the temperature range 150-300 K.

antibonding character of the dd state and the change in electronic structure involved in the transition between states, $(d\pi)^5(\pi^*)^1 \rightarrow (d\pi)^5(d\sigma^*)^1$ [69,70]. In the rigid matrix, expansion along the metal-ligand bond axes may be sufficiently costly energetically that access to the dd state is no longer feasible even under ambient conditions, but rather a fourth ^{3}MLCT state is populated. Nonradiative decay from this high lying ^{3}MLCT does occur, but not to the same degree as from the ligand field excited state (*i.e.* the non-radiative decay rate from ^{3}MLCT is ~ 10^6-10^8 s^{-1} while that from ^{3}MC in solution is ~ 10^{12}-10^{14} s^{-1}). With the loss of this deactivation pathway, decay via the additional MLCT level becomes evident in the temperature-dependent lifetime data.

A similar effect was noticed in our laboratory upon incorporation of $[Ru(bpy)_3]^{2+}$, $[Ru(bpy)_2(dpp)]^{2+}$ and $[Ru(bpy)(dpp)_2]^{2+}$ into a sol-gel matrix. It should be appreciated that because of the small temperature dependence of the lifetime in the sol-gel matrix, the kinetic parameters k_0 and ΔE_i are not as well

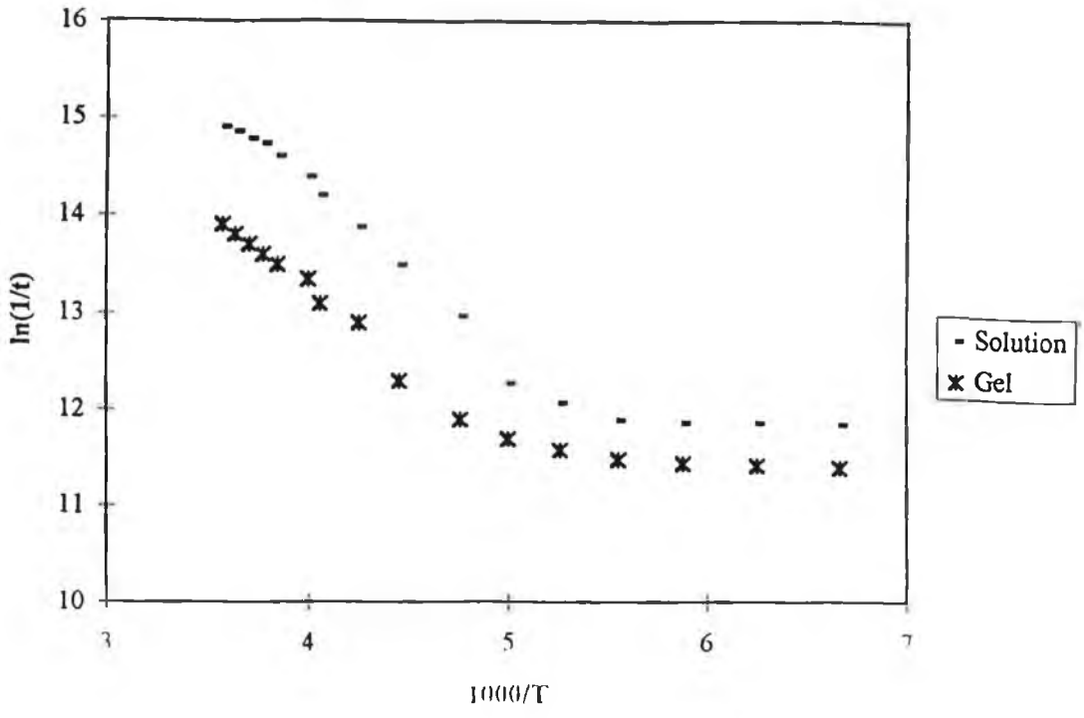

Figure 5.18 Temperature dependence for the luminescence lifetime of $[Ru(dpp)_3]^{2+}$ in 4/1 ethanol/methanol solution and in a sol-gel prepared according to Method 2(5), in the temperature range 150-300 K.

defined as in solution. Nonetheless, the appearance of the temperature dependence is meaningful. Figure 5.17 illustrates the temperature dependence plot for the luminescence lifetime of $[Ru(bpy)_3]^{2+}$ in the sol-gel matrix (Method 2(5)), and the calculated fit in the temperature region 150-300 K. The kinetic parameters presented in Table 5.3 for $[Ru(bpy)_3]^{2+}$, $[Ru(bpy)_2(dpp)]^{2+}$ and $[Ru(bpy)(dpp)_2]^{2+}$ that deactivation of the excited state via the dd level in the sol-gel matrix is no longer feasible. According to those studies reported previously, the low activation energy obtained for these complexes upon immobilisation suggests the population of a fourth ^{3}MLCT level. However, an alternative explanation which has not yet been considered is a reduction in the equilibrium displacement (ΔQ_e). This may result in the nesting of the ^{3}MLCT and the ^{3}MC potential energy surfaces. It is possible that the structural distortion of the excited state may be reduced upon incorporation into the sol-gel matrix. In this situation,

the ^{3}MC state is populated, but the contribution to the radiationless deactivation by k_c (see Figure 5.3) may be zero. In this situation the ^{3}MC and the ^{3}MLCT states may be in equilibrium with deactivation occurring via the ^{3}MLCT state. This option will be discussed in further detail in the following chapter.

3. From the data obtained in Table 5.3, it is evident that the kinetic parameters obtained for temperature dependent lifetime study of the gel doped with $[Ru(dpp)_3]^{2+}$ are consistent with those values which are typically found for the MLCT→dd state conversion in solution. In contrast to the other complexes in this series, the kinetic parameters in the sol-gel matrix (*e.g.* $A = 1.27 \times 10^{12}$ s^{-1} and $\Delta E = 2520$ cm^{-1} in sol-gel prepared at pH 5) are similar in value to those obtained in solution ($A = 3.2 \times 10^{12}$ s^{-1} and $\Delta E = 2675$ cm^{-1}) for this particular complex. Whereas $[Ru(bpy)_3]^{2+}$, $[Ru(bpy)_2(dpp)]^{2+}$ and $[Ru(bpy)(dpp)_2]^{2+}$ exhibit kinetic parameters which are different in the sol-gel matrix to those values in solution, the $[Ru(dpp)_3]^{2+}$ complex displays behaviour that points to population of dd level as was the case for this complex in solution. In fact, as seen in Figure 5.12 and 5.18, both the temperature dependencies of the emission energy and emission lifetime of this complex are somewhat retained in the sol-gel matrix. Unlike the other members of this series, it appears that the excited state properties of $[Ru(dpp)_3]^{2+}$ are very much unchanged within this solid matrix. This suggests that the $[Ru(dpp)_3]^{2+}$ dopants may occupy a solvent-like environment. We will return to this point in Chapter 7. Although emission for all three complexes $[Ru(bpy)_2(dpp)]^{2+}$, $[Ru(bpy)(dpp)_2]^{2+}$ and $[Ru(dpp)_3]^{2+}$ is dpp based in solution, only the $[Ru(dpp)_3]^{2+}$ complex exhibits thermal activation of a ^{3}MC level. While in solution all of the dpp/bpy mixed complexes behave like $[Ru(dpp)_3]^{2+}$, in the sol-gel matrix, they behave like $[Ru(bpy)_3]^{2+}$.

Of the entries in the Table 5.3 above, it is apparent that, for the sol-gel doped samples, the activation parameters associated with the ^{3}MC state for the tris diphenylphenanthroline complex remain similar to that obtained for the complex in solution. Therefore it would appear that for $[Ru(dpp)_3]^{2+}$, the increase in lifetime upon incorporation into a sol-gel matrix is primarily associated with the inhibition of motion of the complex. In addition, the exclusion of oxygen may

also be a contributing factor. Since no change in the position of the emission peak is observed for this complex, the possibility of an increase due to an increase in the ^{3}MLCT-ground state energy gap can be excluded. All of the other complexes in this series exhibit kinetic parameters which again correspond to population of a fourth MLCT level (*i.e.* $A_i < 10^8$ s^{-1}, and $\Delta E_i < 1000$ cm^{-1}).

As yet, there is insufficient data to establish the factors which dictate the magnitude of the energy splitting between the fourth and the lowest three ^{3}MLCT states [31,34]. Furthermore, fits to Equation 5.1 necessarily force the temperature dependence into a single term. In the case of the $[Ru(dpp)_3]^{2+}$ doped xerogel, for example, it is possible that contributions to the experimental data may come from population and decay of both dd and the fourth ^{3}MLCT state. The three rate term given in Equation 5.12, has been shown to give a more satisfactory fit to temperature dependence data in a number of cases [5,13,32,71,72]. Although any model with five parameters should give a better fit than one with three, the assumption of an additional temperature-dependent term is probably reasonable in this case. The major problem is in obtaining sufficient data to determine five independent parameters with reasonable accuracy and to determine that the fit chosen is a more correct representation of the data. For this reason, the temperature dependent lifetime data of all of the examples studied throughout the course of this thesis are fitted to three component model given in Equation 5.1.

5.2.2 The photophysics of $[Ru(bpy)_2(biq)]^{2+}$ and $[Os(bpy)_3]^{2+}$ in a sol-gel matrix.

The complexes studied in the previous section all possess inherently low energy gaps between the lowlying ^{3}MLCT state and the ^{3}MC state. Population of the ^{3}MC state occurs for all of these complexes in solution at ambient temperatures. Depending on the nature of the ligands surrounding the Ru centre, it was found that the excited state kinetic parameters were dramatically altered upon immobilisation. Here we report the effect of the sol-gel matrix on two complexes which are known to possess a ^{3}MLCT-^{3}MC energy gap in solution which is sufficiently large to effectively eliminate this decay pathway from the overall relaxation scheme.

5.2.2.1 Photophysical properties of $[Ru(bpy)_2(biq)]^{2+}$ and $[Os(bpy)_3]^{2+}$ in solution.

As mentioned in Section 1.3.4, studies concerning $[Ru(bpy)_n(L\text{-}L)_{3-n}]^{2+}$ (n = 0,1,2,3) complexes may be important not only to tune the excited state properties in a controlled manner, but also to obtain a better understanding of the photophysical behaviour of the archetype $[Ru(bpy)_3]^{2+}$ itself. The energy of the ^{3}MC state will be influenced principally by the σ-donating strength of the ligands and the ^{3}MLCT state energy depends principally on the energy of the lowest ligand π* orbitals. Preparation of complexes having one polypyridyl ligand with a low-energy π* level and more basic bipyridyl ligands filling the remaining co-ordination sites may result in ruthenium polypyridine complexes having ^{3}MC states which are thermally inaccessible from the ^{3}MLCT. Since most polypyridyl complexes fluoresce at room temperature, it is possible to monitor the ^{3}MLCT to ^{3}MC conversion as a function of systematic structural variations associated with the ligands. Several research groups have presented results of photophysical studies of several ruthenium polypyridyl complexes that suggest such separation of ^{3}MLCT to ^{3}MC states.

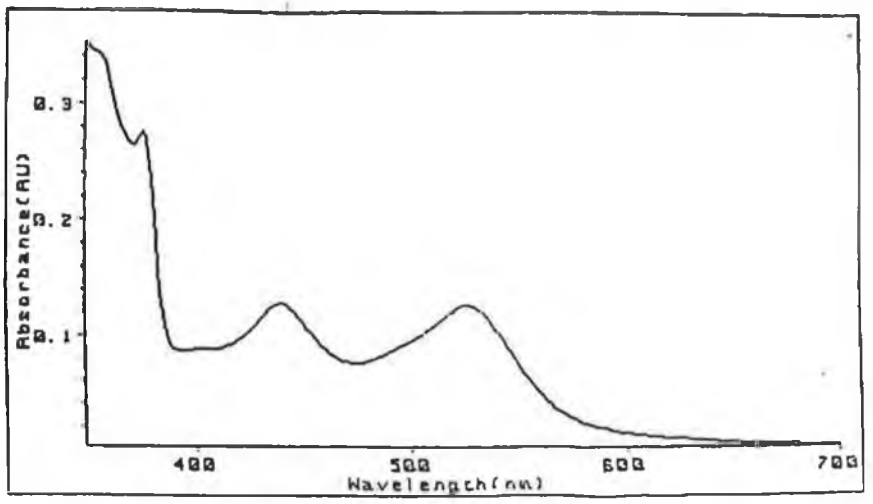

Figure 5.19 UV-Vis absorption spectra of $[Ru(bpy)_2(biq)]^{2+}$ in ethanol (5×10^{-5} M)

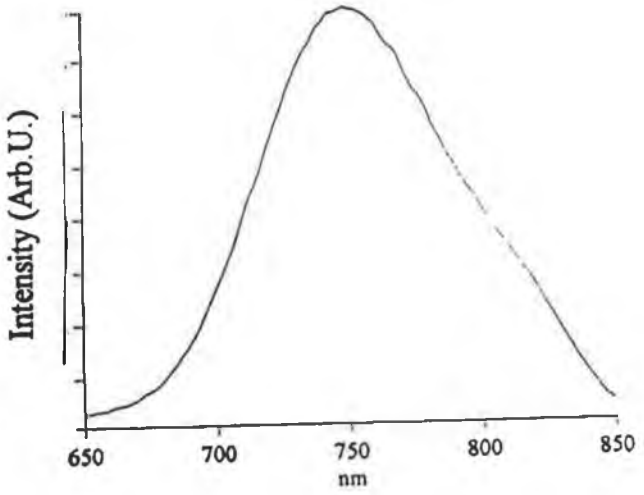

Figure 5.20 Emission spectrum of $[Ru(bpy)_2(biq)]^{2+}$ in ethanol (5×10^{-5} M)

From the latter point of view, the biq (2,2'-biquinoline) ligand is very interesting in the mixed ligand $[Ru(bpy)_2(biq)]^{2+}$ complex, as it plays the role of the lumino-active ligand as far as the properties of the low-energy MLCT excited states are concerned. This complex shows two distinct MLCT absorption bands (Figure 5.19), one at 439 nm corresponding to the Ru→bpy absorption, and the other at approximately 525 nm corresponding to the Ru→biq band [39]. This behaviour indicates that the two bands of $[Ru(bpy)_2(biq)]^{2+}$ are due to Ru→bpy and Ru→biq transitions and suggests that the energies of the π^* orbitals are not significantly influenced by ligand-ligand interactions.

The emission spectrum of this mixed-ligand complex shows only one emission band at approximately 740 nm (Figure 5.20) and the emission decay in solution was strictly monoexponential. No emission was observed in the 600 nm region. These results were obtained regardless of whether the excitation was performed at 450 nm or 520 nm. This behaviour shows that the emission only occurs from the lowest excited state of the complex, which is a Ru→biq charge-transfer state. It also suggests that efficient conversion of Ru→bpy excited states to the lower Ru→biq excited state takes place. These results are consistent with those described by other authors [36,40]. In this particular mixed-ligand complex, the biquinoline ligand is the 'luminoactive' ligand. In effect, the spectroscopic results show that in this mixed-ligand complex, the coupling between excited states involving bpy and excited states involving biq, is too weak to affect the energy levels in a substantial way, but strong enough to allow fast radiationless deactivation of the upper excited states to the lowest one.

Tables 5.4 and 5.5 display the excited state kinetic parameters obtained for $[Ru(bpy)_2(biq)]^{2+}$ and $[Os(bpy)_3]^{2+}$ both in solution and in the sol-gel matrix. For $[Ru(bpy)_2(biq)]^{2+}$, temperature dependent emission and lifetime data in ethanol/methanol (4/1 v/v) revealed a level at approximately 660 cm^{-1} above the emitting Ru→biq charge-transfer state. Barigelletti and co-workers have previously observed only a slight temperature dependence of luminescence lifetimes of this complex between 77 K and room temperature. It has been suggested that replacement of one bpy ligand in $[Ru(bpy)_3]^{2+}$ by biq significantly increases the ^{3}MLCT-^{3}MC energy gap so that population of the ^{3}MC state no

Table 5.4 Kinetic parameters k^r, k^{nr} and k_0, for the decay of the MLCT states of the complexes in 4/1 ethanol/methanol (v/v).

Complex	k^r (s^{-1})	k^{nr} (s^{-1})	k_0 (s^{-1})
$[Ru(bpy)_2(biq)]^{2+}$	1.6×10^4 (7.0×10^5)[a]	7.0×10^5 (9.0×10^5)[a]	7.2×10^5 (1.6×10^6)[a]
$[Os(bpy)_3]^{2+}$	7.1×10^4 (1.6×10^4)[b]	1.1×10^6 (1.11×10^6)[b]	1.2×10^6 (1.13×10^6)[b]

[a] Values in parentheses are from reference [24] (solvent employed was 4/5 v/v propionitrile/butyronitrile). [b] Values in parentheses are from reference [10] (solvent employed was 4/1 ethanol/methanol)

Table 5.5 Kinetic parameters for the decay of the MLCT states of the complexes in a solid matrix.[a]

Complex	Matrix	k_0 (s^{-1})	A_i (s^{-1})	ΔE_i (cm^{-1})
$[Ru(bpy)_2(biq)]^{2+}$	EtOH/MeOH	[a]1.4×10^6 (1.6×10^6)[$]	2.0×10^7 (8.0×10^7)[$]	660 (770)[$]
	Method 2 (1)	[b]7.4×10^5	3.5×10^7	620
	Method 2 (5)	[b]7.9×10^5	2.8×10^7	593
$[Os(bpy)_3]^{2+}$	EtOH/MeOH	[a]4.4×10^6 (3.7×10^6)[*]	1.0×10^8 (7.2×10^7)[*]	495 (312)[*]
	Cell. actetate[c]	4.2×10^6	1.9×10^8	607
	Method 2 (1)	[b]1.7×10^6	1.5×10^8	565
	Method 2 (5)	[b]2.2×10^6	1.0×10^8	540

For definition of parameters, see text. [b] From Equation 5.1. [$] From reference [24] (solvent employed was 4/5 v/v propionitrile/butyronitrile). [*] From reference [10] (solvent employed was 4/1 ethanol methanol). [c] From reference [6].

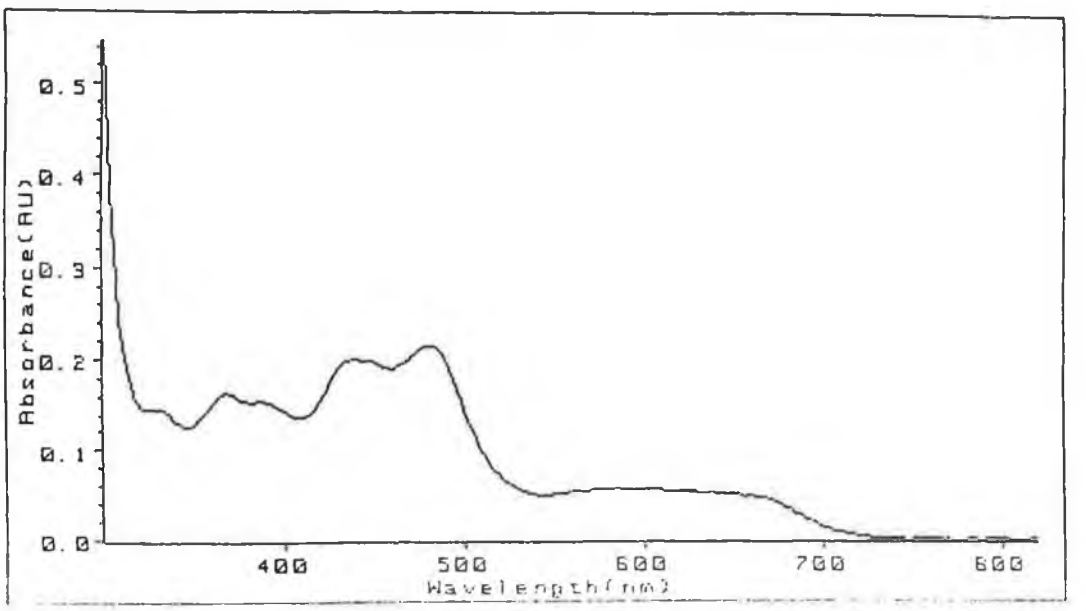

Figure 5.21 UV-Vis spectrum of $[Os(bpy)_3]^{2+}$ in ethanol (5×10^{-5} M).

longer occurs. Our value is somewhat smaller than that obtained by Barigelletti and co-workers (~ 770 cm^{-1}) where 4/5 propionitrile/butyronitrile was employed as the solvent. These authors have also shown that the relative emission intensity does not decrease when this state is populated, indicating that this state is another emitting Ru→biq charge-transfer excited state [22,24,25].

In view of the demonstrated large thermal activation of the luminescence of $[Ru(bpy)_3]^{2+}$ in solution, we have also examined the luminescence of the analogous osmium(II) complex, namely $[Os(bpy)_3]^{2+}$ in both alcoholic solution and indeed in sol-gel glass over a wide temperature range 77-300 K. For $[Os(bpy)_3]^{2+}$, the $\pi-\pi^*$ transitions are all nearly identical to that of $[Ru(bpy)_3]^{2+}$ in solution: most absorptions are around 290 nm and ^{3}MLCT states are approximately at 450 nm. In addition, $[Os(bpy)_3]^{2+}$ has intense MLCT bands which stretch out to 700 nm (see Figure 5.21). Allsopp and co-workers examined the behaviour of the luminescence spectrum and the luminescence lifetime of this complex in both glassy aqueous solution and polymer film and accurately located the energy levels through which energy loss occurs [6]. For $[Os(bpy)_3]^{2+}$ and indeed related Os(II) polypyridyl complexes, ligand loss photochemistry is either

extremely inefficient or non-existent [6,18,42]. The observed kinetic parameters for $[Os(bpy)_3]^{2+}$, are typically in the range $A_i \sim 10^6$ -10^8 s^{-1} and $\Delta E_i \sim$ 300-800 cm^{-1}. In this thesis, the temperature-dependent lifetime data for this osmium complex in solution were fit to the expression given in Equation 5.1 and gave a pre-exponential term, A_i of 1×10^{-8} s^{-1} and is similar in magnitude to the rate constant for excited state decay from the lower lying MLCT states (represented here by k_0). Metal-centred d-d states for $[Os(bpy)_3]^{2+}$ are expected to be thermally inaccessible at room temperature [74,75]. Assuming that the lowest lying dd state in $[Ru(bpy)_3]^{2+}$ is comparable in energy to the emitting MLCT state(s) at 16100 cm^{-1} in acetonitrile and that 10 Dq is greater by 30% for osmium(II), the lowest d-d state for $[Os(bpy)_3]^{2+}$ is expected to lie some 21000 cm^{-1} above the ground state. Since emission from $^*[Os(bpy)_3]^{2+}$ occurs at 13500 cm^{-1} in acetonitrile, it can be predicted that a large energy gap should exist between the MLCT and d-d states for Os(II). Since no other states are expected to appear in the energy region 300-800 cm^{-1}, the only reasonable assignment for the additional state that appears in the lifetime data for this Os(II) complex is an additional fourth MLCT state or states.

5.2.2.2 Photophysical properties of $[Ru(bpy)_2(biq)]^{2+}$ and $[Os(bpy)_3]^{2+}$ in sol-gel.

Table 5.6 is a comparison of the emission properties for $[Ru(bpy)_2(biq)]^{2+}$ and $[Os(bpy)_3]^{2+}$ in solution and in sol-gel under ambient and cryogenic conditions. $[Ru(bpy)_3]^{2+}$ is included in this table for comparative purposes. Before the results of the temperature dependent emission energy and lifetime studies of the immobilised species are presented, a brief account of the photophysical properties of these two complexes in the sol-gel matrix will be given.

We have mentioned previously that on passing from fluid solutions at room temperature to rigid matrices at low temperature, the luminescence energy of the ^{3}MLCT excited state moves to the blue (*i.e.* shorter wavelength). This "rigidochromic effect" has been discussed in the previous chapter [54].

Table 5.6 A comparison of the luminescence properties of these complexes in solution and in the xerogel.

Complex	Medium	RT Emission λ_{max} (nm)[a]	77 K Emission λ_{max} (nm)[b]	RT Lifetime τ (ns)[a]	77 K Lifetime τ (ns)[b]
$[Ru(bpy)_3]^{2+}$	Ethanol	611	580	700 (280)[c]	4500
	Method 2 (1)	597	579	1110	4440
	Method 2 (5)	588	576	2100	4450
$[Ru(bpy)_2(biq)]^{2+}$	Ethanol	744	727	270 (140)[c]	1400
	Method 2 (1)	730	723	650	1425
	Method 2 (5)	713	706	743	1380
$[Os(bpy)_3]^{2+}$	Ethanol	725	712	70 (45)[c]	860
	Method 2 (1)	705	696	70	810
	Method 2 (5)	696	694	95	790

[a] RT. measurements were degassed by purging with argon. Sol-gel samples were not degassed. [b] These measurements were carried out at 77K. The solvent employed was 4/1 ethanol/methanol. [c] Value in parentheses indicates the lifetime of the complex in aerated ethanol solution.

With respect to the emission results observed for $[Ru(bpy)_3]^{2+}$ within a sol-gel matrix, in particular the shift to higher energy upon immobilisation, a similar effect is observed for those gels doped with $[Ru(bpy)_2(biq)]^{2+}$ and $[Os(bpy)_3]^{2+}$. These results indicate that, as is the case for $[Ru(bpy)_3]^{2+}$, it is the destabilisation of the ^{3}MLCT state with respect to the ground state which results in the observed shift in the emission peak. This suggests that regardless of the metal or ligand involved, an increase in the energy gap between the ground and the emitting excited ^{3}MLCT state occurs. Again, the reason for this behaviour is that, in solution, the solvent can reorganise around the excited molecule before the deactivation process occurs. In the gel, emission occurs from an excited state which is not fully stabilised due to the lack of mobility of the matrix. It was found that the energy difference between the solution low and high temperature emissions was larger for $[Ru(bpy)_3]^{2+}$ (611→588 nm *i.e.*~ an energy difference of

640 cm^{-1}) with respect to $[Os(bpy)_3]^{2+}$ (726→705 nm ~410 cm^{-1}) and $[Ru(bpy)_2(biq)]^{2+}$ (744→727 nm ~ 315 cm^{-1}). A similar effect has been previously reported by a number of authors [42,75,76] who suggest that the energy difference between low and high temperature emissions depends on the charge transfer character of the excited state. The emission energies of these two complexes in the sol-gel prepared are not significantly reduced upon lowering the temperature. A possible explanation for this is as follows. We have already described how upon incorporation of these complexes into a rigid matrix a blue shift in the emission energy is induced. As the energy of emission increases, regardless of the origin of the increase, the separation between ground and excited states increase. As the energy gap between states increase, the extent of charge transfer in forming the excited state increases, resulting in a greater shift in emission energy for the sol-gel samples at 77 K. Figures 5.22 and 5.23 illustrate the temperature dependent behaviour of the emission energy of $[Ru(bpy)_2(biq)]^{2+}$ and $[Os(bpy)_3]^{2+}$ in both solution and in the sol-gel matrix.

Notable differences between the three metal complexes were observed upon comparison of the lifetime measurements at room temperature and at 77 K in the sol-gel. Only a small increase in the lifetime of $[Os(bpy)_3]^{2+}$ occurs upon incorporation within the sol-gel matrix. This slight increase is most likely caused by a decrease in k^{nr} due to the inhibition of molecular motion caused by the rigid nature of the surrounding matrix. An important question to ask here is why the lifetime of $[Os(bpy)_3]^{2+}$ does not increase in any great extent upon incorporation into a sol-gel matrix. Perhaps the answer to this question lies in the values of the radiative and nonradiative rates for this complex. The nonradiative rate constant, k^{nr}, is a measure of the radiationless deactivation of the ^{3}MLCT states. Because the ^{3}MLCT of $[Ru(bpy)_3]^{2+}$ is well above the ground state, the energy gap law indicates relatively inefficient nonradiative decay with a resultant emission. According to the energy-gap law, radiationless deactivation rates are determined largely by vibrational overlap between the ground and excited states [77,78]. Because of the "energy disposal" nature of the process, overlap considerations favour high frequency vibrations. The extent of vibrational coupling is determined by the magnitude of vibrational wave function overlap between $v = 0$

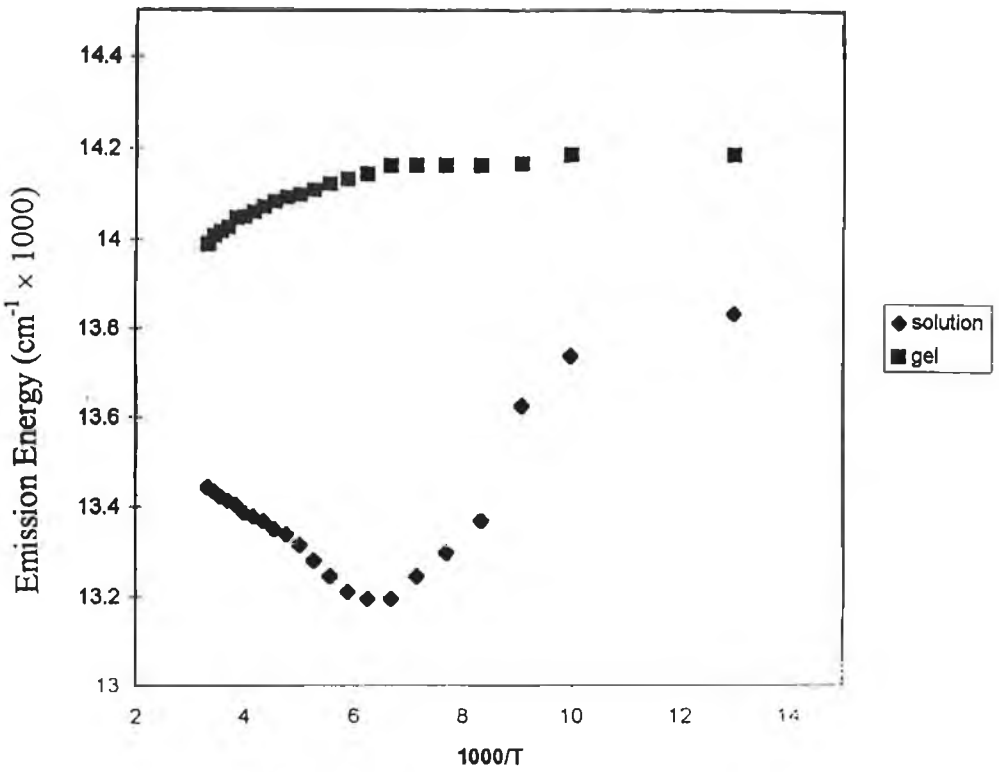

Figure 5.22 Shift of the emission energy of $[Ru(bpy)_2(biq)]^{2+}$ with temperature in a 4/1 ethanol/methanol solution and in a Method 2(5) gel.

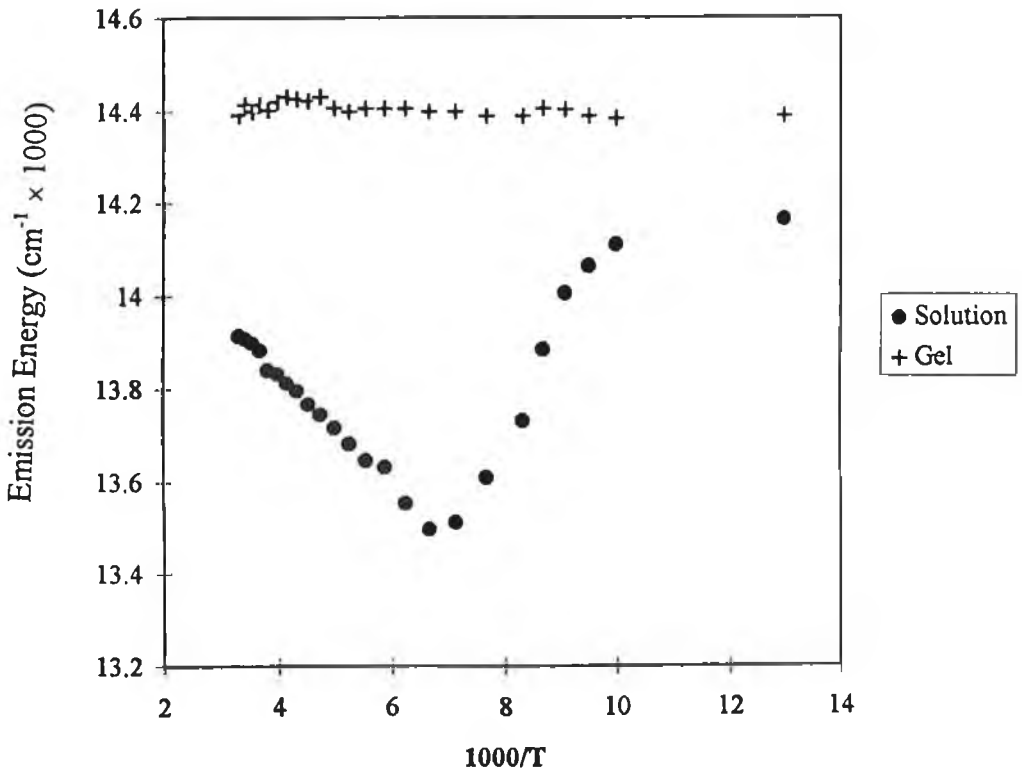

Figure 5.23 Shift of the emission energy of $[Os(bpy)_3]^{2+}$ with temperature in a 4/1 ethanol/methanol solution and in a Method 2(5) gel.

levels in the excited state and highly vibrationally excited isoenergetic levels of the ground state. As mentioned earlier, another deactivating pathway for $[Ru(bpy)_3]^{2+}$ is the population of the metal-centred (^{3}MC) excited state, giving rise to either radiationless deactivation or photodecomposition of the complex. In the case of $[Os(bpy)_3]^{2+}$ the dd state is no longer feasible as an effective decay channel for the excited state decay. However, the ^{3}MLCT state is lower and, therefore quenching to the ground state is more efficient. This is clearly demonstrated by the osmium complex having the lower emission energy of the two species, and an extremely short lifetime at room temperature. Consequently, from Table 5.2, the value for k^{nr} obtained for $[Os(bpy)_3]^{2+}$ exceeds that obtained for $[Ru(bpy)_3]^{2+}$ by almost a factor of 10.

We have mentioned previously, that in solution both of these complexes exhibit a slight temperature dependence which has been attributed to the population of a high lying ^{3}MLCT state. The excited state thermal kinetic parameters associated with Figures 5.24 and 5.25 were previously reported in Tables 5.4 and 5.5. Unlike $[Ru(bpy)_3]^{2+}$, no dramatic change in kinetic parameters is obtained from the temperature dependent emission lifetime study for the $[Os(bpy)_3]^{2+}$ and $[Ru(bpy)_2(biq)]^{2+}$. In both cases, the preexponential term and the activation energy obtained from fitting the temperature dependent lifetime data in the sol-gel to Equation 5.1 are similar in magnitude to their solution value. This suggests that the nature of the excited state of both of these complexes remains unchanged upon immobilisation. Again, the temperature dependent lifetime for both of these complexes originates from an upper MLCT level. It would appear that upon immobilisation, the equilibrium displacement between the ground state and the metal-to-ligand charge-transfer states for these complexes is relatively unchanged.

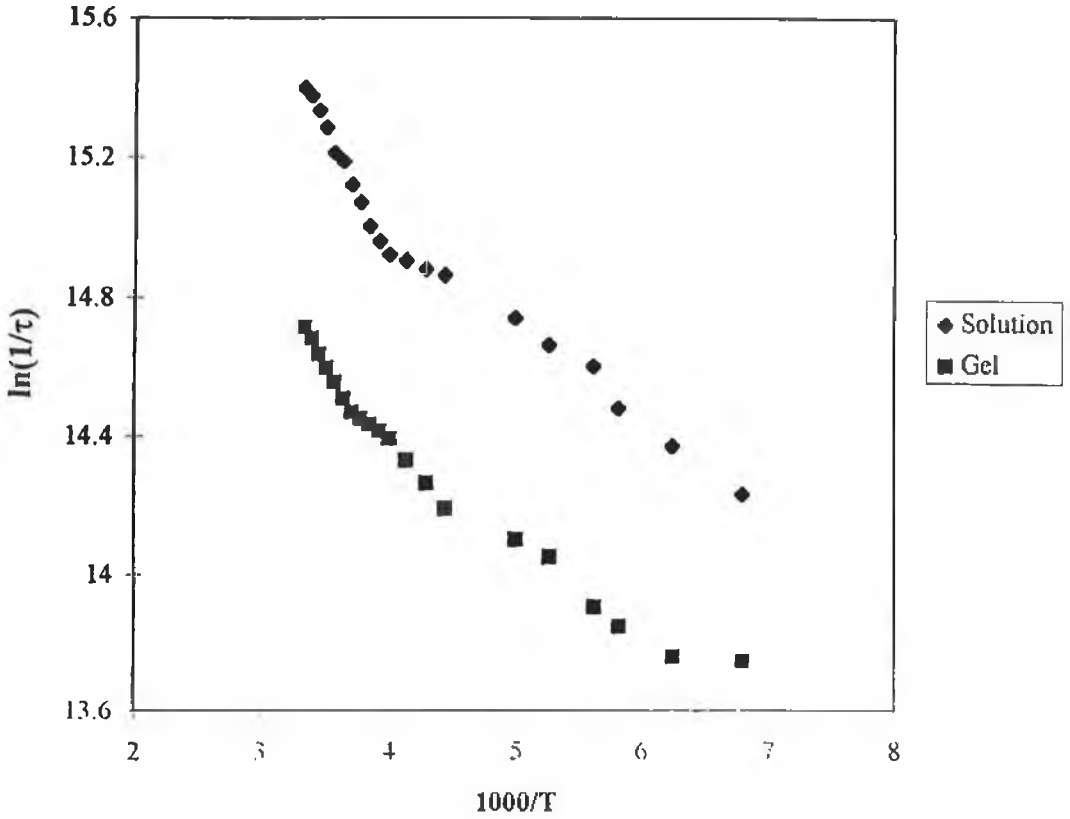

Figure 5.24 Temperature dependence of the luminescence lifetime of $[Ru(bpy)_2(biq)]^{2+}$ in 4/1 ethanol/methanol solution and in a Method 2(5) gel (77-300 K).

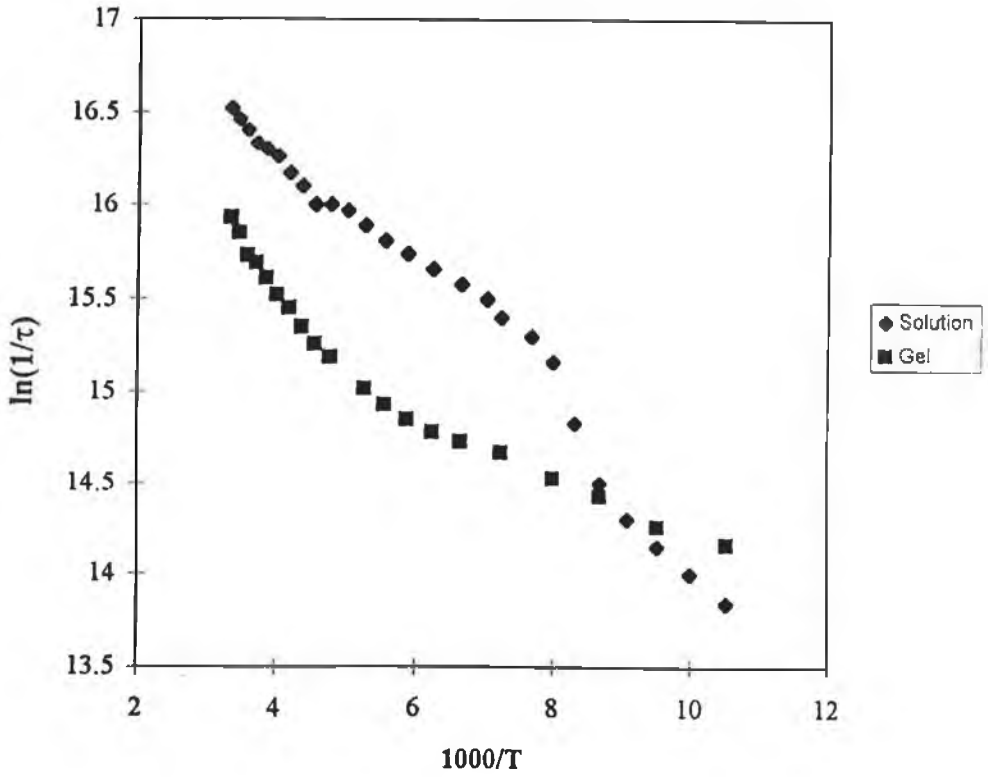

Figure 5.25 Temperature dependence of the luminescence lifetime of $[Os(bpy)_3]^{2+}$ in 4/1 ethanol/methanol solution and in a Method 2(5) gel (77-300 K).

5.3 Conclusion.

Evidence has been presented in this chapter which supports the existence of a thermally accessible higher lying MLCT state in polypyridyl complexes of ruthenium(II) and osmium(II). This state has been shown to exist both in solution for a number of different complexes. This work together with that carried out previously by a number of research groups suggest that this fourth ^{3}MLCT state is typically found to occur at 300-900 cm^{-1} above the lowest lying ^{3}MLCT state and to have a decay rate constant of 10^6-10^8 s^{-1}. This higher lying MLCT state can make a significant to nonradiative decay at room temperature.

In solution at ambient temperatures, excited state decay is dominated by fast nonradiative decay from ^{3}MC, which masks any contribution from a fourth ^{3}MLCT. These results have implications for the use of $[Ru(bpy)_3]^{2+}$ as a sensitiser: The MLCT excited state of this complex has been used extensively as a photosensitiser because of its relatively long solution lifetime and its ability to act as either an electron-transfer acceptor or donor in photoredox applications. One consequence of our work is that it establishes a medium dependence for the excited state lifetime of this complex. At room temperature, the ^{3}MLCT-^{3}MC transition represents a major decay pathway for the excited state complex in solution. In photosensitisation schemes, decay through this metal-centred state represents a major energy loss pathway since the dd state appears to be short-lived, and there is no evidence to suggest that it undergoes redox quenching reactions. Another important aspect of the decay through this channel is that the dd excited state is substitution labile and its population can lead to photodegradation. As such, the accessibility of the dd excited states of $[Ru(bpy)_3]^{2+}$ and related complexes can represent a major problem to their use as photosensitisers. Removing the dd state from the excited state decay scheme of Ru(II) complexes could therefore be advantageous.

5.4 References.

[1] T.J. Meyer, *Prog. Inorg. Chem.*, 39, 389, **1983**.

[2] K.R. Seddon, *Coord. Chem. Rev.*, 41, 79, **1982**.

[3] K. Kalyanasunduram, *Coord. Chem. Rev.*, 41, 159, **1982.**

[4] G.A. Crosby, G.D Hager, R.J. Watts, *J. Am. Chem. Soc.*, 97, 7031, **1975**.

[5] S.R. Allsopp, A. Cox, S.H. Jenkins, S. Tunstal, T.J. Kemp, W.J. Reed, *J. Chem. Soc., Faraday Trans. I,* 74, 1275, **1978**.

[6] S.R. Allsopp, A. Cox, T.J. Kemp, W.J. Reed, *J. Chem. Soc., Faraday Trans. I,* 75, 353, **1979**.

[7] J.V. Houten, R.J. Watts, *J. Am. Chem. Soc.*, 98, 4853, **1976**.

[8] J.V. Houten, R.J. Watts, *Inorg. Chem.,* 17, 3381, **1978**.

[9] W. Wallace, P. Hoggard, *Inorg. Chem.*, 19, 2141, **1980**.

[10] R.S. Lumpkin, E.M. Kober, L.A. Worl, Z. Murtaza, T.J. Meyer, *J. Phys. Chem.*, 94, 239, **1990**.

[11] B. Durham, J.V. Caspar, J.K. Nagle, T.J. Meyer, *J. Am. Chem. Soc.*, 104, 4803, **1982**.

[12] J.V. Caspar, T.J. Meyer, *Inorg. Chem.*, 22, 2444, **1983**.

[13] W. Wacholtz, R. Auerbach, H. Schmehl, *Inorg. Chem.*, 25, 227, **1986**.

[14] D.P. Rillema, D. Taghidira, D. Jones, C. Keller, L. Worl, T. Meyer, H. Levy, *Inorg. Chem.*, 26, 578, **1987**.

[15] V. Balazani, F. Scandola, Supramolecular Photochemistry, Ellis Horwood, London, **1991**.

[16] N.J. Turro, Modern Molecular Photochemistry, Benjamin, New York, **1978**.

[17] G.F. Strouse, J.R. Schoonover, R. Duesing, S. Boyde, W. Jones, T.J. Meyer, *Inorg. Chem.*, 34, 473, **1995**.

[18] D.P. Rillema, D.S. Jones, H.A. Levy, *J. Chem. Soc., Chem. Comm.*, 849, **1979**.

[19] F. Felix, J. Ferguson, H. Gudel, A. Ludi, *J. Am. Chem. Soc.*, 102, 4096, **1980**.

[20] E.M. Kober, T. J. Meyer, *Inorg Chem.*, 21, 3978, **1982**.

[21] J.N. Demas, D.G. Taylor, *Inorg. Chem.*, 18, 3177, **1979**.

[22] A. Juris, V. Balzani, F. Barigelletti, S. Campagna, P. Belser, A. Von Zelewsky, *Coord. Chem. Rev.*, 84, 85 **1988**.

[23] W.P. Krug, J.N. Demas, *J. Am. Chem. Soc.*, 101, 4394, **1979**.

[24] F. Barigelletti, P. Beiser, A. Von Zelewsky, A. Juris, V. Balzani, *J. Phys. Chem.*, 89 3680, **1985**.

[25] A. Juris, F. Barigelletti, V. Balzani, P. Belser, A. Von Zelewsky, *Inorg. Chem.*, 24, 202, **1982**.

[26] R.S. Lumpkin, E.M. Kober, L.A. Worl, Z. Murtaza, T.J. Meyer, *J. Phys. Chem.*, 94, 239, **1990**.

[27] B. O'Reagan, M. Grätzal, *Nature*, 353, 737, **1991**.

[28] A. Hay, M. Grätzal, *J. Phys. Chem.*, 97, 6272, **1993**.

[29] E. Kober, T.J. Meyer, *Inorg. Chem.*, 21, 3967, **1982**.

[30] G.A. Crosby, *Acc. Chem. Rev.*, 8, 231, **1975**.

[31] T.J. Meyer, *Pure and Appl. Chem.*, 58, 1193,

[32] G.H. Allen, R.P.White, D.P. Rillema, T.J. Meyer, *J. Am. Chem. Soc.*, 106, 2613, **1984**.

[33] H. Yersin, E. Galluber, *J. Am. Chem. Soc.*, 6582, 106, **1984**.

[34] E.M. Kober, T.J. Meyer, *Inorg. Chem.*, 23, 3877, **1984**.

[35] J.V. Caspar, T.J. Meyer, Inorg. *J. Am. Chem. Soc.*, 105, 5583, **1983**.

[36] F. Barigelletti, A. Juris, V. Balzani, P. Belser, A. von Zelewsky, *J. Phys. Chem.*, 91, 1095, **1987**.

[37] S. Peterson, J. Demas, *J. Am. Chem. Soc.*, 101, 6571, **1979**.

[38] J. Davila, C.A, Bignozzi, F. Scandola, *J. Phys. Chem.*, 93. 1373, **1989**.

[39] R. Wang, J.G. Vos, R.H. Schmehl, R. Hage, *J. Am. Chem. Soc.*, 114, 1964, **1992**.

[40] P. Belser, A. Von Zelewsky, *Helv. Chim. Acta*, 63, 1675, **1980**.

[41] S. Campagna, A. Bartolotta, G. Di Marco, *Chem. Phys. Lett.*, 206, 30, **1993**.

[42] E.M. Kober, J.L. Marshall, W.J. Dresswick, B.P.Sullivan, J.V. Caspar, T.J.

Meyer, *Inorg. Chem.*, 24, 2755, **1985**.

[43] R. Dallinger, W. Woodruff, *J. Am. Chem. Soc.*, 101, 4391, **1979**.

[44] R. Dallinger, W. Woodruff, P. Bradley, N. Kress, B. Hornberger, *J. Am. Chem. Soc.*, 103, 7441, **1981**.

[45] G. Crosby, W. Elfring, *J. Phys. Chem.*, 80, 2206, **1979**.

[46] C. Kumar, J. Barton, I. Gould, N. Turro, J. Van Houten, *Inorg. Chem.*, 27, 648, **1988**.

[47] J. Baggot, G. Gregory, M. Piling, S. Anderson, K. Seddon, J. Turp, *J. Chem. Soc., Faraday Trans. II,* 79, 195, **1983**.

[48] C. Kumar, J. Barton, I. Gould, N. Turro, *Inorg. Chem.*, 26, 1455, **1987**.

[49] K. Kalyanasunduran, Photochemistry in Microheterogeneous Systems, Academic Press, New York, **1982**.

[50] R. Matsui, S. Sasaki, N. Takahashi, *Langmuir*, 7, 2866, **1991**.

[51] F.N. Castellano, T.A. Heimer, M.T. Tandhasetti, G.J. Meyer, *Chem. Mater.*, 6, 1041, **1994**.

[52] R. Hage, PhD Thesis, Dublin City University, **1991**.

[53] P.C. Alford, M.S. Cook, P.J. Robbins, *J. Chem. Soc. Perkin Trans.*, 705, **1985**.

[54] M. Wrighton, D.L. Morse, *J. Am. Chem Soc.*,96, 988, **1974**.

[55] R.A. Dellaguardia, J.K. Thomas, *J. Phys. Chem.,* 87, 990, **1983**.

[56] J. Wheeler, J.K. Thomas, *J. Phys. Chem.,* 86, 4540, **1983**.

[57] P.G. Bradley, N. Kress, B. Hornberger, R. Dallinger, W. Woodruff, *J. Am. Chem. Soc.*, 103, 7441, **1981**.

[58] C. Creutz, M. Chou, T. Netzel, M. Okumura, N. Sutin, *J. Am. Chem. Soc.*, 102, 1309, **1980**

[59] P. Braterman, A. Harriman, G. Heath, J. *Chem. Soc., Dalton Trans.*, 1801, **1983**.

[60] S. Milder, J. Gold, D. Kliger, *J. Phys. Chem.*, 90, 548, **1986**.

[61] M. Kasha, B. Dellinger, *Chem. Phys. Lett.*, 36, 410, **1975**.

[62] M. Kasha, B. Dellinger, *Chem. Phys. Lett.*, 38, 9, **1976**.

[63] R.J. Watts, D.J. Missimer, *J. Am. Chem. Soc.*, 100, 5350, **1975**.

[64] P.J. Gardiner, M. Kasha, *J. Chem. Phys.*, 50, 1543, **1969**.

[65] W. Jones, R. Smithe, M. Abrano, M. Williams, J. Host, *Inorg. Chem.*, 28, 2284, **1989**.

[66] R. Reisfeld, C. Joergenson, *Structure and Bonding*, 77, 207, **1992**.

[67] H. Yersin, E. Galluber, *J. Am. Chem. Soc.*, 106, 6582, **1984**.

[68] H. Yersin, E. Galluber, E. Vogler, H. Kunkely, J. *Am. Chem. Soc.*, 105, 4155, **1983**.

[69] M. Fetterolf, H. Offen, *J. Phys. Chem.*, 89, 3320, **1985**.

[70] M. Fetterolf, H. Offen, *J. Phys. Chem.*, 90, 1828, **1986**.

[71] W.R. Cherry, L.J. Henderson, *Inorg. Chem.*, 23, 983, **1984**.

[72] W.R. Cherry, F. Seddon, P. Revco, *Inorg. Chem.*, 24, 4078, **1985**.

[73] R. Hage, Ph D. Thesis, Dublin City University, **1991**.

[74] B.N. Figgis, Introduction to Ligand Fields, New York, p242-245, **1966**.

[75] E.M. Kober, J.V. Caspar, B.P. Sullivan, T.J. Meyer, *Inorg. Chem.*, 27, 4587, **1988**.

[76] G. Denti, S. Serroni, L. Sabatino, M. Ciano, V. Balzani, *Inorg. Chem.*, 29, 4750, **1990**.

[77] E.M. Kober, J.V. Caspar, B.P. Sullivan, T.J. Meyer, *J. Am. Chem. Soc.*, 104, 630, **1982**.

[78] J.V. Caspar, T.J. Meyer, *J. Phys. Chem.*, 87, 952, **1983**.

Chapter 6.

The temperature dependence of the emission properties of Ru(II) complexes containing pyridyltriazoles immobilised in a sol-gel matrix.

6.1 Introduction.

The previous chapters report the photophysical behaviour of a number of Ru(II) complexes within the sol-gel matrix. The photophysics of these species were altered to varying degrees upon incorporation into the silica network. The purpose of this chapter was to extend these studies to include a greater number of different Ru(II) complexes and to examine the possibility of any trends which may be occurring. Towards this end, ruthenium compounds (both the monomers and dimers) of $Ru(bpy)_2$ with 3,5-bis(pyridin-2-yl)-1,2,4-triazole (Hbpt) and 3,5-bis(pyrazin-2-yl)-1,2,4-triazole (Hbpzt) were incorporated into the sol-gel matrix and their excited state decay behaviour was investigated.

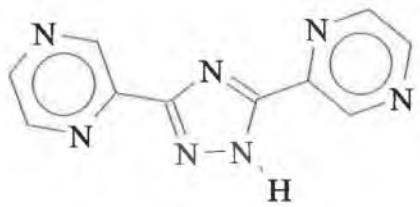

Hbpzt

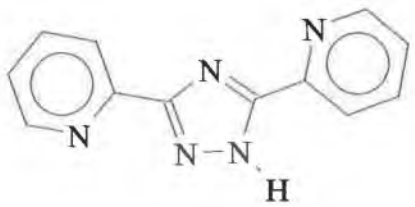

Hbpt

Figure 6.1 Structure of the bridging triazole ligands 3,5-bis(pyrazin-2-yl)-1,2,4-triazole (Hbpzt) and 3,5-bis(pyridyn-2-yl)-1,2,4-triazole (Hbpt).

These complexes were chosen for a number of reasons. Firstly, the synthesis and characterisation of these bridging ligands and their subsequent complexes have been carried out in our laboratories [1-9]. As such, the photophysical properties of these complexes in solution are well understood and documented. Secondly, the acid/base chemistry of the monomeric species leads to significantly different behaviour in the temperature dependent luminescent lifetimes for the protonated and deprotonated complexes in solution. It was of interest to examine whether such differences were evident in the sol-gel matrix. Finally, the incorporation of the dimeric complexes were studied in order to establish the effect of the size or 'bulk' of the species on the photophysical

properties in a rigid matrix by comparison with the analogous monomeric species. Temperature dependent lifetime measurements of the deprotonated and protonated pyridyltriazole complex employed in the Chapter 3 and 4, namely $[Ru(phen)_2(H3Mptr)]^{2+}$, were also carried out to further investigate the photophysical processes of this complex in solution and to allow for comparison to those measurements obtained in the sol-gel matrix.

6.2 Results and discussion.

6.2.1 Electronic properties of Ru(II) complexes containing pyridyltriazoles in solution and in sol-gel matrix.

Table 6.1 presents the emission properties of $[Ru(phen)_2(H3Mptr)]^{2+}$ and also the mono- and dinuclear complexes of the Hbpt and Hbpzt ligands both in solution and in a sol-gel matrix. The electronic properties of $[Ru(bpy)_3]^{2+}$ in solution and in a xerogel are also included in this table for comparison purposes. The photophysical properties of the immobilised complex $[Ru(phen)_2(H3Mptr)]^{2+}$ have been previously discussed in Chapters 3 and 4. For the Hbpt and Hbpzt monomers and dimers, the synthesis and spectroscopic characterisation of these complexes have been previously reported [3-8], and their solution properties have been thoroughly investigated. All the complexes employed here exhibit intense absorption bands in the visible region of the spectrum, which have been assigned as metal-to-ligand charge-transfer (^{1}MLCT) bands. In addition, luminescence at room temperature and at 77 K for all the complexes have been reported previously [7,8].

The bpt^- is a stronger σ-donor and a weaker π-acceptor than bpy. The absorption and the emission spectra of $[Ru(bpy)_2(bpt)]^+$ and $[(Ru(bpy)_2)_2(bpt)]^{3+}$ in solution are in agreement with this expectation [3]. Replacement of a bpy ligand of $[Ru(bpy)_3]^{2+}$ by bpt^- to give $[Ru(bpy)_2(bpt)]^+$ causes an increase in the electron density at the metal (and therefore an increase in the energy of the highest occupied molecular orbital, HOMO), with a consequent red shift of the metal-to ligand (Ru→bpy) charge transfer absorption and emission band. Co-ordination of a second $[Ru(bpy)_2]^{2+}$ unit to the bpt^- bridging results in the sharing of its negative charge between two $[Ru(bpy)_2]^{2+}$ units, with a decrease of electron density on the Ru(II) ions and a consequent blue shift of the Ru→bpy charge-transfer levels.

Table 6.1. Electronic properties of the pyridyltriazole complexes in solution and in sol-gel matrix.

Complex	Medium	λ_{max} nm[a]	λ_{max} nm[b]	τ (ns)[a]	τ (ns)[b]
$[Ru(bpy)_3]^{2+}$	Solution	611	580	700 (280)[c]	4500
	Method 2 (1)	598	579	1100(70), 470(30)[d]	4490(75), 1590(25)[d]
	Method 2 (5)	588	576	2100(80), 660(20)[d]	4450(85), 1800(15)[d]
$[Ru(phen)_2(3Mptr)]^{+}$	Solution	654	606	90 (55)[c]	7200
$[Ru(phen)_2(H3Mptr)]^{2+}$	Solution	606	568	----[e]	9800
	Method 2 (1)	598	566	350(85), 60(15)[d]	9450(80), 2150(20)[d]
	Method 2 (5)	585	568	1920(80), 480(20)[d]	9650(70), 2460(30)[d]
$[Ru(bpy)_2(bpt)]^{+}$	Solution	660	624	355 (160)[c]	5500
$[Ru(bpy)_2(Hbpt)]^{2+}$	Solution	640	612	100 (40)[c]	4200
	Method 2 (1)	618	606	320(65), 80(35)[d]	4170(70), 1630(30)[d]
	Method 2 (5)	612	600	765(75), 170(25)[d]	4300(80), 1500(20)[d]
$[(Ru(bpy)_2)_2(bpt)]^{3+}$	Solution	642	603	85 (50)[c]	4160
	Method 2 (1)	616	599	140(85), 40(15)[d]	4030(80), 1550(20)[d]
	Method 2 (5)	611	600	760 (70), 190(30)[d]	4010(75), 1455(25)[d]
$[Ru(bpy)_2(bpzt)]^{+}$	Solution	662	610	100 (60)[c]	6400
$[Ru(bpy)_2(Hbpzt)]^{2+}$	Solution	675	612	120 (75)[c]	4970
	Method 2 (1)	640	613	180(85), 40(15)[d]	4900(75), 1030(25)[d]
	Method 2 (5)	627	612	615(70), 110(30)[d]	4850(80), 1150(20)[d]
$[(Ru(bpy)_2)_2(bpzt)]^{3+}$	Solution	671	617	105 (70)[c]	7030
	Method 2 (1)	668	615	180(70), 40(30)[d]	6900(75), 1400(25)[d]
	Method 2 (5)	665	612	830(75), 200(25)[d]	7300(75), 1700(25)[d]

[a] RT. measurements were degassed by purging with argon. Sol-gel samples were not degassed. [b] These measurements were carried out at 77 K. For solution values, the solvent employed was ethanol/methanol 4/1 v/v. [c] Value in parentheses indicates lifetime of the complex in aerated ethanol solution. [d] Value in parentheses are the lifetime components pre-exponential factor given in percent. [e] This value was outside the range of the instrumentation (*i.e.* < 20 ns).

Replacement of the bpt$^-$ bridging ligand with bpzt$^-$ results in higher maximum wavelength of the absorption and the emission maxima at both room temperature and at 77 K [6,9]. This can be explained by the weaker σ-donor and stronger π-acceptor properties of the bpzt$^-$ ligand compared with the bpt$^-$ ligand, which causes less electron density to be present on the metal and consequently a shift to higher energy of the lowest unoccupied molecular orbital (LUMO) [6]. The electrochemical and resonance Raman data have shown that, for $[Ru(bpy)_2(bpzt)]^+$, the emitting state is bpy based [6]. For $[Ru(bpy)_2(Hbpzt)]^{2+}$ the situation is different as the resonance Raman spectra exhibited both bpy and Hbpzt vibrations. Upon protonation of the bpzt$^-$ ligand a significant lowering of the π^* (bpzt) orbital takes place. In effect, a switch over from bpy-based emission for the deprotonated complex to a bpzt-based emission for the protonated complex is observed. The ^{3}MLCT state of $[(Ru(bpy)_2)_2(bpzt)]^{3+}$ has also been found to be bpzt-based. When going from the mononuclear to the dinuclear compound with bpzt$^-$, two effects have been observed. Firstly, a lowering of the π^* level of the bridging ligand has been observed [7-9]. Because of the switch from the bpy-based reduction for the mononuclear compound, the decrease in energy of the lowest π^* level upon formation of the dinuclear compound is much smaller than that observed for other bridging ligands with low-lying π^* levels. Secondly, the higher oxidation potential observed for the bpzt$^-$ dinuclear complex [8,9], compared to the analogous monomer exhibited that a stabilisation of the d orbitals occurred. This is caused by the fact that in the dinuclear compound two $Ru(bpy)_2$ moieties share the σ-donor capacity of the negatively charged bridging ligand.

For the bpt$^-$ and the bpzt$^-$ monomers, it is important to determine whether the protonated or deprotonated species is present in the final xerogel. The sol-gels prepared at pH 1 pose no real problem, and it is evident from the emission data in Table 6.1 that both of these monomers are protonated in Method 2(1) xerogels. However, for the sol-gels prepared at pH 5, the question of which species is present is not as straightforward. Directly after preparation (*i.e.* zero time) of the Method 2(5) samples, the gel doped with the bpt monomer emits at 661 nm while that doped with the bpzt monomer emits at 663 nm. In both cases,

the emission maximas are indicative of the deprotonated complexes. Since the starting systems were liquid, composed of TEOS, ethanol, water and catalyst (HCl) the emission behaviour indicates that the effective pH value of the surrounding mixture is approximately 5. However, as the sol-gel reactions proceed, it is uncertain as to whether the pH which the dopant experiences remains at 5. Fujii and co-workers have recently reported the absorption spectra of Thymol Blue during the sol-gel-xerogel transition in TEOS based systems under both mild acid and base conditions [10]. These studies suggest that the doped systems increase in acidity throughout the transitions regardless of the catalysts used. The authors suggest that the surface silanols act as proton donors towards the Thymol Blue probe molecules.

In Chapter 3, it was suggested that the protonated pyridyltriazole complex, $[Ru(phen)_2(H3Mptr)]^{2+}$, was the eventual species in the final xerogel for the gel at pH 5. This was suggested by following the absorption and the emission spectra of the complex as the sol-gel-xerogel reactions proceeded. We have mentioned previously, that the absorption profile of the $[Ru(L\text{-}L)_3]^{2+}$ complexes studied are unchanged in the final xerogel when compared to the initial sol. As such, the blue shift in the absorption spectrum of $[Ru(phen)_2(3Mptr)]^{+}$ noted during the early stages of the sol-gel reactions for those samples prepared at pH 5 (see Chapter 3) strongly suggests that the deprotonated complex reverts to the protonated complex during this time. Further evidence that the protonated form, $[Ru(phen)_2(H3Mptr)]^{2+}$, exists in the final xerogel was also obtained from the emission spectrum of the immobilised complex. Placing the doped Method 2(5) xerogel in an aqueous basic environment for 12 hours resulted in a red shift in the emission maximum from 585 nm to 630 nm, which suggests that under these conditions the immobilised deprotonated form of the complex was formed.

For both monomers studied in this chapter, a significant blue shift in the absorption energy was observed during the initial sol-gel reactions. In addition, the position of the emission maxima of these samples was also shifted to higher energy upon formation of the xerogel (from 661→612 nm, an increase of 1210 cm^{-1} for the bpt monomer, and 663→627 nm, an increase of 870 cm^{-1} for the

bpzt monomer). With respect to the bpzt$^-$ monomer in solution, the protonated species luminesces at a higher wavelength than the deprotonated form. If in the sol-gel the deprotonated form of this complex reverts to the protonated form, we would expect a similar red shift. However, it is likely that such a red shift in emission energy is counteracted (or masked) by the blue shift induced by the rigid nature of the gel matrix. However, comparison of the excited state pK_a of these complexes ($[Ru(phen)_2(H3Mptr)]^{2+}$ = 2.7, $[Ru(bpy)_2(Hbpzt)]^{2+}$ = 2.8 [8], $[Ru(bpy)_2(Hbpt)]^{2+}$ = 3.7 [8]) suggests that the latter two complexes will also be protonated in the sol-gel matrix prepared at pH 5.

As regards the pH at which the gels were prepared, similar trends in the emission energy and excited state decay were observed for both monomers as were previously reported for $[Ru(bpy)_3]^{2+}$ in Chapters 3 and 4. The most pronounced effect of the sol-gel matrix on the bpt monomer is the destabilisation of the ^{3}MLCT excited state which can be contributed to the larger dipole moment in the excited state relative to that in the ground state. Again, both the gels prepared at pH 5, where the surface of the xerogel is known to be deprotonated, exhibited not only a larger increase in emission energy with respect to the analogous solution value, but also an extended luminescent decay lifetime when compared to the analogous gels prepared at pH 1.

However, although the emission energy of the bpzt monomer behaved in a very similar fashion to the bpt monomer and indeed $[Ru(bpy)_3]^{2+}$ upon incorporation into a sol-gel matrix, it was noticed that the energy of the photoluminescence peak of the dimer $[(Ru(bpy)_2)_2bpzt]^{3+}$ was only slightly altered upon incorporation into the sol-gel matrix (by 70 cm^{-1} at pH 1 and 130 cm^{-1} at pH 5). This behaviour is very different from that which was observed for the bpt$^-$ dimeric species (which was altered by approximately 660 cm^{-1} at pH 1 and 790 cm^{-1} at pH 5). A possible explanation for this is as follows: It has been previously reported that, in the case of the bpt$^-$ dimer, upon excitation, both ends of the complex have equal chance of being excited [9]. Furthermore, since in the bpt$^-$ compound, the lowest π^*-level is based on the bpy ligands, both bpy-based ^{3}MLCT levels can be occupied. However, in the case of the bpzt$^-$ dinuclear molecule, the lowest π^*-level is based on the bridging ligand which is more

central in the molecule [6-9]. Therefore, upon excitation the change in dipole moment for the bpt$^-$ dimer as experienced by the sol-gel environment would appear to be more significant than that of the analogous bpzt$^-$ species where the excited electron resides on the central bridging unit. As such, the excited state of the bpzt$^-$ dimeric species may be shielded to an extent by the $Ru(bpy)_2$ units.

6.2.2 Temperature dependent studies.

6.2.2.1 Solution measurements.

As mentioned previously, for Ru(II) complexes at room temperature, the lifetime of the ^{3}MLCT states is affected by the magnitude of a number of energy gaps. For example, increasing the energy gap with respect to the ground state tends to increase the lifetime [11]. Also, decreasing the energy gap with respect to upper metal-centred (^{3}MC) ligand-field states is known to decrease the lifetime (these states are in the strong coupling regime with the ground state and provide an efficient thermally activated deactivation pathway [12-15].

Luminescent temperature dependent lifetime experiments were carried out on all of the monomer and dimer doped gels. As before, the temperature dependent lifetime data of the complexes studied in this chapter were fit by assuming that the excited state decay consists of a temperature independent intrinsic decay from the ^{3}MLCT state and a single thermally activated non-radiative decay process. Table 6.2 lists the exponential prefactors and activation energies obtained from these measurements, together with those previously reported for the complexes in solution [19,24]. Plots of $\ln(1/\tau)$ versus 1000/T in the temperature range 150-300 K are presented in Figures 6.2-6.6.

As discussed in the previous chapter, with regard to a solution of $[Ru(bpy)_3]^{2+}$, the kinetic parameters A_i and ΔE_i obtained are associated with an activated surface crossing to an upper lying ^{3}MC excited state, which can then undergo fast deactivation to the ground state and/or ligand dissociation.

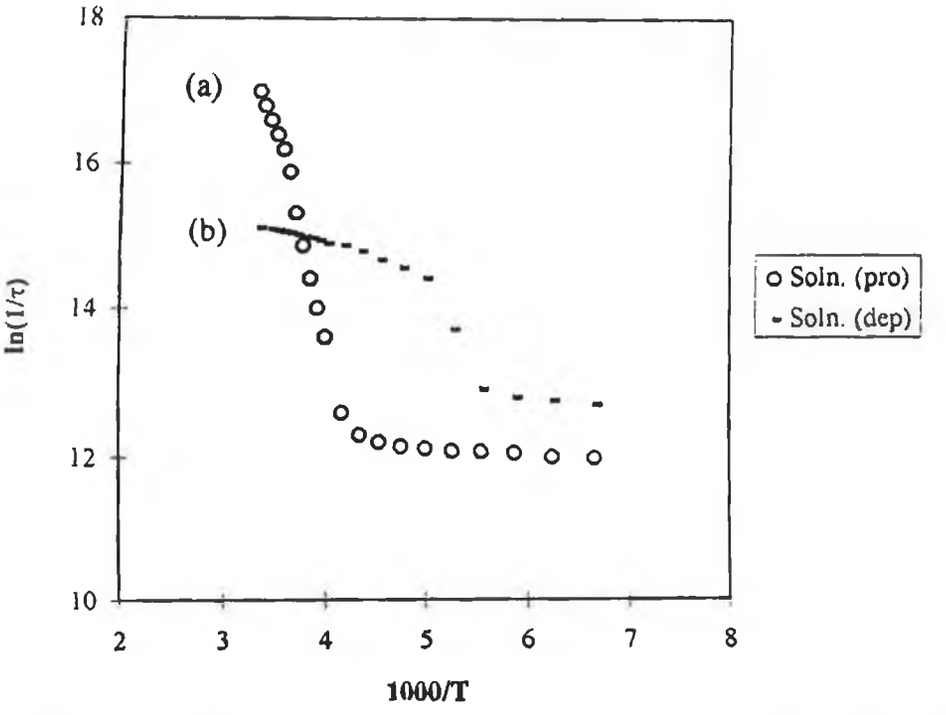

Figure 6.2(a) The temperature dependence for the luminescence lifetime of (a)[Ru(phen)$_2$(H3Mptr)]$^{2+}$ and (b) [Ru(phen)$_2$(3Mptr)]$^+$ in 4:1 EtOH:MeOH, in the temperature range 150-300 K.

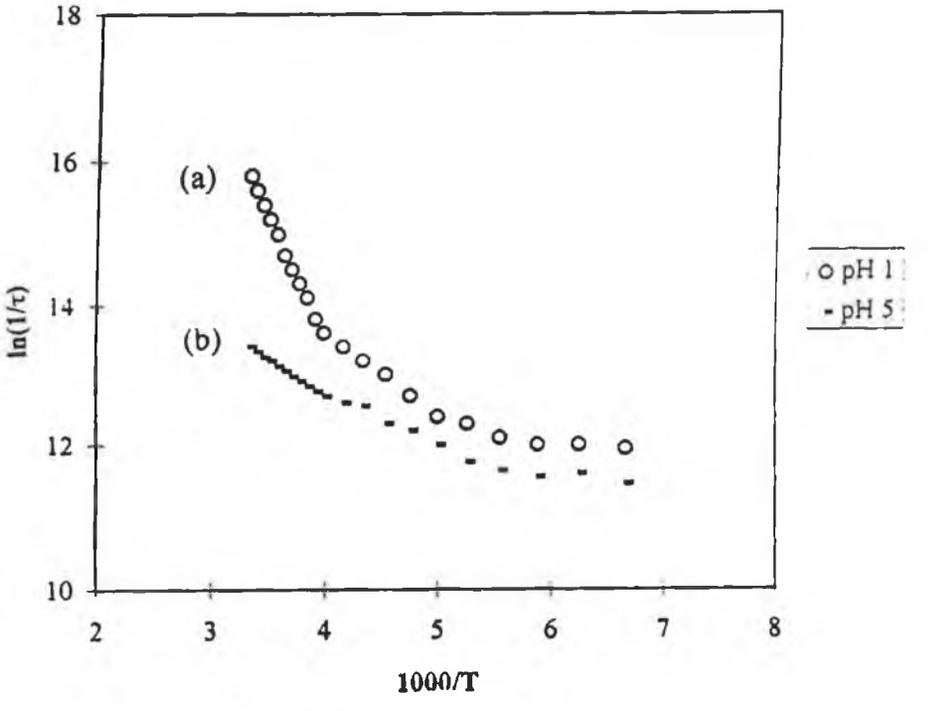

Figure 6.2(b) The temperature dependence for the luminescence lifetime of [Ru(phen)$_2$(H3Mptr)]$^{2+}$ in (a) a Method 2(1) sol-gel and (b) a Method 2(5) sol-gel, in the temperature range 150-300 K.

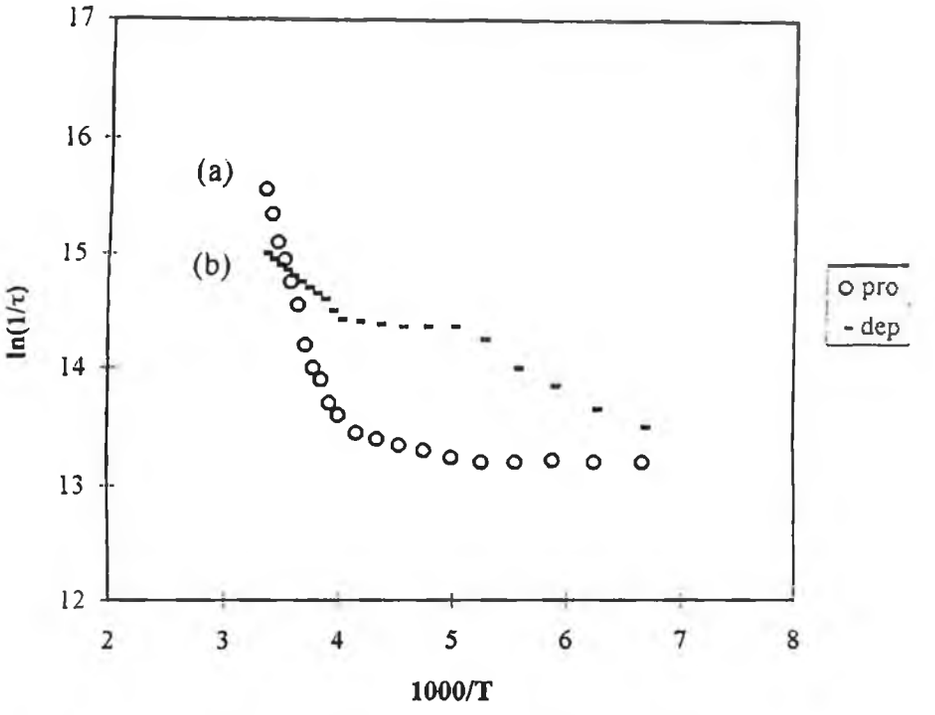

Figure 6.3(a) The temperature dependence for the luminescence lifetime of (a) $[Ru(bpy)_2(Hbpt)]^{2+}$ *and (b)* $[Ru(bpy)_2(bpt)]^{+}$ *in 4/1 EtOH/MeOH, in the temperature range 150-300 K.*

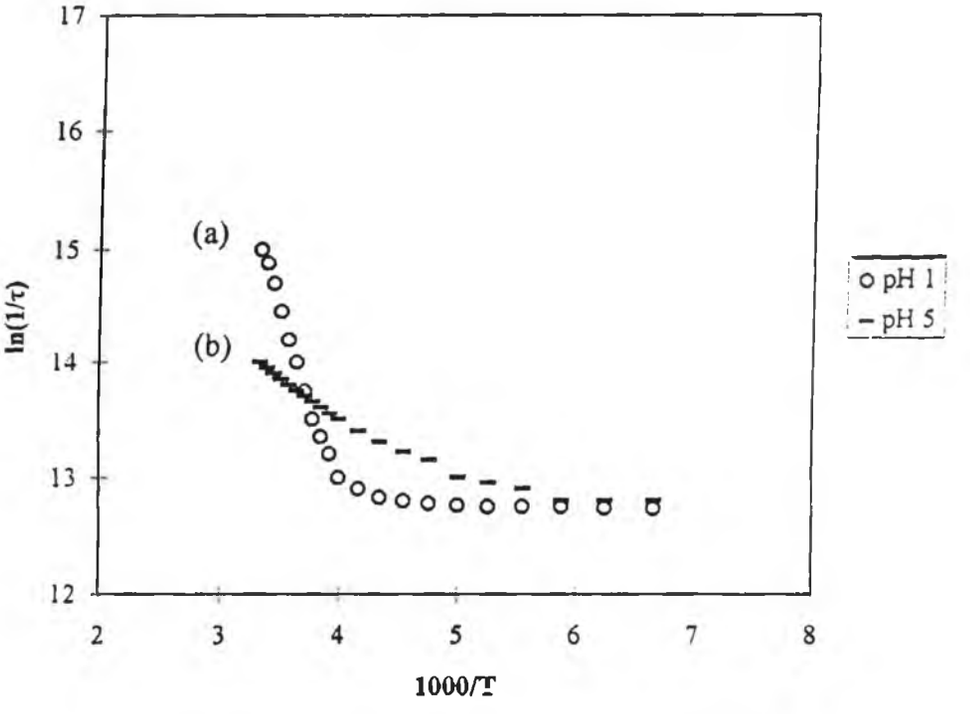

Figure 6.3(b) The temperature dependence for the luminescence lifetime of $[Ru(bpy)_2(Hbpt)]^{2+}$ *in (a) a Method 2(1) sol-gel and (b) a Method 2(5) sol-gel, in the temperature range 150-300 K.*

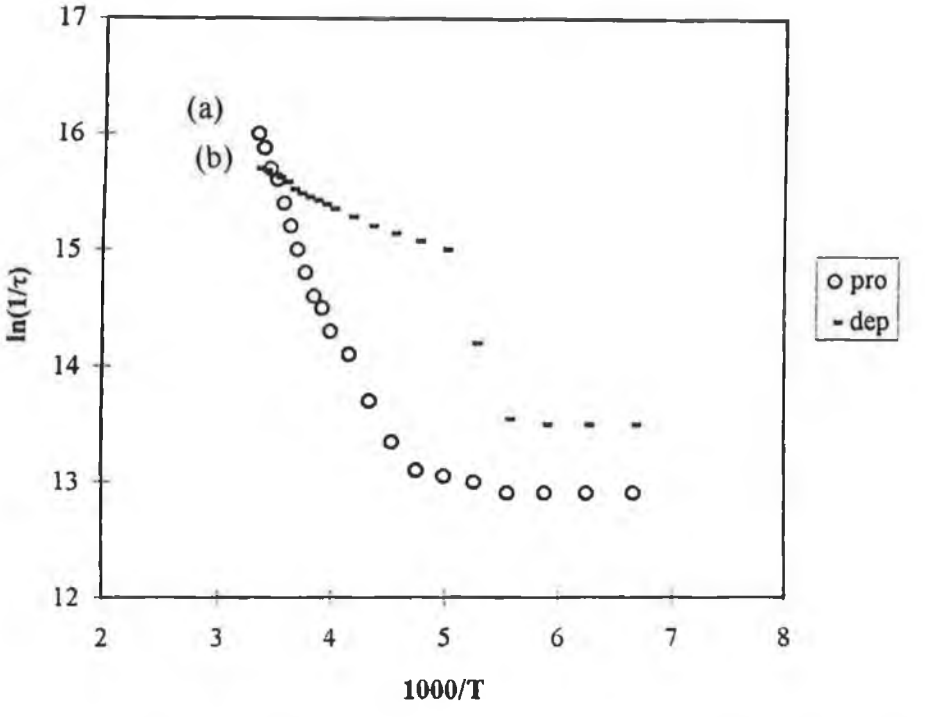

Figure 6.4(a) The temperature dependence for the luminescence lifetime of (a) $[Ru(bpy)_2(Hbpzt)]^{2+}$ *and (b)* $[Ru(bpy)_2(bpzt)]^{+}$ *in 4/1 EtOH/MeOH, in the temperature range 150-300 K.*

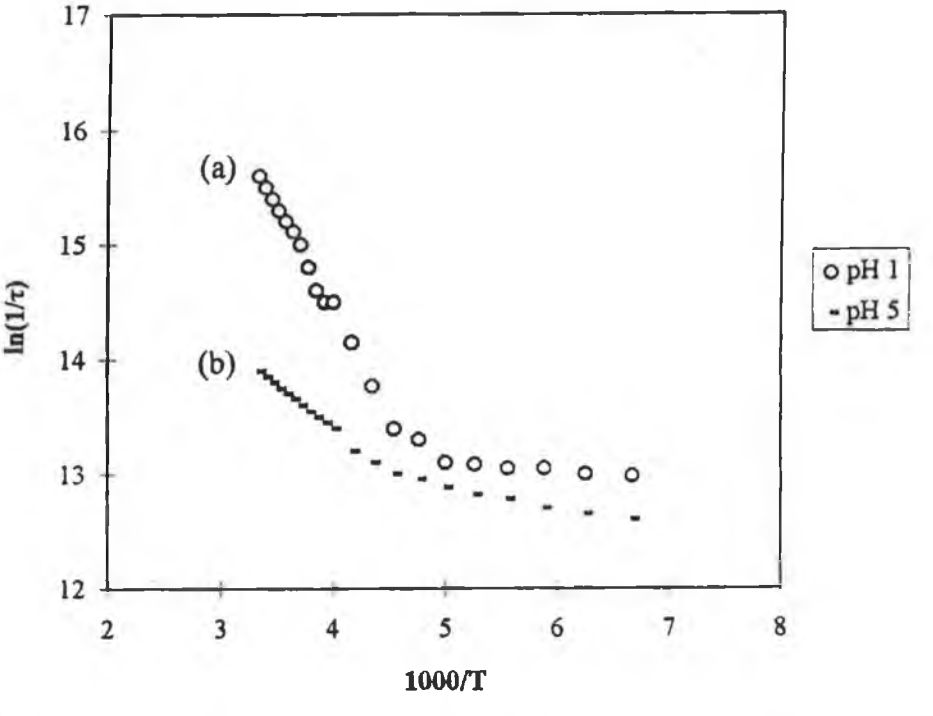

Figure 6.4(b) The temperature dependence for the luminescence lifetime of $[Ru(bpy)_2(Hbpzt)]^{2+}$ *in (a) a Method 2(1) sol-gel and (b) a Method 2(5) sol-gel, in the temperature range 150-300 K.*

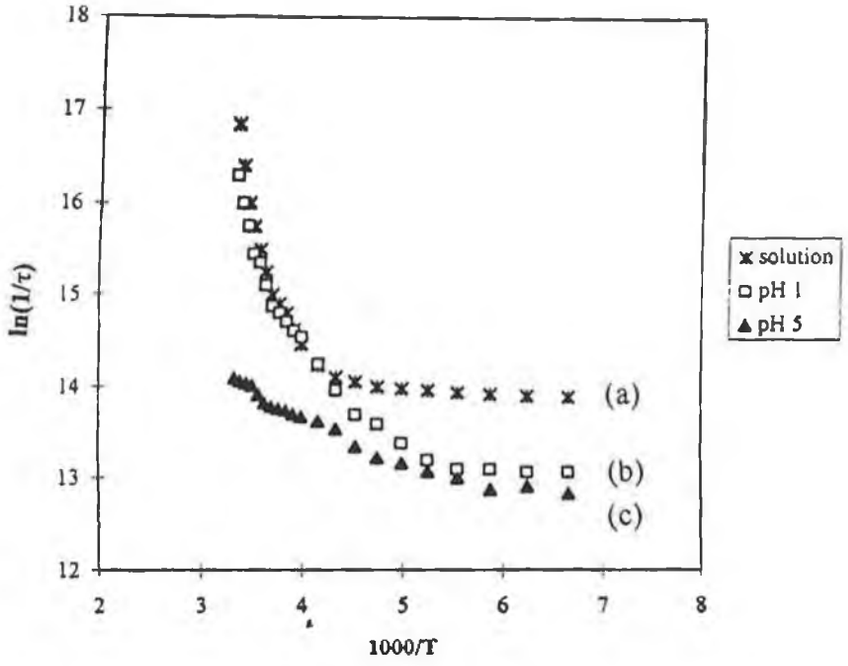

Figure 6.5 The temperature dependence for the luminescence lifetime of $[(Ru(bpy)_2)_2(bpt)]^{3+}$ in (a) 4:1 EtOH/MeOH, (b) a Method 2(1) sol-gel and (c) a Method 2(5) sol-gel, in the temperature range 150-300 K.

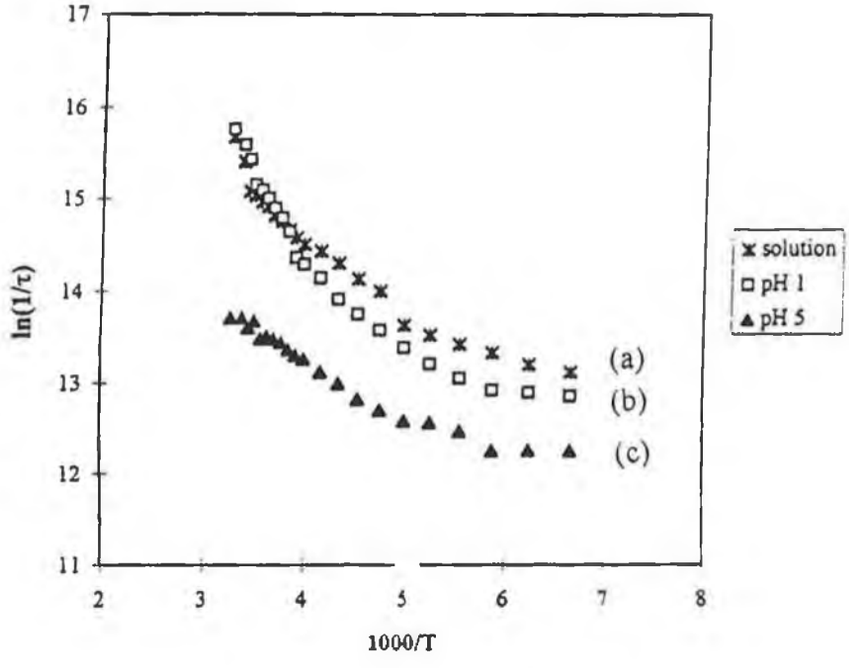

Figure 6.6 The temperature dependence for the luminescence lifetime of $[(Ru(bpy)_2)_2(bpzt)]^{3+}$ in (a) 4:1 EtOH/MeOH, (b) a Method 2(1) sol-gel and (c) a Method 2(5) sol-gel, in the temperature range 150-300 K.

Table 6.2 Excited state decay parameters of pyridyltriazole complexes both in solution (4/1 ethanol/methanol, v/v) and in sol-gel matrices.

Complex	Medium	k_0 (s-1)	A_i (s^{-1})[b]	ΔE_i (cm^{-1})[b]
$[Ru(bpy)_3]^{2+}$	[b]Solution	2.22×10^5	1.4×10^{14}	3900
	[b]Method 2 (1)	2.42×10^5	6.77×10^6	520
	[b]Method 2 (5)	2.51×10^5	2.9×10^6	660
$[Ru(phen)_2(3Mptr)]^+$	[b]Solution	1.38×10^5	2.9×10^7	320
$[Ru(phen)_2(H3Mptr)]^{2+}$	[b]Solution	1.60×10^5	2.0×10^{13}	3006
	[b]Method 2 (1)	1.56×10^5	6.36×10^{12}	2655
	[b]Method 2 (5)	1.22×10^5	1.44×10^7	800
$[Ru(bpy)_2(bpt)]^+$	[c]Solution	2.41×10^5	3.8×10^8	1127
$[Ru(bpy)_2(Hbpt)]^{2+}$	[c]Solution	2.33×10^5	8.55×10^{14}	3600
	[b]Method 2 (1)	3.75×10^5	5.45×10^{14}	3525
	[b]Method 2 (5)	3.48×10^5	7.28×10^7	900
$[(Ru(bpy)_2)_2(bpt)]^{3+}$	[c]Solution	2.40×10^5	5.3×10^{15}	4061
	[b]Method 2 (1)	4.92×10^5	2.84×10^{14}	3600
	[b]Method 2 (5)	3.64×10^5	4.63×10^7	800
$[Ru(bpy)_2(bpzt)]^+$	[c]Solution	1.6×10^5	2.9×10^9	1370
$[Ru(bpy)_2(Hbpzt)]^{2+}$	[c]Solution	1.4×10^5	1.66×10^{13}	3100
	[b]Method 2 (1)	3.19×10^5	2.42×10^{13}	3225
	[b]Method 2 (5)	3.21×10^5	3.84×10^8	1000
$[(Ru(bpy)_2)_2(bpzt)]^{3+}$	[c]Solution	1.4×10^5	9.9×10^{13}	3735
	[b]Method 2 (1)	4.11×10^5	1.26×10^{13}	3020
	[b]Method 2 (5)	2.37×10^5	1.46×10^{11}	2500

All of the samples (both solution and sol-gels) were degassed prior to temperature dependent measurements. [b] Present work. [c] From reference [8]

The $\ln(1/\tau)$ vs. 1/T plots for both the protonated and the deprotonated $[Ru(phen)_2(H3Mptr)]^{2+}$ complex in 4/1 ethanol/methanol are illustrated in Figure 6.2(a). As in Chapter 5, the analysis of the temperature dependent lifetime of the immobilised complexes was restricted to only the longer lived, most dominant lifetime component. The protonated complex exhibits a steep decrease in lifetime above 220 K and the high activation energy (3006 cm^{-1}) and prefactor (2.0×10^{13} s^{-1}) obtained suggest a photochemically unstable complex. As is the case with $[Ru(bpy)_3]^{2+}$ an activated surface crossing to a ^3MC excited state is occurring [19,30]. The population of such an excited state causes a fast deactivation to the ground state and/or photodecomposition of the complex. On the other hand, the deprotonated form of the complex has a low prefactor (2.9×10^7 s^{-1}) and a small activation barrier (600 cm^{-1}) characteristic of a photoinert complex [15]. Such values are typically obtained for those complexes which are unreactive towards ligand substitution. The slight temperature dependence observed for this complex above 220 K may be attributable to population of other MLCT excited states. Kober and Meyer have suggested that this activated process corresponds to the population of an MLCT state of largely singlet character [16,17,18].

As mentioned in Chapters 3 and 4, for this particular complex the pyridyltriazole acts as a "spectator" ligand. Protonation results in an increase in the emission energy. The decrease in the emission lifetime is the consequence of the increased π-acceptor ability of the pyridyltriazole upon protonation and the consequent stabilisation of the t_{2g} orbitals of the metal. Due to the concomitant decreased σ-donor ability of the protonated pyridyltriazole and the consequent stabilisation of the e_g^* orbitals, the energy of the ^3MC is expected to undergo a much smaller change than that of the MLCT state upon protonation. Therefore, the energy gap between the ^3MLCT and ^3MC states is expected to decrease upon protonation, leading to fast thermally activated decay for the protonated form of the complex. This phenomenon has been previously observed by Scandola and co-workers for the protonation of $[Ru(bpy)_2(CN)_2]$ [15].

In solution, the deprotonated species, $[Ru(phen)_2(3Mptr)]^+$, a step was been observed around 170 K in the $\ln(1/\tau)$ versus 1000/T plot. A similar behaviour was also observed by Barigelletti and co-workers for $[Ru(bpy)_2(CN)_2]$

[13], and has been attributed to reorientation of the solvent molecules due to a strong change in dipole moment caused by the Ru→bpy charge-transfer. $[Ru(phen)_2(3Mptr)]^+$ can be compared with $[Ru(bpy)_2(CN)_2]$ because, in both cases, strong σ-donor ligands are present (CN^- and $3Mptr^-$), that do not participate in the emission process (bpy/phen-based emission) and because both ligands can interact with the solvent molecules *via* hydrogen bonds.

From Table 6.2 and Figures 6.3(a) and 6.4(a), it appears that the temperature dependent behaviour of the emission lifetime of the Hbpt and Hbpzt monomers behave in a similar manner to that observed for the $[Ru(phen)_2(H3Mptr)]^{2+}$ complex. The protonated species exhibit kinetic parameters which are indicative of the population of the ^3MC state. No steep rise was observed in the $\ln(1/\tau)$ versus 1000/T plot for either of the deprotonated monomers. For $[Ru(bpy)_2(bpt)]^+$, because of the strong σ-donor power of bpt^-, the metal centred levels are expected to lie at higher energy than that of $[Ru(bpy)_3]^{2+}$ [18]. Coupled with the lower energy of the luminescent ^3MLCT level, this leads to the conclusion that the ^3MC-^3MLCT energy gap for the deprotonated monomer is considerably higher than that of $[Ru(bpy)_3]^{2+}$. Thus the slightly activated radiationless decay process which occurs with $A_i = 3.8 \times 10^8\ s^{-1}$ and $\Delta E_i = 1127\ cm^{-1}$ for $[Ru(bpy)_2(bpt)]^+$ does not concern the population of the ^3MC state, but more likely, the additional MLCT level discussed in the previous chapter [19-22]. Similarly, the kinetic parameters of $[Ru(bpy)_2(bpzt)]^-$, $A_i = 2.9 \times 10^9\ s^{-1}$ and $\Delta E_i = 1370\ cm^{-1}$, predict that this compound is photostable. Both deprotonated complexes exhibit a steep rise in the $\ln(1/\tau)$ vs. 1000/T plots in the temperature range of 180-210 K. This step has already been encountered for the $[Ru(phen)_2(3Mptr)]^+$ complex and was attributed to reorientation of the solvent molecules due to strong changes in the dipole moment caused by the Ru→phen charge transfer.

A value of $3735\ cm^{-1}$ was obtained for ΔE_i and a value of $10^{14}\ s^{-1}$ for the preexponential factor of the $[(Ru(bpy)_2)_2(bpzt)]^{3+}$ complex [9]. These values are quite similar to those obtained for the analogous bpt dimer, where ΔE_i and A_i were found to be $4060\ cm^{-1}$ and $5.3 \times 10^{15}\ s^{-1}$ respectively [9].The high values obtained for the kinetic parameters for both of the dimer species in solution

indicate that the activated process observed for these complexes is the population of the triplet metal-centred (^{3}MC) state. As mentioned previously, the ligand field strength of bpt$^-$ for $[(Ru(bpy)_2)_2(bpt)]^{3+}$ and of Hbpzt in $[(Ru(bpy)_2)_2(bpzt)]^{3+}$ are smaller than for the analogous deprotonated mononuclear compounds and as such, the ^{3}MC state of the dinuclear complexes should be lower in energy than in the ^{3}MC states of the mononuclear complexes. This decrease in energy gap between the ^{3}MC and ^{3}MLCT state allows for the population and subsequent deactivation of this ^{3}MC state in the dimer complexes.

6.2.2.2 Sol-gel measurements.

Tables 6.2 also lists the exponential prefactors and activation energies obtained for each of the complexes in two different sol-gel matrices. Concerning $[Ru(phen)_2(H3Mptr)]^{2+}$ and the two monomers $[Ru(bpy)_2(Hbpt)]^{2+}$ and $[Ru(bpy)_2(Hbpzt)]^{2+}$, the temperature dependent behaviour of the immobilised protonated complexes seems to depend greatly on the surface charge of the sol-gel matrix. For example, when the surface charge of the sol-gel is negative (*i.e.* for those gels prepared at pH 5), the temperature dependency of the immobilised $[Ru(phen)_2(H3Mptr)]^{2+}$ is manifested as only a slight rise in the $\ln(1/\tau)$ vs. 1000/T plot, and low values were obtained for both the prefactor and ΔE_i (*i.e.* $A_i = 1.44 \times 10^7$ s^{-1} and $\Delta E_i = 320$ cm^{-1}). In contrast, the gels prepared at pH 1 exhibited a steep rise in the $\ln(1/\tau)$ vs. 1000/T plot, and the kinetic parameters obtained for this sample ($A_i = 6.36 \times 10^{12}$ s^{-1} and $\Delta E_i = 2655$ cm^{-1}) suggest population of the ^{3}MC state. Similar results were found for the immobilised Hbpt and Hbpzt monomers (see Figures 6.4(b) and 6.5(b)). In contrast to the results outlined above, for $[Ru(bpy)_3]^{2+}$, population of the ^{3}MC state was not observed, irrespective of the pH at which the gel was prepared.

For those gels prepared at pH 5, it could be argued that the low kinetic parameters obtained from the temperature dependent studies of each of these pyridyltriazole complexes suggest the presence of the deprotonated form of the complexes. However, although we cannot rule out this possibility, for the reasons

outlined in the previous section, we suggest that the protonated form of the pyridyltriazole complexes are present in the final xerogel. If indeed the protonated form of these complexes is present in the final xerogel, the question remains as to why the kinetic parameters are dramatically altered upon going from a gel prepared at pH 1 to one prepared at pH 5. We will return to this point shortly.

As mentioned earlier, upon incorporation into the sol-gel matrix the photophysical properties (in particular the position of the λ_{max} and the lifetime) of the dimeric complexes were found to depend very much on the surface charge of the matrix as well as the residency of the LUMO. It was of interest therefore, to investigate the temperature dependent excited state decay behaviour of the immobilised species. Figure 6.5 and 6.6 illustrate the $\ln(1/\tau)$ versus 1000/T plots for the bpt^- and $bpzt^-$ dimers in solution and in the sol-gel matrices. In both cases, the gels prepared at pH 1, where the surface is known to be positively charged due to the presence of protonated silanols (*i.e.* $Si\text{-}OH_2^+$), a steep rise in the temperature-dependent lifetime plots was observed, similar to that of each particular complex in solution. This observation, together with the kinetic parameters obtained for these samples ($A_i = 2.84 \times 10^{14}$ s^{-1} and $\Delta E_i = 3600$ cm^{-1} for the Hbpt dimer and $A_i = 1.26 \times 10^{13}$ s^{-1} and $\Delta E_i = 3020$ cm^{-1} for the Hbpzt dimer) indicate that for these immobilised complexes an activated surface crossing to the ^3MC states followed by subsequent deactivation of these states is occurring. However, for the bpt^- dimer complex, a profound change occurred in the kinetic decay parameters between the sol-gel prepared at pH 1 and at pH 5. Where the surface is negatively charged, *i.e.* for those gels prepared at pH 5, the temperature dependent lifetime analysis of this species revealed a low prefactor and a small activation barrier ($A_i = 3.84 \times 10^8$ s^{-1} and $\Delta E_i = 1000$ cm^{-1}). For the $bpzt^-$ dimer, the kinetic parameters obtained for temperature dependency of the emission lifetime of this complex in a negatively charged gel ($A_i = 1.46 \times 10^{11}$ s^{-1} and $\Delta E_i = 2500$ cm^{-1}), fall into an intermediate category, which suggests that the ^3MLCT and ^3MC states are in equilibrium.

In order to explain the observed effects for the temperature dependent behaviour of the lifetime of the immobilised complexes (both monomers and

dimers) a number of possibilities exist. As mentioned previously, the negatively charged surface of the Method 2(5) sol-gels appears to have a significant effect on the kinetic parameters of the immobilised monomers and the kinetic parameters of these immobilised species fall into the category of low pre-factors and low activation. One possible explanation involves the argument that the location of the dd states relative to the luminescent excited states (*i.e.* the ^{3}MLCT-^{3}MC energy gap) in the Method 2(5) matrix is significantly altered upon incorporation. This interpretation maintains that the negatively charged surface destabilises the crystal field levels, which are populated in fluid media near room temperature, to such an extent that that population of the ^{3}MC state from the ^{3}MLCT is no longer possible at ambient temperatures. However, the present study shows that for these complexes, the ^{3}MLCT state is also destabilised upon incorporation into a sol-gel matrix (a blue shift in emission energy). This explanation suggests that the ^{3}MC state is destabilised to a greater extent than the ^{3}MLCT.

These results can be also be accounted for in terms of a rigid matrix perturbation of the potential wells. A general discussion of the phenomenology of solvent matrix spectroscopic effects has been presented by Dellinger and Kasha [23]. Their report suggests that the potential wells are made steeper by the viscosity of the rigid matrices formed at 77 K and/or a change in the equilibrium distance (ΔQ_e). In addition, Watts and Missimer report an application of such rigid matrix perturbations of molecular potentials to an interpretation of the luminescence rigidochromic effect [24]. With regard to the present study, under the influence of a rigid matrix perturbation caused by the sol-gel, steepening of potential wells would in turn lead to an increase in the activation energy. This explanation suggests that the perturbation varies according to the surface charge of the sol-gel matrix. As such, those species experiencing a large rigid matrix perturbation populate the ^{3}MLCT level only, while those experiencing a small perturbation may populate the ^{3}MC state (from the ^{3}MLCT level) at ambient temperatures.

Finally, small changes in the equilibrium distance ΔQ_e between the ^{3}MLCT and the ^{3}MC state, or between the ^{3}MC state and the ground state upon

immobilisation of the complexes may occur. This in turn would influence vibrational overlap of the potential surfaces and hence alter the value of k^{nr} [25]. A further discussion of each of these possible explanations is given in Chapter 7.

6.3 Conclusion.

In this chapter, a number of Ru(II) complexes containing pyridyltriazole ligands were successfully incorporated into the sol-gel matrix and their photophysical properties were examined. With the exception of the bpzt$^-$ dimer, all of the complexes exhibited a blue shift in the emission energy upon immobilisation into the sol-gel matrix. This shift was attributed to dipole reorientation with the excited state being energetically destabilised in the gel with respect to solution. For the bpzt$^-$ dinuclear molecule, the lowest π^*-level is based on the bridging ligand and the excited state of the bpzt$^-$ dimeric species appears to be shielded to an extent by the $Ru(bpy)_2$ units.

The pH at which the sol-gels were prepared was found to significantly alter the kinetic parameters obtained from the temperature dependent lifetime analysis of these immobilised complexes. We have mentioned previously, that the pH plays an important role in determining both the surface charge of the matrix and also the evolution of the gel structure. It would appear that the negatively charged surface of the sol-gel samples prepared at pH 5 distorts the excited states of the immobilised complex to a greater extent than when the surface is positively charged (*i.e.* at pH 1).

6.4 References.

[1] R. Hage, R. Prins, J.G. Haasnoot, J. Reedijk, J.G. Vos, *J. Chem. Soc. Dalton Trans.*,1389, **1987**.

[2] R. Hage, A. Dijkhuis, J.G. Haasnoot, R. Prins, J. Reedijk, B. Buchanan, J.G. Vos, *Inorg. Chem.*, 27, 2185, **1988**.

[3] F. Barigelletti, L. De Cola, V. Balzani, R. Hage, J.G. Haasnoot, J. Reedijk, J.G. Vos, *Inorg. Chem.*, 28, 4344, **1989**.

[4] H. Hughes, D. Martin, S. Bell, J. McGarvey, J.G. Vos, *Inorg. Chem.*, 32, 4402, **1993**.

[5] Y. Fuchs, S. Lofters, T. Dieter, W. Shi, R. Morgan, T. Strekas, H. Baker, *J. Am. Chem. Soc.*, 109, 2691, **1987**.

[6] R. Hage, J.G. Haasnoot, J. Reedijk, R. Wang, J.G. Vos, *Inorg. Chem.*, 30, 3263, **1991**.

[7] R. Hage, Ph. D. Thesis, Leiden University, The Netherlands, **1991**.

[8] H. Hughes, Ph. D. Thesis, Dublin City University, Ireland, **1993**.

[9] H. Hughes, J.G. Vos, *Inorg. Chem.*, 34, 4001, **1995**.

[10] T. Fujii, K. Toriumi, *J. Chem. Soc. Faraday Trans.*, 89, 3437, **1993**.

[11] J.V. Caspar, T.J. Meyer, *Inorg. Chem.*, 22, 244, **1983**.

[12] T.J. Meyer, *Pure and Appl. Chem.*, 58, 1193, **1986**.

[13] F. Barigelletti, A. Juris, V. Balzani, P. Belser, A. von Zelewsky, *J. Phys. Chem.*, 91, 1095, **1987**.

[14] S. Peterson, J. Demas, J. Am. Chem. Soc., 101, 6571, **1979**.

[15] J. Davila, C.A. Bignozzi, F. Scandola, *J. Phys. Chem.*, 93, 1373, **1989**.

[16] E.M. Kober, T.J. Meyer, *Inorg. Chem.*, 21, 3978, **1982**.

[17] E.M. Kober, T.J. Meyer, *Inorg. Chem.*, 23, 3877, **1984**.

[18] E.M. Kober, J.V. Caspar, B.P. Sullivan, T.J. Meyer, *J. Am. Chem. Soc.*, 104, 630, **1982**.

[19] G. Denti, S. Serroni, L. Sabatino, M. Ciano, V. Balzani, *Inorg. Chem.*, 29, 4750, **1990**.

[20] P. Bradley, N. Kress, B. Hornberger, R. Dallinger, W. Woodruff, *J. Am. Chem. Soc.*, 103, 7441, **1981**.

[21] R.S. Lumpkin, E.M. Kober, L.A. Worl, Z. Murtaza, T.J. Meyer, *J. Phys. Chem.*, 94, 239, **1990**.

[22] J.V. Caspar, T.J. Meyer, *J. Am. Chem. Soc.*, 105, 5583, **1983**.

[23] B. Dellinger, M. Kasha, *Chem. Phys. Lett.* 38, 9, **1976**.

[24] R.J. Watts, D. Missimer, *J. Am. Chem. Soc.*, 100, 5350, **1978**.

[25] G.F. Strouse, J.R. Schoonover, R. Deusing, S. Boyde, W.E. Jones, T.J. Meyer, *Inorg. Chem.*, 34, 473, **1995**.

Chapter 7.

Final Remarks.

7.1 Summary and final remarks.

7.1.1 Probing the sol-gel process.

This thesis investigates the photophysical properties of a range of Ru(II) diimine complexes immobilised in sol-gel matrices. Chapter 1 gives a general introduction to the sol-gel process. In this first chapter, an introduction to the photophysical properties of the tris(bipyridine)ruthenium(II) complex and related complexes are also given. Finally, details of previous research involving Ru(II) polypyridyl complexes in heterogeneous environments is presented in this chapter.

Chapter 2 deals with the preparation of the sol-gel matrices and the synthesis of the ruthenium complexes. In this chapter, the experimental details of the different physical measurements used for the elucidation of the properties of the ruthenium complexes both in solution and in the sol-gel matrix are given.

Initially, the primary concern of this thesis was to employ Ru(II) complexes as photoprobes of the sol-gel process and to investigate the parameters which affected the sol-gel-xerogel transition. In Chapters 3 and 4, the emphasis was on the ability of these transition metal complexes to probe local chemical and structural changes which occur as the matrix evolves from a sol through the sol-gel transition, the ageing process and the drying stages. Optical spectroscopic techniques were used to detect the changes and to interpret the chemical and structural environment responsible for them.

More specifically, Chapter 3 deals with the influence of the sol-gel matrix on the emission maxima of $[Ru(L\text{-}L)_3]^{2+}$ (where L-L = 2,2'-bipyridine (bpy), 1,10'-phenanthroline (phen), or 4,7-diphenyl-1,10-phenanthroline (dpp)). The absorption spectra of these complexes were found to be largely preserved before and after gelation. This suggested that there was no significant ground state interaction between the complex and the gel matrix. However, the emission spectra were significantly blue shifted. This has been previously reported and discussed in detail for related charge-transfer compounds doped into sol-gel materials [1-3]. This hypsochromic shift was attributed to dipole reorientation

and the excited state is energetically destabilised with respect to the solution. The destabilisation of the excited MLCT triplet state and the extent of this shift was found to vary, depending on the complex. Concerning this perturbation, the most sensitive complexes to the sol-gel environment, as in solution, were the bpy and phen complexes: indeed, whereas the emission maximum of $[Ru(dpp)_3]^{2+}$ exhibited no blue shift upon incorporation to the sol-gel matrix, $[Ru(bpy)_3]^{2+}$ and $[Ru(phen)_3]^{2+}$ were shifted by 590 cm^{-1} and 670 cm^{-1} respectively, in Method 2(5) xerogels. As such, the emission maxima of these latter two complexes were employed as spectroscopic probes, whereby the degree of sol-gel reaction most likely determined the position of the photoluminescence peak. These two photoprobes successfully followed the early stages of the sol-gel process and were used to monitor the following parameters;

- pH effects,
- thermal effects, and
- solution water content (R).

The observations were rationalised in terms of changes in the kinetics of the hydrolysis and polycondensation reactions which accompany the different pH regimes, temperature or water/silane ratio.

In Chapter 3, the potential application of $[Ru(phen)_2(H3Mptr)]^{2+}$ as a spectroscopic probe in order to monitor changes in the acidity of the surrounding environment was also investigated. Considerable electronic redistribution occurs between protonation and deprotonation of this pyridyltriazole complex, which is reflected in the absorption and emission spectroscopy of the complex. Unlike the previously studied $[Ru(L\text{-}L)_3]^{2+}$ complexes, the absorption spectra recorded for those sol-gels prepared at pH 5 exhibited a blue shift during the early stages of the sol-gel reactions. In addition, this change in the absorption profile was accompanied by a significant blue shift in the emission maxima during this time. These spectroscopic changes were consistent with the initially deprotonated complex accepting H^+ to become protonated and suggested that the sol-gel reactions induce local shifts of the pH around the complex to values lower than

the initial mixture of water, TEOS and ethanol. In effect, the acidity of the environment as experienced by the complex increased. The reason for this increased acidity is uncertain, but it is thought that the silanols, which are potential adsorption sites for the pyridyltriazole complex molecules, become deprotonated (to form SiO^-) as they are formed at this pH (*i.e.* pH 5) with $[Ru(phen)_2(3Mptr)]^+$ accepting this proton to become $[Ru(phen)_2(H3Mptr)]^{2+}$.

Chapter 4 deals with the effect of the sol-gel matrix on the luminescent lifetimes of these Ru(II) complexes. In fluid solution, the decay of the emission of each of these Ru(II) complexes is strictly first order. Deviations from first-order decay for these complexes upon immobilisation suggest the heterogeneous nature of the sol-gel matrix. The lifetimes of the incorporated complexes were quantitatively characterised by using a double exponential equation. The appearance of a second lifetime component for the immobilised complexes are in agreement with recent studies carried out recently by Castellano and co-workers whereby the photoluminescence decay data were modelled by a sum of two exponentials or by a single, asymmetric distribution of relaxation rates [2]. In addition to the introduction of a second lifetime component, in general, the overall lifetime of the complexes increased upon incorporation. The luminescent decay of $[Ru(bpy)_3]^{2+}$ and $[Ru(phen)_3]^{2+}$ were found to probe the early stages of the sol-gel transition with the emission decay lifetime increasing almost immediately. In contrast to these Ru(II) species, the emission lifetime of the $[Ru(dpp)_3]^{2+}$ complex was employed to monitor changes in the rigid nature of the gel matrix during the drying stage. The differences noticed between the immobilised $[Ru(bpy)_3]^{2+}$ and $[Ru(phen)_3]^{2+}$ complexes as compared to the $[Ru(dpp)_3]^{2+}$ suggest that while the former two complexes tend to be adsorbed on to the sol-gel particles during the early stages of polymerisation, the latter complex molecules possibly remain dissolved in the solvent filled pores in the gel during this time. In effect, no large increase in the emission lifetime occurred for this complex even at the gelation point although the solution had turned into to a solid amorphous material on the macroscopic scale suggesting that, at this stage, these dopants were unconstrained in a solvent-like environment. Consequently, the eventual observed increase in the emission lifetime for $[Ru(dpp)_3]^{2+}$ could

simply be explained by the shrinkage of the sol-gel medium, leading to the constriction of the silica network surrounding the dopants, which would thus decrease their vibrational degrees of freedom and thus the nonradiative rate constant (k^{nr}). Future work in this area might include observation of the change in weight which accompanies this increase in emission lifetime.

Finally in this chapter, the luminescent decay of $[Ru(phen)_2(H3Mptr)]^{2+}$ was investigated as a function of time, as the sol-gel reactions proceeded. It has been recently reported that the construction of a well-defined rigid cage only occurs under certain preparation conditions [4]. It is possible that during the initial stages of the sol-gel reaction at pH 5, (*i.e.* before the drying process) the dopants are not incorporated into a well-defined rigid cage but rather in a flexible three-dimensional network of Si-O chains. The dopants may be separated from one another by Si-O bonds. The final state of cage construction, resulting in complete encapsulation of the dopant is during the drying process.

7.1.2 Photophysical aspects of the immobilised Ru(II) complexes.

The second objective of this thesis concerned the examination of the excited state processes of Ru(II) polypyridyl complexes under a novel environment. Photophysical studies of Ru(II) complexes in solution [5], have revealed that the lifetimes are often dominated by the surface crossing from the ^{3}MLCT state to the non-luminescent ^{3}MC state. The study of the temperature effect on the emission lifetime of these complexes in solution allows the estimation of the ^{3}MLCT-^{3}MC energy gap. In Chapters 5 and 6, the temperature dependence of the emission properties of a range of Ru(II) polypyridyl complexes in the sol-gel matrix were investigated. Before further discussing the possible causes for the temperature dependent behaviour of the immobilised complexes, the important observations of these studies will be reviewed here;

- For the $[Ru(bpy)_{3-n}(dpp)_n]^{2+}$ series, only $[Ru(dpp)_3]^{2+}$ retains the high prefactor and activation energy upon immobilisation which are characteristic of the surface crossing from the ^{3}MLCT to the ^{3}MC and which occurs for all of these complexes in solution

- For the complexes $[Ru(bpy)_2(biq)]^{2+}$ and $[Os(bpy)_3]^{2+}$, where the ^{3}MC states are effectively removed from the ^{3}MLCT state so as not to be populated in solution, an increase in the emission lifetimes was observed upon immobilisation.

- The activation parameters obtained for the immobilised Ru(II) pyridyltriazole containing complexes depended significantly on the pH at which the sol-gel matrix was prepared. In general, high activation parameters were obtained when the gels were prepared at pH 1 while those prepared at pH 5 yielded low prefactors and low activation energies. It is likely that the surface charge of the silica cage plays an important role in the determination of these parameters. We shall return to this point shortly.

In solution, once populated, the ^{3}MC state undergoes radiationless decay to the ground state or ligand loss and net substitution [6,7]. In an excited dd state an electron occupies an antibonding, metal-based orbital, $(d\pi)^6 \rightarrow (d\pi)^5(d\sigma^*)^1$. The expected structural consequences of electron occupation of $d\sigma^*$ include large distortions along metal-ligand axes and weakening of the Ru-N bonds. Recently, Castellano and co-workers [8], carried out ground state Raman spectra of $[Ru(bpy)_3]^{2+}$ doped sol-gels. These samples displayed three symmetric bpy modes similar to those for the complex in aqueous solution suggesting that the ground state structure of $[Ru(bpy)_3]^{2+}$ is similar to that in fluid solution. While the mixed ligand complexes (*i.e.* $[Ru(bpy)_2(dpp)]^{2+}$ and $[Ru(bpy)(dpp)_2]^{2+}$) behave like $[Ru(dpp)_3]^{2+}$ in solution, it appears that in the sol-gel matrix their behaviour resembles that of $[Ru(bpy)_3]^{2+}$. This would seem to suggest that for the mixed ligand complexes in the sol-gel matrix, the lowest excited state may be located on the bpy ligand. In effect, a switching from dpp-based emission in solution to bpy-based emission in the xerogel may be occurring. To clarify this issue, time resolved excited state resonance Raman measurements were carried out on the immobilised mixed ligand complexes. However, the Raman spectra of these doped glass samples were dominated by features characteristic of the dpp ligand (see Figure 7.1) [9]. This suggests that, contrary to what was expected, the lowest excited state of the incorporated mixed ligand complexes remain dpp based as in solution.

We now turn to the question of the origin of the changes in the activation parameters of the temperature dependent lifetime decay upon immobilisation into the sol-gel matrix. There are a number of possible explanations as to why the activation parameters are significantly lowered.

One possibility, which has been previously reported to account for the loss of temperature dependence of $[Ru(bpy)_3]^{2+}$ in a cellulose acetate matrix [10,11], suggests that the low activation parameters can be attributed to the presence of a fourth ^{3}MLCT state. This suggests that the ^{3}MLCT-^{3}MC transition is inhibited in the solid xerogel matrix.

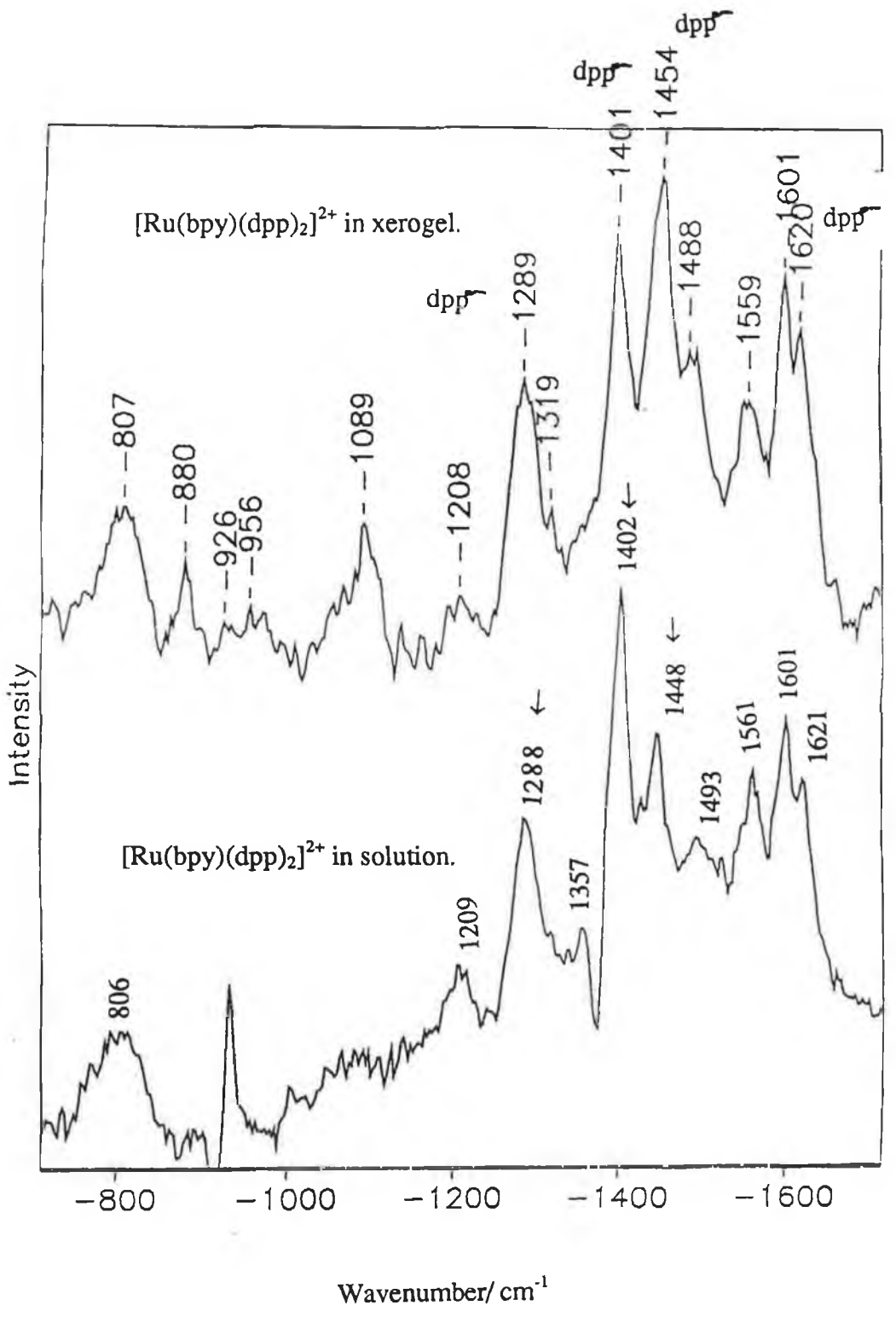

Figure 7.1 Excited state resonance Raman spectra of $[Ru(bpy)(dpp)_2]^{2+}$ in (a) xerogel and (b) acetonitrile.

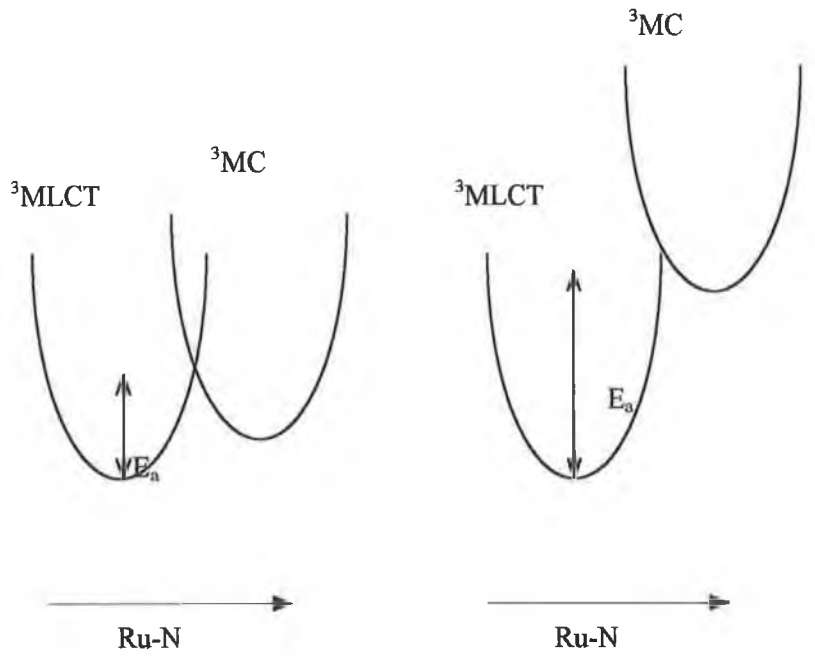

Figure 7.2 Possible destabilisation of the ^{3}MC potential energy surface relative to that of the ^{3}MLCT.

It is possible that, in the sol-gel matrix, the dd state may be destabilised to such an extent that population of this state from the ^{3}MLCT state is no longer feasible, even under ambient conditions (see Figure 7.2). However, with respect to the $[Ru(bpy)_n(dpp)_{3-n}]^{2+}$ series, the question remains as to why the ^{3}MC state would be destabilised to a large extent upon immobilisation for the first three complexes in this series and not for $[Ru(dpp)_3]^{2+}$. It is possible that the $[Ru(dpp)_3]^{2+}$ molecules remain dissolved to some extent by the residual solvent molecules even after drying. If this is the case, then the temperature dependent lifetime behaviour of the immobilised $[Ru(dpp)_3]^{2+}$ would resemble that of the complex in ethanol/methanol solution.

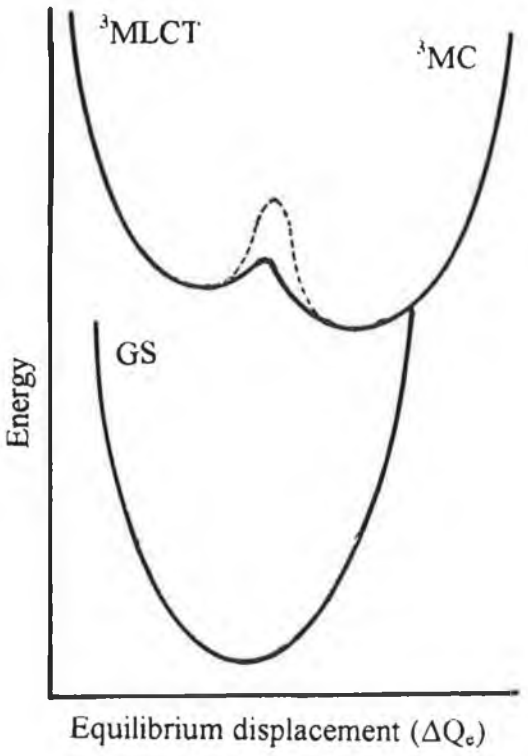

Figure 7.3 Possible rigid matrix perturbations (dotted lines) of the ^{3}MLCT and ^{3}MC states caused by the xerogel.

An alternative explanation for the inability to populate the ^{3}MC state involves the "rigid matrix effects" [12,13] caused by the sol-gel matrix which were previously discussed in Chapter 6 [14]. This interpretation maintains that the potential energy surfaces of the excited ^{3}MLCT and ^{3}MC states are perturbed in such a manner that surface crossing from the ^{3}MLCT to the ^{3}MC level can no longer occur in the temperature range studied in this thesis. Effectively, significant steepening of the potential wells may occur (see Figure 7.3) which may in turn lead to an increase in the activation energy such that population of the ^{3}MC state is no longer feasible. Again, in this situation, the activation parameters obtained for the analysis of the temperature dependent lifetime data of the immobilised species are most likely related to the population of the previously reported fourth ^{3}MLCT state [15,16].

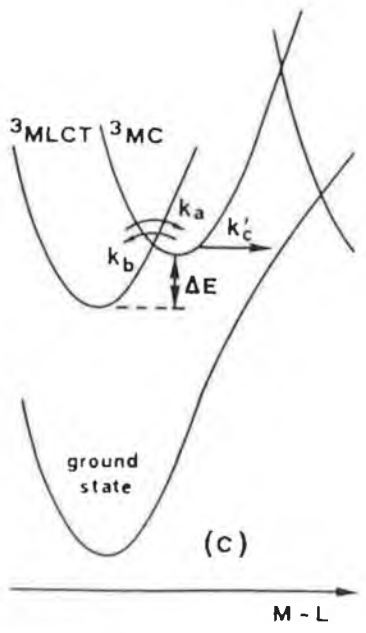

Figure 7.4 Schematic representation of the potential energy surfaces [19].

A third possibility is related to the displacement (ΔQ_e) of the potential energy surfaces from the equilibrium position. We have mentioned previously that changes in ΔQ_e influence the vibrational overlap between the ground- and excited-state (see Figure 5.1). The rate constant for non-radiative decay decreases as vibrational overlap decreases. Figure 7.4 depicts the possible situation of the potential energy surfaces of an Ru(II) complex in solution. It is possible that the sol-gel matrix induces some constraint on the complex and a decrease in ΔQ_e for the ^{3}MC state relative to the ground state may result.

In the gel matrix, the ^{3}MC geometry may be less substantially distorted from the ground state geometry. This may be caused by the rigid nature of the xerogel. As a consequence, the ground state and ^{3}MC state may be nested rather than strongly coupled as in solution. That is, decreasing ΔQ_e may sufficiently reduce the surface crossing of the ^{3}MC and the ground state potential surfaces so much so, that the contribution to k_c' as shown in Figure 7.4 may be effectively zero. This would account for the increased emission lifetime of the immobilised complexes. Furthermore, a change in ΔQ_e may result in the nesting of the ^{3}MLCT and the ^{3}MC potential energy surfaces. In effect, upon immobilisation subtle

changes in the equilibrium displacement of the excited states may give rise to non-activated processes with low prefactors.

It has been suggested that the Ru(II) dopants occupy two very different types of sites within the gel [2,8,17,18]. The first site, which gives rise to the shorter lifetime, is thought to provide a solvent rich environment for the dopants. This is most likely due to the presence of residual solvents from the sol-gel processing conditions (*i.e.* ethanol/water molecules). The Ru(II) sites with longer lifetimes are likely those well entrapped within the gel. The kinetic parameters obtained from the temperature dependence of the emission lifetime of the immobilised $[Ru(dpp)_3]^{2+}$ complex were found to be relatively unaltered when compared to those measured in solution. This suggests that the sol-gel matrix places no constraints on the immobilised complex which are observable by the spectroscopic techniques employed. This may be due to the shielding effect of the bulky diphenyl moieties which extend from the phenanthroline portion of the ligand. It is possible that the sol-gel network forms around the large $[Ru(dpp)_3]^{2+}$ molecule, in which case the dopant is responsible for creating the pore in which it is housed. Another explanation is that this immobilised complex remains solvated to a large extent by the remaining ethanol/water solvent molecules. At ambient temperatures, sufficient solvent molecules may allow for environmental relaxation processes to occur in which strongly distorted species are created as in ethanol/methanol solution.

$[Ru(bpy)_2(biq)]^{2+}$ and $[Os(bpy)_3]^{2+}$ were chosen in order to report the effect of the sol-gel matrix on complexes known to possess a ^{3}MLCT-^{3}MC energy gap in solution which is sufficiently large to effectively eliminate this decay pathway from the overall relaxation scheme. In all, there are less non-radiative processes involved in the excited state decay of these complexes. An increase in the lifetimes of these complexes was noticed upon immobilisation. A subtle decrease in the equilibrium displacement of the ^{3}MLCT state may lead to a decrease in vibrational overlap of the ^{3}MLCT and ground states, thereby increasing the lifetime of these complexes.

We have mentioned previously that the activation parameters of the pyridyltriazole containing complexes depend significantly on the surface charge

of the silanols. It appears that when these complexes are embedded in a negatively charged microenvironment, population and subsequent deactivation of the ^{3}MC state is no longer evident. That is, low activation energies and prefactors are obtained upon analysis of the temperature dependent emission lifetime data. This difference may have its origin in the negatively charged silica surface producing greater steric restrictions on the immobilised cationic pyridyltriazole complexes than the positively charged surface. As such, the rigid matrix effects mentioned above may be significantly more pronounced for gels prepared at pH 5 than at pH 1.

One question, which as yet has not been addressed, is why the monomeric pyridyltriazole complexes exhibit high kinetic parameters for gels prepared at pH 1 (as in solution), while the kinetic parameters obtained for $[Ru(bpy)_3]^{2+}$ immobilised under identical conditions are dramatically lowered (when compared to solution values). This is quite curious, since the relative size of these species are not un-alike. In solution, the activation energies and prefactors for both $[Ru(bpy)_3]^{2+}$ and the protonated pyridyltriazole complexes fall into the higher category indicative of thermal population of the ^{3}MC level. However, differences in the relative position and overlap of the excited states (*i.e.* the ^{3}MLCT and ^{3}MC states) and perhaps also the ground state may exist between $[Ru(bpy)_3]^{2+}$ and the pyridyltriazole complexes. As such, while subtle changes in the equilibrium distances of the excited states or the narrowing of potential wells may have a dramatic effect on the kinetic parameters of $[Ru(bpy)_3]^{2+}$, the pyridyltriazole complexes may be relatively unaffected.

7.2 Future work.

Photophysical studies in solution have shown that the short lifetime of many Ru(II) polypyridyl complexes in solution is due to the surface crossing between the ^{3}MLCT and the non-luminescent ^{3}MC that controls the emission lifetime. Population of the ^{3}MC state is accompanied by some geometric distortion of the molecule that is responsible for photodecomposition of these

molecules. It appears that the sol-gel matrix induces some constraint on the Ru(II) dopant, the extent of which depends very much on the particular Ru(II) complex and also the preparation conditions of the sol-gel matrix. It has been suggested that for $[Ru(bpy)_3]^{2+}$ for example, that the ^3MC state is most likely inaccessible from the ^3MLCT state. If this explanation is correct then a significant decrease in the photodecomposition of the incorporated complex should be observed, which should consequently improve the quality of this complex as a photosensitiser.

A further experiment which could confirm this hypothesis is the measurement of the photodecomposition of these Ru(II) complexes in the gel matrix. In solution, this experiment is quite straightforward. It involves dissolving the complex in a solvent (*e.g.* dichloromethane) with a suitable source of counter anion (*e.g.* benzyl tetraethyl ammonium chloride (0.005 mol/L)) and irradiating the solution. During photolysis, displacement of one of the co-ordinating ligands by the counter anion can occur. This photodecomposition process can be monitored by HPLC methods. However, in the gel matrix, a number of complexities are likely to arise. Firstly, the choice of solvent and counter anion must be such that both are capable of permeating the gel structure. This is by no means trivial, since the surface silanols are known to be charged and may repel certain species through electrostatic interactions thus preventing their entry into the porous gel. Secondly, it is possible that a portion of the immobilised Ru(II) dopants within the gel structure are contained within glassy regions [8] thereby rendering them inaccessible to the chosen solvent and counter anion. Finally, a qualitative method of detection must be chosen which allows for the distinction between the Ru(II) dopant and the product of photolysis.

Presently, the excited-state and ground-state resonance Raman spectra of these doped sol-gel glasses are

It would also be interesting to examine the behaviour of the bpt diphenylphenanthroline dimer ($[(Ru(dpp)_2)_2(bpt)]^{3+}$) and also the mixed ligand dimer ($[Ru(bpy)_2(bpt)Ru(dpp)_2]^{3+}$) upon incorporation into the sol-gel matrix.

7.3 References.

[1] K. Matsui, K. Sasaki, N. Takahashi, *Langmuir*, 7, 2866, **1991**.

[2] F.N. Castellano, T. Heimer, M. Tandhassetti, G.J. Meyer, *Chem. Mater.*, 6, 1041, **1994**.

[3] R. Reisfeld, C. Joergensen, *Structure and Bonding*, 77, 207, **1992**.

[4] M.M.E. Severin-Vantilit, E.W.J.L. Oomen, *J. Non-Cryst. Solids*, 159, 38, **1993**.

[5] A. Juris, V. Balzani, F. Barigelletti, S. Campagna, P. Belser, A. Von Zelewsky, *Coord. Chem. Rev.*, 84, 85, **1988**.

[6] B. Durham, J.V. Caspar, J.K. Nagle, T.J. Meyer, *J. Am. Chem. Soc.*, 104, 4803, **1982**.

[7] W.M. Wallace, P.E. Hoggard, *Inorg. Chem.*, 19, 2141, **1980**.

[8] F.N. castellano, J.G. Meyer, *J. Phys. Chem.*, 99, 14742, **1995**.

[9] K. Mongey, J.G. Vos, J.J. McGarvey, C. Gates, To be published.

[10] S. Allsopp, A. Cox, T.J. Kemp, W. Reed, *J. Chem. Soc., Faraday Trans. I*, 74, 1275, **1978**.

[11] R.S. Lumkin, E.M. Kober, L. Worl, Z. Murtaza, T.J. Meyer, *J. Phys. Chem.*, 94, 239, **1990**.

[12] B. Dellinger, M. Kasha, *Chem. Phys. Lett.*, 36, 410, **1975**.

[13] B. Dellinger, M. Kasha, *Chem. Phys. Lett.*, 38, 9, **1976**.

[14] R.J. Watts, D. Missimer, *J. Am. Chem. Soc.*, 100, 5350, **1978**.

[15] E.M. Kober, T. J. Meyer, *Inorg Chem.*, 21, 3978, **1982**.

[16] E.M. Kober, J.L. Marshall, W.J. Dresswick, B.P.Sullivan, J.V. Caspar, T.J. Meyer, *Inorg. Chem.*, 24, 2755, **1985**.

[17] U. Narang, R. Wang, P. Prasad, F. Bright, *J. Phys. Chem.*, 98, 17, **1994**.

[18] U. Narang, J. Jordan, F. Bright, P. Prasad, *J. Phys. Chem.*, 98, 8101, **1994**.

[19] A. Juris, V. Balzani, F. Barigelletti, S. Campagna, P. Belser, A. Von Zelewsky, *Coord. Chem. Rev.*, 84, 85 **1988**.